Diss. ETH No. 20508

Quantification of vegetation root induced cohesion in non cohesive river beds by experiments, monitoring and modeling

A dissertation submitted to
ETH Zurich

for the degree of
Doctor of Sciences

presented by
NICOLA PASQUALE
Dipl. Civil Eng. Politecnico di Torino
born July 14, 1981
citizen of Italy

accepted on the recommendation of
Prof. Dr. P. Burlando, examiner
Prof. Dr. P. Perona, co-examiner
Prof. Dr. A. Dittrich, co-examiner

2012

Abstract

River restoration has become a common measure to repair anthropogenically-induced alteration of fluvial ecosystems. The inherent complexity of ecohydrologic systems leads to limitations in understanding the response of such systems to restoration over time. Therefore, in the recent years a significant effort has been dedicated worldwide to document the efficiency of restoration actions and to produce new effective guidelines that may help overcoming existing deficiencies in designing such actions.

At the same time little attention was paid to illustrate the reasons and the use of certain monitoring and experimental techniques in spite of others, or in relation to the specific ecohydrologic process being investigated. In this context, the research project RE.COR.D. (REstored CORridor Dynamics) provided an interdisciplinary framework, which aimed at investigating, by means of extensive field work and modeling, the effects of restoration on several components of river corridor dynamics, from groundwater river quality to river morphology. In particular, the project addressed the morphodynamic evolution of the restored reach of the River Thur near Niederneunforn (Switzerland) is studied, also in relation to the role of pioneer vegetation roots in stabilizing the alluvial sediment. Indeed, the use of riparian tree cuttings for river rehabilitation is widely used and it relies on a good understanding of cutting survival and growth responses to environmental variables.

This work describes the methodology chosen for monitoring the river morphodynamics, the dynamics of riparian and of in-bed vegetation and their mutual interactions, as well as the need of complementing such observations with experiments and with the hydraulic modeling of the site.

A series of experiments aimed at studying the effects of water table fluctuation induced by streamflow variability on the development of below-ground biomass of riparian tree cuttings were performed on the Thur River. Willow cuttings were installed in gravel bar plots at various locations to develop an understanding of how topography and flow variability control cutting root development strategies, which in turn can lead to observed different vertical root density distributions in response to varying forms of tropism. In particular, it is shown how

the transient root growth dynamics eventually create a distribution reflecting the hydrologic conditions experienced towards the end of the growing season.

A scaling relationship is presented that is useful to predict the expected depth with the highest root density as a function of soil topography and river discharge statistics. The results have implications for predicting cutting survival and growth, along with a corresponding strengthening of the alluvial sediment, in different flow regimes.

Finally a model of root reinforcement based on the Shields approach is formulated and validated with data collected from field site experiments. This approach is therefore useful to incorporate in morphodynamic models covering the ecological and hydraulics responses of below-ground biomass to floods.

Zusammenfassung

Flussrestaurierung ist eine verbreitete Methode, um anthropogene Veränderungen von fluvialen Ökosystemen zu korrigieren. Aufgrund der Komplexität von ökohydrologischen Systemen ist das Verständnis der Entwicklung solcher Systeme im Laufe der Zeit ungenügend. Daher wurde in den letzten Jahren weltweit ein beträchtlicher Aufwand betrieben, die Effizienz von solchen Restaurierungen zu dokumentieren und neue Richtlinien zu erstellen, die helfen sollen, die bestehenden Mängel in solchen Projekten zu beseitigen.

Jedoch wurde die Wahl von bestimmten Beobachtungs- und Experimentiertechniken nicht ausführlich diskutiert und begründet in Bezug auf die spezifischen ökohydrologischen Prozesse, die untersucht werden sollten. In diesem Kontext hat das Forschungsprojekt RE.COR.D. (REstored CORridor Dynamics) ein interdisziplinäres Umfeld geschaffen, in dem anhand von umfangreicher Feldarbeit und Modellierung die Effekte der Restaurierung auf verschiedene Komponenten des Flusssystems, wie zum Beispiel Grundwasserqualität und Flussmorphologie, untersucht werden. Konkret wurde in diesem Projekt die morphodynamische Evolution des restaurierten Abschnitts des Flusses Thur bei Niederneunforn (Schweiz) untersucht. Weiter wurde auch die Rolle des Wurzelgeflechts der Pioniervegetation in der Stabilisierung des alluvialen Sediments untersucht. Die Verwendung von Stecklingen von der Ufervegetation ist in der Flussrestaurierung weit verbreitet und sie erfordert ein detailliertes Verständnis des Wachstums und des Fortbestands der Stecklinge unter Einfluss verschiedener Umweltfaktoren.

In dieser Arbeit beschreiben wir die gewählte Methode zur Beobachtung der Flussmorphodynamik, der Dynamik der Ufer- und Flussbettvegetation und deren Interaktion, sowie die Notwendigkeit solche Beobachtungen mit Experimenten und hydraulischer Modellierung zu ergänzen.

Um die Effekte der Wasserstandsfluktuationen, die durch Abflussveränderung induziert werden, auf die Entwicklung der unterirdischen Biomasse der Stecklinge zu untersuchen, wurde am Fluss Thur eine Serie von Experimenten durchgeführt. Weidenstecklinge wurden an verschiedenen Stellen auf einer Kiesinsel gepflanzt, um zu untersuchen wie Topographie und Abflussvariation die Strategie des Wurzelwachstums beeinflussen. Dies kann zu Unterschieden in der vertikalen

Verteilung der Wurzeldichte führen, als Antwort auf verschiedene Formen von Tropismus. Insbesondere wird gezeigt, wie die Dynamik des Wurzelwachstums zu einer Verteilung führt, welche die hydrologischen Bedingungen am Ende der Wachstumsperiode wiederspiegelt. Eine Skalierungsbeziehung wird präsentiert, welche nützlich ist, für die Vorhersage der Tiefe mit der höchsten Wurzeldichte als Funktion von Bodentopographie und Abflussstatistik. Die Resultate sind von Bedeutung für die Vorhersage des Wachstums und Fortbestands von Stecklingen im Zusammenspiel mit der Verstärkung des alluvialen Sediments unter verschiedenen Abflussbedingungen.

Zum Schluss wird, basierend auf dem Shields Ansatz, ein Modell für die Bodenverstärkung durch das Wurzelgeflecht formuliert und anhand der gesammelten Daten validiert. Es ist sinnvoll, diesen Ansatz in morphodynamische Modelle zu integrieren, die die ökologischen und hydraulischen Reaktionen der unterirdischen Biomasse auf Überflutung untersuchen.

Sommario

La pratica di *restoration* di tratti fluviali è divenuta una misura sempre più diffusa allo scopo di rimediare alle alterazioni antropogenetiche degli ecosistemi fluviali. L'insita complessità dei sistemi eco-idrologici porta a forti limitazioni nella comprensione delle risposte nel tempo agli interventi di *restoration* su tali sistemi. Per tale motivo, negli anni recenti, in tutto il mondo è stato dedicato un significativo impegno per documentare l'efficienza degli interventi di *restoration*, al fine di produrre nuove ed efficaci linee guida che possano aiutare a colmare le lacune esistenti in tale campo. Allo stesso tempo, tuttavia, si è prestata poca attenzione nel cercare di spiegare le ragioni alla base dell'uso di determinate techiniche di monitoraggio o di intervento sperimentali in luogo di altre. Lo stesso dicasi in relazione allo studio e alla valutazione di specifici processi eco-idrologici.

In questo contesto, il progetto di ricerca RE.COR.D. (REstored CORridor Dynamics, vale a dire Dinamiche dei Corridori Fluviali a seguito di interventi di *restoration*) ha fornito una cornice di lavoro fortemente interdisciplinare allo scopo di studiare, per mezzo di estensive campagne di esperimenti *in situ* e di modellazione, l'effetto degli interventi di *restoration* su diverse componenti delle dinamiche fluviali e riparie, dalla qualità delle acque di falda sotteranea alla morfologia fluviale. In particolare, il progetto si focalizza sull'evoluzione morfodinamica del tratto di fiume Thur sottoposto a interventi di *restoration*, nei pressi di Niederneunforn (Thurgau, Svizzera), e in maniera più specifica, in relazione al ruolo svolto delle radici delle specie vegetali pioniere (salici) nello stabilizzare la dinamica dei sedimenti fluviali. Talee di piante provienenti dalla vegetazione riparia sono largamente utilizzate nel campo della rinaturalizzazione e riabilitazione fluviale. Quest'uso fa inoltre affidamento su una buona comprensione della risposta ai fattori ambientali delle talee piantumate.

In questo lavoro vengono descritte le metodologie adottate per monitorare l'evoluzione della morfodinamica fluviale, la dinamica della vegetazione riparia e di quella in alveo e la loro mutua interazione, così come la necessità di accompagnare tali osservazioni con esperimenti e con la modellizzazione idraulica del sito investigato.

Sul fiume Thur, è stata condotta una serie di esperimenti volti a studiare l'effetto della flut-

tuazione della falda riparia (quindi controllata dalla variabilità del livello d'acqua in alveo) sullo sviluppo della biomassa sotterranea di talee di specie riparie. Talee di salice sono state piantumate, sparse in gruppi su un'isola fluviale in ghiaia allo scopo di studiare come la topografia e la variabilità del livello d'acqua dovuta alla portata influenzino le strategie delle piante nello sviluppo delle radici. Tali strategie possono a loro volta portare ad osservare diverse distribuzioni nella densità delle radici in rapporto alla profondità, come risposta a vari fattori di tropismo. In particolare, si mostra come la dinamica di crescita delle radici, nelle farie fasi di crescita, durante la stagione, possa eventualmente produrre una distribuzione, verso la fine della stagione di crescita, che riflette le condizioni idrologiche susseguitesi nel tempo.

Viene illustrata una relazione di taratura (scaling) molto utile per predire la profondità attesa della massima densità delle radici in funzione dell'elevazione topografica del suolo e delle statistiche di portata del fiume. I risultati hanno notevole importanza nel predire la sopravvivenza e la crescita delle talee di salice, insieme a implicazioni per ciò che concerne il rinforzo di sedimenti alluvionali non coesivi, contro l'erosione, a diversi regimi di portata.

In conclusione viene proposto un modello di rinforzo del terreno da parte delle radici basato sull'approccio di Shields. Il modello viene validato sulla base dei dati raccolti durante gli esperimenti e i rilievi di monitoraggio *in situ*. Questo approccio si rivela quindi molto utile per includere all'interno di modelli morfodinamici la risposta ecologica e idraulica della biomassa sotterranea delle radici rispetto ai fenomeni di piena.

Acknowledgments

This study was funded by the Competence Center Environment and Sustainability (CCES) of the ETH domain in the framework of the RECORD project[1].

Thanks to Prof. Paolo Burlando. The contribute he gave to this work as a leading guide is difficult to describe. He has always been helping and open to discussions.

Thanks all the people, Ph.D. students and P.I.s who participate to the record project and in particular Prof. Mario Schirmer for coordinating the project, Dr. Joerg Luster for interesting discussions and Dr. Philipp Schneider for his help in everything concerning installation, field work and project coordination and co-operation.

Thanks to Romeo Favero, Ulrich Guettelmann, Robert Holzschuh, Andreas Scholtis, and Marco Baumann from "Amt fur Umwelt" of Canton Thurgau and Urs Spychiger, Franz Bieler, Kurt Nyfenegger, and Matthias Oplatka from AWEL, Canton Zurich for their support and close cooperation.

Thanks to the ETH technicians. Above all to René Weber and Thomy Keller. Thanks also to Manuela for all her help, her patience and her understanding, together with my apologize for the times I messed rules up.

Thanks also to Prof. Andreas Wombacher at the University of Twente, NL and Prof. Robert Francis at the London King's College (UK) for their precious help.

Thanks to Prof. Paolo Perona for never letting me down and for his help on the field. The contribute he gave to this work as well as to my personal formation has been too precious to describe. It was an enormous pleasure to work with and beside him.

[1] http://www.cces.ethz.ch/projects/nature/Record

Thanks to all my all Ph.D. students in the hydrology group. Especially, to Maurizio Savina for being not only a great office mate but also a precious, unique friend; to Bettina Schäppi for her help and for all the nice conversations; to Marco Carenzo for all our late evening run, for his help, for the nice conversation and for always keeping his door open.

To Francesca Casini also my thanks for helping me with the grain size curve analysis. She is the one that made it possible.
For the field work (cutting transplantation and uprooting) and for the laboratory analysis, special thanks are due to: Bettina Schäppi, Roger Bordoy Molina, Grigorios Anagnostopoulos, Maurizio Savina, Francesca Verones, Giovanni Maccioni, Paolo Cavatore and my father.

Thanks to the Italian guys that help me not to feel too much homesick in those three years: Francesca Casini and Giovanni Maccioni, above all. I wish them all the best for their life and their scientific and professional careers.
Thanks to Andreas and Deniz: they have been my family during the time I spent in Zurich.

Thanks to Giulia, for having always been waiting for me, for her support and her love.

Grazie alla mia mamma e al mio papà. Se oggi sono arrivato fino a qui è solo grazie al loro affetto, ai loro insegnamenti, alla loro pazienza e al supporto che non hanno mai smesso di farmi mancare.

Nicola Pasquale

Contents

1 Introduction **1**

1.1 River Restoration 2

1.2 RECORD project 3

1.3 Quantification of vegetation root induced cohesion rationale 6

1.3.1 State of the art 6

1.3.2 Research questions 10

1.3.3 Research plan and structure of the thesis 10

2 Study site, field investigations and experimental set up **13**

2.1 Thur river and hystory (field site) 13

2.2 Field experiment set up 15

2.2.1 Local meteorogical and soil moisture measurements 16

2.2.2 Sediment size and nutrient spatial variability 16

2.2.3 Terrestrial and aerial photography 19

2.2.4 Digital terrain models and river bathymetry 20

2.3 Hydrodynamic simulations 21

2.3.1 Introduction to 2D hydrodynamic models 21

2.3.2 Grid and mesh generation 22

2.3.3 The model BASEMENT and the software AQUAVEO SMS 10 23

2.4 Hydrodynamic Model calibration 26

2.4.1 Classical Methods 27

2.4.2 Calibration from terrestrial photography 28

2.5 Bedload transport . . . 36
2.5.1 Basic Theory . . . 36
2.5.2 Meyer-Peter and Müller equation . . . 38
2.6 Vegetation cutting experiments . . . 39
2.7 Root sampling and analysis . . . 42

3 Morphodynamic evolution of the study site 47
3.1 Annual erosion-deposition balance . . . 47
3.2 Morphodynamic evolution of the Thur river after restoration . . . 51
3.3 Erosion-deposition pattern and their interaction with vegetation . . . 55
3.3.1 Bed-form scale . . . 55
3.3.2 Salix plots scale . . . 57
3.4 Effects of the restored morphological dynamics . . . 59

4 Vegetation cuttings growth: experiments and analysis 63
4.1 Experimental set up . . . 63
4.2 Cutting Growth Statistics . . . 65
4.2.1 Above ground biomass: surviving, growth and growth rate . . . 65
4.2.2 Below ground biomass . . . 69
4.2.3 Link between above- and below-ground biomass . . . 72
4.3 Survival rate in relation to morphodynamic processes . . . 74

5 Effects of streamflow variability on the root system evolution 79
5.1 River hydrology . . . 79
5.2 Water table dynamics . . . 81
5.2.1 Water table estimation . . . 81
5.2.2 Water table frequency distribution . . . 81
5.3 Root frequency distribution . . . 83
5.4 Root scaling relationship . . . 84
5.5 Root scaling map and root mode depth . . . 87

5.6 Sources of uncertainties 89

6 Root anchorage and soil reinforcement 91

6.1 Application to river banks and slopes 91

6.2 Model of root reinforcement for river bedforms (alluvial sediments) 93

6.2.1 Energetic Method 93

6.2.2 Simplified root reinforcement method: theory 98

6.2.3 Quantification of root reinforcement and model validation from data . 102

7 Conclusions 107

8 References 111

A Normalized Difference Vegetation Index 131

B Shallow water equation and finite volume method of integration 137

B.1 Derivation of the shallow water equations 137

B.2 Discretisation with the finite volume method 139

C "Quasi-Automatic" Pattern Recognition 143

C.1 Matlab code 144

C.2 Conversion pixel-to-area 155

D Willow cuttings transplantation and monitoring 157

E Root empirical histograms 161

F Formulation of the velocity profile in presence of a canopy layer 167

List of Figures

1.1 Field test site at Neunforn, partly restored and partly channelized. 5

1.2 Theoretical trajectories for tree recruitment and growth and sediment aggradation on bar surfaces of a braided river (Gurnell and Petts (2002)). 8

1.3 Flow chart of the Ph.D. project 11

2.1 Location of the river Thur in Switzerland and river basin. 14

2.2 Conceptualization of the interaction among river hydrology and hydrodynamics, root structure and architecture and sediment erosion and uprooting. 15

2.3 Field installation: meteorologiacal and soil moisture stations, remote sensing devices and paraglider for aerial pictures. 17

2.4 Grain Size Distributions on the main island. 18

2.5 Mesh generation for hydraulic modeling. 25

2.6 Calibration of the hydraulic model with classic methodologies. 29

2.7 Aerial view of the restored reach of the Thur River, together with three representative cross section and pictures from the cameras taken at different flow rates. 30

2.8 Automatic pattern recognition output. 31

2.9 Location of the green and blue tarps used for remote calibration. 31

2.10 Computation of the island area-to-pixel conversion function using over a boundary ω. 33

2.11 Optimum roughness coefficient values changing according to the discharge. . . 36

2.12 Forces acting on a submerged particle. 37

2.13 Shields diagram of sediment particle's incipient motion. 38

2.14 Planning and monitoring strategy of the transplanted cuttings 40

2.15 Map of the investigated island showing the location of the vegetation plots in 2008, 2009 and 2010. 41

2.16 Example map of the simulated shear used to plan the location of the *Salix* plots. 43

2.17 Pictures showing the steps for cutting uprooting. 44

3.1 Pattern of the yearly erosion deposition balance in the river corridor since the end of the restoration project. 49

3.2 Relative frequency histograms of the observed and simulated erosion/deposition during the year 2007-08. 51

3.3 State plane projection showing the spatial variability of the modeled hydraulic variables (h,v) for the straight and the restored reaches. 52

3.4 Morphodynamic evolution of the Thur river from the end of the restoration project to the present. 54

3.5 Difference computed from the DEM with resolution 50cm x 50cm gives the pattern of erosion - deposition due to hydrodynamics. 56

3.6 Simulate bed shear stress on the island for the highest recorded peaks. 56

3.7 Erosion deposition balance at the vgetation plot scale in 2009 and 2010. . . . 58

3.8 Conceptual representation of the restored corridor evolution trajectory in the state space. 60

4.1 Example of correlation between vegetation mortality and highly impulsive natural floods. 64

4.2 Cuttings growth within a representative plot in 2009 and 2010 throughout the corresponding season. 65

4.3 Survival of the cuttings and hydrogram of the river together with growth curve of the canopy biomass in 2009 and 2010. 67

4.4 Growth rate (mm/day), computed as average of the single cuttings, for each plot in 2009 and 2010. 68

4.5 Root length density (RLD) and root volume ration (RVR) relative to 2009 and 2010 field campaign. 71

4.6 Discharge, air temperature and water temperature recorded at the Thur river field site for the growing season in 2009 and 2010. 72

4.7 Regression analysis linking the main stem length [cm] to the root volume [cm^3]. Regression coefficients are reported in Table 4.1. 74

4.8 Plot mortality (expressed as percentage) in relation to class of scouring and deposition (a) and to the distance from the water table (b). 75

4.9 Consequences of the different root distribution due to hydrotropism or oxytropism on cutting surviving. 77

4.10 Flood frequency and duration curves computed on the basis of 12 years (1999-2010) daily records for the field site at the Thur River. 77

5.1 Streamflow regime during the growing season (april - september) in 2008, 2009 and 2010. 80

5.2 Gravel island of the restored reach of the Thur River near Niederneunforn showing the location of the plots of installed willow cuttings for the 2009 campaign and simulated flow depth. 82

5.3 Cross section used to compute the relative frequency of water table in correspondance of the plot using the rating curve method. 82

5.4 Experimental relationship between the vertical root density distribution and the histogram of water table oscillations at each plot location for a number of exemplary plots located at different elevation. 84

5.5 Temporal evolution through the season of the root structure of Plot 10 (2009 field campaign) showing how the root density histogram adjusts in time to the experienced water table fluctuations. 85

5.6 Scaling relationship relating the depth of the highest root density (histogram mode) to that of the most frequent water table position, and the soil surface elevation. 86

5.7 Map of expected highest root density depth for the 2010 campaign as obtained from the scaling on 2009 data. 88

5.8 The coefficient of determination R^2 for observed vs computed data points for the 2010 campaign at the end of the growing season (Pasquale et al., 2012a). 89

6.1 Conceptual model for shooting deformation due to dragging on stem and leaves (Schnauder and Moggridge, 2009). 94

6.2 Conceptual model of the flow energy method to assess quantification of root reinforcement in presence of a canopy layer. 95

6.3 Scheme of the cells within and surrounding the vegetation plot. The geometry here represented is used to compute vegetation root reinforcement. 99

6.4 Modified Shields curve of incipient motion according to percentage of root volume in the soil. 102

6.5 Coefficient of determination R^2 of the observed erosion value within the plot Δz and the expected depth of the root mode. 104

A.1 NDVI computed for representative pictures selected within single month set in 2009. 133

A.2 NDVI computed for the island only. 134

A.3 Histograms of the percentage of pixels for each class (waterm bare soil and vegetation) computed with the NDVI. 135

A.4 NDVI analysis of the flood effects in July 2009. 136

B.1 Finite volume discretization of the model problem 139

B.2 FV cell-centered method (left) and node centered method (right) and associated volume definitions. 141

C.1 Example of water and non-water classes recognition from digital photographs under changing light and surface albedo. 143

D.1 Phases of the cutting transplantation. 158

D.2 Monitoring of the transplanted *Salix* cuttings thoughout the growing season. . 159

D.3 Effect of floods on the plot of transplanted *Salix* 160

E.1 Black and White pictures of the three samples taken from plot 5 in Semptember 2009. 161

E.2 Graphical User Interface (GUI) of the MATLAB code for calculating the empirical histogram for each cutting. 162

F.1 Conceptual model developed by Katul et al. (2011) for the force balance above the canopy and the assumed mean velocity profile $\overline{U}(z)$ in streams. 167

List of Tables

2.1 Nutrient content and soil type analysis results. 19

2.2 Manning's *n* value of the roughness coefficients used for calibration and corresponding errors. 34

2.3 Summary of the field campaign activities. 42

3.1 Input data and results of the solid transport analysis based on shear stress computed in the straight non-restored channel. 50

4.1 Coefficients and index of goodness resulting from the regression analysis between root volume and stem length. 73

6.1 Results of validation of the root reinforcement model for plots in 2009. 105

6.2 Results of validation of the root reinforcement model for plots in 2010. 106

C.1 Conversion pixel-to-Area at each tarp location. The conversion factor is computed in correspondence of the center of mass of the tarp (X_G,Y_G). 155

E.1 Excel sheet with the output of the root analysis for sample "Plot5 r1c1". 163

E.2 Excel sheet with the output of the root analysis for sample "Plot5 r2c1". 164

E.3 Excel sheet with the output of the root analysis for sample "Plot5 r3c1". 165

...to my roots,
to my homeland.

There's a lot of people leaving town now
Leaving their friends, their homes
At night they walk that dark and dusty highway all alone.
Well Papa go to bed now it's getting late
Nothing we can say can change anything now
Because there's just different people coming down here now
and they see things in different ways
And soon everything we've known will just be swept away.

B. Springsteen

"Tu sai che le cose immortali le avete a due passi"

C. Pavese

Chapter 1

Introduction

In the past century the main streams of many rivers have been straightened and channelized worldwide for both hydraulic and socio-economic reasons such as, for instance, flood protection, land use changes, agriculture or spreading of infectious diseases (Lacey, 1930; Inglis, 1949; Brookes, 1988). However, later it has become clear that such corrections affect considerably the associated riverine ecosystem, which typically reacts to artificial perturbations on multiple time scales (Malmqvist and Rundle, 2002; Tockner and Stanford, 2002). For instance, straightening the main water course affects both the river sediment dynamics and the lateral exchanges and connectivity with the floodplain on short temporal scales (e.g., weeks), whereas morphological changes and the related effects in habitat availability and in local biodiversity occur over longer temporal scales (e.g., months, years).

In the last decade, many projects of river restoration have been initiated in order to bring local sections of rivers back to an improved natural appearance and thus to partially remediate to the consequences of large scale river straightening. Among other it is worth to mention the restoration projects on the Platte River, Kissimmee River and Grand Canyon in the U.S. (Wohl et al., 2005) or the restoration projects on the Rhone River and the Thur River in Switzerland.

Water demand and conversion of wetlands to agricultural, urban and traffic areas competes with protection of aquatic ecosystems and ecological services (MEA 2005[1]). The Water Framework Directive (WFD[2]) - "the most substantial piece of water legislation ever produced by the European Commission" - is a key driver for achieving "good ecological status" of rivers, their catchments and associated groundwater bodies. Swiss legislation has similar goals, requiring river revitalization actions as part of flood protection measures (BWG, 2001). These actions aim at increasing the variability of habitats in a restored corridor of the river in order to increase the resilience of the ecosystem in terms of functional biodiversity. Worldwide, the number of

[1] http://www.maweb.org/en/index.aspx

[2] www.euwfd.com

restoration projects has increased significantly during the past few years and is expected to raise further (Wohl et al., 2005; Nakamura et al., 2006; Palmer and Bernhardt, 2006).

1.1 River Restoration

River bed and floodplain morphologies play a big role in determining the lateral connectivity between the main stream dynamics and the moisture condition of the side terraces, which are critical for the ecotone development. Thus, forcing changes of river bed morphology by either artificial or natural widening actions is one of the most common restoration techniques for those rivers that in origin showed a braided morphology (Formann et al., 2007; Peter et al., 2006; Schweizer, 2007). Restoration is usually intended as "the complete structural and functional return of the river to a pre-disturbance state" (Cairns, 1991). Soar and Thorne (2001) notice that full-restoration to an anthropogenic *pre-disturbance* state is an ideal concept. Hence, in the context of this work, river restoration is defined as "the input actions that serve to trigger the fluvial ecosystem evolution toward a new self-sustaining statistical equilibrium (if existing)" (Wohl et al., 2005).

The main goal of restoration is to link the sustainable use of rivers and wetlands with human wellbeing. Following the initiation of restoration, it is also important to address the question of quantifying its success (Peter et al., 2006; Palmer et al., 2010), especially as far as coupled hydro-ecological processes are concerned. In this respect, useful hydrologic and ecologic indicators have been developed to evaluate the present status of rivers (Woolsey et al., 2007). However, today's literature about river restoration mostly deals with practical guidelines that have gradually been built on results, observations and lessons learnt by comparing pre- and immediate post restoration on case study (e.g., Mitsch, 2003). The literature is apparently missing systematic studies addressing an integrated mechanistic understanding of the evolution after restoration over longer time periods. Densmore and Karle (2009), for instance, recognize the value of long-term monitoring of restored streams.

River restoration extent and rates are influenced by a range of factors including ecological heterogeneity, water quality and soil fertility. Riparian vegetation typically occurs in patches (i.e., areas that differ from their surroundings in structure or function) that are controlled by the hydrological regime of the river (frequency and magnitude of flooding events), the soil substrate and the time since the patch was colonized. Conversely, vegetation influences hydrological, chemical and morphological conditions via transpiration, root-microbe-soil interactions and mechanical stabilization (e.g., Abernethy and Rutherfurd, 2001; Gyssel et al., 2005; Pollen and Simon, 2005).

The interactions between soil-water content, plant growth, microorganisms and soil cohesion determine how and which vegetation develops on juvenile soils in the restored corridor, and how resistant it is against minor floods. Thus, the practice of considering vegetation cover as merely passive mechanical elements that increase the local river (or bank) roughness has given way to the awareness of the active role of both flora and fauna. Indeed, the life cycle of vegetation influences the river morphodynamics and vice versa (e.g., Camporeale et al., 2006; Perucca et al., 2006).

It is known that streambank instability poses a number of economic and ecological problems including land loss and destabilization of structures (e.g. bridges), while the delivery of excessive sediment to channels can cause downstream aggradation and impairment of water quality (Casagli et al., 1999). In the same way it is known that vegetation roots contribute to stabilize hill slopes, river banks and more in general non cohesive soils. However the hydrologic effects of vegetation on shear resistance and stream bank stability were not quantified until the work in unsaturated soil mechanics by Fredlund et al. (1978) and the application of these techniques to vegetation-covered stream banks (Simon and Collison, 2002).

On alluvial sediment, still now the impact of increasing morphological variability on water quality is currently under debate. River restoration aims at enhancing the hyporheic exchange, which is claimed to increase the self-cleaning capacity of the river. Conversely, concerns have been raised that river restoration may facilitate early breakthrough in pumping wells adjacent to revitalized rivers, which may lead to contamination of drinking water, e.g., by bacteria. Swiss legislation prohibits river revitalization in the inner protection zone of drinking water wells, defined by an average travel time of ten days (BUWAL 2004[3]), although it is not clear whether this precautionary measure is justified.

1.2 RECORD project

Investigating river restoration issues was the goal of the RE.COR.D. (REstored CORridor Dynamics) project, which was financed by the CCES of the ETH Zurich[4]. Along with Densmore and Karle (2009) the main aim of the project was specifically to quantify the results of an ongoing restoration project and to approach scientifically the study of the river and riparian zone dynamics after restoration, in order to identify a mechanistic approach for future restoration process.

Because the Thur River flows through an area of intensive agriculture and substantial urban-

[3] http://www.bafu.admin.ch/publikationen/publikation/00378/index.html?lang=de

[4] http://www.cces.ethz.ch/projects/nature/Record

ization, it is also impacted by anthropogenic activities, and so is typical for rivers in the Swiss Plateau and Central Europe. The research performed in the project consists of three major components:

1. Comprehensive field measurements of ecological-status components and their major influencing factors at the main study site, including 3D surveys of sedimentary materials, identification of subsurface spatial travel-time distributions, continuous recording of hydrological variables in air, water and ground, frequent observation of vegetation, monitoring of root zones and repeated sampling for hydrochemical parameters. Data collected at the highly instrumented test sites will form the basis to test hypotheses on flow, transport, and biogeochemical cycling in the heterogeneous system of the restored corridor.

2. Well targeted laboratory and field experiments on key processes and relations, such as oxygen replenishment in riparian sediments, the impact of vegetation on mechanical soil stability, the dependence of C and N fluxes and transformations on plant-soil-microbe interactions at varying dry/wet cycles, and the influence of flow paths on nutrient and organic matter transformation.

3. Process-based numerical simulations for testing understanding and quantification, and for linking processes and data collected at various scales.

Several other ecological and hydrological aspects, such as groundwater quality (Schneider et al., 2011), flood protection efficiency, long-term river morphology and biodiversity changes (Schirmer et al., 2012) are all eco-hydrological processes influenced by the new river hydraulics and morphodynamics.

In particular, the idea behind the RECORD project was to achieve this goal by means of field experiment, monitoring and modeling. The main field site chosen for installation was a restored reach of the Thur river (Figure 1.1 shows an overview of the area and of the installations).

In general, the main questions addressed by the RECORD project were:

- What is the role of vegetation with a particular focus on vegetation roots in influencing soil cohesion? More in detail, how is the the root system increasing soil reinforcement against bed erosion and therefore in influencing the local stream morphology (which are the tasks of this work)?

- How does the maturity of the vegetation influence local hydrology and resistance to hydrological stresses? and how important is variability of hydrological forcing for the ecological functioning of the restored corridor?

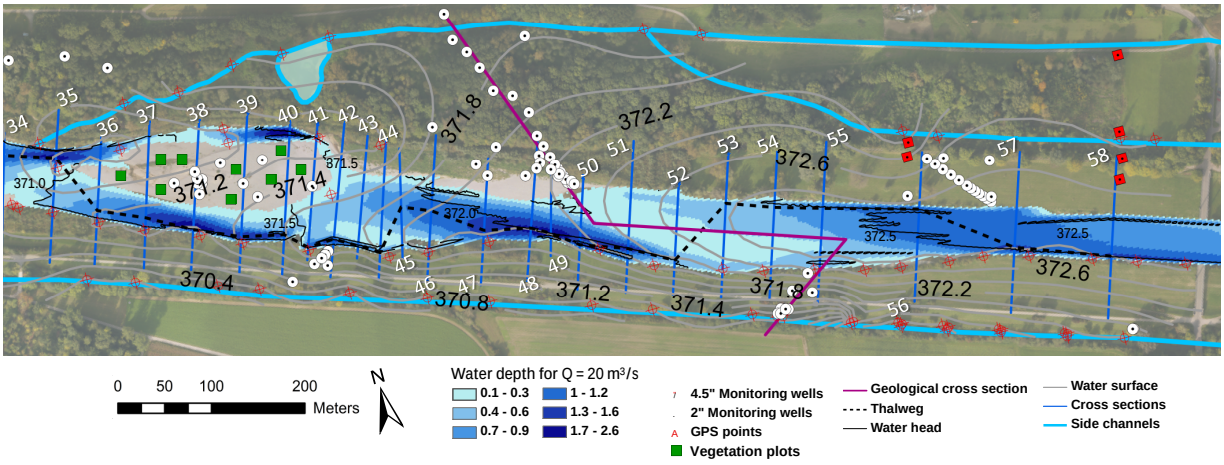

Figure 1.1: *Test site Neunforn, partly restored and partly channelized with monitoring-well transect. Thalweg, surface water levels and water depths for River Thur under low-flow conditions (20 m^3/s). Contour lines of groundwater heads are based on interpolated surface-water levels in the river and the side channels with a differential GPS. Bathymetric surveys are conducted annually in September by measuring predefined cross-sections blue lines with white numbering. Figure taken from Schneider et al. (2011).*

- How do morphological variability of the river and variability of hyporheic zone processes influence the quality of water resources? and which characteristic time/spatial scales are relevant to biocomplexity of riverine corridors?

- How does the spatial distribution of sedimentary materials influence distributions of microbial activity, hydro-chemical status and vegetation?

- How can the complex hydrological and ecological interactions in the heterogeneous restored corridor be aggregated in models that can be used for prognostic investigations of river restoration?

More specifically, within the RE.COR.D. project, the task involved for this thesis aims at separating the components coming from the above ground biomass (the canopy) from that of the below ground biomass (the root system). This work aims at focusing the effect of different flow conditions on root structures and biomass development with the purpose of deriving a useful constitutive relationship linking streamflow properties (e.g., flow rate and bed shear stress), sediment properties and vegetation root structure. Accordingly, the aim is to investigate the role of vegetation roots at those locations, spatial and time scale where the active role of vegetation starts affecting river morphodynamics.

1.3 Quantification of vegetation root induced cohesion rationale

1.3.1 State of the art

The role of vegetation and in particular the role of plant roots in the stability of hillslopes was largely ignored until the 1960s (Greenway, 1987). Application of the root reinforcement on stream bank stability and other channel processes did not occur until the 1990s (Thorne, 1990), when tensile strength testing and mapping of roots of woody, riparian species were conducted and quantified as an additional cohesion (Abernethy and Rutherford, 1998; Simon and Collison, 2002). Empirical studies have shown that vegetated channels erode more slowly, and are deeper and narrower than similar nonvegetated banks (Hickin, 1984; Hey and Thorne, 1986). Vegetation type and density particularly affects lateral channel erosion (e.g., Graf, 1978; Andrews, 1984; Hey and Thorne, 1986), but the complexity of natural, vegetated streams often makes difficult to formulate a direct mechanistic relation between riparian vegetation and channel characteristics (Gran and Paola, 2001). However, tools for quantifying the interactions between vegetation and river morphological processes are necessary (Pollen and Simon, 2005).

In particular when there is the need of quantifying vegetation effects on erosion and aggradation dynamics after channel widening with an accurate prediction. It is therefore critical to understand and quantify the key controlling processes and more accurately predict the role vegetation can play in stabilizing streambanks (Pollen and Simon, 2005; Pollen, 2007) as well as alluvial bed. Stream bank instability and associated sedimentation are major issues of environmental concern due to their detrimental effects on agricultural land, infrastructure, and the overall ecological health of waterways. In addition to the ecological benefits of vegetated stream banks, it is commonly recognized that the root networks of plants and trees act to increase the apparent cohesion of soil through a combination of mechanical ad hydrologic effects. Roots anchor themselves into the soil to support above-ground biomass, producing a reinforced soil matrix. This effect may become negative, when vegetation weight (in particular mature trees) acts as an additional load to the streambanks, thereby reducing bank stability. The hydrologic effect on streambanks may have positive and negative effects, as described by Selby (1993) and Simon and Collison (2002).

The hydrologic and hydraulic effects on alluvial sediment are much broader. Pioneer vegetation (grass, bushes) locally modifies velocity profile (e.g., see Nepf, 1999; Rominger et al., 2010; Zong and Nepf, 2010; Katul et al., 2011) during a flood event, diverging scouring forces away from the area where there is vegetation canopy. As a consequence, velocity, shear stress and dragging forces within the canopy are sensitively smaller then the same in bare soil river bed,

thus often resulting in deposition of material within vegetation canopy and scouring of the bare bed.

Quantification of the interactions between vegetation and bank erosion processes has been unreliable due to limited knowledge regarding the way in which roots affect the geotechnical, hydrological and hydraulic processes within a bank and its adjoining channel. To quantify vegetation effects on increasing soil stability, several properties of the root network need to be established (Pollen and Simon, 2005).

Possibly the most challenging aspect of root investigations is the acquisition of data pertaining to root architecture and root distributions throughout the bank. The inherent complexity of root networks and the spatial and temporal variability of the soil in which they grow (Nielson et al., 1997), and their opaque growing medium, creates numerous impediments to data collection and sampling. Current stream restoration designs are, therefore, based on empirical methods and standardized practices (Gregory and Gurnell, 1988; Wynn et al., 2004), with process-based models examining vegetation largely unavailable or untested.

Up to the end of the past century, attempts to quantify root reinforcement of soil have been dominated by the use of simple perpendicular root models such as those developed by Waldron (1977) and Wu et al. (1979), which simply require knowledge of the tensile strength of the roots, and the cross-sectional area of fibers crossing the shear plane. Perpendicular root models can be considered to be static models, in that they estimate maximum root reinforcement at a single instance in time, when all of the roots contained in the soil matrix have reached their maximum tensile strength. However, in reality as a soil-root matrix shears the roots contained within the soil have different tensile strengths and thus break progressively, with an associated redistribution of stress as each root breaks. The assumptions made by static models of root reinforcement therefore overestimate the increased apparent cohesion provided to the soil by a root network, as essentially they simply sum the tensile strengths of all of the roots.

It becomes evident how it is important to begin with an accurate investigation in order to address a better and deeper comprehension of the root system as well as the investigation of how plants establish, grow and survive an alluvial bare soil.

Plant roots perform a number of ecological and structural functions (e.g., Coutts, 1983; Waisel et al., 2002) and develop according to complex interactions among soil properties, hydrologic and climate conditions and nutrient availability, altogether representing different forms of tropism (e.g., Gregory, 2006). In some species, the tendency of roots to bend downward (gravitropism) has been explained as the action of gravity on hormonal fluxes (Aloni et al., 2006). In general, hydrotropism is the tendency to grow towards regions with higher soil moisture, oxytropism towards greater oxygen availability, and thigmotropism indicates the reaction of roots to mechanical impedances, e.g. obstacles such as stones.

The vertical density distribution of phreatophyte plant roots in textured soil in different ecosystems and climatic conditions has widely been studied and is nowadays well documented by both experimental observations (Oyanagi et al., 1995; Bouma et al., 2001; Schenk and Jackson, 2002b,a; Xie et al., 2006) and models (Laio, 2006; Guswa, 2008). A density distribution decreasing with depth seems to be a common pattern (Bengough et al., 2000; Schenk and Jackson, 2002a), also captured by models in response to soil moisture changes induced by precipitation fields (Laio et al., 2006; Guswa, 2008; Preti et al., 2010). Lateral spreading may show preferential directions reflecting particular nutrient availabilities or stress conditions (Waisel et al., 2002).

In this contest it is essential to study vegetation establishment, growth and survival on bare soil of river bedforms. The interactions between soil-water content, plant growth and soil cohesion determine how and which vegetation eventually develops on bare exposed soils. Gurnell and Petts (2002) proposed that the mode of reproduction (sexual or vegetative) and whether vegetation is (A) dispersed across open bar surfaces, (B) aggregated in areas of fine sediment that have accumulated in the shelter of large pieces of driftwood, or (C) in the form of sprouting large wood pieces, control the rate of biomass production and the associated rate of aggradation of fine sediment around the growing biomass (see Figure 1.2).

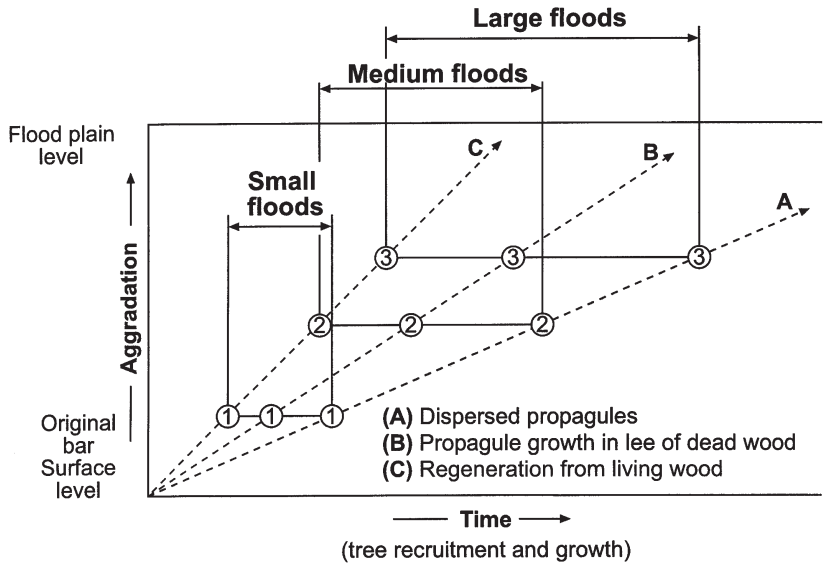

Figure 1.2: *Theoretical trajectories for tree recruitment and growth and sediment aggradation on bar surfaces of a braided river. Trajectories are initited by: (A) dispersed propagule establishment; (B) propagule establishment in the shelter of large wood pieces; (C) vegetation regeneration from living wood pieces (taken from Gurnell and Petts (2002)).*

Vegetation cover is not only a passive mechanical element that increases the local river rough-

ness. Vegetation life cycle actively influences indeed river morphodynamics and vice versa (e.g., Camporeale et al., 2006; Perucca et al., 2006). It becomes thus crucial to know whether those forms are likely going to be vegetated in natural conditions or not. Many studies have demonstrated the importance of riparian vegetation in preventing erosion (Karrenberg et al., 2003; Gurnell and Petts, 2006; van der Nat et al., 2002) mainly due to the interaction between the above ground mass of plants (stems, leaves) and the local hydrodynamic.

Salix species in particular can tolerate flooding and prolonged periods of inundation and have developed evolutionarily to cope adapt to such conditions (see Karrenberg et al., 2002). Additionally, their chance of establishment increases with increasing inundation duration (Vreugdenhil et al., 2006). The easier establishment of *Salix*, may also be explained with inundation characteristics. For instance, rather than the total inundation duration per year, *Salix*, suffers the average duration of inundation (Vreugdenhil et al., 2006). Salicaceae generally have several adaptations that enable them to survive prolonged inundation, which many other species lack, like rapid growth to avoid total inundation (Karrenberg et al., 2002), the ability to restart growing after inundation, the production of adventitious roots in order to deal with soil anoxia (Vandersande et al., 2001), and high uprooting resistance (Karrenberg et al., 2003). In particular, both *Salix* and *Populous*, have the capacity to produce roots and shoots from disseminated branch fragments when they are deposited in suitable locations, a process that is essentially replicated with the planting of cuttings (Francis and Gurnell, 2006; Pasquale et al., 2012a).

Several riparian tree genera, such as Salix and Populous, have the capacity to produce roots and shoots from these disseminated fragments when they are deposited in suitable locations (Francis and Gurnell, 2006).

Experimental observations concerning vegetation growth on gravel bars and fluvial islands (Gurnell et al., 2001; Francis and Gurnell, 2006; Francis, 2007) also inspired conceptual models about the "engineering" role of pioneering species and their contribution to river morphodynamic processes (Corenblit et al., 2007). Whilst many studies relate the above-ground biomass to the morphodynamic activity of the river, not much is known about how the below-ground biomass develops according to water table oscillations as induced by streamflow variability. Bouma et al. (2001) reported clear evidence of how inundation frequency on coastal marshes may affect the topology of the root system of many halophytic species.

As far as laboratory experiments are concerned, Francis et al. (2005) showed that the rising and the recession speed of water level would play a role in controlling the depth of the root biomass in riparian cuttings. On alluvial bedforms, given the vicinity to the stream and the soil properties of the alluvial material, precipitation events can be assumed to be uniformly distributed, whereas the vertical location of the saturated water table oscillates with time

scales practically equal to those of river discharge (Pasquale et al., 2011). Hence, provided that nutrient distribution is not a limiting factor for vegetation to develop, streamflow variability is reasonably expected to influence the vertical density distribution of the root system.

1.3.2 Research questions

In this contest an important research question concerns the understanding of the active (biological) role of vegetation (e.g., Jang and Shimizu, 2007; Gurnell and Petts, 2006; van der Nat et al., 2002) in relation to several other ecological and hydrological aspects, such as morphodynamics. Specifically, it is worth to investigate: i) the morphologic changes of the restored reach in response to hydrologic disturbances, ii) the interaction between flow, sediment and local vegetation, and iii) the mechanical anchoring due to vegetation roots and its contributions to reach a dynamically stable restored river configuration.

A first research question should address the influence of vegetation roots in controlling the movement of sediment, which, in turn, may limit the migration of alternate bars. Indeed, mechanical anchorage is one of the main functions of plant roots (Fitter, 1987) and it gives strong contribution to soil reinforcement (Pollen and Simon, 2005; Pollen, 2007; Millar, 2000).

A second research question concerns the amount of vegetation that can colonize the bare sediments. This is obviously related to the ability of the plant to anchor roots into the alluvial non-cohesive soil and to their resistance to flood drag and uprooting actions (e.g., Edmaier et al., 2011). Despite vegetation germinates on the bare sediment of the restored reach (see later sections), it does not seems to be able to colonize it. The gravel bars of the restored reach are still showing mainly grass and sporadic willow bushes about 6 years after the first restoration activities ended. Poorly vegetated sediment would in principle indicate a slow regeneration capacity as far as the creation of new terrestrial habitat is concerned. Indeed the absence of vegetation cover limits fine sediment trapping, which represents a fundamental component of the hydrogeomorphic resilience and adjustment dynamics.

1.3.3 Research plan and structure of the thesis

On the basis of the research questions raised in the previous section, a research plan has been drawn up. Figure 1.3 shows a schematic flow chart summarizing all the set up, experiments, modeling and analysis planned to reach the goal of a mechanistic understanding of both post restoration river dynamics and root reinforcement. In thesis the structure of the Chapters also represents the different fields explored along with the experimental work: instruments set up,

field experiments, morphological analysis, vegetation dynamics and the model of root reinforcement. In order to access a model of root reinforcement, many installations have been set up and many experiment and analysis carried out. During the first year, a complex variety of instruments have been installed to monitor meteorological and soil moisture dynamics. In parallel transplantation of *Salix* cuttings have been carried out for three consecutive years of field campaign, including monitoring of the above- and below-ground biomass growth and surviving. Aerial survey of the river corridor produced detailed Digital Elevation Models (DEMs). Together with river bathymetry and sediment sorting data, DEMs have been used to study the local hydrodynamic at restored reach scale.

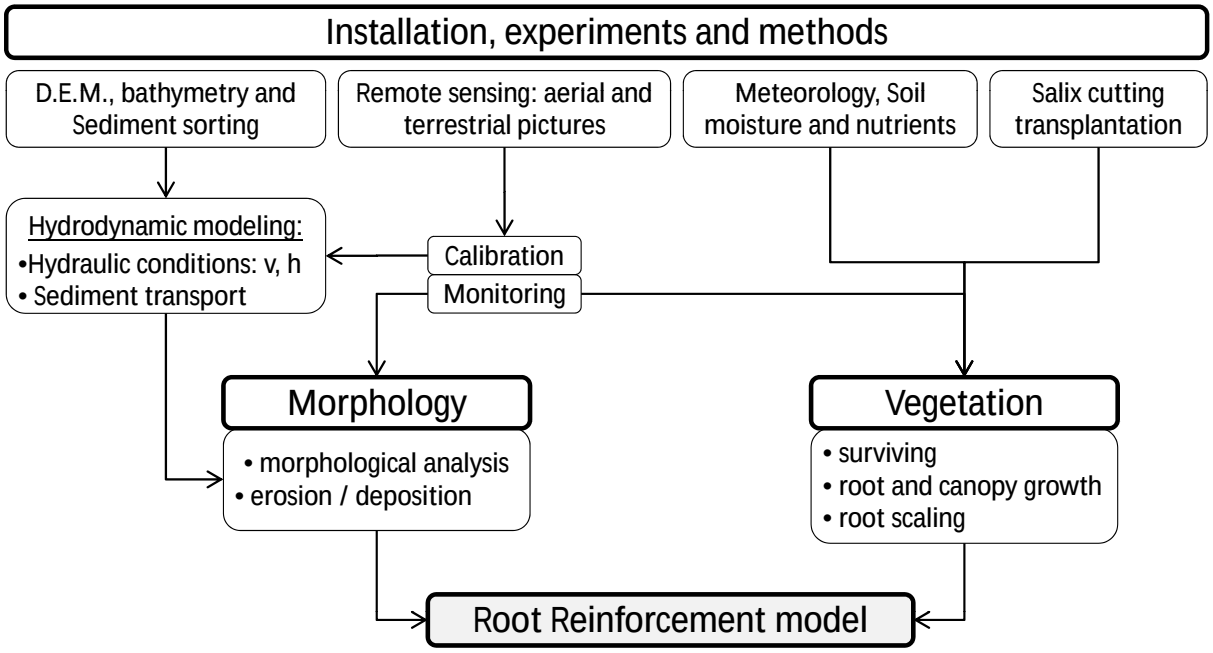

Figure 1.3: *Flow chart of the Ph.D. project: in order to access root reinforcement quantification, during the first two years a series of field installation have been set up and experiments carried out. Analysis on morphology and vegetation dynamics (above- and below-ground) lead to the formulation of a experiment-based model.*

Aerial and terrestrial photography, produced on a regular basis have been used to monitor both vegetation dynamics and morphodynamic evolution of the river corridor after restoration. Terrestrial pictures have been used to develop a new promising technique to calibrate hydrodynamic models via remote sensing. Some preliminary morphological analysis at the reach scale and at the river bed form scale have been produced, in order to investigate the effect of restoration on river dynamics and possibly, to link river morphodynamic to vegetation establishment, surviving and growing. In this contest, particular attention was dedicated to the erosion deposition pattern on a yearly basis at different spatial scales. Analysis on erosion-deposition balance of the river bed, vegetation statistics on above-ground growth and survival together

with statistics on root morphology and architecture are finally used to formulate a simple root reinforcement model. The model is based on the Shields' theory and on Meyer-Peter and Müller formula and it is validated on the basis of the data measure and collected in the contest of this project.

The comprehensive framework of experimental activities adopted to monitor the evolution of the restored river corridor of the Thur River is described in Chapter 2 and in the scientific publication of Pasquale et al. (2011). Hydraulic modeling and the techniques for the hydraulic model calibration are presented in this Chapter. Briefly, the theory on shallow water equations and their numerical integration, together with some basics of sediment transport are reported. The development of a new non-invasive technique for model calibration is also presented and object of a scientific publication currently under review (Pasquale et al., 2012). Methodologies adopted for the field campaign of *Salix* cuttings transplantation, monitoring and uprooting, together with the tools and methods used for analysis are described in detail.

Chapter 3 shows results of the preliminary morphological analysis. The analyses are supported by observation and aerial surveys of the field site. Morphological evolution and implications of the restored corridor, advantages and disadvantages, in time and space, are briefly discussed as well. Particular attention is given to the erosion-deposition pattern, in order to be able to link the presence of pioneer and riparian vegetation to river dynamics.

In Chapter 4 a detailed description of the *Salix* transplantation campaigns is presented. Results on *Salix* growth, surviving and mortality in relation to river hydrology are shown together with statistics on root system growth (length and volume) throughout the growing season. A regression function to extract root statistics from above-ground biomass measurement is also presented (Pasquale et al., *to be submitted*).

The results of a study on how river hydrology and in particular the water table influences root architecture and the vertical root distribution is reported in Chapter 5 and in the scientific publication of Pasquale et al. (2012a). Here a scaling of the highest root density in depth is formulated and validated on the data produced along the field campaigns of root transplantation.

After presenting a brief overview of the methods available in literature to quantify root reinforcement, in Chapter 6 the model of root reinforcement formulated in the contest of this work is presented and validated (Pasquale et al., *in preparation*).

Chapter 7 reports the conclusive remarks for further projects and investigations on the basis of the experience matured with this work.

Chapter 2

Study site, field investigations and experimental set up

This chapter outlines the methodologies, the monitoring strategies and the field and numerical experiments that were carried out to provide evidence of vegetation survival and development in relation to the hydraulic regime.

2.1 Thur river and hystory (field site)

The Thur River is a perennial river in the north-east part of Switzerland (Figure 2.1.a, b). The catchment area is about 1750 km^2 and the river has a length of about 127 km. It is the longest river in Switzerland that flows continuously without any regulation by artificial reservoir or natural lakes.

The hydrologic regime of the river is nivo-pluvial with the characteristic presence of rapid floods. In spring and autumn flood pulses are generated as a combination of snow melt and intense precipitation. Discharge may increase dramatically within a few hours and trig both bed load and suspended sediment transport. The mean annual discharge (MQ) is 47 m^3/s. Peak flows (HHQ) up to 1130 m^3/s have been observed, thus leading to a HHQ/MQ ratio of 24. Observed low flows can be as low as 2.2 m^3/s.

Originally, the lower Thur River showed a clear braided morphology (Figure 2.1.c). Before the first half of the 20^{th} century the river was channelized like most of the major rivers in Europe to avoid frequent flooding and gain arable land. Such first river correction basically transformed the floodplain into a double trapezoidal channel with a 45 m wide low-water channel (flow capacity 230 m^3/s) with embankment and artificial floodplains (total flow capacity 1100 m^3/s) confined within levees. Spacing between the levee crests was 160 m and the vertical distance

between riverbed and levee crest averaged 6 m.

The failure of the levees during the large 1977 and 1978 floods suggested to enlarge the floodplain between the levees in order to increase the channel conveyance capacity (today the low flow channel and the total flow capacities are about 300 m^3/s and 1300 m^3/s, respectively) by removing fluvial deposits from the forelands between the levee (Figure 2.1.d). However, these corrections caused erosion of the river bed. This triggered the plan for a second Thur River correction, which had to consider both flood protection goals and the ecological status of the river. Since 1993 this correction equally promotes river restoration and flood protection measures. In 2002, a 2 km long section of River Thur near Neunforn/Altikon (see the box in Figure 2.1.b) was restored by completely removing the right side foreland, so that the nearby alluvial forest became part of the active floodplain again.Soon after the remodeling ended, the large widening forced the river to deposit sediments and to enhance the alternating bar patterns. Such pattern is the essential river attribute (Trush et al., 2000) that is fundamental for the creation of physical habitats for pioneer species (Figure 2.1.e, f). The restoration attempt had also a positive impact to mitigate the damages of flood events observed in the recent years.

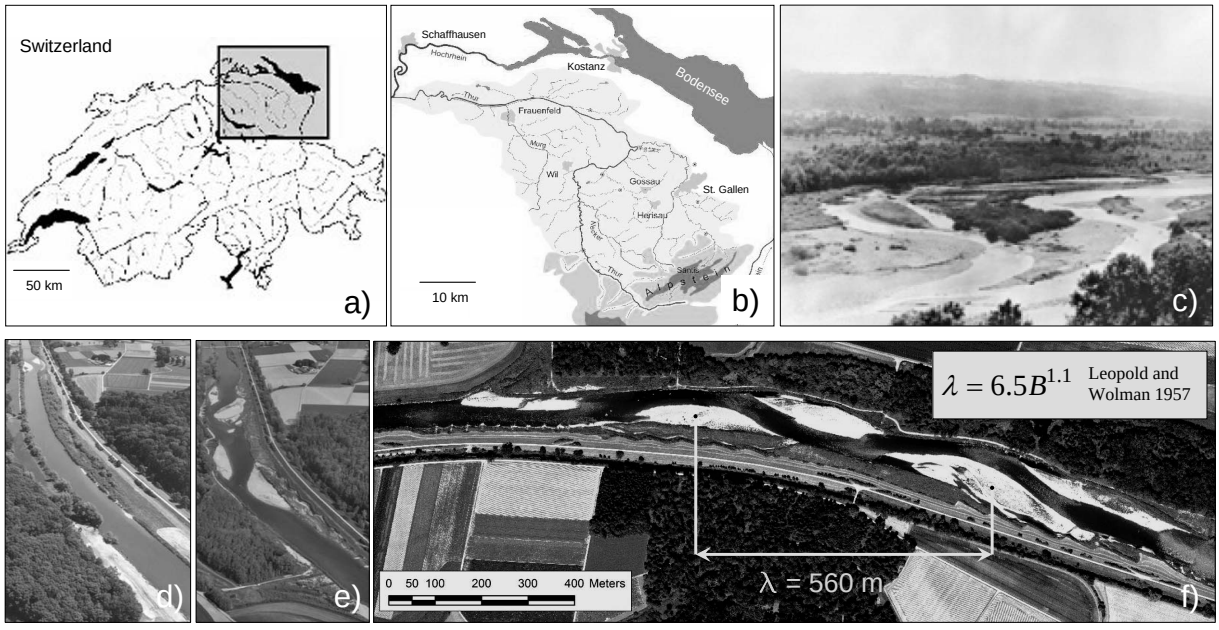

Figure 2.1: *Location of the river Thur in Switzerland (a) and river basin (b). From a natural braiding state (Rodhe, 2004) (c) the river was straightened (d) in the past century to improve flood protection, to increase agriculture areas and to reduce spreading of disease. As a consequence river bed faced serious erosion problems. After the restoration project started in 2002 the river naturally formed an alternate bar system (e, f).*

2.2 Field experiment set up

One of the naturally formed sedimentary island of the Thur River represents an almost ideal research area for the research questions identified in the previous section. The island is located in a slight bend of the river where the Thur flows through a rural area with many field crops and a riparian forest (Figure 2.1.f). The shape and size of such island are obviously not constant, but changing in time because of erosion and aggradation induced by hydrodynamic forcing during floods. In order to capture the morphodynamic activity after restoration an active monitoring strategy was adopted, which is summarized in Figure 2.2.b.

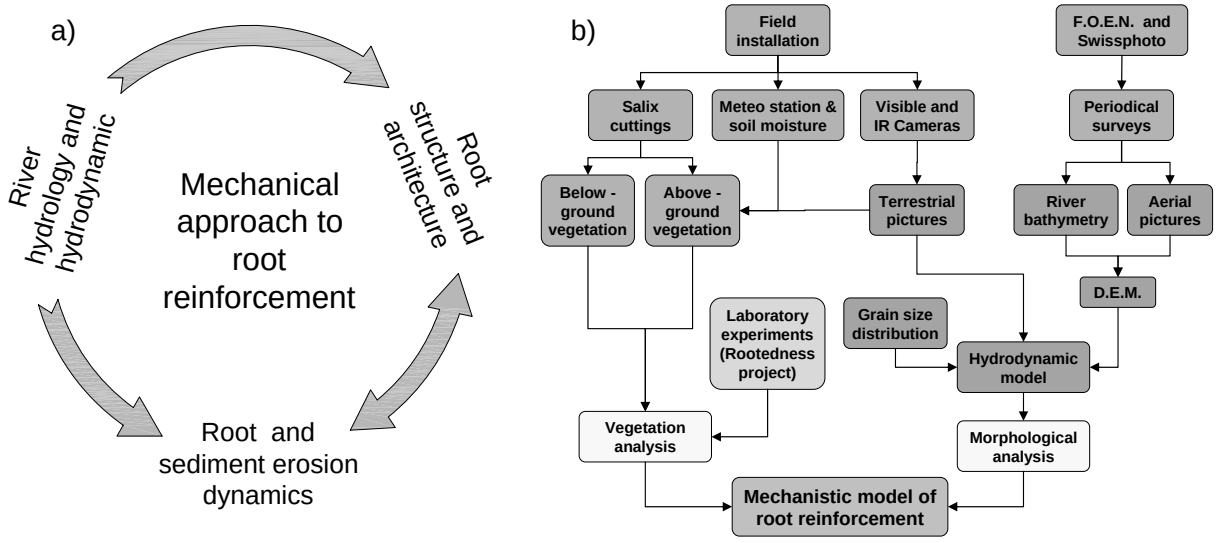

Figure 2.2: *Conceptualization of the interaction among river hydrology and hydrodynamics, root structure and architecture and sediment erosion and uprooting (a) and (b). Architecture of the investigation strategy to reach a mechanical understanding of root reinforcement (b).*

The field installations consist of a meteorological station, soil moisture monitoring clusters (see section 2.2.1), visible and near-infrared (NIR) cameras for terrestrial remote sensing (see section 2.2.3) and three campaigns of *Salix* cuttings transplantation on the island (see section 2.6). Since the beginning we have also taken advantage of the hydrological and topographic data provided by the Federal Office for the Environment (FOEN) and of aerial surveys, the latter being periodically updated on an annual basis. Meteo- and soil moisture station, jointly with observation of *Salix* (willow) cuttings evolution via direct and remote sensing carried out together with a parallel project (Edmaier et al., 2011) have been used for vegetation analysis. Topographic data such as river bathymetry (see section 2.2.4) or digital elevation models (DEMs) from aerial pictures, grain size distribution analysis (see section 2.2.2) and hydrodynamic simulations (see section 2.3) have been used for morphological analysis. Results

from vegetation response to river hydrology and observations of morphological changes (Figure 2.2.a) will be later used to formulate a mechanistic model of non-cohesive soil reinforcement by roots (Figure 2.2.b).

2.2.1 Local meteorogical and soil moisture measurements

In order to monitor the micro meteorological variables necessary to compute a correct water balance at the reach scale, a complete meteo-station was installed on an aluminium frame tower (see Figure 2.3.a) located on the top of the left side levee (Figure 2.3.c). The higher position of the tower with respect to the river corridor allows for measurements to be representative of the mean local meteorology surrounding the restored reach. The meteo-station consists of recording raingauge, two sensor pairs measuring air temperature and relative humidity at 2.5 m and 8 m above the ground level, a complete solar radiation device (i.e., measuring the four radiation at 4 m above the ground), two anemometers (also at 2.5 m and 8 m above the ground level) and an atmospheric pressure sensor. The station is connected via optic fiber wires to a remote computer, located in a small hut about one kilometer upstream on the levee (Figure 2.3.b, c). Thus, it is possible to remotely access the meteo-station to download data in real time and eventually to reprogram the logger settings according to current needs. The installation includes also four soil moisture measuring spots installed on the island (Figure 2.3.f, g), which are wireless connected to a second tower (Figure 2.3.b). Each soil moisture sensor, based on capacitance technology, measures soil moisture and temperature at three different elevations (20, 40 and 60 cm) below the ground surface.

2.2.2 Sediment size and nutrient spatial variability

Grain size distribution curves of the alluvial sediment forming the island were obtained from six representative locations that were identified by simple visual survey (Figure 2.4.a). At each chosen location we took two samples, one at the surface and the second one about 40 cm underneath. The purpose is to spatially identify and map sediment armoring and aggradation profiles (Lanzoni, 2000), as these control both sediment resistance to erosion and vegetation establishment. The two samples have been sieved to build grain size distributions, which are shown in Figure 2.4.b,c. Generally, the sample taken at the surface (Figure 2.4.b) shows a higher percentage of coarse sediments than the sample at 40 cm depth (Figure 2.4.c). Moreover consistently with experimental observation reported by Lisle et al. (1991), Diplas and Parker (1992), Lisle and Madej (1992), Ashworth et al. (1992) the island is characterized by a longitudinal sorting.

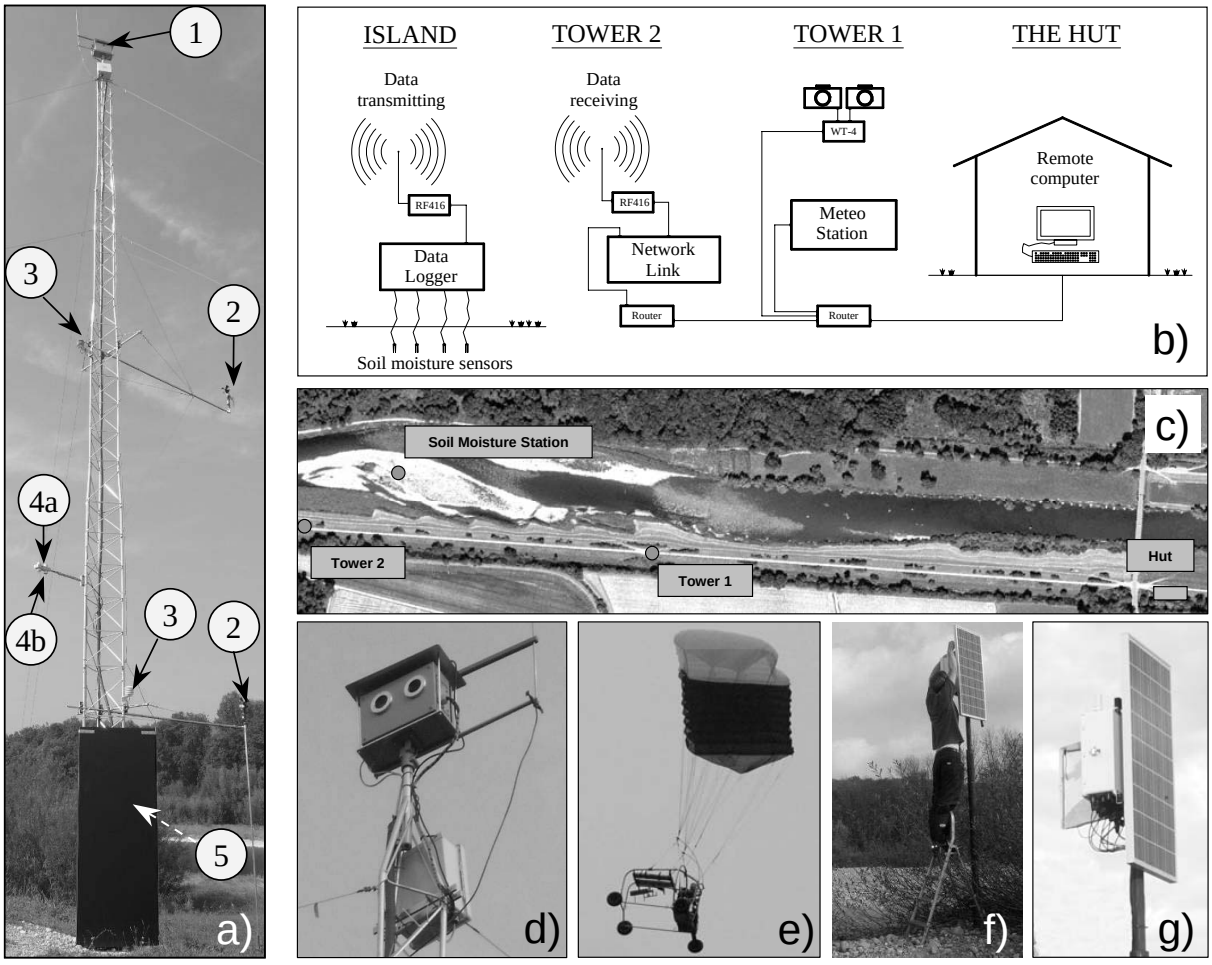

Figure 2.3: *Field installation: (a) shows the tower (Tower 1) with the meteorological station with the camera box (1,d), the two wind sensors (2), two temperature and relative humidity sensors (3), the incoming and reflected radiation sensors (4a,b) and the pressure sensor (5). The soil moisture station on the island is wireless connected to the second tower on the levee. The second tower (Tower 2) has one box with two cameras and it is connected via optical wires to Tower 1 (b). The system is controlled by a computer located in a hut on the levee (b, c) and connected via optical fiber to Tower 1 (b). Picture (e) shows the motorized paraglider used for aerial pictures, whereas the soil moisture station on the island and a particular of the solar panel used to charge the data logger battery are shown in (f) and (g).*

From coarse particle deposition upstream we move to fine sand deposition downstream (Lanzoni, 2000), where also stratification is not anymore evident. Successive visual observation have confirmed this pattern, leading to assume that the grain size distribution is substantially independent from the macroscopic morphological changes of the island. Sedimentation is the main source of fine materials and nutrients supply. Hence, soil texture, organic carbon and nutrient (nitrogen and phosphorus) contents in the lateral gravel bar upstream the island have been measured in the context of another scientific task of the RECORD project (Battle-Aguilar

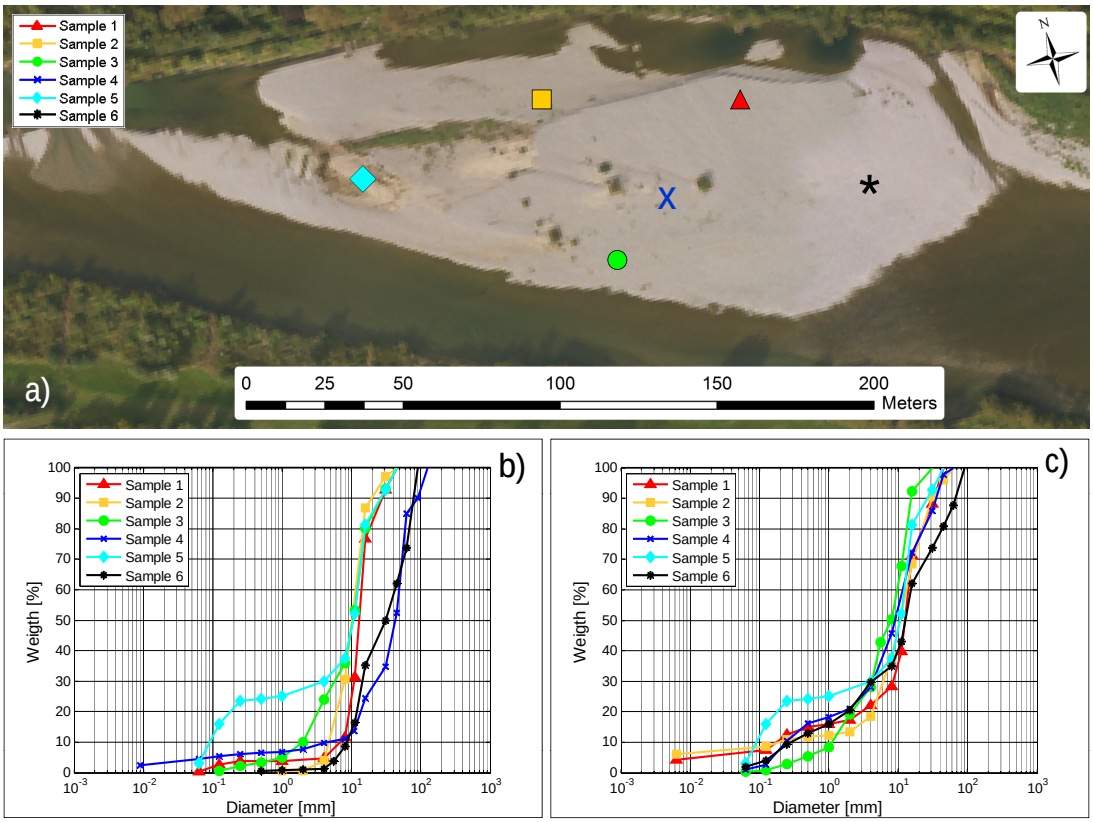

Figure 2.4: *Grain Size Distributions for the six different locations on the main island indicated in (a). Samples were taken on the surface (b) and at 40 cm depth (c). d_{50} and d_{90} are generally higher on surface layers (b) than at 40 cm (c). Surface samples (b) show also a higher spatial sediment sorting, from coarser material upstream (sample 6) to finer material downstream (sample 5). Sediment at 40 cm depth are more spatially similar and d_{50} is practically equal for all samples (c). Comparing (c) and (d) it is evident the vertical sorting typical of river bed forms.*

et al., 2011; Samaritani et al., 2011). In particular, six sampling plots have been taken on the right hand side bar (from 50 to 150 m upstream the island). As both the riverside bar and the island are formed by the same alluvial material, we assume that also the nutrient contents are similar. However, six additional samples have been taken from sparse location on the island inside the vegetation plots (see Section 2.6) to validate this assumption. The collected soil samples have then been dried at 40° C and sieved at 2 mm for analysis of above-mentioned chemicals. The texture has been measured using the pipette method (Gee and Bauder, 1986).

Organic carbon and total nitrogen have been measured in finely ground fine soils by using the method by Walthert et al. (2010). Available phosphorus has been measured colorimetrically by following the approach of Kuo (1996).

Eventually, both the island and the lateral bar show a similar amount of nutrients, the statistics

Soil type - Nutrients	Units	Average	Standard Dev.
Sand	%	81	5
Silt+Clay	%	19	4
Organic carbon	gC kg^1soil	9.2	3.2
Total nitrogen	gN kg^1soil	0.6	0.2
Available phosphorus	mgP kg^1soil	24.9	8.7

Table 2.1: *Nutrient content and soil type analysis results. Soil samples were dried at 40° C, and then sieved at 2 mm.*

of which, averaged over the bar and the island, are reported in Table 2.1. The nutrient content in the gravel bar (with the exception of ammonium, which was quite uniformly distributed) is spatially variable, but does not follow any particular pattern. This suggests that differences in both quantity and quality of sediment deposition within the gravel bar are likely to occur. For instance, the organic carbon and nitrogen content is known to be strongly related to soil texture, whereas the quantity of sediment deposition is typically more important for phosphorus (Steiger and Gurnell, 2003). Although the nutrient content on the island is lower than in other part of the floodplain (data not reported here), its range is normal for sediment deposits of other large rivers in Europe (Steiger and Gurnell, 2003; Olde Venterink et al., 2006). Hence, as far as the gravel bars and island are concerned, we conclude that the nutrient content of the fine material is not the main limiting factor for plant growth. Elevation and grain size may both be more crucial than nutrient contents due to their control on soil water dynamics (Gilvear et al., 2008).

2.2.3 Terrestrial and aerial photography

The high cost of aerial surveys makes them economically not feasible more than once a year. However, periodical extensive surveys are very important to monitor morphological changes and riparian vegetation patterns and evolution along rivers. Thus, it has been decided to explore the possibility to replace periodical surveys by means of continuous monitoring through terrestrial photography. If successful, this technique may lead to promising applications in the field of river engineering and restoration. For instance, calibration of river hydrodynamic flow models is typically a difficult and demanding task, which requires adequate information about the corresponding water depth for different flow rates. The many points that are required across the river domain cannot be measured through manual survey, either because of excessive time demand or because of inherent difficulties in the presence of high flow conditions, which limit the access to the area. Remote survey techniques, for instance based on aerial photographs,

are welcome.

To produce a continuous time series of aerial-like photographs two boxes (Figure 2.3.d) have been installed on the top of each monitoring tower at 16 meters above the levee level. Each box contains two high resolution digital cameras shooting pictures in both the visible and the NIR range. By combining the visible and NIR images it is possible to compute the Normalized Difference Vegetation Index (NDVI) (Qi et al., 1994), which is useful to quantify vegetation patterns, growth and mortality (Appendix A shows more in detail the NDVI analysis carried out for 2009). All the digital cameras are connected to the remote computer, from which it is possible to change their shooting parameters and, in particular, the frequency, to better capture flood events evolution. Images from the tower have been complemented with photographs taken from a remotely controlled motorized paraglider (Figure 2.3.e), which has been equipped with the same type of high resolution digital camera and with a GPS for more convenient geo-referencing. The paraglider has been used to detect important morphologic changes, similar to what was shown by Lejot et al. (2007) soon after a flood occurred and without waiting for the annual airborne LIDAR flight. Using both image sets we have thus been able to test and improve several techniques based on pattern recognition analysis to calibrate both hydraulics and ecosystem models (Molnar et al., 2008; Perona et al., 2009).

2.2.4 Digital terrain models and river bathymetry

An important element in hydraulic and morphodynamic modeling is the availability of detailed topographic data of the river bed and the floodplain area. The Federal Office for the Environment (FOEN), together with Canton Zurich and Canton Thurgau, provides detailed cross sections of the restored reach once a year. Surveys take place generally in late September-October. Summer season is characterized by the most important floods which are responsible of morphological changes. From annual LIDAR airborne flights, the corresponding Digital Terrain Model (DTM) is produced with a horizontal resolution 50 cm and vertical precision of +/- 5 cm. River bathymetry is generally obtained by manual cross sections measurements just few weeks after or before the aerial flight, depending on flow and weather conditions. Cross sections along the river are measured on average every 20 meters. For each cross section, the profile of the river bed is obtained by measurements spaced every 50 cm.

Cross section data are then merged with the DTM in order to obtain a new DEM which includes the river bathymetry. To this purpose we use the method developed by Schäppi et al. (2010), which requires as inputs: i) cross section profiles data, ii) a raster of the DTM that needs to be corrected and iii) the identification of breaklines (Lane et al., 1994; Keim, 1999; Brasington et al., 2000). The algorithm is designed to deal with longitudinal unequally spaced cross section

profiles. It performs two linear interpolations in the lateral and longitudinal direction of the river. DTM grid points situated in between two adjacent cross section profiles are replaced by values obtained from the cross section interpolation. This method was chosen because it is more robust than the nonlinear ones and those based on spline interpolations (Schäppi et al., 2010), which often introduce spurious oscillations due to not equally spaced data (Schäppi et al., 2010).

2.3 Hydrodynamic simulations

The development experienced by hydraulic models in the last decades allows simulating with increasing accuracy many of the flow characteristics that are an important boundary condition for aquatic ecosystems. In order to characterize the hydrodynamics of the restored river reach under different flow scenarios numerical simulations were used in this contest. Those simulation were useful to plan field campaign of vegetation cutting transplantation and to study the influence of hydrodynamic stresses on erosion and deposition processes and consequently on vegetation growth and surviving.

The grid of the interpolated DTM (see Section 2.2.4) has been first pre-processed by means of the AQUAVEO SMS-10.1 software (described in Section 2.3.3) to create an unstructured triangular mesh, which is particularly suitable for fast and more efficient computing. For the hydrodynamic simulations we have used the 2D hydrodynamic model BASEMENT (Section 2.3.3).

2.3.1 Introduction to 2D hydrodynamic models

2D shallow water equations

Mathematical models of the so-called shallow water type govern a wide variety of physical phenomena. An important class of problems of practical interest involves water flow with a free surface under the influence of gravity such as: i) tides in oceans, ii) flood waves in river, iii) dam break waves, iv) tsunami waves.

The validity of the shallow water equations (SWE) implies the following three conditions and assumptions: i) hydrostatic distribution of pressure: this is fulfilled if the vertical accelerations are negligible, ii) small slope of the channel bottom, so that the cosine of the angle α between the bottom and the horizontal can be assumed to be one (i.e., $\sin\alpha = \tan\alpha$) and iii) steady-state resistance law can are valid for unsteady flow too. A key assumption made in derivation of the approximate shallow water theory concerns the first aspect, the hydrostatic pressure

distribution. Supposing that the vertical velocity acceleration of water particles is negligible, a hydrostatic pressure distribution can be assumed. This eventually allow for integration over the flow depth, which results in a non-linear initial value problem, namely the shallow water equations. They form a time-dependent two-dimensional system of non-linear partial differential equations of hyperbolic type. Derivation of the SWE for flood waves in rivers is shown in Appendix B together with the closure conditions.

Numerical integration

Due to the rapid developments in the field of computer technology, computing capacities are available to the user today, which just a few years ago were possible only on a super computer. This computing capacity allows us to use numerical solutions, where in the past estimates obtained via simplified approaches had to be used. In the field of flow calculations, the term "Computational Fluid Dynamics" (CFD) is often used. CFD deals with the numerical solution of partial differential equations (PDE) in the area of fluid mechanics, i.e. with the Navier Stokes-, Reynolds- or shallow water equations, among other things. For the solution of these differential equations, mainly three different methods are used: the Finite Differences method (FD), the Finite Volumes method (FV) and the Finite Elements method (FE). The model BASEMENT uses the FV method. An overview on the discretisation in space and time of the SWE is reported in Appendix B.

2.3.2 Grid and mesh generation

Structured grids are the simplest grids that can be used for the discretization of a rectangular domain. They can be characterized by the fact that the number of subdivisions in one direction, independently of the number of subdivision in another direction, is always constant, i.e. a 2D grid has a certain amount of cells n_x and n_y in x and y direction. Therefore, each cell in the computational grid or every calculation node can be identified unambiguously using two indices (for a 2D grid). Structured grids can be further subdivided into: *regular grids*, where the cell length in each direction is always constant, *orthogonal grids*, where the grid lines in the different directions are normal to each other and *curvilinear grids*, where the grid lines can be arbitrary curves in space.

Structured, and especially regular structured grids are very suitable for the FD-method. Thanks to the properties of this type of grid, the derivatives in all spatial directions can be determined well, without a need for coordinate transformations. A great advantage of the structured grids lies in the small storage requirements, since the nodes of a cell and its neighbours are straightforwardly determined using their indices. This is also of advantage for computation times. The

laborious calculation of contributions to a node from neighbouring cells is not necessary and the structure of the solution matrix is known in advance. The main disadvantage of structured grids is that they are not flexible enough to discretize complex domains. Unstructured grids are the most complex to generate, but on the other hand they offer the highest flexibility. On an unstructured grid the number of neighbours of a cell is variable. Therefore it is no more possible to identify a cell using two (2D) or three (3D) indices only. Moreover, the nodes forming a cell are not known a priori, but they have to be identified. An unstructured grid must contain at least two types of information: all nodes and their coordinates, and all cells and the related information, which nodes constitute each individual cell. Unstructured grids are mostly used in conjunction with the finite elements method. Partly they are also employed in the FV method. Unstructured grids have the disadvantage of requiring significantly higher computation time. They have, however, the advantage that they can be refined locally. For simple domains, which require only a small number of cells, the grid generation can eventually also be done by hand. For more complex domains with a large number of cells this would be too time consuming. Therefore tools are used, which, for a given domain contour automatically subdivide the domain into cells. Such a tool is called grid generator. Algebraic grid generators create cells by using algebraic relations. Hereby they take different criteria into account, e.g., maximize the cell area, angle criteria, etc. Alternatively there are grid generators, which solve PDEs to subdivide the domain. Depending on the type of PDE used, the grid generators are denominated accordingly, e.g. elliptic grid generators use an elliptic PDF like the Poisson equation. The procedure is that a simple initial grid is transformed over the complex domain by solving a PDE, where the boundary coordinates of the new domain are the boundary conditions of the PDE.

2.3.3 The model BASEMENT and the software AQUAVEO SMS 10

Surface Water Modelling System (SMS) is a software produced by Aquaveo[1] used for importing topographic and hydraulic data for visualization as well as analyzing solution. It interfaces with a range of numerical models such as river flow analysis, contaminant, sediment transport and costal dynamics. In terms of this project, the SMS software has the function to provide topographic data for further use in the sediment analysis. The topographic input is a mesh of the desired domain provided in *.2dm format. In order to create a mesh for the River Thur, external input data required is usually in an ascii format. It will be read inn SMS as a scatter map, which are sets of points representing the domain with x, y, and z information data. Creating a mesh from a scatter set is one direct way to generate it, but usually this conversion method cannot distinguish different type of land use/ material that has different

[1] http://www.aquaveo.com/sms

roughness coefficient. Domain will only have one material roughness type. Hence, to generate different material type, map module is used with the base of scatter set or aerial photos to distinguish one material boundary to another. One can create arcs then connect to one another to produce a polygon. The properties in the polygon can be changed according to the desired objective. Having different polygon show the difference of type of land use, therefore the model is more realistic representing real life property character. In the case of River Thur, the domain is diversified in four type of land use: river bed, grass, levee and forest (2.5.a).

Finite volume typically requires heavy computation. In order to avoid it, the mesh must be created in a compromising number of nodes or elements. The term not too much, not too little is practical in this model. Usually finer mesh is created in the river bed or certain levees, then coarser meshes approaching the undesired part of the domain. After all the above described is fulfilled, a mesh can be generated. The Thur River mesh model will nearly look like in 2.5.b. To see a deeper extrusion of the mesh, one can eventually increase the elevation height in the general tab within display option. Checking mesh element quality is an important step to avoid model instability. Several rules of mesh element construction help to cread a robust finite element network. These violations of mesh quality consist of:

- *Minimum/Maximum Interior Angle*: For triangular elements, if the angle is between 10 to 150 degrees, computation problem can be avoided.
- *Concave quadrilateral*: For quadrilateral elements, if angles are between 30 to 150 degrees, computation problem can be avoided
- *Maximum Slope*: Highly steep in slope can cause computational instabilities
- *Element Area Change*: Nodes need to be plentiful and elements smaller in areas where solution variables (u, v, and h) change rapidly. Size of elements need to change gradually when moving from an area described by small elements to an area modeled with large elements, or vice versa. A rule of thumb is to keep areas of neighboring elements within a factor of two, meaning an element is twice as big or half as big as its adjacent elements.
- *Connecting Elements*: Limiting the number elements connecting at a node to fewer than eight
- *Ambiguous Gradient*: All triangular elements are planar by definition. However, quadrilateral elements may vary significantly from a plane. It is recommended to construct elements as close as to a plane as possible.

The most common mesh quality violation is 2.5.c. There are many green highlighted elements due to these elements reaching the maximum slope values. There is some extent in maximum

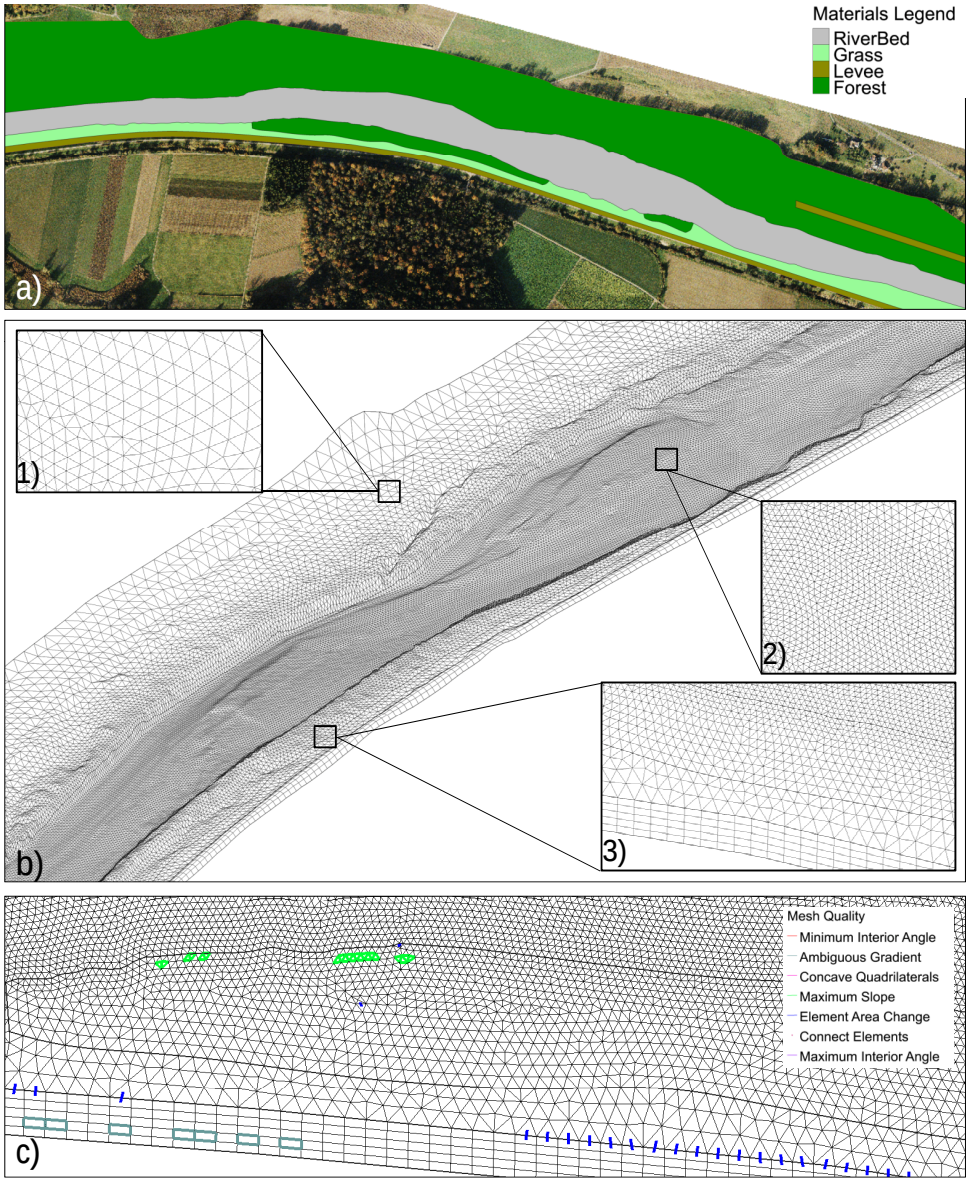

Figure 2.5: *Mesh generation for hydraulic modeling: first, classes of areas, characterized by same hydraulic roughness are defined (a). An unstructured irregular triangular mesh grid is created (b). Spatial resolution is not uniform, in order to reduce running time of the simulation and at the same time producing more information where needed. The last step (iterative) concerns checking and improving the mesh quality (c) in order to have an efficient, performant and stable model.*

slope value that can be set. The maximum slope violation can usually be neglected, since it does not have extreme effect on the river stability. Ambiguous gradient can sometimes be found in the meshes, mostly rectangular shape ones; which is why in this case triangular grid is used to avoid this violation. Triangular grid is more flexible for abrupt elevation difference.

Element area change can be found in some areas located in the middle between finer to coarser meshes, but making the gradual change of the nodes distribution when making boundary line is possible way to reduce this violation. The most crucial violations that one must avoid are minimum/maximum interior angle for triangular grids and concave quadrilateral. Element must be in a way that it respects certain angle limitation to avoid such problematical computation. After finish checking mesh quality, then the last procedural steps are to check whether the meshes are linear (which means vertices or nodes and less computation than quadratic) and then renumber the nodes so smaller numbers are located in upstream and bigger in the downstream. Renumbering is optional; however it is easier to have sets of numbers in order when assigning boundary condition in the nodes. Once, all procedures above are completed, next is to proceed in BASEMENT.

This open source software BASEMENT (BAsic Simulation EnvironMENT) developed at the Laboratory of hydraulics, hydrology and glaciology of ETH Zurich[2],[3] uses the finite volume method to integrate the shallow water equations. The explicit Euler scheme implemented deals both sub- and supercritical flow regimes, thus resulting a suitable code to perform hydrodynamic simulations across a broad range of natural streamflows (e.g., Ruf et al., 2008; Perona et al., 2008, 2009). The software package is freely available on the web[4]. Particularly, it is a numerical software tool for the computation of fluvial, hydraulic and morphological scenarios. It is developed by the VAW in order to conduct research and teaching in the fields of hydraulic engineering, river engineering and glaciology. The software itself is still under development and newer versions of with more advanced features are coming out periodically.

2.4 Hydrodynamic Model calibration

The reliability of hydraulic model simulations strongly depends on the accuracy of calibration, which is a lon-term investigated issue in hydraulic engineering (e.g., Chow, 1973; Aronica, 1998; Horritt, 2010). Therefore it is important to perform an accurate calibration of hydraulic models that works at any discharge rate: at low flow conditions for ecological reasons (e.g. Diez-Hernandez 2008), at medium flow conditions to verify the inundation hazard in the floodplain (e.g., Girard et al., 2010), and at high flow conditions to study the impact of flood waves (e.g., Junk et al., 1989) and how to mitigate them (e.g., Bernardara et al., 2010). Recently, many authors have investigated the use of automatic techniques for calibration of hydrodynamic models, such as those often implemented for watershed models (e.g., Fabio et al., 2010; Dung

[2] http://www.vaw.ethz.ch/
[3] http://www.vaw.ethz.ch/divisions/an
[4] http://www.basement.ethz.ch

et al., 2011). Calibration methods can be classified in two main groups: traditional methods relying on field measurements and techniques based on remote sensing imagery. Both methods are based on an output error criterion, used to determine river bed roughness parameters.

Traditional methods (e.g., Beker and Yeh, 1972; Fread and Smith, 1978; Wasantha Lal, 1995; Wohl, 1998), although still largely used to calibrate hydrodynamic models, are expensive, time consuming and often not practical. First, such measures represent only discrete information of the flow conditions for selected sections. Therefore, an accurate calibration requires as many observations as possible. In order to be representative of the flow conditions, the number of measures increases in case of complex river sections such as braided rivers. Second, measuring flow depth or water surface elevation may not be practical, especially during high flow when the access to the river is difficult or even precluded for safety reasons.

More recently, non-invasive techniques based on remote sensing partially allowed solving such problems by using aerial and satellite pictures. In recent studies, hydrodynamic models were calibrated by using either topographic information produced by airborne laser altimetry (e.g., Cobby, 2001; Castellarin et al., 2009) or satellite synthetic aperture radar (SAR) sensors (e.g., Horritt et al., 2007). However, inundation maps generated from a single observation often produce uncertain prediction (Aronica, 1998; Romanowicz and Beven, 1998; Aronica et al., 2002; Romanowicz and Beven, 2003; Hall et al., 2005; Pappenberger et al., 2005). The use of aerial georeferenced images is another popular non-invasive technique, which usually relies on just one shot for economic reasons. Hence, no information about varying flow condition is available. In addition, image ortho-rectification may often be a time consuming procedure not feasible when the shooting angle is too flat (Pasquale et al., 2012).

In the contest of the RECORD project there was the need of a specific calibration method that allows an accurate calibration of complex geometry (braided) alluvial rivers. Locally, in correspondence of the main bedforms, it was very important to have a reliable and accurate estimation of water depth, velocities and shear stress, in order to investigate the effect of river hydraulic on vegetation and therefore to plan field campaigns.

2.4.1 Classical Methods

As a first validation test, the hydraulic model performance at low discharge through the simulation of the discharge of 15 m^3/s and 50 m^3/s were verified. For those flow rates a precise measure of the island shore-line was available from a differential GPS survey. Figure 2.6a, b show the comparison of the simulated areas of the island to those obtained from the GPS survey. In both cases the results show a very good overlap of the surveyed and computed shorelines. The two star points in Figure 2.6b show that the roughness coefficient ($n = 0.028$

$m^{-1/3}s$), obtained by calibrating the model against the GPS surveyed island shoreline for the two available flow rates of 15 and 50 m^3/s, is in accordance with the ones obtained with the proposed technique.

A simulation for the largest flood of 2009 was also performed (peak flow equal to 760 m^3/s) and then compared the water level recorded by the camera at the peak flow instant (Figure 2.6c) to the simulated one (Figure 2.6d). Simulations using a roughness parameter n =0.022 $m^{-1/3}s$ provided good results, though mainly qualitative at this time. Among standard methodologies we may also find calibration with scaled rod. However, due to the irregular topography of the restored reach, calibration based on traditional techniques would need several rods positioned at different locations. Installing them on the island would disturb the flow with the additional risk that poles may easily bend, break or be removed during floods. Moreover, the distance between the camera and the monitored river reach (in our case 150÷300 m) may result in a resolution not enough detailed to allow reading scale bars on the rods (Pasquale et al., 2012).

2.4.2 Calibration from terrestrial photography

In the context of this work, a technique was used (Pasquale et al., 2012), which uses low cost terrestrial photography digital images of the investigated river reach and obtains from them the information about the inundated area corresponding to different flow rates. By comparing the simulation of the inundated area to the pictures taken at a known flow rate, the calibration of the riverbed roughness, expressed as Manning's roughness coefficient (Aronica, 1998) is performed. This method offers a new perspective of calibration and validation of 2D hydraulic models and can be applied to a wide range of flow conditions, even to flood events, since no field measurement is needed. In addition, it is rather cheap, since the photographs used for the calibration are taken from a high resolution, but common digital camera and no orthorectification is needed. Moreover this method allows obtaining spatial calibration of velocity and water level at different flow rate for river reach characterized by complex geometry such as braided river system.

The calibration technique described in this work consists of three steps: i) pattern recognition, ii) digital mapping and iii) model fitting. To illustrate the procedure, here, a sequence of terrestrial pictures taken from the restored reach of the Thur River near Niederneunforn, in Switzerland (Figure 2.7a) is shown.

The site is currently monitored in order to understand its evolution dynamics after restoration (Pasquale et al., 2011; Schneider et al., 2011). Three representative images taken by mean of high resolution digital cameras installed on the monitoring tower located on the left levee (Figure 2.7a) are shown in Figures 2.7e, f, g. Such images show that only few vegetation spots

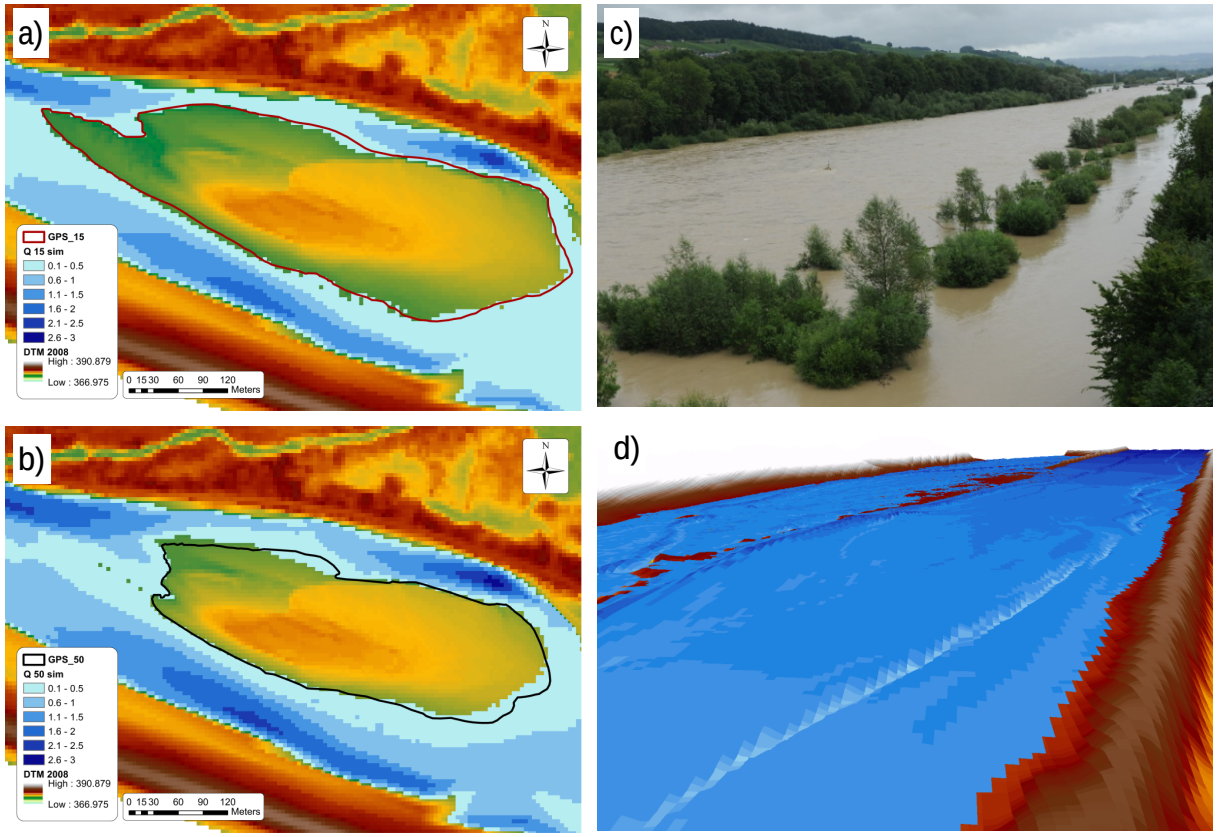

Figure 2.6: *Simulations run for topography 2009 at 15 m^3/s (a) and 50 m^3/s (b) show the comparison between the observed island shoreline (measured by a differential GPS) and the simulated one. In July 2009 the installed camera recorded a 760 m^3/s flood (c). The flood was then simulated using the calibrated roughness coefficient $n = 0.022\ m^{-1/3}s$ (d), which although not considering the presence of vegetation, still gives qualitatively good results.*

colonize the emerging bedforms, thus not contributing too much to the equivalent riverbed roughness. The first step requires the recognition and extraction of river bed forms such as bars and islands from selected terrestrial photographs under different flow conditions. It has been developed an automatic recognition procedure to classify the pixels with the highest probability of being non-water, which represents the island surface and the surrounding shore areas. While the first version of the automatic classifier presented by (Pasquale et al., 2011) required a large amount of training classified data, the approach presented here is improved and does not require this anymore. The classification approach is based on several features, which perform similarly to the approaches used by autonomous off-road navigation (Rankin et al., 2004) and on water level detection (Iwahashi and Udomsiri, 2007).

The first feature is a combination of saturation and value of the HSV (Hue Saturation Value) representation of the image, which in particular classifies the bare soil on the island. The

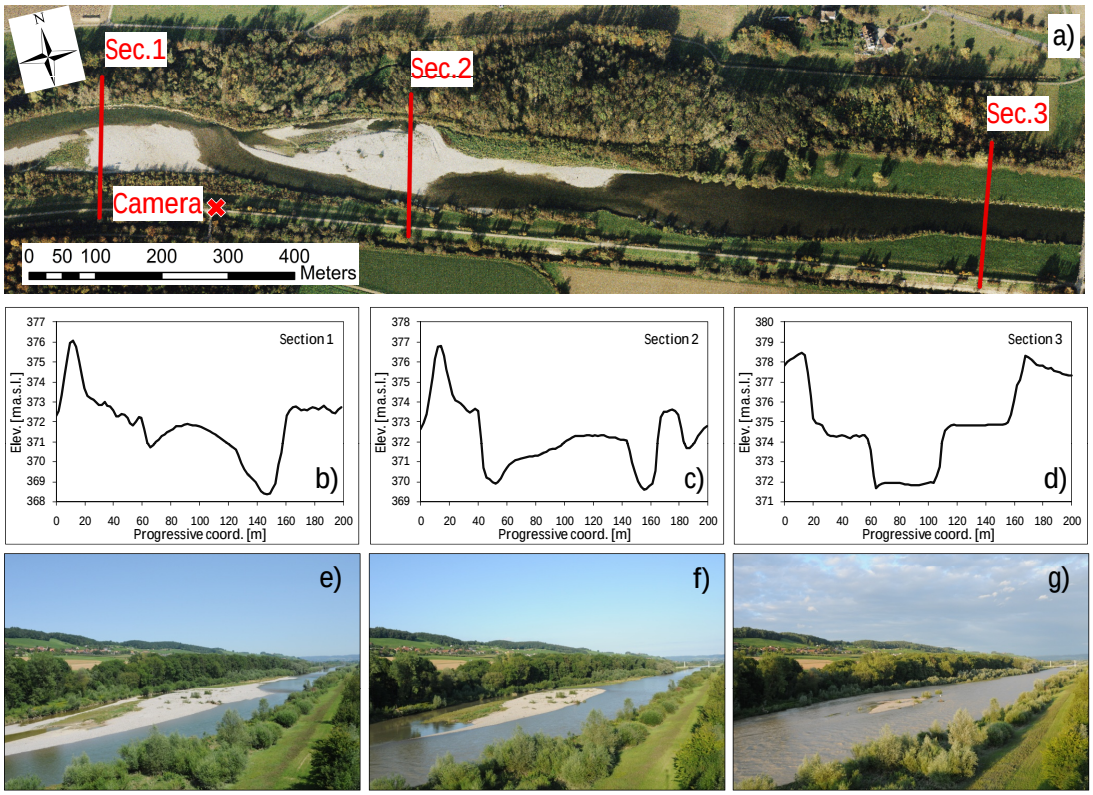

Figure 2.7: *Aerial view of the restored reach of the Thur River (a). An example of three cross sections is given: section 1 (b) and section 2 (c) in correspondence of a gravel bar and the research island respectively refer to the restored reach in comparison with section 3 (d) in the non restored reach. Three representative pictures taken from the digital camera at 20 m^3/s (e), 100 m^3/s (f), and 250 m^3/s (g) show how the access to the river becomes impossible at high flow rates.*

remaining features classify vegetation on the island and the shore line. The second feature is based on the amount of edges detected in the image. The third feature is based on the difference between hue and saturation values of the HSV representation of the image, while the forth feature is based in the difference between green and blue channel of the RGB representation of the image. The last two features are error prone since they also classify reflections of vegetation in the water as non-water under certain conditions. The classified picture is then matched within scenarios from the selected pictures, which we recommend to be representative of a wide range of hydrodynamic conditions. Figure 2.8 shows an example of the output results. At the present stage, the method allows recognizing and classifying with satisfactory precision the non- water pixels, represented by the red masked areas by means of a series of Matlab codes (see Appendix C).

The second step is the digital mapping and consists of building a metric to compute the actual area of the island as seen through a perspective view point, that is obtaining the actual area

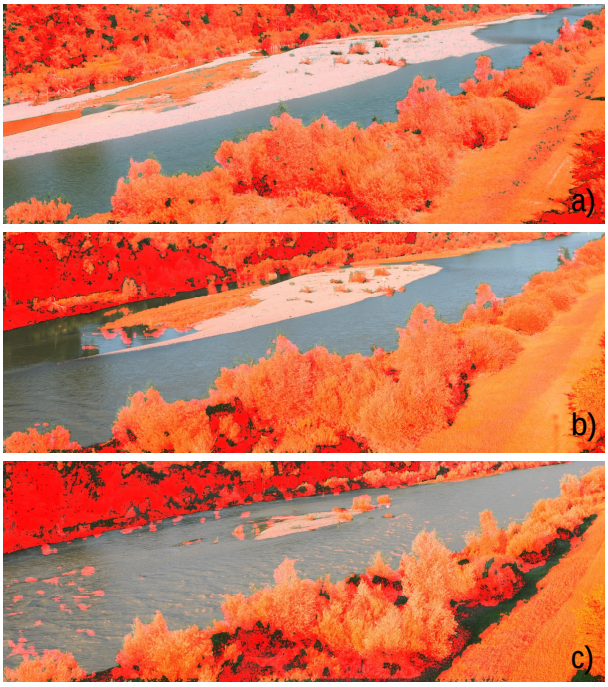

Figure 2.8: *The automatic algorithm for pattern recognition allows delimitation of water and non-water classes from digital photographs. The reddish mask over the pictures represents the pixels classified as non-water.*

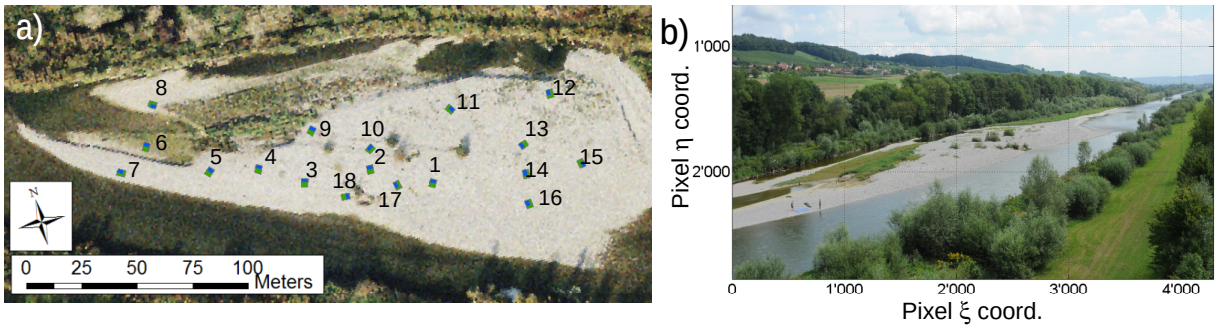

Figure 2.9: *Aerial photo of the research island in 2009 with the green and blue tarps (a). Coordinate are in meters (E, N). Example of photograph used for the calibration (b). The discharge represented in the picture is 20 m^3/s and the coordinate are in pixel number.*

from pixels of the 2D non-orthorectified digital image. In the case study, this task was achieved by positioning two rectangular tarps of known and different areas (blue, 5.1 m^2 and green, 10.9 m^2) at 18 different locations on the reference island (Fig. 2.9a). We chose the locations in order to almost uniformly cover the entire island and for each of them, a photograph was taken in August 2009 under homogenous conditions of light and flow (Fig. 2.9b). Then, a Matlab script was developed in order to compute the number of pixels (RGB channels) that each tarp

occupies in each photograph. Thus, by knowing the actual area of the tarps, a Pixel-to-Area ratio (PA) could be calculated for each tarp location and each picture (see Appendix C, Table C.1). The final pixel-to-area ratio at each location is the average of the ratios of the blue and green tarps at the same location. The average values of the two tarps at each of the 18 locations are associated to the averaged center of area of the tarps (Table C.1, Appendix C). The pixel-to-area conversion ratio for every pixel of the island is then obtained by fitting a second order polynomial to the values computed for each (ξ, η) coordinate of the tarp locations:

$$\mathrm{PA}\left(\xi,\eta\right) = a\cdot\xi^2 + b\cdot\eta^2 + c\cdot\xi\eta + d\cdot\eta + e\cdot\xi + f \tag{2.1}$$

where ξ, η are the coordinate of each pixel of the photograph and a, b, c, d, e and f are fitting parameters given by the regression analysis (a = -7.46·10^{-09}, b = 1.27·10^{-07}, c = -7.48·10^{-08}, d = 1.59·10^{-04}, e = -4.97·10^{-04}, f = 4.9·10^{-01}). The value of the corresponding coefficient of determination (R^2_{adj}) is equal to 0.9365. At this point, for a given picture the 2D area of the island (delimited by a shore-line) through the automatic pattern recognition is known. A last step is necessary in order to crop the island surface from the original picture thus defining the domain of validity of the (2.1). This is done manually. The cropped area (Figure 2.10a) is the domain ω of the function PA by means of which we convert each pixel within ω into an actual area. The integral computed over the domain ω delimited by the shoreline of the function PA(ξ, η) gives the total area of the island A:

$$\mathrm{A} = \iint_{\omega} \mathrm{PA}\left(\xi,\eta\right) d\xi d\eta. \tag{2.2}$$

The 3D chart of the interpolating surface PA for the investigated case is shown in Figure 2.10b, whereas an example of the conversion ratio (in m^2) for each pixel of the research island is shown in Figure 2.10c. The third step consists of comparing the area of the island obtained in the steps 1 and 2 for different flow rates with that obtained by the 2D hydrodynamic simulation, for different values of the Manning's coefficient. The calibration is done by choosing the value of n that best matches the simulated island area with the one obtained through photographs.

The areas computed by the pattern recognition method for different observed discharges were finally used as ground truth to analyze the sensitivity of the BASEMENT model to variable Manning coefficients in simulating the correct island area. Simulations were run on a mesh built on a high resolution Digital Terrain Models (DTM, produced by LIDAR airborne flight with horizontal resolution of 50x50 cm^2 and vertical precision of $\pm$ 5cm) corrected with the code of Schaeppi et al. 2010 in order to account for the actual river bathymetry. A homogeneous roughness coefficient was used to represent a complex grain distribution (see Pasquale et al. 2011 for details) and to take into account local roughness due to sand, gravel and shallow

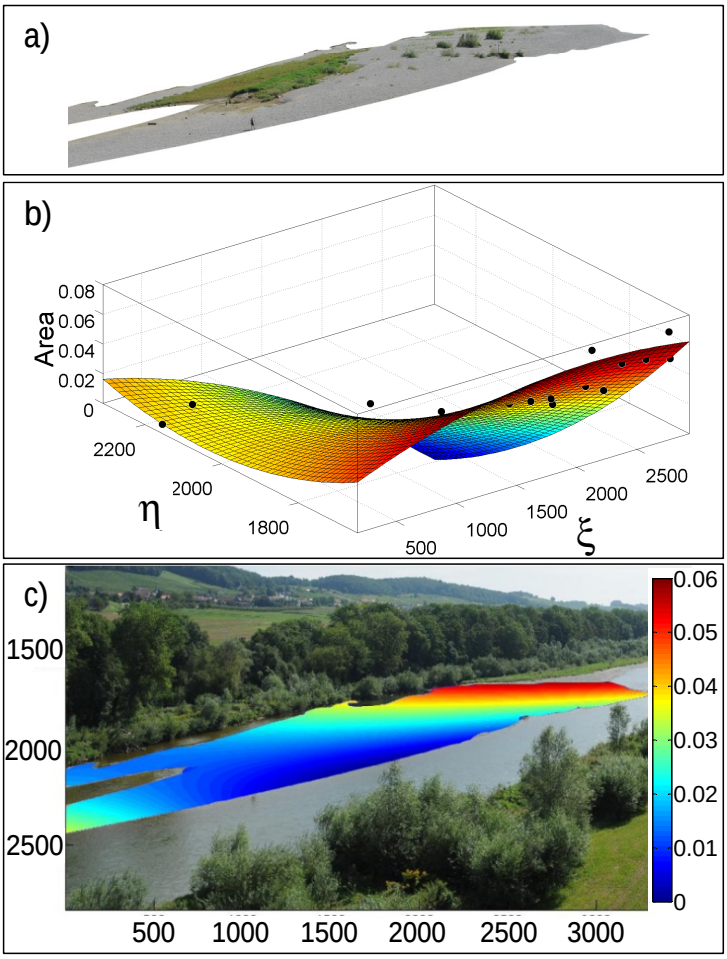

Figure 2.10: *On the basis of the results shown in figure 2.8 the area of the island is then extracted manually (a) and used as a boundary ω for the second order polynomial interpolation function (Eq. 2.1). The 3D representation of the fitting surface is shown in (b). Equation 2.1 computed over the boundary ω gives the pixel-to-area (PA) conversion for each pixel of the surface (c).*

vegetation. The roughness coefficient was allowed to change in the range $n = 0.017 \div 0.028$ $m^{-1/3}s$ and simulations were run for six different discharges (ranging in the interval $Q = 20 \div 250$ m^3/s). The output in terms of water surface elevation was imported in a GIS environment to compute the area of the research island (simulated by the model) and the actual area computed from digital image (step 1 and 2) at the same flow rate. The results and the percentage errors for varying Manning's coefficients *n* are shown in Table 2.2.

The application of the proposed calibration technique to the restored reach of river Thur provided promising results. By comparing the percentage error between simulated and observed areas for different Manning's we found the roughness coefficient that minimizes such error at a given discharge (Figure 2.11a shows and example for the simulation with $Q = 140$ m^3/s).

	Q=20 m^3/s A_{photo} = 13880 m^2		Q=60 m^3/s A_{photo} = 9539 m^2		Q=100 m^3/s A_{photo} = 8328 m^2		Q=140 m^3/s A_{photo} = 6394 m^2		Q=200 m^3/s A_{photo} = 3666 m^2		Q=250 m^3/s A_{photo} = 1780 m^2	
n [$m^{-1/3}s$]	A_{sim}	Error	A_{sim}	Error	A_{sim}	Error	A_{sim}	Error	A_{sim}	Error	A_{sim}	Error
[$m^{-1/3}s$]	[m^2]	[%]	[m^2]	[%]	[m^2]	[%]	[m^2]	[%]	[m^2]	[%]	[m^2]	[%]
0.017	15560	10.8	10868	12.2	8596	3.1	6968	8.2	3712	1.2	1500	-18.7
0.018	15480	10.3	10700	10.9	8544	2.5	6712	4.7	3604	-1.7	1376	-29.4
0.019	15424	10.0	10460	8.8	8490	1.9	6580	2.8	3412	-7.4	1244	-43.1
0.020	15364	9.7	10404	8.3	8440	1.3	6372	-0.3	3216	-14.0	1144	-55.6
0.021	15304	9.3	10356	7.9	8316	-0.1	6124	-4.4	3048	-20.3	1028	-73.2
0.022	15104	8.1	10092	5.5	8024	-3.8	5976	-7.0	2928	-25.2	848	-109.9
0.023	15012	7.5	10056	5.1	7888	-5.6	5832	-9.6	2860	-28.2	680	-161.8
0.024	14828	6.4	9984	4.5	7464	-11.6	5752	-11.2	2548	-43.9	488	-264.8
0.025	14824	6.4	9752	2.2	7272	-14.5	5652	-13.1	2324	-57.7	436	-308.3
0.026	14804	6.2	9620	0.8	7120	-17.0	5392	-18.6	2080	-76.3	372	-378.5
0.027	14688	5.5	9564	0.3	7024	-18.6	5248	-21.8	1876	-95.4	308	-477.9
0.028	14624	5.1	9500	-0.4	6828	-22.0	4912	-30.2	1728	-112.2	288	-518.1

Table 2.2: *Manning's n value (or the corresponding Strickler's c) of the roughness coefficients used for calibration. The table shows also the discharges range of value simulated and the corresponding area of the island produced and the related error.*

Considering the best performing *n* (minimum error) at each discharge (Table 2.2), one notices that at high flow rates the percentage error with respect to the simulated area increases. This is due to the progressive decrease of the exposed area of the gravel bar, which makes the conversion pixel-to-area gradually less precise. Figure 2.11b shows an interesting result clearly reflecting the role of the relative submergence, i.e. the ratio between the equivalent sediment diameter and the average flow depth. As expected, riverbed roughness decreases as the discharge increases. At low flow rates indeed (Fig. 2.11b, Q<60 m^3/s), grain size is the main factor influencing the roughness coefficient (e.g., Julien, 1995; Bathurst, 2002). This is due to shallow submergence, when the relative roughness ϵ (the ratio between mean sediment diameter *d* and water depth *h*) is between 0.01 and 0.1. As discharge increases, *h* increases too and therefore the relative roughness decreases.

At high flow rates (Q>200 m^3/s) when most of bed forms are submerged the grain size has, generally, less effect on the river roughness which is rather influenced at large scale by river bed forms (Julien, 1995). From Figure 5b, in correspondence of abrupt gradient changes of the plot, three different ranges of *n* can be identified: for Q<60 m^3/s, the average *n* is equal to 0.0275 $m^{-1/3}s$, for 60<Q<180 m^3/s, the average *n* is 0.022 $m^{-1/3}s$ for Q>180 m^3/s, $n = 0.017$ $m^{-1/3}s$. The set of pictures used for calibration allowed to only considering discharges lower than 300 m^3/s. This is indeed the critical discharge for which all river bed forms are submerged and therefore, not visible in the picture anymore. Figure 2.11b also seems to suggest that, for discharges higher than 250 m^3/s, the relation between roughness coefficient and discharge is likely to become asymptotic.

However, at present it is not possible yet to advance any conclusion in direction, but we would

rather expect that the effects of submerged bedforms and bank vegetation start playing a role and determine a successive increase of the equivalent roughness. In order to identify the best *n* value for all investigated flow rates two statistical measures were adopted, the root mean square error (RMSE) and the mean absolute error (MAE), as suggested for instance by Papanicolaou et al. (2011). There are respectively defined as:

$$\mathrm{RMSE} = \sqrt{\frac{1}{N}\sum_{j}^{N}(O_j - S_j)^2} \tag{2.3a}$$

$$\mathrm{MAE} = \frac{1}{N}\sum_{j}^{N}|O_j - S_j| \tag{2.3b}$$

where N is the number of field measurements, O_j are the observed values and S_j are the simulated areas. The lower these errors are, the better simulated values fit observed ones. The plot of RMSE and MAE vs. *n* (Figure 2.11c) shows that the best *n* value is 0.020 $m^{-1/3}s$ according to MAE and it is 0.022 $m^{-1/3}s$ according to RMSE.

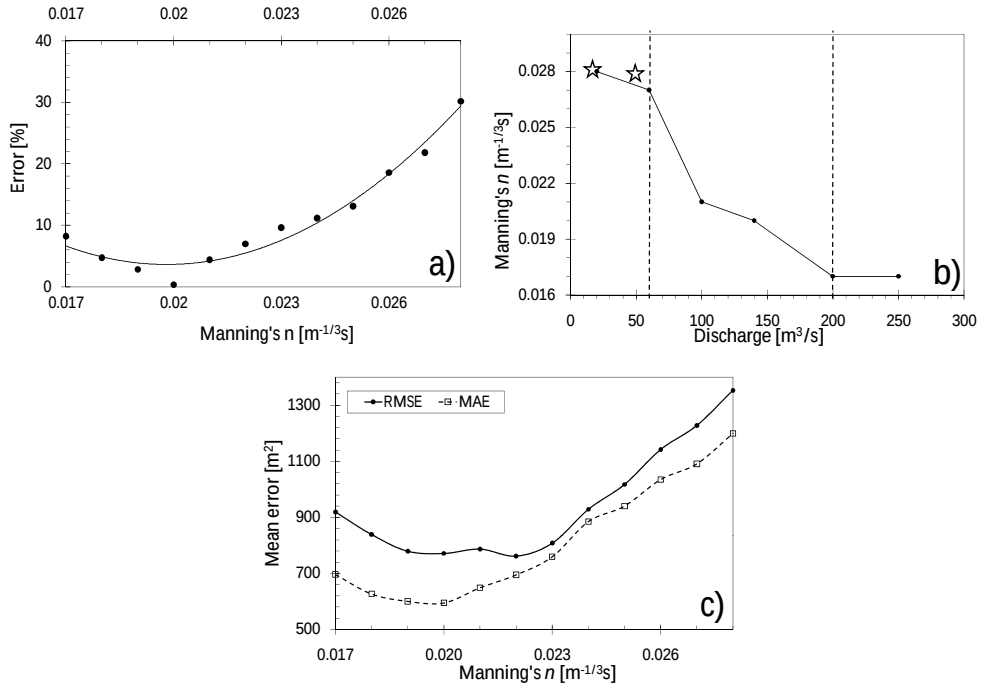

Figure 2.11: *Percentage errors at a fixed discharge for different roughness parameters and Q = 140 m^3/s (a). Plot (b) represents the best roughness values for each discharge. The optimum value changes according to the flow rate. Stars represent the calibrated values obtained from dGPS survey of the island shoreline at 15 m^3/s and 50 m^3/s. Chart of the mean errors computed for all flow rates using eqs. 2.3a and 2.3b (c).*

Assuming that the average grain size of the alluvial sediment is not time dependent, the digital mapping function can in principle be implemented only once, i.e. at very low flow conditions. This metric is used to convert 2D photographs into actual river bed forms area that is exposed under certain flow conditions. This methodology allows then extracting the optimal equivalent roughness coefficient for each flow rate, which can later be used for hydraulic simulations. Considering the uncertainties in calculating Manning's roughness from empirical relationships depending only on roughness height (the aforementioned values range from 0.017 to 0.028 $m^{-1/3}s$), the proposed technique can be considered a valuable alternative to standard methodologies. Some hints should be taken into account for further improvements of this technique: the number of tarp locations should be as high as possible, especially far from the camera where the mapping function converting pixels to actual area gives high errors. In alternative, the analyzed area should be contained within a small distance from the camera to avoid low visibility of far tarps. Beside those recommendations, the reliability of this technique has been tested and proven by all the simulations and analysis carried out in this project, in particular in terms of accuracy.

2.5 Bedload transport

All the erosion and deposition process is leaded by sediment transport dynamics and particularly bedload transport. In the contest of this work bedload transport analysis was the starting point for more detailed morphodynamic analysis or root reinforcement model formultation.

Section 2.3.1 gave an overview on open channel flow within rigid boundaries. In natural rivers, however, the boundaries are generally loose, leading to the complex phenomena of interrelated movement and sediment movement. Thus it is necessary to introduce some basics to understand the principles of sediment transport.

2.5.1 Basic Theory

Considering the complex topic of sediment transport, first of all one should distinguish three different transport mechanisms: bed load, suspended load and wash load. Wash load depends on the quantity of material coming from upstream, while both bed load and suspended load take material from the river bed. It is usually hard to distinguish the last two from each other; literature analyzes them in separate ways. Some authors were also capable of analyzing the overall phenomena, thus leading to total solid transport equations.

Both cohesive and non-cohesive sediments take part in morphological processes. For the non-

cohesive sediments there is no physical-chemical interaction between individual particles. All the treatment in this thesis deals with non-cohesive sediments. A first measure with which to characterize non-cohesive sediments is the particle size or diameter. There are various definitions for the particle diameter such as: *sieve diameter* (size of sieve opening through which the particle will just pass), *nominal diameter* (diameter of the sphere with the same volume as the particle) and *sedimentation diameter* (diameter of a sphere with the same density and fall velocity as the given particle). Other important factors to characterize sediment transport are particles' shape, density and fall velocity. In order to create a parameter to characterize shape, the shape factor had been defined as: $\mathrm{SF} = c/\sqrt{ab}$, in which a, b and c are respectively the longest, intermediate and shortest of the three mutual perpendicular axes of the particle.
The density of the particle depends on mineral composition: a common value for sand and gravel beds is 2650 kg/m^3. The fall velocity is defined as:

$$w = \left[\frac{4}{3\mathrm{C}_D}\left(s-1\right)gd\right]^{1/2} \tag{2.4}$$

in which C_D is a coefficient function of the Reynolds number, *s* is the ratio between the grain density and the water density, *g* is the gravity acceleration and *d* is the diameter of the particle.

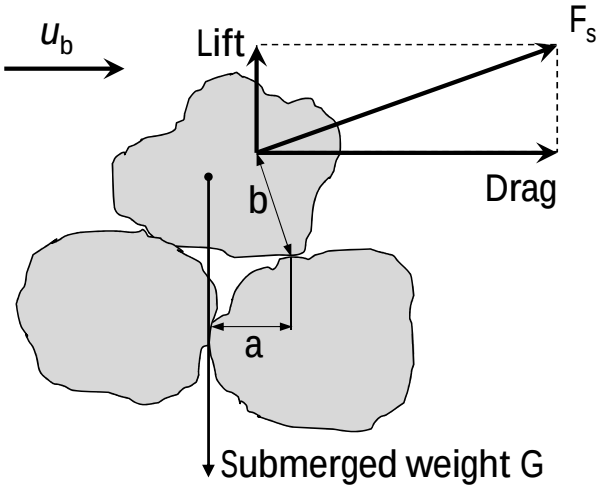

Figure 2.12: *Forces acting on a submerged particle.*

The stability of a non-cohesive particle on the bed of a channel depends on the forces acting on it, such as the submerged weight, drag forces and lift forces. The two latter forces are due to the flow around the particle causing pressure differences and shear stresses on the particle surface. These forces are shown in Figure 2.12 and the condition for equilibrium can

be expressed by

$$\tau_* = \frac{\rho u_*^2}{(\rho_s - \rho)\, gd} \tag{2.5}$$

in which $u_* = \sqrt{\tau_0/\rho}$ is the shear velocity and τ_* depends on the particle shape, velocity profile, etc. Shields (1936) demonstrated experimentally that the parameter $Re_* = u_* d/\nu$ is sufficient to characterize the flow pattern near the particle. He has given an empirical relation between τ_* and Re_* which is shown in figure 2.13. When flow conditions reach the critical stage, the loose bed material starts moving.

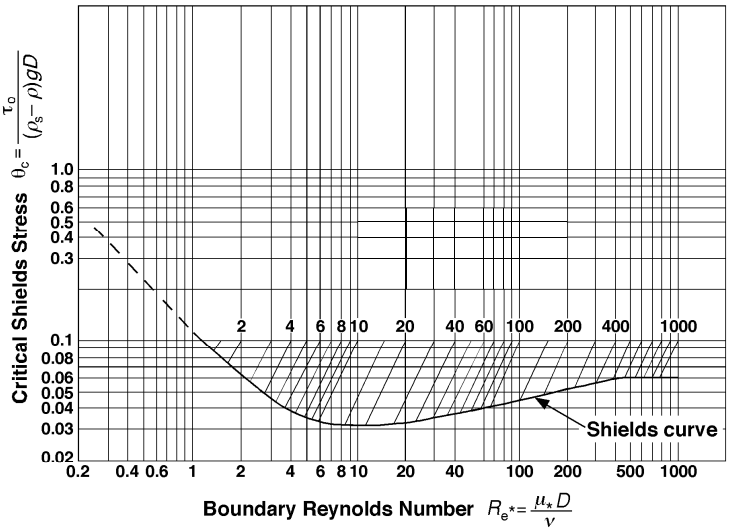

Figure 2.13: *Shields curve: for a given Boundary Reynolds number, if the dimensionless stress on a particle is below the curve, then there is no motion, if it is above the motion can start (picture taken from the web page: http://serc.carleton.edu/NAGTWorkshops/sedimentary/activities/14100.html).*

2.5.2 Meyer-Peter and Müller equation

The sediment particles which start moving in send-bed streams or rivers induce perturbation of the bed surface elevation. There are pattern covering bed surface that develop called bedforms. From the practical engineering point of view they are of importance for the following reasons: first, the bedform reflects the stochastic nature of bed load transport. Thus the measurement technique must be based on it. Second, in determining the depth available for navigation the bedform has to be considered, especially if its amplitude is not small compared to the average depth. The prediction of bedform employs a great deal of empiricism. The unsteady conditions found in nature are responsible for the scatter of data compared with laboratory data obtained under controlled steady conditions. Sediment transport formulae link the sediment transport to

the properties of the sediment and the hydraulic properties of the stream. However, considering the complex physical phenomena and the relatively simple formulae in use, it is not surprising that the sediment transport can only be estimated with low accuracy. Another indication that the accuracy is poor is the fact that there are a considerable amount of formulae. Nobody can say which formula is the most reliable and therefore it should be chosen depending on river characteristics. Indeed most formulae have a strong experimental character and so their validity is restricted to rivers which have a behavior similar to experimental condition. As stated in the beginning of this chapter, there are different formulae for bed load and sediment load. The analysis carried out on river Thur with the software Basement in this thesis deals only with bed load and the Meyer-Peter and Müller (Meyer-Peter and Müller, 1948) formula was adopted. The formula originally was calibrated for mixed grain sizes and undulating bed and best suits river Thur features. Meyer-Peter and Müller formula modified by Chien (1954) is:

$$q_s^* = 8\left(\tau^* - \tau_c^*\right)^{3/2} \tag{2.6a}$$

$$q_s^* = \frac{q_s}{\sqrt{(G-1)\,g d^3}} \tag{2.6b}$$

in which: $\tau^* = \frac{\tau_b}{(\gamma_s - \gamma)d}$ is the Shields' shear stress, $\tau_c^* = 0.5\left[0.22\mathrm{Re}_*^{-0.6} + 0.06 \cdot 10^{\left(-7.7 \cdot \mathrm{Re}_*^{0.6}\right)}\right]$ is the Shields' threshold as defined by Parker et al. (2003), Re^* is Shields' Reynolds number as defined in Section 2.5.1 and G is the ratio between γ_s, sediment specific weight, and γ_w, water specific weight.

2.6 Vegetation cutting experiments

The last element of the project investigations concerns the understanding of the interaction between river hydrology and vegetation. This requires accurate monitoring of the vegetation growth dynamic and survival (see Figure 2.14). Since the final goal of this project is to achieve a mechanistic quantification of root-induced soil cohesion, it is first fundamental to know if and how vegetation grows on such bare soils and which factors influence root sprouting growth and surviving.

Clearly, successful ecological engineering in the riparian zone requires a thorough understanding of interactions among plants, hydrology and fluvial geomorphology. Naturally occurring riparian plant communities exhibit strong sensitivity to physical factors (Mallik and Rasid, 1993), and several environmental factors such as moisture and soil texture have been identified as being critical in determining survival and performance of planted willow cuttings (Pezeshki et al., 2007).

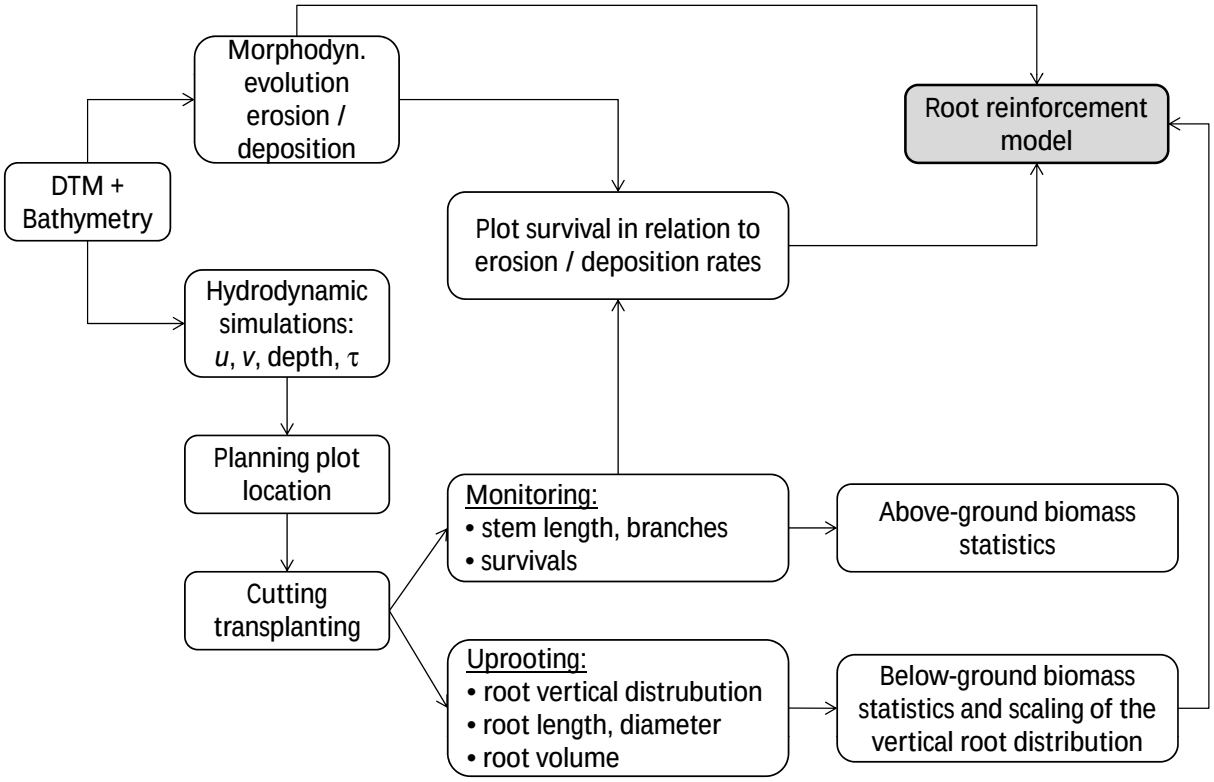

Figure 2.14: *Planning and monitoring stategy of the transplanted cuttings: first, vegetation plot location is decided according to hydrodynamic simulation at detailed scale of the island. Second, after tranplantation, monitoring campaign is carried out. In average every two weeks cutting growth and survival is measured. Starting in the middle of May, every month cutting samples are also uprooted for root analysis (see Section 2.7). On the base of the morphological analysis and cutting survival rate a relation between erosion-deposition and surviving is formulated. Root analysis, together with morphological analysis are used, in the constest of this work to formulate a model of soil root-reinforcement.*

Periodic monitoring of the survival rates, of the main stem length and of the number of branches for each cutting has regularly been carried out every 15-30 days. Throughout the whole monitoring process cuttings were regarded to be dead when they were completely covered with sediment and thus invisible, or if they had been eroded and washed away or if they had failed to sprout. Cuttings uprooted for further root analysis were not considered 'dead' in the survival statistics of the monitoring on the day they were uprooted, since they would have lived if they had not been uprooted.

The campaign of cutting transplantation was initiated with the long term purpose of investigating the role of vegetation roots in anchoring the alluvial sediment, particularly in relation to vegetation growth and flood interarrival time scales. Willow cuttings (*Salix Alba* and *Salix Viminalis*) were installed toward the end of March each year in square plots (2m x 2m). In 2008,

26 plots for a total number of 1272 cuttings were distributed across the island, but an early flood in May (2.15, red hydrograph) removed nearly all of them and replacement installation was not possible for that year. In 2009, the field campaign was repeated (Figure 2.15) with the installation of 1188 cuttings within 26 plots, while 1152 cuttings distributed over 32 plots were installed in March 2010. A summary of the field campaign of cutting transplantation is listed in Table 2.3.

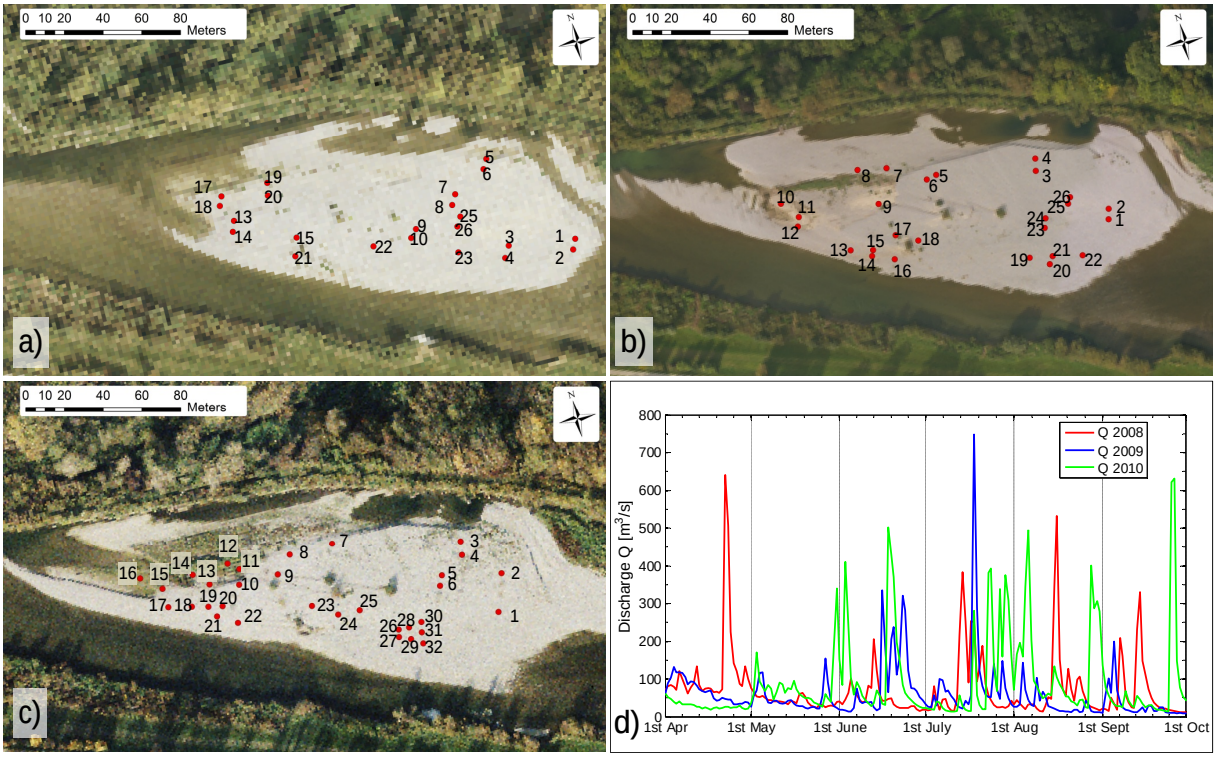

Figure 2.15: *Map of the investigated island showing the location of the vegetation plots in 2008 (a), 2009 (b) and 2010 (c). Plot location have been identified mainly according to hydraulic parameters (flow, shear stress and velocity) and to topography (elevation). Frame (d) shows the hydrographs of the corresponding years.*

Each year, the location of the plots was changed in order to let them experience different hydrologic and hydraulic stress conditions. In particular, the plot location to hydraulic stress was tested by simulating the local hydrodynamics by means of the 2D hydrodynamic model BASEMENT (e.g., Schäppi et al., 2010; Pasquale et al., 2011).

Cuttings have been selected among the indigenous species growing in the area (i.e., *Salix Alba* and *Salix Viminalis* Verones, 2009). The campaign has been repeated in each year of the project and about 1200 cuttings of *Salix Alba* and *Salix Viminalis* have been planted each year in early springtime. Cuttings have been organized in plots with different density, respectively 9 and 16 plants·m^{-2}, following the structure of a regular square matrix (see box in Figure

Year	Plot type			Transplanted cuttings	Monitoring campaign	Uprooting		Survived cuttings
	Plot 6x6	Plot 8x8	Total			Times	Numbers	
2008	14	12	26	1272	1	-	-	308
2009	17	9	26	1188	9	4	57	603
2010	32	-	32	1152	8	5	81	457

Table 2.3: *Summary of the activities carried out for the field campaign of cutting transplantation. For each year, the number of plot and the size of the plot is listed. The table shows the total number of monitoring and uprooting, together with the quantity of uprooted cuttings and the number of cuttings survived ad the end of each year.*

2.15), in which cuttings are planted in correspondence of the nodes (see Appendix D, Figure D.1 for further datails). Plots have been located all over the main island (Figure 2.15) with the purpose of testing the resistance of cuttings stressed by different drought and inundation conditions. In this respect the location of single plots has been decided also according to the shear stress patterns (Figure 2.16) simulated by the numerical model discussed in section 2.3.3. Within each consecutive year we have changed the location of the plots on the basis of the experience acquired during the preceding campaigns in order to validate previous observations or to increase the statistical significance of others. Additional flow simulations were performed using different annual morphologies and flow conditions in order to establish a relationship between morphological and hydraulic variability and the related time dependency. This concept is well illustrated by Figure 2.16, which shows the simulated bed shear stress for a flood peak of 650 m^3/s over the 2005 topography. The shoreline of the main island for a (low) flow rate of $10 \div 15$ m^3/s is shown in the aerial pictures (Figure2.15).

Periodic monitoring of the survival rates, of the main stem length and of the number of branches for each cutting has regularly been carried out every 15-30 days (see Appendix D, Figure D.2). An accurate monitoring of the root-soil system has also been done in order to identify factors linking topological and functional differences of root growth in relation to bar and island topography and hydraulic conditions as observed by other authors (Waisel et al., 2002).

2.7 Root sampling and analysis

All cuttings were periodically monitored (Pasquale et al., 2011). In 2009 and 2010, starting at the beginning of May and ending at the beginning of October, cuttings were uprooted from selected plots 4-5 times in the season following as far as possible van Noordwijk et al. (2000), though the non-cohensive nature of the sediments meant that standard techniques could not be

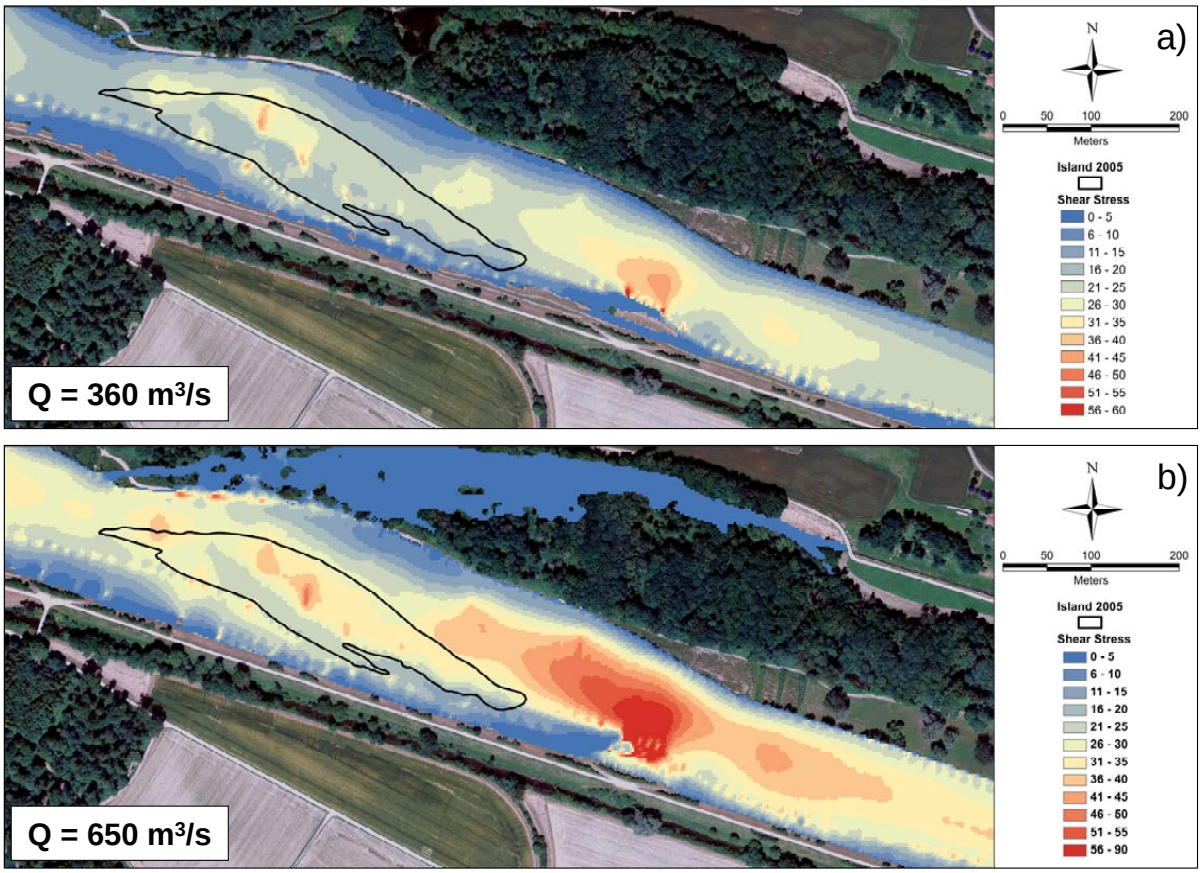

Figure 2.16: *Simulated bed shear stress produced by the maximum peak flow (corresponding to 650 m^3/s) registered in the period 2005-2006. Simulation of this type have been used to decide the location of Salix plots as well as for morphodynamic analysis. The shoreline of the island for 30 m^3/s for the 2005 topography is indicated in black.*

applied throughout (Pasquale et al., 2011). Since the initial sizes (length and diameter) of the transplanted cutting influence their initial growth (Hartman and Kester, 1975; Burgess et al., 1990), three cuttings were systematically uprooted from each plot following a technique that aims at maintaining the highest level of integrity of the roots. Such technique consists of three steps: First, digging a deep trench about 1 meter beside the cuttings (Figure 2.17.a,b), second, searching for the deepest point of the root system (Figure 2.17.c), third, gently removing the soil from the cutting and the root system to preserve the highest level of integrity of its three dimensional structure (Figure 2.17.d).

The uprooted cuttings have been first washed to remove the excess particles of soil and organic material. Each cutting has been then separately layered down on a white paper to re-arrange it to the original three-dimensional structure that we have carefully reconstructed from pictures taken during uprooting. The high resolution picture showing the spatial distribution of the

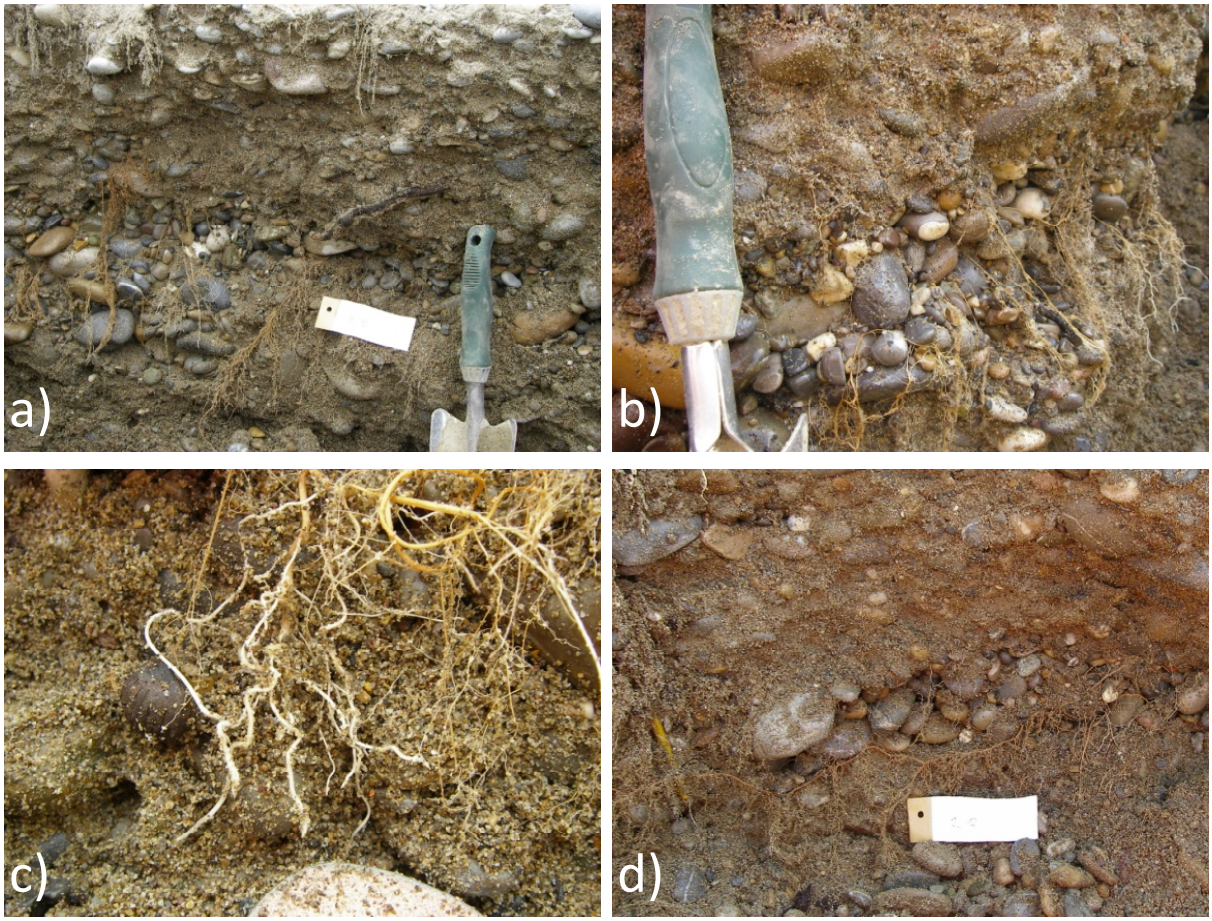

Figure 2.17: *Pictures showing the steps for cutting uprooting. A trench beside the cutting root system is dug, paying attention to not damage any root (a, b). Once the deepest root has been found (c) the last step consists in removing the soil surrounding the cutting, trying to preserve the root system integrity (d).*

roots was then turned into a grey scale image (see Appendix E for further details) and used to compute histograms (See Appendix E) of the vertical root density (Pasquale et al., 2011). By processing the grey-scale image using a filter to remove noise (due, for instance, to dust or fine soil particles) and a binary threshold that classifies pixels as 0 (black) and 1 (white), it has been possible to discriminate root segments from empty spaces. From the resulting binary matrix we have computed an empirical histogram (Table E.1, E.2, E.3 in Appendix E) of the root distribution (resulting from an average of three cuttings) with an appropriate number of classes (Verones, 2009). The histogram bins from the three uprooted samples from each plot were averaged to obtain a single histogram representative of the cuttings forming the plot at a given time (Pasquale et al., 2012a). The proceedure, together with the Matlab Graphical User Interface (GUI) and an example of output results is shown in Appendix E. Spatial variation within plots that could influence the sampling methodology and results (Bengough et al., 2000)

was considered negligible given the small distances between cuttings (tenths of centimeters). Results on vertical root distribution analysis are presented and discussed in Chapter 5.

Reliable statistics of the below ground biomass for the uprooted samples (mean diameter, length, volume, density), and of the related vertical density distribution were obtained (Richner et al., 2000; Pasquale et al., 2011) and further discussed in this work in Chapter 4. Uprooted samples have been additionally processed to quantify their main morphological characteristics. For this purpose, roots have been first cut away from the primary root (i.e., the cutting, in this case, the size of which is measured by hand) and then spread in the water-filled transparent tray of a root scanner. The scanner - an EPSON Expression 10000XL - uses one light source from below as typical for common flat-bed scanners and a second, additional light transparent unit (TPU) from above. It is optimized extra for root images analysis by Regent Instrument, Inc. that also provides the processing software WinRhizo (Regent Instruments, 2009), which is appositely designed for detecting morphology, topology and architecture of root systems through the analysis of their images. The software returns the total root length, average root diameter, surface area, volume of the root system and number of tips and forks of the roots in the morphology package.

Chapter 3

Morphodynamic evolution of the study site

The objective of this chapter is to understand erosion-deposition patterns, in order to be able to link the presence of pioneer and riparian vegetation to river dynamics. This is achieved by showing results of several morphological analysis, supported by observation and aerial surveys of the field site, and of system sensitivity analyzed by modelling. Morphological evolution, in time and space, and implications of the restored corridor, as well as its benefits and negative effects, are also discussed.

3.1 Annual erosion-deposition balance

The natural phenomena of sediment erosion and deposition are an essential feature of the river morphological dynamics. Sediment transport, which is strongly related to catchment hydrology, river geology and hydraulic conditions both at large and small scale, is responsible of bar and island formation in any natural reach (Leopold and Wolman, 1957; Bridge, 1993). An important and non-negligible mutual interaction links sediment transport, hydrology and riparian vegetation (Perona et al., 2009). Camporeale et al. (2005); Perucca et al. (2006, 2007); Tealdi et al. (2010) for instance, have been studying those interactions for meandering rivers and in particular, the developing of vegetation patterns according to flood pulses and regimes. In the context of the RECORD project it is thus very important to monitor the consequences of the restoration also in terms sediment dynamics in the restored reach of the Thur river.

The Digital Terrain Model, interpolated in order to take into account river bathymetry (as described in Chapter 2.2.4), is used to compute erosion deposition balance in the restored

corridor of the Thur river. The balance is obtained in two steps: first the interpolated DTM is cropped to delimitate only the area of the restored reach. Then, by subtracting year-by-year two interpolated DTMs a map with the erosion-deposition pattern is obtained. Figure 3.1 shows the erosion deposition pattern obtained from DTMs analysis.

Considering the portion of river reach shown in Figure 3.1, the balance is $8.434 \cdot 10^3$ m^3 of eroded material for the year 2006−2005, $8.581 \cdot 10^3$ m^3 of deposition for the year 2007−2006, $5.818 \cdot 10^3$ m^3 of deposition in 2008−2007 and $2.027 \cdot 10^3$ m^3 of erosion during 2009−2008. Data do not show any clear trend of erosion, rather than deposition, however, in absolute terms it seems that the magnitude of sediment transport is decreasing.

From a detailed spatial analysis of the in situ grain size distribution, it is found that the median grain size d_{50} ranges in the interval 10÷45 mm (Pasquale et al., 2011). We use the equation $n = 0.0417 \cdot {d_{50}}^{1/6}$ (Chow, 1973) to compute the theoretical d_{50} corresponding to the roughness coefficient determined from the calibration. In the range of $0.017 < n < 0.028$ $m^{-1/3}s$ (Figure 2.11), Chow's equation leads to $5 < d_{50} < 92$ mm, particularly to $d_{50} = 22$ mm for $n = 0.022$ $m^{-1/3}s$.

The spatial distribution of the bed shear stress for varying flow conditions has allowed identifying the locations where critical conditions of incipient (bedload) sediment motion were first reached. Bed shear stress simulated with BASEMENT (see Section 2.3.3) in an almost regular trapezoidal section of the non-restored reach were then used to do a sediment transport analysis based on Meyer-Peter and Müller (1948) formula (see Chapter 2.5.2). Given the average grain size distribution curve of the surface sediment (see section 2.2.2) with $d_{10} = 4$ mm, $d_{30} = 10$ mm, $d_{50} = 20$ mm, $d_{70} = 50$ mm and $d_{90} = 90$ mm, an analysis of sediment transport based on the Shields' theory of incipient motion predicts particles equal to 20 mm moving for flows equal or greater than 200 m^3/s (Table 3.1). For this analysis a critical shear stress τ_c^* = 0.027÷0.030 was used, in accordance with the modification of the Shield's curve reported by Parker et al. (2003), where the asymptotic value of τ_c^* is corrected from it's original value of 0.06. However, the threshold of incipient motion at 200 m^3/s seems a little too low for the Thur river. Therefore Meyer-Peter and Müller (1948) value of the critical shear stress $\tau_c^* = 0.047$ was used for analysis and simulations leading to threshold of 400 m^3/s which is more realistic for the case study. $\tau_c^* = 0.047$ was then used to validate root reinforcement model in Chapter 6. Results are shown in Table 3.1.

Several morphodynamic simulations were performend using the mobile riverbed package of BASEMENT (see Section 2.3.3). The median sediment size d_{50} of the model has been varied several times and it was applied to the sequences of floods recorded in 2008 in order to find out the optimal grain size producing statistically similar changes between the model and two successive DTMs, taken with a time delay of one year, approximately. Five single-grain sizes

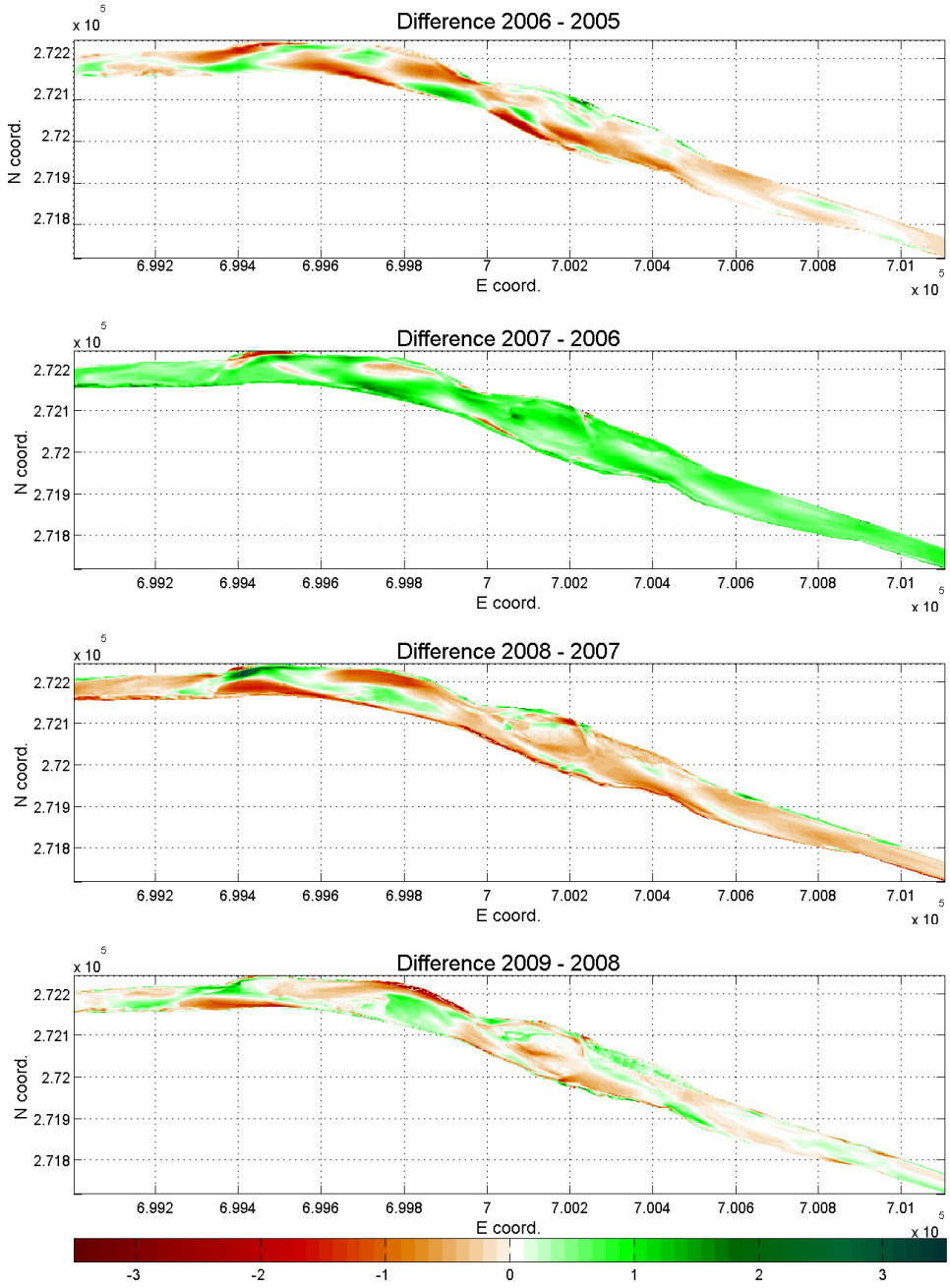

Figure 3.1: *Pattern of the yearly erosion deposition balance in the river corridor since the end of the restoration project.*

were used to produce simulations starting from the terrain configuration of the DTM 2007. Only flood peaks of 2008 exceeding 200 m^3/s were used in the simulatation. This value represents the critical discharge for which particles equal to d_{50} start to move in the non-restored channel according to the analysis conduced using Parker et al. (2003)'s τ_c^*.

Physical and geometrical quantities									
S_o [m/m]	g [m/s^2]	r_w [kg/m^3]	g_w [N/m^3]	r_s [kg/m^3]	g_s [N/m^3]	n [m/s^2]	G [-]	d_{50} [m]	b [m]
0.00169	9.81	1000	9810	2650	25997	1.01E–06	2.65	0.025	50

Measured data			Shield Curve for d_{50}			Meyer Peter & Muller		
Q [m3/s]	t_0 [Pa]	u* [m/s]	t^* (d_{50}) [Pa]	Re* (d_{50})	t^*_c (d_{50}) [Pa]	q^*_b	q_b [m^2/s]	Q_s [m^3/s]
15	0.5	0.02	0.001	5.71E+02	0.023	-	-	-
20	0.8	0.03	0.002	6.88E+02	0.023	-	-	-
30	1.2	0.03	0.003	8.60E+02	0.024	-	-	-
40	1.8	0.04	0.004	1.04E+03	0.024	-	-	-
50	2.2	0.05	0.005	1.17E+03	0.025	-	-	-
75	3.2	0.06	0.008	1.41E+03	0.025	-	-	-
100	4.6	0.07	0.011	1.68E+03	0.026	-	-	-
125	5.9	0.08	0.015	1.90E+03	0.026	-	-	-
150	7.1	0.08	0.018	2.08E+03	0.026	-	-	-
180	8.4	0.09	0.021	2.27E+03	0.026	-	-	-
200	9.5	0.10	0.023	2.41E+03	0.026	-	-	-
230	10.8	0.10	0.027	2.58E+03	0.027	0.0000	0.0000	0.000
250	12.1	0.11	0.030	2.72E+03	0.027	0.0014	0.0000	0.001
280	13.4	0.12	0.033	2.87E+03	0.027	0.0040	0.0001	0.003
300	13.6	0.12	0.034	2.89E+03	0.027	0.0046	0.0001	0.004
360	16.0	0.13	0.039	3.13E+03	0.027	0.0113	0.0002	0.009
400	19.1	0.14	0.047	3.42E+03	0.027	0.0229	0.0004	0.018
450	21.1	0.15	0.052	3.60E+03	0.027	0.0318	0.0005	0.025
500	24.1	0.16	0.059	3.84E+03	0.027	0.0463	0.0007	0.037
550	27.4	0.17	0.068	4.10E+03	0.027	0.0651	0.0010	0.052
600	31.0	0.18	0.077	4.36E+03	0.027	0.0874	0.0014	0.070
650	33.7	0.18	0.083	4.54E+03	0.027	0.1053	0.0017	0.084
700	39.1	0.20	0.097	4.90E+03	0.028	0.1452	0.0023	0.115
760	44.3	*0.21*	*0.110*	*5.21E+03*	0.028	*0.1873*	*0.0030*	*0.149*

Table 3.1: *Input data and results of the solid transport analysis based on shear stress computed in the straight non-restored channel. The computation is done using Eqs. 2.6. The critical shear stress is given by Parker et al. (2003).*

The final river bed topography obtained with numerical simulation was then compared to the DTM 2008 in terms of histograms of the amount of erosion and deposition per single DTM cell. Erosion and deposition patterns as well as relative (and cumulative) frequency of cells affected by erosion or deposition were used to compare and thus calibrate the median grain size, d_{50}. Histograms in Fig. 3.2a-e show the empirical frequency distribution of cells affected by erosion or deposition. The observed data follow a Gaussian distribution. The median grain size that best approximates the distribution of observed data is 30 mm (Figure 3.2e and 3.2g). This result suggests that the model can be calibrated to a value of *n* and d_{50} that make it able to capture both the hydrodynamics and, in a statistical sense, the morphodynamics of the investigated river reach.

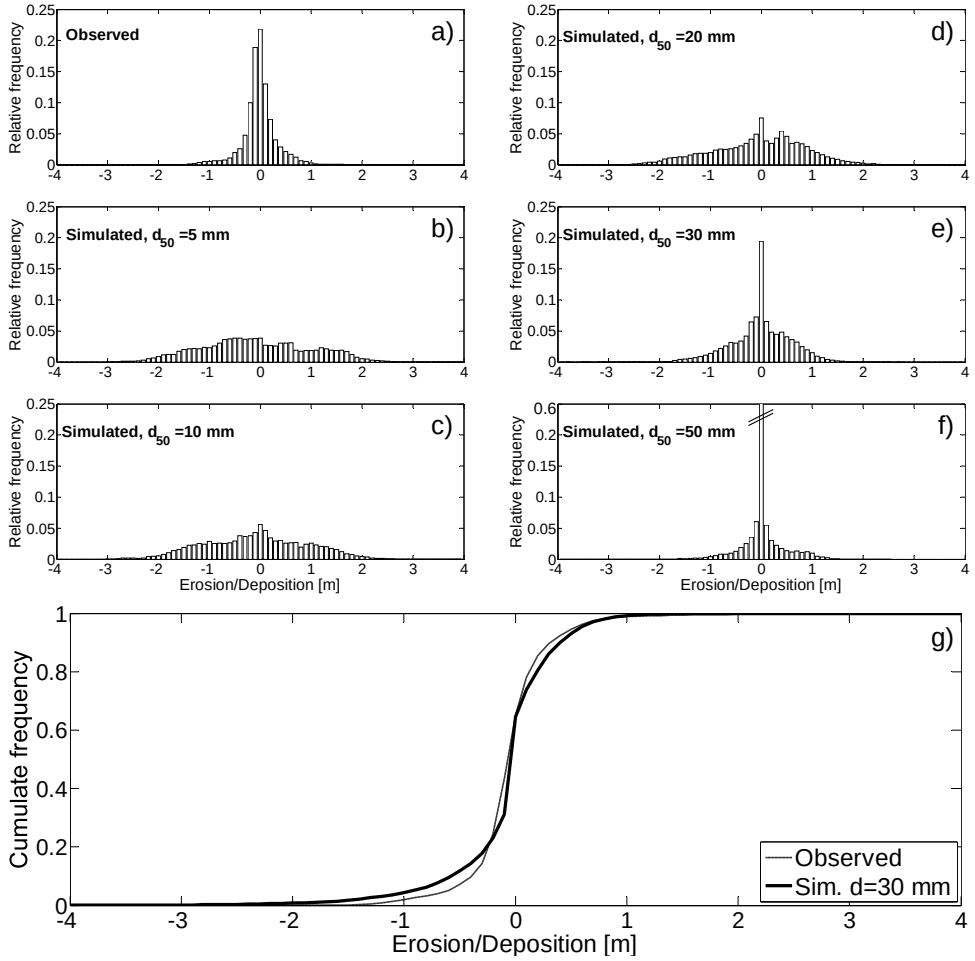

Figure 3.2: *Relative frequency histograms of the observed erosion/deposition during the year 2007-08 (a). Relative frequency histogram of the simulated erosion/deposition for a unique diameter of 5 mm (b), 10 mm (c), 20 mm (d), 30 mm (e), and 50 mm (f). (g) shows the cumulative frequency of the best simulation result (30 mm) and the observed data.*

3.2 Morphodynamic evolution of the Thur river after restoration

The experimental and modeling setup has been used to investigate the interaction among river hydraulic regime, vegetation establishment and its role in sediment anchoring, which, together, dictate the temporal dynamics of the river morphology. In particular, attention was paid to flood magnitude, frequency and duration, as these are crucial parameters to understand plant growth and survival dynamics and their role in determining river morphodynamics. While the return period of specific flow conditions can be estimated by flood frequency analysis, understanding spatial inundation patterns and consequent impacts on vegetation requires integrating multiple

sources of information.

A series of 2D flow simulations at different flow rates for both the restored and the upstream straight reach have allowed to compute both the spatial and temporal variability of a number of flow related variables such as velocity components, water depth, water surface elevation, bed shear stress, etc. Hydrological indicators of river restoration efficacy are often based on flow variables such as flow depth, velocity, shore line length, exposed area, wet perimeter and their gradients under variable flow conditions, because they are well correlated with ecological indicators (Emery et al., 2003; Clifford et al., 2005). A high spatial variability of these variables indicates areas with high habitat diversity (e.g., Lamouroux et al., 1992; Allan and Castillo, 2007). Thus, empirical approaches have been thus proposed in the literature to relate the form and shape of velocity and depth distributions to predictor variables that are relatively easy to determine (Lamouroux, 1995, 1998). However, these approaches show some limitations to comprehensively describe the degree of spatial variability, especially with respect to temporal dynamics that are generated by disturbances, such as flood events, which contribute substantially to rework the river morphology.

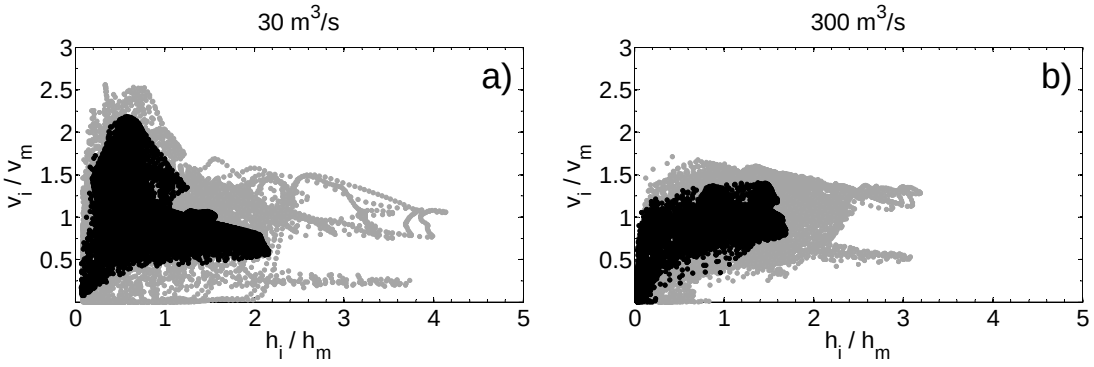

Figure 3.3: *State plane projection showing the spatial variability of the modeled hydraulic variables (h,v) for the straight (black) and the restored (gray) reaches at two different flowrates (right).*

As far as the Thur River is concerned, an example of the changed hydrodynamic regime can be made by plotting modeled flow velocities vs water depth for both the restored and the upstream straight reaches (e.g., Schweizer, 2007), i.e. assuming the latter as a reference of the pre-restoration situation. An example of such variability is shown in Figure 3.3, which illustrates the dimensionless modeled flow velocities v_i/v_m versus the dimensionless water depths h_i/h_m, which we have simulated for both the restored and the original (straight) Thur river reach using the 2005 topography.

The higher spread of points simulated for the restored reach than for the straight one under low flow conditions points to the variability in velocity and depth produced by restoration.

This is a fundamental factor regulating ecosystems (Allan and Castillo, 2007), which strongly influences, e.g., benthic plants, invertebrates as well as fishes (Quinn and Hickey, 1994; Bovee, 1982; Jowett, 2003). Figure 3.3 is also consistent with Stewardson's hypothesis (Stewardson and MacMahon, 2002), which suggests the existence of two fundamental bivariate distributions of water depth and velocity. One is characterized by a centered form with a positive correlation resulting from significant cross-channel effects and weak along-channel effects whereas the other is characterized by a skewed shape resulting from longitudinal bed undulations (e.g., pool-riffle sequences) and minimal lateral variation. Increasing the discharge produces a shift from a positively skewed (Figure 3.3.a) to a symmetric (Figure 3.3.b) distribution. At higher flow rate more and more fluvial forms are submerged, and the similarity between the restored and the non-restored reaches, as expected, increases.

looking at the aerial picture of the study area near Niederneunforn taken in 2005 (see Figure 2.1.f), i.e., soon after remodeling ended, the alternate bar configuration is a flow-sediment bedform instability well known in river mechanics (Ikeda et al., 1981; Colombini et al., 1987; Tubino and Seminara, 1990; Federici and Seminara, 2003). Compared to the bedforms observed in the non restored channel, river bars in the restored reach are larger and are submerged for flows (250 m^3/s) much higher than the annual average (MQ). A first quantitative analysis of the alternate bars pattern can be done by comparing the observed channel width with that predicted by both hydrodynamically-based (e.g., Ikeda et al., 1981; Federici and Seminara, 2003) or empirically-based (Leopold and Wolman, 1957) relationships. For instance the empirical equation proposed by Leopold and Wolman (1957) predicts the typical periodicity that characterizes such bedforms as

$$\lambda = 6.5 \cdot B^{1.1}. \tag{3.1}$$

When measuring the curvilinear distance between bars on the aerial picture (Figure 2.1.f), one obtains $\lambda = 560$ m, that yields from Equation 3.1, $B = 57$ m, which is approximately the average river width between the channelized and the restored reach. This is a first confirmation of the natural origin of the developed morphology. This development stage of the system seems also to suggest the tendency of the river to meander if lateral banks or levee were removed. Figure 2.16 suggests a future of slow migration of the island toward the right-hand river side, i.e., according to the downstream migrating nature of alternate bars (Federici and Seminara, 2003). From the sequential analysis of successive morphologies over the next years it is expected to understand whether alternate "free" bars will gradually concentrate around the river bend, thus assuming a punctual character, eventually forced by the local river curvature (Tubino and Seminara, 1990), or the establishment of vegetation (either natural or planted throughout the project) will be able to influence, at least locally, the expected morphology. The observation of

this evolution will have important implication as far as the stability of the lateral banks (e.g., the right-hand side one in this case) is concerned.

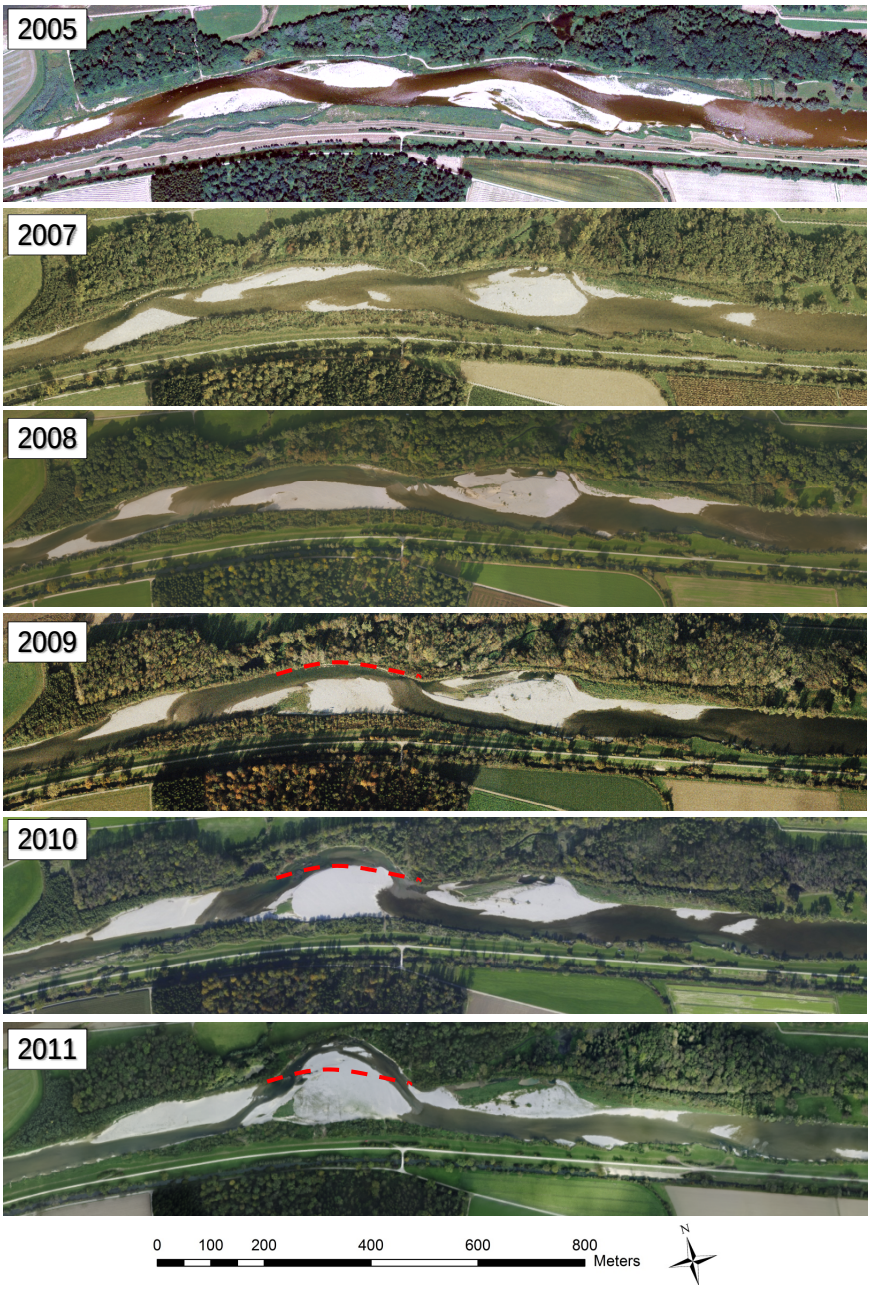

Figure 3.4: *Morphodynamic evolution of the Thur river from the end of the restoration project to the present.*

Figure 3.4 shows morphodynamic evolution of the Thur river in the last seven years, i.e., after restoration. During the period between 2005 and 2009 aerial pictures of the restored river corridor seem to confirm the alternate river bars theory mentioned before. All fluvial forms

slowly migrated toward the opposite bank. This suggests that river bedforms migrate of nearly half wave length in a period of five years. However, in 2010 a quite fast erosion process began on the right side bank, just in front of the left side gravel bar. The red dashed line in picture frame 2009, 2010 and 2011 tracks the position of the right bank in 2009 before the erosion process started. In two years, for a curvilinear distance of about 300 m there was a huge scour phenomenon. The amount of volume scoured is estimated in about 40000÷60000 m^3. One may speculate that the free alternate bar system is evolving towards a meandering system and the "free" bar has become a punctual bar in a bending meander.

3.3 Erosion-deposition pattern and their interaction with vegetation

3.3.1 Bed-form scale

Quantifying the influence of roots on the bed form erosion mechanism and, consequently, root reinforcement requires preliminary accurate field observations. As described in Section 2.2.4, each year, a LIDAR flight survey over the restored corridor produced a detailed DTM with resolution 50cm x 50cm. Focusing the analysis on the exposed area of the island only and differentiating DTMs of two consecutive years, a detailed map of the erosion - deposition pattern is produced. Results for each of the three years of the cutting transplantation field campaign (i.e., 2008, 2009 and 2010) are presented in Figure 3.5. Through the years, there is a sharp separation of the areas which experienced erosion and the ones which had deposition of bed material.

The island shape, its position and orientation toward the flow strongly influences local hydrodynamics and at the same time it is the hydrodynamic that produce contribute in reshaping, creating or moving river bars. Bed shear stress plays an important role in this respect. For this reason the output of the hydrodynamic simulation for the highest peak flow, recorded each year, are used to produce maps of shear stress on the island (Figure 3.6). Comparing the year-by-year erosion/deposition pattern (Figure 3.5) with the map of the simulated bed shear stress (Figure 3.6), one can observe that the scoured portion of the island also experienced higher shear stress values whereas the area of the island where there was deposition of material is also the area where shear stress was lower. This confirms the strong dependence of the scouring - deposition on hydrodynamics and in particular on shear stress value. Being the cutting length about 40 cm, all the portion of the island where an erosion of $\Delta z^{-} > 40$ cm is recorded through the season (April - September) also experienced an almost total cutting mortality. Plots have been removed completely, together with bad material, and flushed away by the flow.

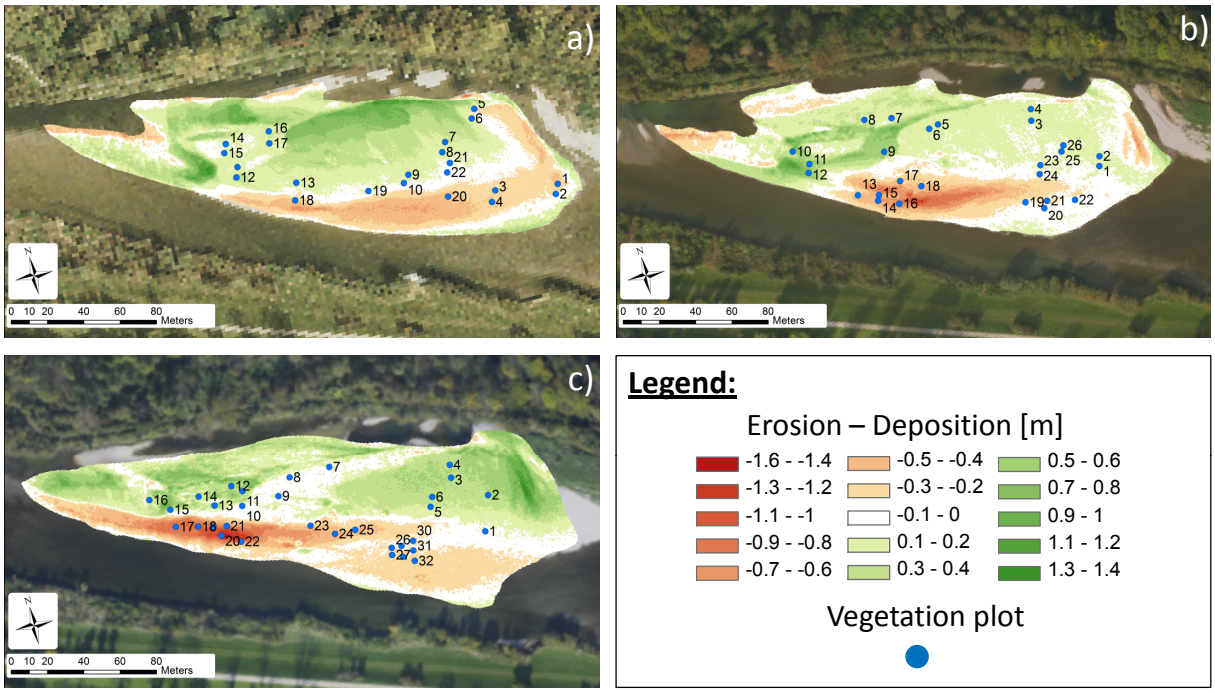

Figure 3.5: *Difference computed from the DEM with resolution 50cm x 50cm gives the pattern of erosion - deposition due to hydrodynamics.*

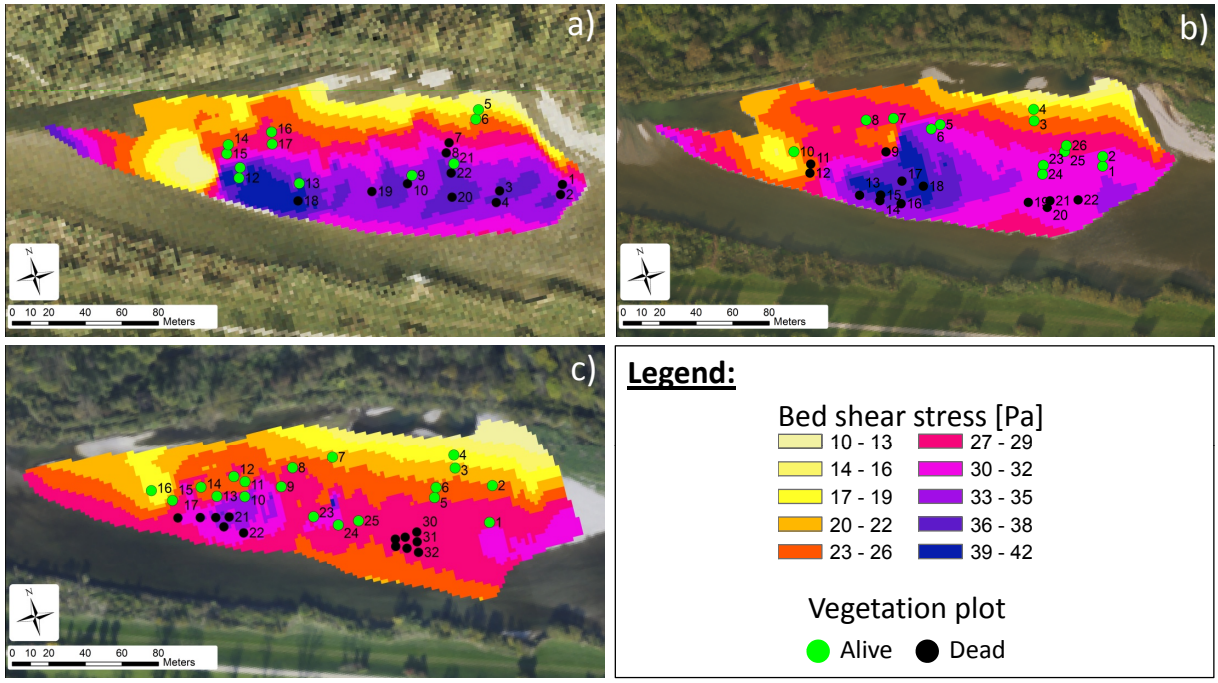

Figure 3.6: *Map of the bed shear stress simulated, with the model BASEMENT, on the island surface for the highest flood peak recorded during each year.*

Being the cutting length about 40 cm, all the portion of the island where an erosion of Δz^{-} $>$ 40 cm is recorded through the season (April - September) also experienced an almost total cutting mortality. Plots have been removed completely, together with bad material, and flushed away by the flow. On the contrary, portion of the island where there was more than $\Delta z^{+} >$ 50 cm of deposited material during a single flood event, rarely allowed surviving of the plots there too. Such an amount of deposition is indeed often too much to allow re-spreading of the buried *Salix* shootings. Further details and analysis of plot surviving and mortality in relation to scouring and deposition phenomena are presented and discussed in Section 4.3.

3.3.2 Salix plots scale

Hydrodynamic strongly influences vegetation establishment and growth (van der Nat et al., 2002; Corenblit et al., 2007). Flood pulses are the major disturbance, both for juvenile pioneer plants (Francis et al., 2005) and for older woody plants (Gurnell and Petts, 2006) although at difference scale of magnitude. At the same time, water flow transports debris wood and branches that may spread along the river facilitating colonization of gravel bars and riparian zones (Gurnell et al., 2005). Another important factor playing a big role on fluvial vegetation dynamics is the transport of sediment which comes together with erosion or aggradation of bed material.

In the former Sections, a brief overview on the morphological dynamics and consequences of the post restoration project has been given. For the purpose of this study, i.e., the quantification of induced root reinforcement, it becomes very important to focus the attention on such a scale closer to the transplanted vegetation plot. For this reason in the area within the plot and nearby the plot, erosion - deposition output from Figure 3.5 have been averaged to produce an output re-sampled to a resolution of 2m x 2m, which is the plot dimension (see Section 2.6). Thus a unique value representative for the plot is available and so, the amount of soil scoured or deposited within the plot can be compared to the surrounding plot areas (where there are no root into the soil).

Figure 3.7 show the erosion or deposition balance, locally nearby vegetation plot, in 2009 and 2010 respectively. Locally, small aggradation may results, for instance in a supply of nutrient. Plants can therefore benefit, in this case of a small flood. However, for juvenile *Salix* shootings, deposition of layers thicker than 40 cm during a single event practically always resulted in a complete covering of the plot. It is the case of plots 9, 11 and 12 in 2009 (Figure 3.7). In 2010 plot 3, 4, 5 and 6 suffer high rate of cutting mortality or more in general damage (Figure 3.7).

When a plot, during the whole growing season, experienced more than 40 cm erosion, instead,

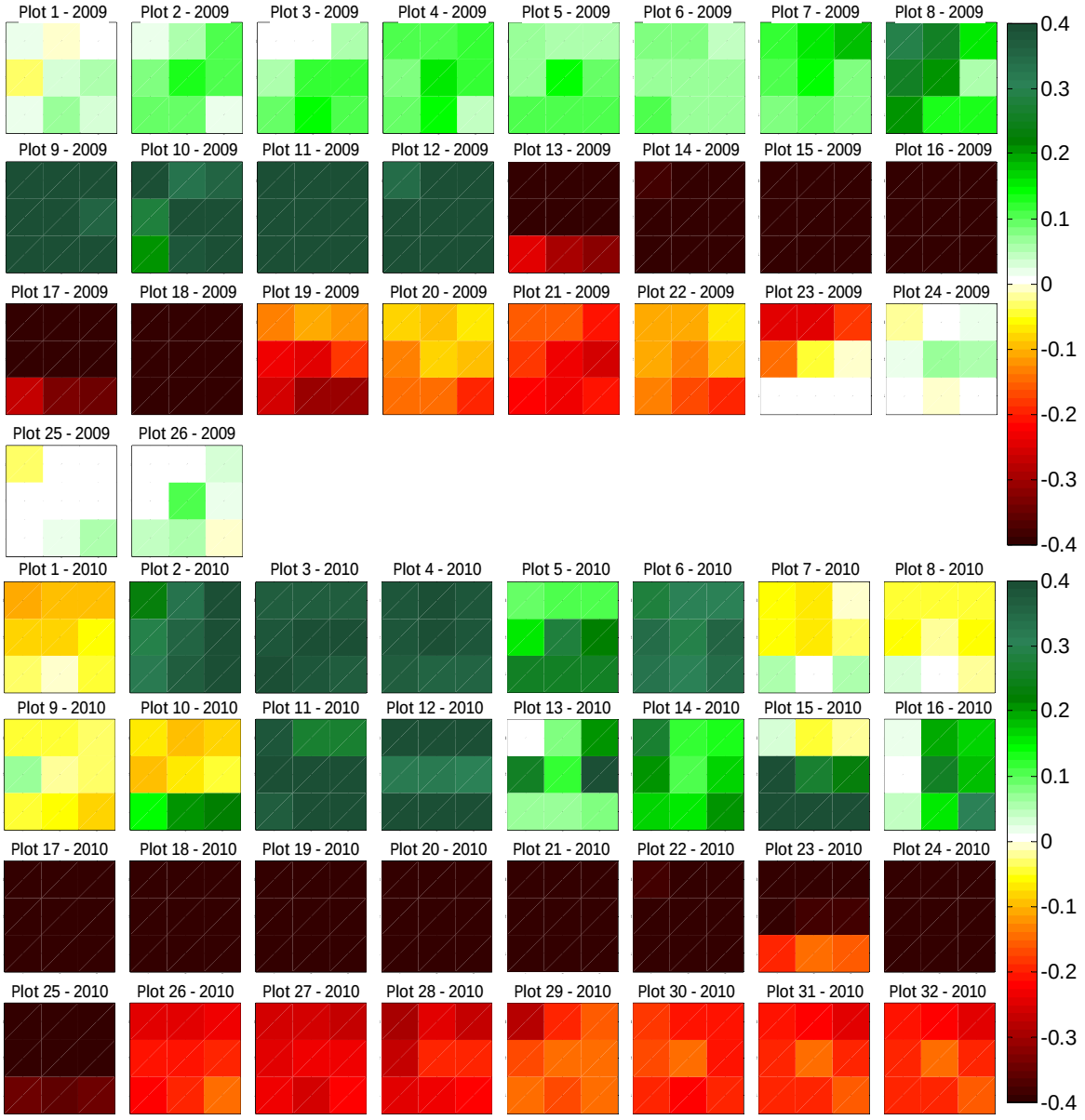

Figure 3.7: *Erosion deposition balance for plots in 2009 and 2010. Cells are 2m x 2m and vegetation plot is located in correspondence of the center cell. The interval is kept in the interval -0.4< Δz<0.4 m because the cutting length is about 40 cm. Scouring higher than 40 cm produce removal of the cutting whereas more than 40 cm of sediment deposition is often too much for cuttings to spread new shootings and stems.*

often all cuttings have been removed and flushed away by the same flood that provoked erosion or later events. It is the case of plots 13, 14, 15, 16, 17, 18 in 2009 (Figure 3.7) and plot 18, 19, 20, 21, 22 in 2010 (Figure 3.7). Figure 3.5 shows that many portion of the island experienced more than just 40 cm of scouring or aggradation. However, being somehow 40 cm the threshold of surviving for the transplanted plot at the Thur field site, both in Figure 3.7 the scale bar is set in the range $\pm$ 40 cm for a better graphical readability.

Plot mortality in relation to scouring or aggradation is further investigated in Chapter 4.3, where data hereby presented have been used for statistics and analysis on cuttings surviving and mortality influencing factors.

3.4 Effects of the restored morphological dynamics

Beside the morphological dynamics due to erosion and deposition phenomena, restoration of a more active fluvial dynamics, which had a broader impact on the river corridor.

Restoration allowed the natural formation of alternate bars and the formation of a diversity of habitats due to intense channel reworking with fast turnover rates. This attracted the scientific interest of ornithologists, ecologists, biologists, as well as the recreational sphere of local inhabitants also generating several studies, which have been carried out in order to assess the restoration success. A study of organic C dynamics in the Thur River floodplain by Samaritani et al. (2011) revealed that in the restored section characterised by low total organic carbon (TOC) contents and coarse-textured soils, frequent flood disturbance increased SR and the otherwise low base-levels of organic C pools. On the other hand, in the stable forested zone, the finer texture of the soils leads to higher TOC contents and water retention capacity, thus leading both to high base-levels of C pools. Results from Samaritani et al. (2011) show that the large range of soil properties and flooding frequencies in the gravel bars and willow covered riparian areas together with the high spatial heterogeneity of soil properties and environmental conditions, increased the spatial and temporal variability of organic C pool and fluxes in the restored section of the Thur River floodplain as compared to the channelized section. Together with the much higher plant biodiversity in the restored section, this suggests that restoration has led to a strong increase in functional diversity. These results support the recent findings of Wilson et al. (2011). This suggests that river restoration, in order to achieve maximum recovery of ecosystem functions, should aim at creating near-natural floodplains comprising both dynamic gravel bars and stable alluvial systems.

Bertrand et al 2012 studied a biomonitoring approach based on functional traits that may allow overcoming biogeographical limitations. They studied testate amoebae (TA) which are a polyphyletic group of free-living protozoa that play important roles in soil nutrient cycling and especially the cycles of C, N, and Si in soils (Aoki et al., 2007). Bertrand et al. (2012) report that *"TA produces shells that differ in their composition, size and shape. These morphological differences are believed to represent adaptations to the soil environment especially the soil moisture regime"*. At the Thur river field site contrasted patterns of TA density, diversity and functional traits have been found. Dissolved organic matter (DOM), including dissolved organic C and, is an important controlling factor for the ecological functioning of forest soils and

grasslands, as well as a major C source to mineral soils. The presence of vegetation, naturally or artificially grown after restoration influences directly the soil moisture through transpiration and the mineral N stock via plant root uptake.

The system evolution after restoration can be descrybed by conceptually integrating the information conveyed from different ecohydrologic indicators into a single system trajectory, showing how and toward which statistical equilibrium the restored system evolves to. To the purpose a technique from classic mechanics is here recall, known as the "state space" (e.g., Sprott, 2003).

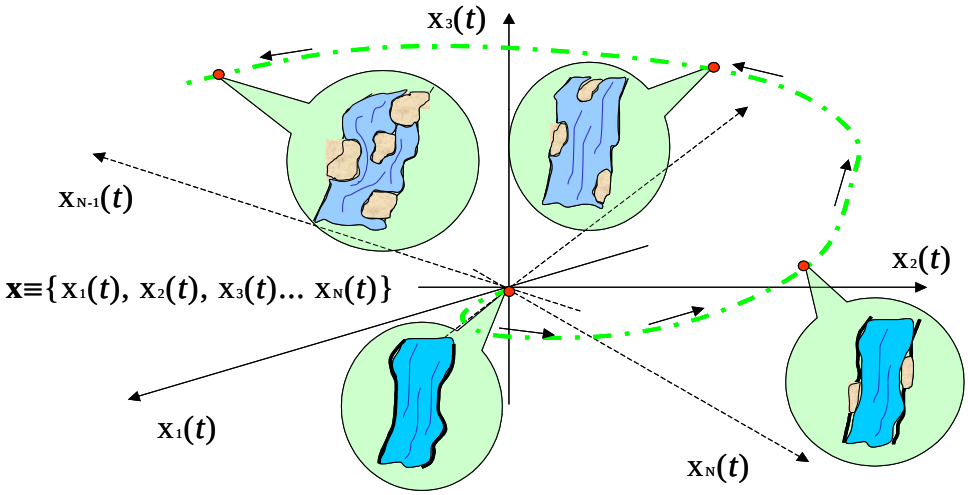

Figure 3.8: *Conceptual representation of the restored corridor evolution trajectory in the state space (left) assuming the variables* $x_1(t), x_2(t), x_3(t), ..., x_N(t)$ *as indicators representing the state of the system at successive time instants.*

The state space is a multidimensional space, the axis of which represent the evolution of the (theoretically) independent system variables in time. Time does not appear explicitly in this space in that it is now a parameter of the dynamics. The variables can be for instance flow velocity, water depth and the shoreline length for certain flow conditions. Considering the situation from when restoration starts, i.e. such as the case of the Thur River, and considering this as the initial state of the system, the river is in average straight as depicted in the exemplary panel of Figure 3.8. All state variables have average values and this state corresponds to a single point in the state space. Then, by means of restoration works (e.g., in the Thur case the lateral banks are made erodible) the system starts to evolve in subsequent times under the action of floods, which reshape the river reach through erosion and aggradation, possibly forming alternate bars. At this time the variables identify another point in the state space corresponding to the actual river configuration and the associated ecohydrologic variables. Gradually, restoration leads to an evolution with more complex eco-morphologies characterized

by different eco-hydrologic indicators, and possibly an accurate systematic monitoring allows identifying the related trajectory, as well as possible equilibrium (statistical) points (Argyris and Faust, 1994; Sprott, 2003).

Among the somewhat unexpected results of this restoration action there is the return of the "Little Ringed Plover". This bird species preferentially breeds on bare or poorly vegetated alluvial sediment, and it visited the restored site after nearly 150 years from its disappearance from the region, i.e., from the time when the correction took place. This shows that the new river morphodynamics can control, even after relatively short time since restoration measure took place, the establishment of bird species that abandoned the river corridor after its channelization.

Chapter 4

Vegetation cuttings growth: experiments and analysis

The purpose of this Chapter is to discuss quantitatively the characteristics of the above-ground and the below-ground biomass growth of a number of cuttings of *Salix*, which were transplanted on the frequently inundated alluvial sediment, in relation to the morphodynamic of the restored reach of the Thur river which was analyzed in the previous Chapter. A relationship to link stem length and root volume is also produced. Finally, the survival rate of vegetation is linked to the scouring and deposition of material on the bedforms due to floods.

4.1 Experimental set up

Data from repeated campaigns of cutting transplantation are not easily available in the literature. Hence, an experimental field campaign started in spring 2008, and was repeated in 2009 and 2010, as described in Section 2.6. Unfortunately, due to a big flood occured at the end of April 2008 (see Figure 2.15) for that year all cutting installations have been lost and a new transplantation campaign was not repeatable. Data from 2008 are consequently missing.

In this Chapter, spatial statistics of vegetation growth from both above- and below-ground biomass are derived and discussed in relation to sediment size distribution, nutrient availability and river hydrology. As hydrology represents the primary driving force for morphological and ecological processes in floodplains (Junk et al., 1989; Tockner and Stanford, 2002), the survival and growth rate mainly in relation to river hydrology and morphology is discussed.

Bed shear stress produced by the largest flood, for each year of field campaign, was simulated in order to quantify mechanical stress experienced by vegetation plots. Figure 3.6 shows how, for each of the three field campaigns, plot mortality is strongly related to the magnitude of shear

stress. The evidence of a positive relation between plot mortality and magnitude of bed shear stress leads to the need of analysing the probability of vegetation establishment and surviving in relation to river morphodynamic processes, such as erosion and deposition.

Quantitative observation of cuttings collected during monitoring campaigns together with aerial photographs have allowed quantifying vegetation plots growth (or mortality) rates in relation to the natural river hydrologic regime.

In order to clarify the meaning the results shown in this Chapter, here Figure 4.1 is commented, which shows a representative data set of four plots in 2009. (Pasquale et al., 2011) define *potential* growth as the average cutting length of each plot computed by excluding the death ones and *effective* growth as the average cutting length of the whole including damaged, removed or died plants. This definition of growth average allows considering that a damaged biomass may indeed have single branches (i.e., cuttings in this case) growing at the effective rate despite the biomass has decreased.

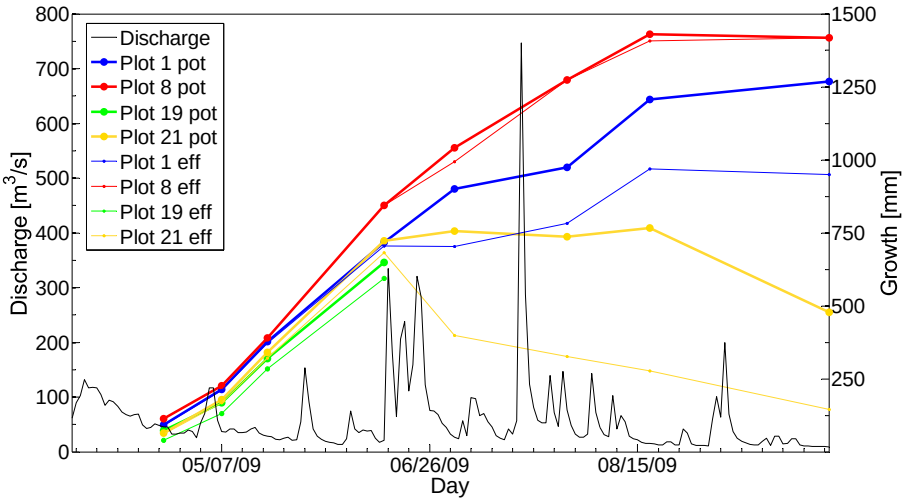

Figure 4.1: *Example of correlation between vegetation mortality and highly impulsive natural floods. Plot located at higher elevations (1 and 8) are less frequently inundated and experience also less stresses during floods. Their growth is therefore almost linear and monotonic during the whole season. The effect of inundation is more evident on plot 21 sited at a lower elevation. In the period of the three consecutive peaks in June we register a negative growth for plot 21 (stems are broken). The same three floods cause the complete removal of all plot 19 cuttings, the one at the lowest elevation. Thicker lines represent the potential growth whereas thin lines are the effective growth. Effective growth is always smaller than the potential and shows more evidently flood effects.*

From Figure 4.1 it is evident that Plot 1 and plot 8 are located at high elevation on a portion of the island less frequently inundated. Accordingly, they have experienced a much lower velocity and shear stress intensity, so that their potential and effective growth has been practically

monotonic. On the contrary, plot 19, located at really low elevation, has been removed by the first big flood in June 2009. This is not surprising, as the location of this plot is characterized by much higher frequency and duration of inundation (it is inundated for all floods higher than 50 m^3/s). Compared to such two extreme situations, plot 21 (located at intermediate elevation) shows that, on average, it survives the season despite some plants are either partially damaged or died due to main floods, in June and July 2009. It is worth to note that, after the first flood has affected the plot, the potential growth is always higher than the effective one. Thus, the more the two curves differ, the more the plots are expected to be located at lower and more flood risk prone elevations.

4.2 Cutting Growth Statistics

4.2.1 Above ground biomass: surviving, growth and growth rate

The periodic monitoring of the main stem length and of the cutting survival produced a spatially (i.e., over the plot) and temporally (i.e., through the season) very detailed set of data on *Salix* establishment. Figure 4.2 shows the growth of the single cuttings within two representative plots throughout the season, in 2009 and 2010. The coloured squares in each matrix represent individual cutting lengths recorded the day of monitoring. White squares indicate cuttings that did no re-sprout or which have died. The number of white squares increases, usually, after a flood event, indicating flood-induced mortality.

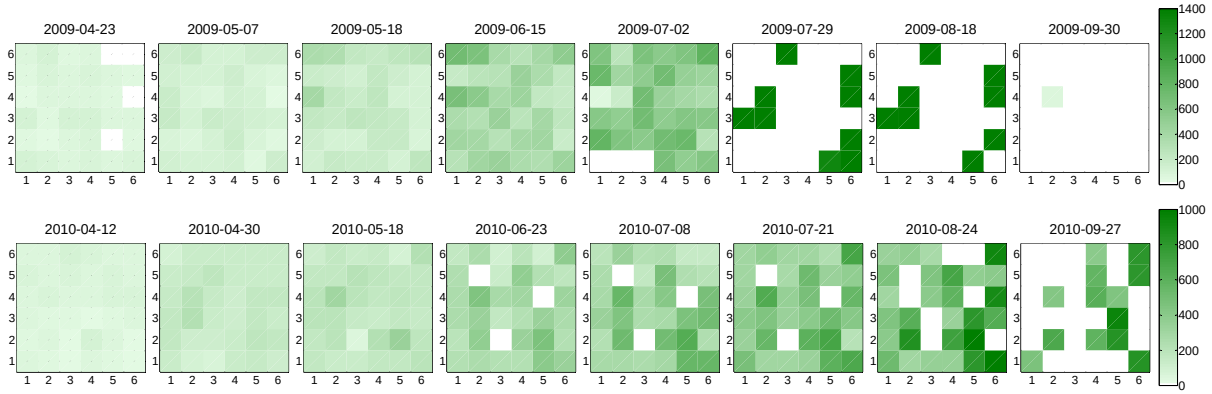

Figure 4.2: *Cuttings growth (in mm) within a representative plot in 2009 (a) and 2010 (b) throughout the corresponding season. Cutting length has been measured periodically during the growing season, each year. For Each plot the single cutting growth and survival is later counted to compute average growth, growth rate and survival. Along the season, several cuttings disappear from the plot. White spots represent dead cuttings. The main source of mortality is represented by flood events.*

With the purpose of obtaining representative statistics at a larger scale, the number of white squares in the matrix (i.e., dead cuttings) is used to compute cutting mortality or inversely, cutting surviving rate. Three weeks after planting the monitoring campaign of Salix growth on the gravel bar started, mainly by measuring the length of the highest stem of every cutting for all the plots. A measure of growth (what Pasquale et al. (2011) call *effective growth*) per plot was obtained by calculating the average stem length of the surviving cuttings at each monitoring period. Results are shown in Figure 4.3.
Observation on the growth of more than 1000 Salicaceae seedlings in their first year of growth (approximately 19 weeks after germination) on the Tagliamento River in 2004 (Moggridge, 2007) showed that around 96% of the seedlings had a simple single stem structure, shown by the similarity between the longest stem length and the total stem length(Schnauder and Moggridge, 2009). For this reason, in the contest of the experiments carried out in this work, the measure of the main stem length is meant to be representative of the above-ground biomass. During the first two months of the 2009 campaign a fast growing is observed. This trend slows down a little following the large flood in June and July. Many plants were seriously damaged, cut or broken by the power of the flow. In 2009, the growing increases again in August, aided in this year by the absence of serious floods and higher temperatures. In contrast, in 2010, prolonged and repeated flood events in August were responsible for further strong disturbances, and consequently higher mortality and reduced plant growth (Figure 4.3).

The variance of the stem length increases very much proceeding with growing season until the final monitoring. This can be explained by the fact that the initial dimension (size and diameter) of the transplanted cuttings influences their initial growth (Hartman and Kester, 1975). Also the location of the plots on the bar was important. Plots closer to the water and therefore more frequently inundated suffered more stresses, whereas the ones further from the water suffered a lack of water during dry periods. The success of establishment depends on the relative elevation of the plots (as it relates to depth to water table and frequency of inundation or flow disturbance) and with sediment size distribution (as it relates to permeability and hydraulic conductivity). The average length reached by the longest stem spread by cuttings was about 1 m, with peaks of 1.80 m, which are measurements generally in accordance with those reported by Glenz et al. (2006) and by Moggridge (2007).

The survival of the Salix cuttings in both 2009 and 2010 was very high until the end of June (Figure 4.3). The explanation for the apparent 'increase' of the survival rate during the first two months is that some of the cuttings that had been covered by sediment started shooting from below the sediment. Salix seeds can germinate in darkness (Farmer and Bonner, 1967), therefore, it seems comprehensible that they can also start shooting below the sediments. Some other cuttings started sprouting only with a small delay.

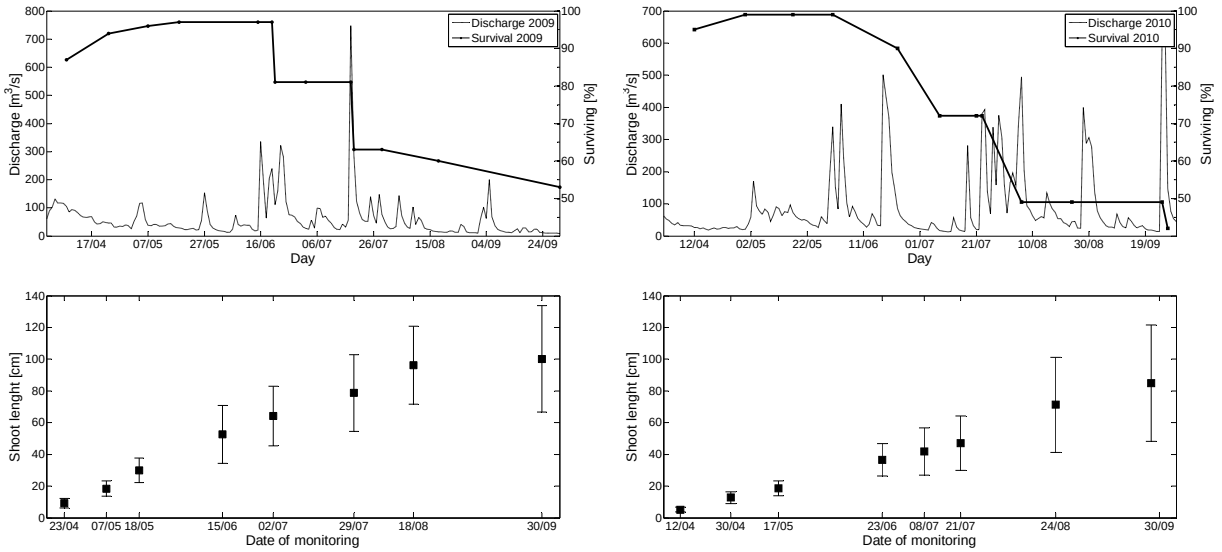

Figure 4.3: *Survival of the cuttings and hydrogram of the river (upper frames). At the beginning, after transplantation there is an increasing because some cuttings take more time than others to spread branches. The curve decreases dramatically in correspondence of the two main floods registered. Flood and large events represent the main cause of death for vegetation growing on gravel bars and islands. Growth curve of biomass during the growing season from April, when cuttings were planted, to the end of September (lower frames).*

In 2009 two large floods on June, 16^{th} and 23^{rd}, led to considerable erosion along the edge of the island and changed its shape considerably. During the first flood no cuttings were uprooted and carried away, but some were bent, and of some roots exposed and branches broken. However, on the 2^{nd} of July after the second flood many cuttings had been carried away or were completely uprooted and dying or covered by debris wood. The survival ranged from 87 percent (1030 plants) when first monitored in April 2009 to 97 percent on June 15^{th} and 81 percent on the 2^{nd} of July (Figure 4.3). On the 18th of July a large flood inundated the island, the river banks and the riparian forest. The island morphology was sensitively reshaped during this flood. All the plots sited nearby the main channel were completely removed because of the high erosion rate there (higher water depth, higher velocity and higher shear stress during the flood). Downstream on the island surface there was a lot of sediment deposition (about one meter of coarse sediment). The survivorship of cuttings is visible in Figure 4.3, represented by the second negative peak. The survival after the flood in July was 63 percent (730 plants) and only 53 percent (603 plants) at the end of the monitoring season in October.

In 2010, two large floods, a double peak between June 1^{st} and 3^{rd}, and a 500 m^3/s on June 18th, caused large damage to all cuttings (Figure 4.3). At this growth stage, stem shootings are, for a large part, still not woody but rather green and soft. Such sizeable floods can destroy most of the juvenile shootings. Unfortunately, due to the presence of protected birds breeding

on the bar between the two events, it was not possible to access the island to monitor growth and damage. Survival rate decreases from a 99 percent at the end of May to 90 percent at the end of June. Two weeks later (July, 8^{th}) only 78 percent of the plants are still alive. Many cuttings, despite still being alive after the floods, suffered too severe damage and died later.

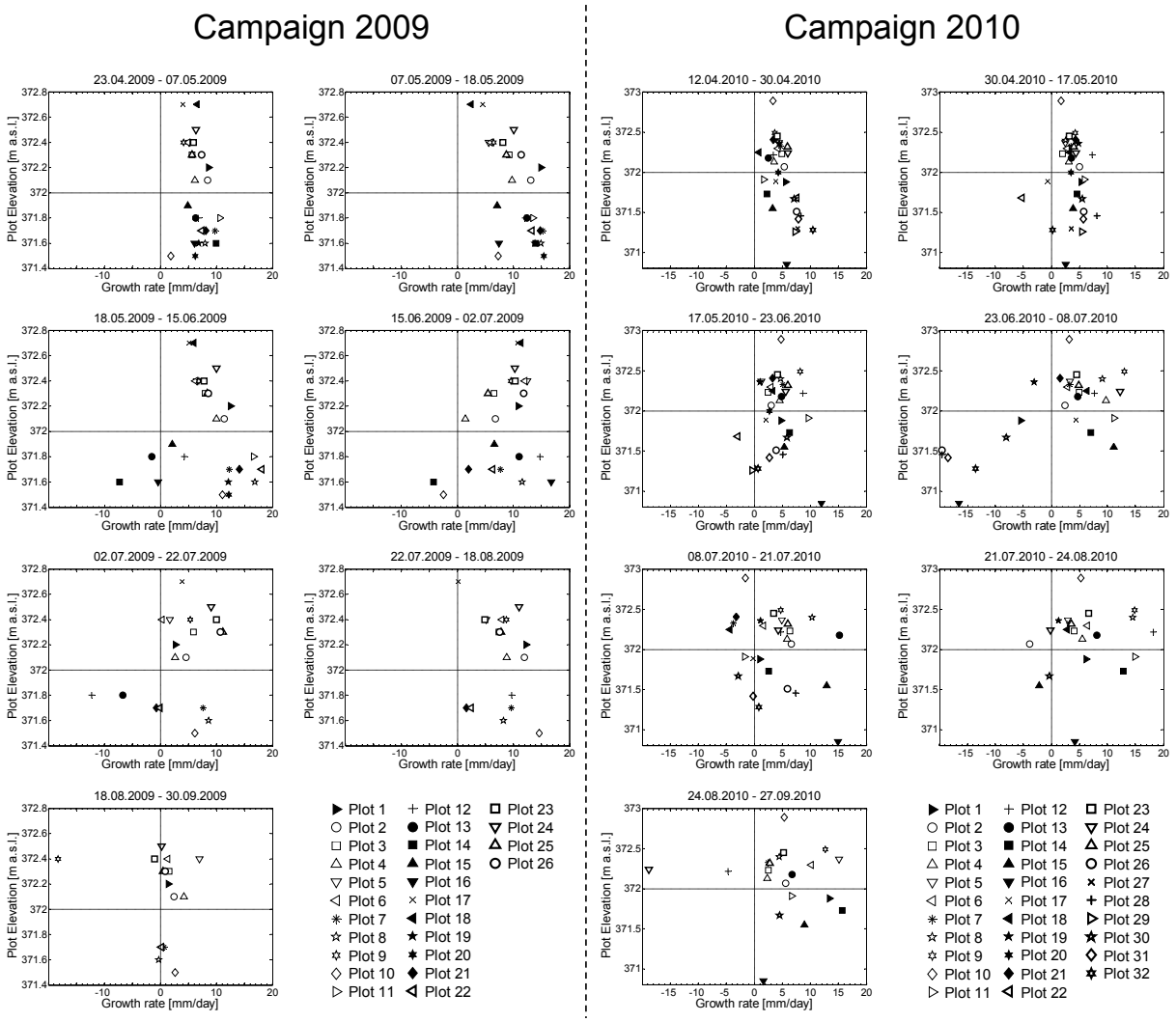

Figure 4.4: *Growth rate (cm/day), computed as average of the single cuttings, for each plot is reported. At early stage all plots have a positive growth rate. Along with the season plots experiencing more flood disturbance show a negative growth rate. In this case the severe damage produced by the flood on the above-ground biomass is greater than growing.*

Plant suffering is visible also in Figure 4.4. The second row of Campaign 2010 shows a negative growth rate for many plots between June and early July. Compared to beginning of July 2009, when the average cutting growth was 64 cm, in the same period of 2010 the average cutting growth was only 42 cm. Between July 18^{th} and August 8^{th}, 2010, five consequent floods up

to 490 m^3/s inundated the island and the river banks. All cuttings sited near to the main channel were fatally damaged or broken, and plots 18 to 21 completely removed because of the severe scouring. The high mortality for the plots is visible in Figure 3.6.c (black dots), and the survivorship of cuttings is visible in Figure 4.3, represented by the second fall in the surviving rate, from 78 percent (early July) to 49 percent by the middle of August. Average growth, on August 18^{th}, 2010 was only 71 cm compared to 96 cm in the same period of 2009. At the end of 2010 the average growth over the survived cutting on the island was 92 cm (in 2009 it was 100 cm) and the survival rate 42 percent.

The survivorship of *Salix* cuttings, was very high compared to the information available in literature, even in 2010, when cuttings experienced intense hydrological disturbance. Francis and Gurnell (2006), after long investigation on the River Tagliamento (Italy) reported that where riparian restoration involves the planting of cuttings along rivers that are climatically comparable to the River Tagliamento, at least 20 percent survivorship can be achieved with 40 cm cuttings in substrates with low moisture and organic matter, suggesting that these pioneer species would be a good choice for planting on newly-created substrates.

Figure 4.4 shows the growth rate recorded between each monitoring point related to plot elevation in a quite peculiar way. At the beginning there is a positive and more or less similar growth rate for all plots of about 5 - 10 mm/day (Figure 4.4). Figure 4.4 show that after May, there is a progressive scattering of the plot growth rate for those plots located at an elevation lower than 372 m AMSL. Plots below this elevation experience also very often a negative growth rate and they are more affected by mortality (shown as missing squares below the threshold in Figure 4.4). The elevation of 372 m AMSL is a sort of threshold for this specific test site. This elevation corresponds to the water level reached in correspondence of the island for a streamflow of 75 m^3/s which in average lingers on for 310 day/year. This further indicates that plots experiencing greater levels of inundation are those that experience greater mortality and reduced growth. This evidence is clearer in 2009 than in 2010. The abundance and the repetition of flood events in 2010 is indeed a strong source of disturbance that may obscure this trend.

4.2.2 Below ground biomass

The first few months of growth are the period during which adventitious roots seek to make contact with the water table (many riparian trees are obligate phreatophytes relying on ground water to survive). Therefore the early growth stage object of this analysis corresponds to the period when hydrology plays the strongest effect on root development.

Besides the total root length, the average root diameter and the total root volume we also refer

to specific indexes in order to have more representative and comparable results. Therefore the Root Volume Ratio (RVR) and the Root Length Density (RLD) are introduced, which relate root length and volume to the soil matrix volume in which they are sampled. Root volume and length are spatially averaged and non-dimensionalized to a specific volume as follows: first, for one plot, the average length (or volume) obtained from the sampled cuttings is multiplied by the number of cuttings within the plot. Hence, the total root length (or volume) representative of that plot is given; second, the above obtained length (or volume) is divided by the soil matrix volume in which the plot is contained. For the RVR, also the volume of the original cutting is added to the output volume given by WinRhizo. An average cutting 40 cm long and with a diameter of 1.2 cm is considered. The reference soil volume of the plot is computed considering a 2m x 2m surface area times 60 cm of depth. Although the cutting length is only 40 cm, here we consider that root system might have grown to a notable depth, as is common, to reach soil moisture or water table (Francis et al., 2005).

Results of the analysis and the two index, RVR and RLD, produced in this way for 2009 and 2010 are shown in Figure 4.5. Both RLD and RVR were much higher at the end of season 2009 than 2010. In any case, the RVR is relatively low, even in September, mainly due to the young growth stage of the plants. The total growth time, at the end of September was only six months. The RVR at the end of September 2009 was 0.15 %. Instead, in September 2010 the same ratio was 0.09 %, only 60 percent of the value recorded the previous year.

Air (T_a) and water (T_w) temperature have been recorded at the field site during the growing season 2009 and 2010 (Figure 4.6). Water temperature is nearly in phase with air temperature, through the season. During the first two months the two years recorded differences in the average temperatures, higher in 2009 ($T_{a,\mathrm{April09}} = 13.2^\circ$ C and $T_{a,\mathrm{May09}} = 18.9^\circ$ C) than in 2010 ($T_{a,\mathrm{April10}} = 11.6^\circ$ C and $T_{a,\mathrm{May10}} = 18.1^\circ$ C). Looking at the period August - September, in 2009 the temperature was $T_{a,\mathrm{Aug.09}} = 20.8^\circ$ C and $T_{a,\mathrm{Sept.09}} = 18.6^\circ$ C, whereas in 2010 was much lower: $T_{a,\mathrm{Aug.10}} = 19.6^\circ$ C and $T_{a,\mathrm{Sept.10}} = 15.9^\circ$ C. Generally higher temperature brings a greater level of physiological plant activity, above all in terms of photosynthesis and consequently biomass production of both shoots and roots. This fact can only explain in part, the lower growth of the below-ground biomass in 2009. Therefore, another important external force has to be considered. As previously mentioned, in 2010, cuttings experienced a more frequent flood disturbance activity. The resources available to the plants (sun light, water, nutrients, etc...) have likely been used to re-sprout following inundation, or producing adventitious roots in order to better survive the continuous hydrological disturbance. This might have produced a lack of resources for root structure and biomass. This is also supported by the fact that water volume from April to the end of September 2010 ($9.5 \cdot 10^8$) was 39 % higher than that in 2009 ($6.8 \cdot 10^8$), implying an average higher water level (and therefore higher water table) and easier water availability for root uptake during the season.

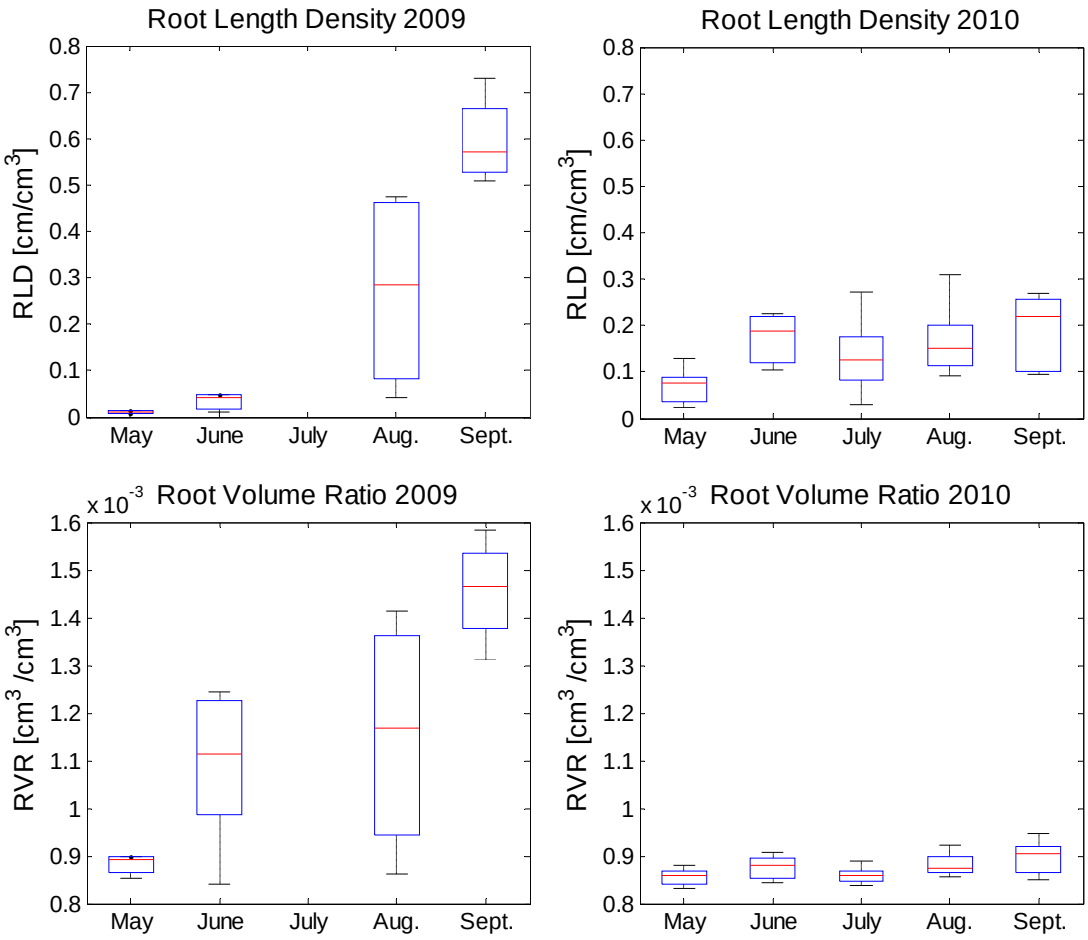

Figure 4.5: *Root length density (RLD) and root volume ration (RVR) relative to 2009 and 2010 field campaign. Values refer to the plot average. Each year, for each monitoring results of sampling analysis is spatially averaged in order to produce a unique representative length or volume for the island. Therefore, RVR and RLD hereby reported do not take into account the different hydrological stresses experienced by plot located in different position.*

The large variance in the RVR of August 2009, in respect with other samples in 2009 may be explained by the fact that one of the plots that sample cuttings were uprooted from had experienced a lot of scouring due to the flood in July. On the contrary, plot 8, for the same year recorded a growth much above the average. Moreover, as for the above ground biomass, the greater the below-ground biomass growth, the larger the expected variance is. This is confirmed by the general increase of variance through the season in 2009. Looking at the variance of the RVR, in 2010, the order of magnitude remains more or less the same, and comparable to the one in May 2009, that has the same average value. Another non-negligible factor that surely influences the goodness of the analysis is the sampling operation on the field. This operation has been carried out as much accurate as possible. The last factor which

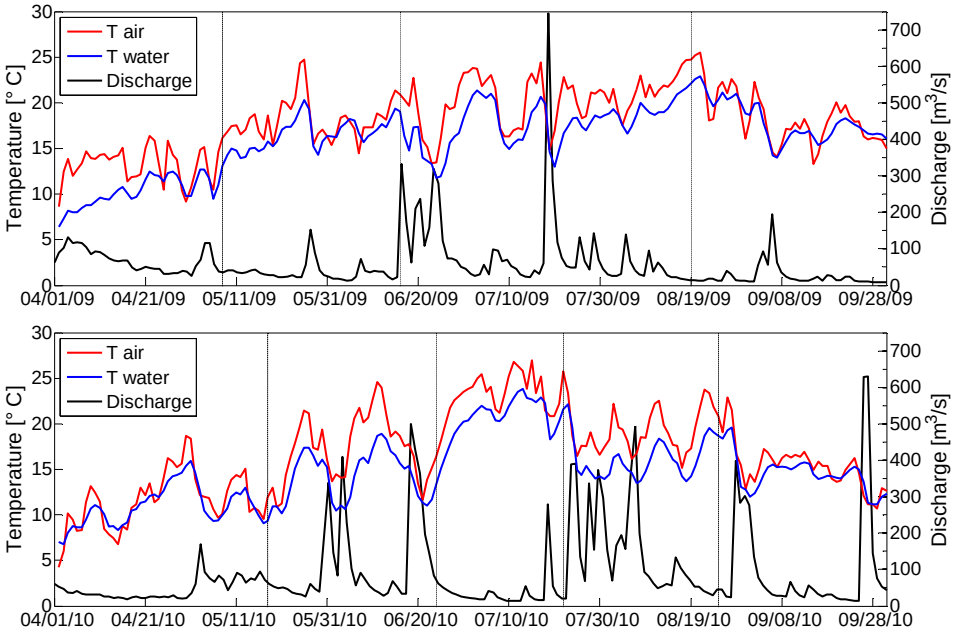

Figure 4.6: *Discharge, air temperature and water temperature recorded at the Thur river field site for the growing season (April - September) 2009 (upper frame) and 2010 (lower frame).*

might explain the higher variance of 2009 in respect with 2010 is hydrology. 2009 was a much warmer and dryer year than 2010, and may have resulted in a generally lower water level and less precipitation. Plots located closer to the water table and yet not in areas affected by erosion and high dragging forces might have benefitted a lot, in comparison with plots installed at higher relative elevations (i.e., more distant from the water table), even though those plots may be less disturbed by floods.

This might be important for an estimation of root reinforcement of the river bed. However in Figure 4.5 no information is available concerning the distribution of the root volume with depth. Root vertical distribution has a lot of implications regarding uprooting resistance as further discussed in Section 4.3 and detailed in Chapter 5. Chapter 5 shows that, according to hydrological forcing, there might be a vertical root redistribution during the growing season. In order to better face external stresses, the plants reorganize the root system according to hydrotropism or oxytropism (Pasquale et al., 2012a).

4.2.3 Link between above- and below-ground biomass

Root analysis is a complicated, time consuming and expensive activity requiring an accurate planning of the field campaign for monitoring and sampling with the risk that unpredictable

flood may thwart an entire year of measurements. Moreover, while sampling requires time and man power, laboratory analysis may become very expensive. Prediction of root biomass from above-ground measurements would therefore be useful in order to save time and man power when repeated analyses have to be don both in space and time.

For these reasons, an analysis with the purpose of linking above- and below-ground biomass, based on field data has been carried out. A classical literature measure focuses at the ratio between the dry below and above ground biomass. However, in our environment the presence of beavers frequently chewing the lowest branches of the cuttings would eventually make this measure not necessarily meaningful. Hence, we preferred to look for correlations between the length of the main stem and the root volume.

The best fitting equation was found to be a power law in the form: $y = ax^b$. Results of the regression analysis are shown in Figure 2.10. Data from all samples in 2009 give quite good results: $R^2_{adj} = 0.74$ (a). Root volume in 2010 was significantly lower in respect to 2009, whereas the stem growth is more similar for the two years. These unbalanced data produce a regression with a lower $R^2_{adj} = 0.53$ (b). Frame c) shows the regression analysis month-to-month for 2009-10 and the regression from the two years together. The last case, probably the more physically meaningful, considering that it takes into account more all data from the two field campaing, gives $R^2_{adj} = 0.65$. Regression coefficients together with the RMSE and the coefficients of determination R^2_{adj} are reported in Table 4.1.

Once measured the stem length on a field site, one may use those regression coefficient to derive root volume according to his needs. For cuttings that experienced a full rowing season the best regression would be the one considering all data from 2009 and 2010 field campaign. Using this linking model, particular attention has to be paid regarding the variation that can be generally expected in growth rates.

Case	Frame (line color)	Regression Type (equation)	Coefficients (95%) a	b	R^2_{adj} [-]	RMSE [cm]
Vr, Ls - 2009	a) -----	Power law: $y = a \cdot x^b$	15.66	0.5404	0.7405	23.781
Vr, Ls - 2010	b) -----	Power law: $y = a \cdot x^b$	18.05	0.7598	0.5485	20.355
Vr, Ls - may	c) ------	Power law: $y = a \cdot x^b$	15.59	0.2681	0.1830	4.344
Vr, Ls - june	c) ------	Power law: $y = a \cdot x^b$	27.1	0.2187	0.3250	12.520
Vr, Ls - aug.	c) ------	Power law: $y = a \cdot x^b$	31.05	0.3991	0.6903	20.038
Vr, Ls - sept.	c) ------	Power law: $y = a \cdot x^b$	60.94	0.1802	0.3950	22.899
Vr, Ls	c) -----	Power law: $y = a \cdot x^b$	26.02	0.3959	0.6499	22.633

Table 4.1: *Coefficients and index of goodness resulting from the regression analysis between root volume and stem length. The regression equation better fitting the input data, in all cases, is a power law of the type:* $y = a \cdot x^b$.

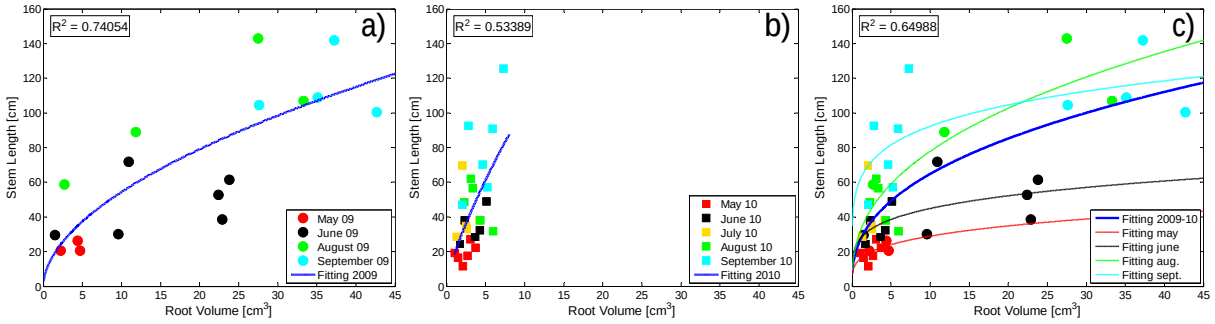

Figure 4.7: *Regression analysis linking the main stem length [cm] to the root volume [cm^3]. Regression coefficients are reported in Table 4.1.*

4.3 Survival rate in relation to morphodynamic processes

From differentiating successive DTMs, evident signatures of the reach morphodynamic after restoration emerge. At a rather local scale, patterns of erosion and deposition can be well identified (Figure 3.5). At the reach scale, such patterns clarify the symptomatic trend of the gravel bar to establish on the right hand side of the river bank.
Based on locations, plots are divided in two groups: those situated in an erosion zone and those located in a deposition zone (see Figure 3.5, where red shading stands for eroded area and green for areas with aggradation). Plots are also divided into those which survived and died. All dead plots from field campaign 2008, 2009 and 2010 are combined together as a function of the scouring - deposition rate. The outcomes of this analysis are presented in Figure 4.8. On the left side of the y-axis are the values of erosion zones; on the right are deposition zones. Erosion or deposition value is an independent variable and the number of plots and total percentage of surviving and dead at same range are the dependent variables. The independent variables are categorized into a range of 10 cm difference of height values; hence the range starts from 0-10 cm, 10-20 cm, 20-30 cm, and so on.

Plot mortality is asymmetric, thus the minimum is found for relatively low deposition rates. Up to 30 cm of aggradation (over the whole season), mortality recorded during the three years is in the interval 17÷23 percent (Figure 4.8.a). When the deposited layer exceeds 30 cm mortality rate increases dramatically and where there was aggradation of material higher than 50 cm, practically no plot survived. Figure 4.8.a shows that *Salix* plots are more sensitive to erosion than deposition. Plots located in the erosion class 0-10 cm already show 40 percent of mortality. When erosion is in the range 10-20 cm mortality increases to 65 percent and remains constant up to 40-50 cm of scouring. Where erosion higher than 50 cm was recorded,

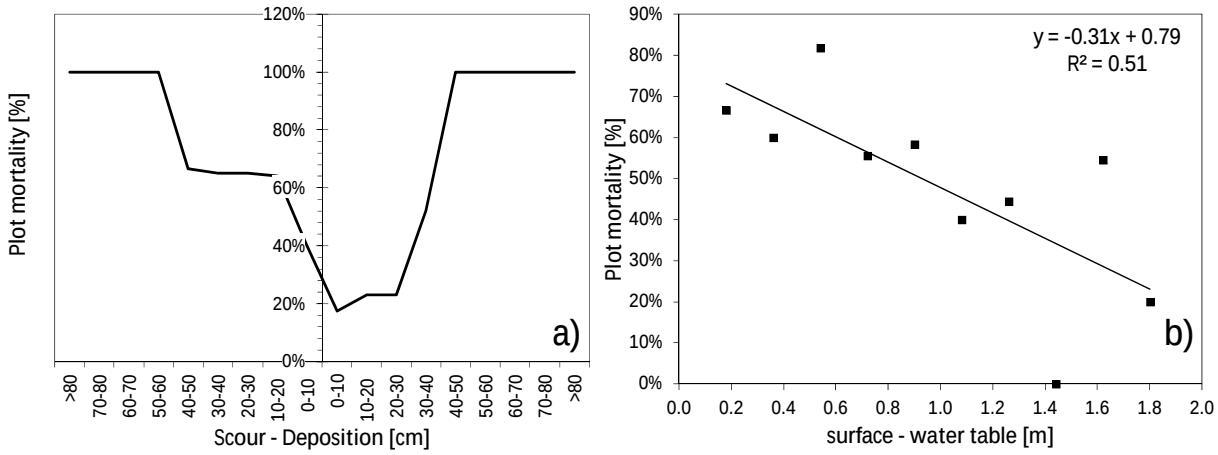

Figure 4.8: *Plot mortality (expressed as percentage) in relation to class of scouring and deposition (a). Plot more frequently inundated are exposed to higher disturbance and consequently experience higher mortality. A higher inundation frequency is expressed as relative distance from the mode of the water table (b).*

practically no plot survived. As the cutting length was 40 cm, higher scouring is likely to remove all the substrate surrounding the majority of th cutting, and cuttings are consequently flushed away by the flow. According to Edmaier et al. (2011), where plots experience erosion, plot mortality may be described as erosion Type II. Type II is a combination of local sediment erosion around the plant decreasing the anchoring force, until drag force prevails and, as such, it is a delayed mechanism possibly requiring multiple events before actual uprooting takes place.

Figure 4.8.b shows the relation between plot mortality and plot relative distance from the mode of the water table. Plot mortality is computed as percent of plots (relative frequency) located at the same distance from the mode of water table. The mode of the water table is computed on the basis of an empirical histogram of water table elevation frequency (see Pasquale et al. (2012a) for further details). In the case study, for the field site at the restored corridor of the Thur river, the mode of the water table corresponds to the water table elevation given by a steady river flow of 20 m^3/s. The general trend shows that the further the plots distance from the water table, the lower the plot mortality. This result suggests that plots located at higher relative elevation (i.e., those inundated less frequently) have more chance of surviving. This result supports the theory that floods are the major disturbance for *Salix* establishing on fluvial landforms and is in accordance with Bendix and Hupp (2000). While Figure 4.8.a gives information concerning surviving and mortality only as a function of erosion and deposition, 4.8.b contains also information about river hydrology (elevation of the water table). This result has to be interpreted considering the vertical root distribution too. As shown by Pasquale et al. (2012a) the relative distance between plot surface elevation and water table leads to different vertical distribution. The skew of the distribution may have implication on uprooting resistance

or even on root reinforcement of soil.

Pasquale et al. (2012a) synthetically illustrates how cutting surviving is influenced by river hydrology. On the basis of that work, linking root vertical distribution and hydrologic regime, a conceptual model is here proposed that considers two opposite cases: the first case refers to a cutting located very close to the water table and therefore also more frequently inundated. In Figure 4.8.b this cutting would be located on the left site of the chart. The second case refers to a cutting located far from the water table (Figure 5.4.b) which therefore would be located on the right side of the chart in 4.8.b. This cutting is also less frequently inundated.

According to Pasquale et al. (2012a), cuttings more frequently inundated develop a root system closer to the soil surface driven by oxytropism. Those cuttings are more resistant to erosion forces at the beginning of plant regeneration. However, removal of the more superficial material leaves the majority of cutting roots exposed and greatly increased risk of mortality. In the case of cuttings that are less frequently inundated, Pasquale et al. (2012a) suggest that roots grow more towards the cutting bottom driven by hydrotropism. In this case plants first take advantage of the less frequent disturbance represented by flooding and secondly, even when the cuttings experience a high erosion rate, they still have a good chances to survive as the majority of the root system maintains access to water and nutrients. Hence, classic return time theory for floods should be corrected in order to account for such a growing strategy if plant uprooting by floods has to be analyzed in relation to flow disturbances statistics. Figure 4.10 shows the frequency and duration curves for the river Thur. From this chart, it comes that plot transplantation on the island should be avoided in those area inundate by floods lower than 100 m^3/s, since in this case the flood duration would be always longer than one day.

Obtaining good survivorship is particularly important in restoration activities involving cuttings. Planting should not be at extremes of elevation to avoid sites prone to extreme drought conditions or to prolonged inundation and fluvial scour. If engineering is taking place before the restoration effort, attempts should be made to provide a range of sediment types, particularly with abundant coarser gravel-sized sediments where possible, to maximize cutting survivorship (Francis and Gurnell, 2006).

Bendix and Hupp (2000) note that floods play at least a three-fold role in the establishment and survival of riparian plants. First, most riparian plants germinate in alluvium that is deposited during floods. Fresh deposits provide sites for colonization, and the energy conditions of the floods determine the texture of the new substrate. Second, floods may create colonization sites by destroying pre-existing vegetation. Third, the occurrence or lack of floods subsequent to germination may determinate whether seedlings survive maturity. In some cases, floods may also play a significant role in dispersing propagules to colonization sites. Hydrological impacts that may influence survival include mechanical damage, saturation and propagule transport.

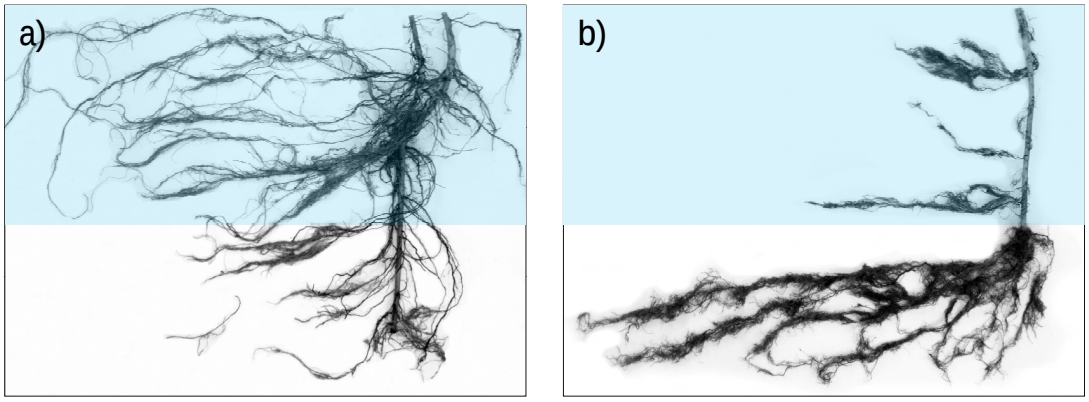

Figure 4.9: *Consequences of the different root distribution due to hydrotropism or oxytropism (Pasquale et al., 2012a) on cutting surviving. The same amount of eroded material leads to cutting death (a) when root distribution is close to the surface. The opposite situation when root are concentrated at the cutting bottom (b). The deeper root system gives the cutting still good chances to survive. (a) and (b) show two examples of cuttings (only below-ground biomass) uprooted for RVR and RLD analysis and for root vertical distribution analysis carried out in Pasquale et al. (2012a).*

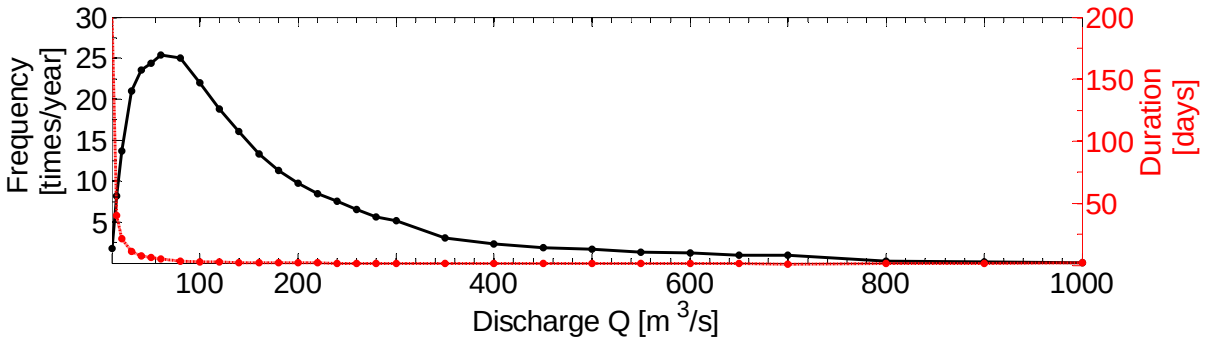

Figure 4.10: *Flood frequency and duration curves computed on the basis of 12 years (1999-2010) daily records for the field site at the Thur River. The mean yearly discharge (47 m^3/s) occurs about 23 times per year for a total duration of nearly 140 days. A discharge double than the mean ($Q = 100$ m^3/s) has a frequency of 25 times per year and a duration of 170 days.*

Geomorphological impacts involve the destruction and creation of substrate through erosion and deposition processes. Plants may be broken (often resulting in mortality) by the force of floodwaters, or by the impact of floating debris. They may be killed by prolonged saturation of the root zone. They also may be destroyed by the erosion of the substrate in which they are rooted (Bendix and Hupp, 2000).

Analysis and data shown in this chapter support the thesis that hydrological time scales strongly influence vegetation establishment first and subsequently growth (Crouzy and Perona, 2012;

Perona et al., 2012). Root growth, in terms of RVR and RLD support the analysis on vertical root distribution of Pasquale et al. (2012a) who have shown that hydrotropism and oxytropism are important in driving root growth and distribution.

As reported by Karrenberg et al. (2002), in order to overcome inundation during the growing season, *Salix* allocates investments from propagation to survival. However, hydraulic stress and burial of sediments have stronger effects on other woody and herbaceous species and therefore they create bare substrates that are highly favourable for the establishment of Salicaceae. In general this shows the high plasticity of response found in *Salix* species.

Based on results shown before, in order to reach the highest surviving rate of the transplanted cuttings one would have to locate vegetation plots where bed changes are not expected to be significant. More, the relative elevation of the plot must not be too low, and therefore too frequently exposed to inundation, but at the same time not to high, in order to guarantee water availability for root uptake (see Figure 4.8). Considering cutting transplantation and pioneer vegetation establishment as a tool for restoration projects, the results shown in this chapter represent an important and useful step toward assessing the success of future operation of river re-naturalization and stabilization of river forms using vegetation as *river engineer*.

Chapter 5

Effects of streamflow variability on the root system evolution

In Chapter 4 the analysis of above- and below-ground vegetation growth and surviving in relation to river hydrology and aggradation-sedimentation was shown. The next step to study the root anchoring mechanism and the root contribute to soil reinforcement is the analysis of the root vertical profile. This chapter analyses the effects of river hydrology, and in particular the water table, on root architecture and on the vertical root distribution. The experimental evidence suggests the existence of a scaling relationship between the root density and the water table.

5.1 River hydrology

Salix is rather sensitive to prolonged droughts, but at the same time it is able to withstand long periods of submergence (Glenz, 2005; Glenz et al., 2006). In the experiments carried out, the transplanted plots are spread on the island, so that they may have experienced both situations depending on river hydrology. However, long periods of submergence may be associated with larger floods that can induce erosion and uprooting. For a given above-ground canopy, cutting resistance to floods will eventually depend on the root architecture, which in turn is also the result of river hydrology.

Figure D.3 (Appendix D) shows the effect of a flood on a plot in 2009, documenting the survival of the plot despite the deep scouring of sediments around the cutting, which has also partially exposed the roots. Although this picture reflects a situation quite often observed in natural systems, it is quite difficult to obtain in controlled experimental field campaigns. This partial erosion depicts the type II mechanism of rooted sediment erosion dynamics conceptualized by

Edmaier et al. (2011) and suggests the nonlinear role that root architecture plays in locally stabilizing and anchoring the sediment.

While in this contest it is recognized that more experimental observations are necessary to understand rooted sediment erosion dynamics, this first set of experiments has allowed us to carry out some preliminary investigation. First, it has been investigated if the vertical root density distribution correlates with the statistical location of the saturated water table in the sediment. Because precipitation can be considered spatially homogeneous at the island scale, soil moisture changes in deep soil are likely dependent on streamflow statistics. Figure 5.1 shows the discharge fluctuations for the three year when the field campaings were carried out.

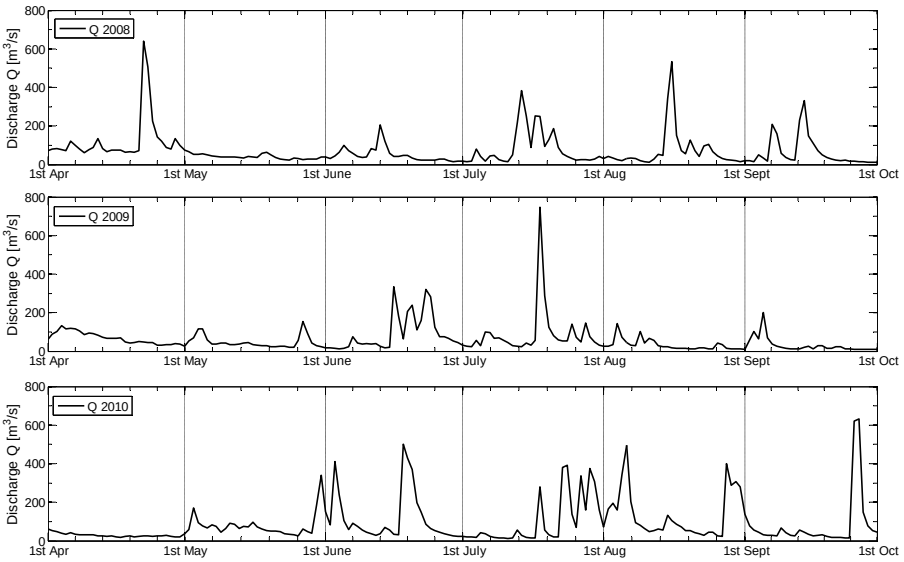

Figure 5.1: *Streamflow regime during the growing season (april - september) in 2008, 2009 and 2010.*

At the beginning of the season (April-May) cuttings need at the same time enough water availability and the absence of flood pulses. At this stage the stems shooten by cuttings are too soft and weak to resist any prolonged dragging force. If this happens, as it was in 2008 (Figure 5.1,a), it results in breaking, damaging or complete removal of the short and fine shootings. The small canopy, in the first two months is not yet woody, indeed. When a flood with magnitude higher than 360 m^3/s happens, scouring forces, together with prolonged heavy bed sediment transport may result in morphodynamic changes of the island topography with consequent erosion or aggradation, often fatal for vegetation surviving. Floods in 2009 only damaged part of the cuttings, resulting in a decrease of the total growth rate (see Figure 4.3) and a peak of mortality. However, due to the absence of events in august and September, there were no relevant consequences for the field campaign. 2010 river hydrological dynamic was more complicated. After a first prolonged period of drought (April and May) there has been a series of frequent flood pulses, although never higher then 500 m^3/s. This continuous disturbance

damaged continuously shootings and stems (Figure 4.3), but the monitoring campaign was not compromised.

5.2 Water table dynamics

5.2.1 Water table estimation

Flow scenarios in the range 10 $\div$ 700 m^3/s were generated for the current 2x2 m resolution DEM corrected for the river bathymetry according to Schäppi et al. (2010) by means of the hydraulic model mentioned in Section 2.3.3. Given the relatively coarse size of the alluvial material (saturated hydraulic conductivity about $2 \div 3$ cm/s), and the fact that the water level at the island rises quite slowly during floods, the water table beneath the island rises nearly simultaneously with the stream. One may reasonably expect the vertical water front to infiltrate at a rate which is comparable to the hydrograph dynamics. Therefore, it was assumed the water table to propagate in quasi-steady state dynamics for common river hydrograph conditions. Thus, the position of the water table within the island is found along a straight line perpendicularly joining the simulated velocity vectors in the two side channels (Figure 5.2). This has allowed to obtain a "rating curve" of the saturated water table for all plots of the island, as function of the water surface elevation in quasi-steady state conditions.

5.2.2 Water table frequency distribution

For each plot a rating curve can be drawn with the outcome of the cross sections. At the location of the plots, as shown in figure 5.3.a, the elevation of the local water table is read for every stream flow. With this information a rating curve can be drawn for each plot, showing the relationship between the stream flow and the local water table (Figure 5.3.b). The values of the calculated daily stream flow at the island for the 10 year period between 1999 and 2008 were sorted in an ascending way from the smallest (3.965 m^3/s) to the largest (771.6 m^3/s) value.

In order to get a detailed histogram from the data a class width of 10 m^3/s was chosen, i.e. 77 classes were established. The stream flow values from 10 m^3/s to the value that completely covers the island (360 m^3/s) which have been simulated for the island's site each received a discrete relative frequency value that corresponds to the value of the respective class of stream flow values from the histogram with 10 year data, and these values are corrected in order for the sum to augment to 1. The result is a histogram for the total range of used flow rates. With the rating curves, which give the relation between the stream flow and the elevation

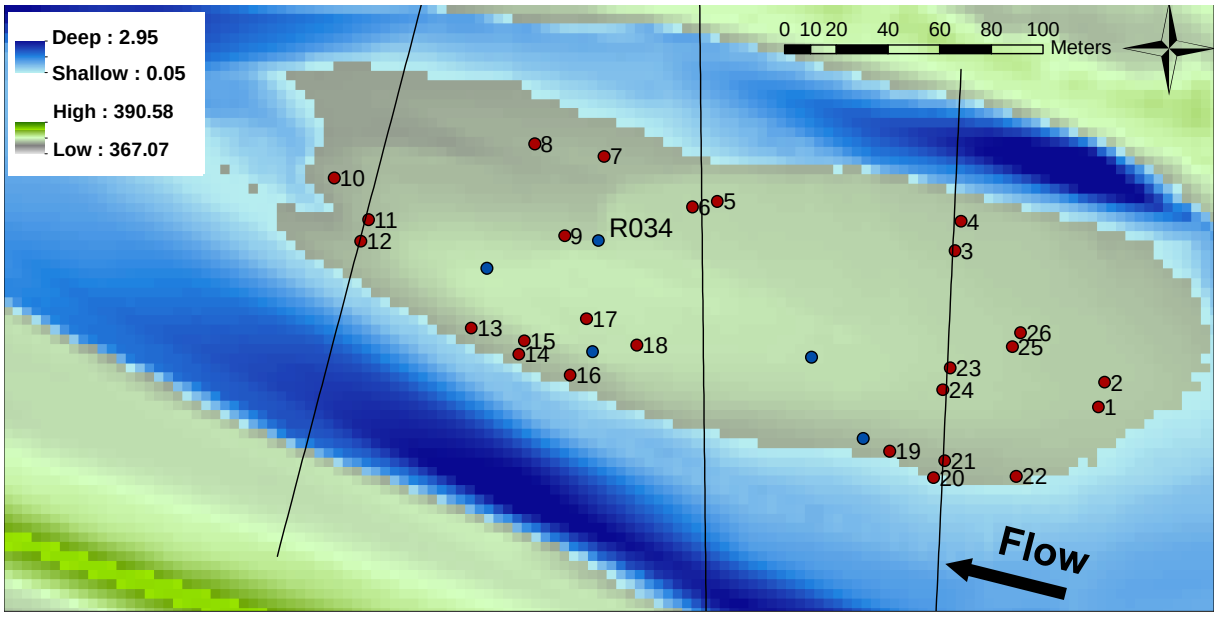

Figure 5.2: *Gravel island (∼11000 m^2) of the restored reach of the Thur River near Niederneunforn showing the location of the plots of installed willow cuttings for the 2009 campaign and simulated flow depth (BASEMENT 2D model) for the exemplary flow rate of 60 m^3/s). Blue dots indicate piezometers among which R034 (close to Plot 9) is used as control. Thin black lines represent exemplary transects along which the water table in the sediment was computed by using the water elevation information at the island shoreline (Pasquale et al., 2012a).*

of the water level, the histogram can be translated. For each plot the respective histogram is translated to a discrete relative frequency distribution of reaching certain water elevations instead of only obtaining a relative frequency of certain stream flows. For the plots where root data is available the histograms of the water table are rescaled to the same bin width in order to facilitate comparison.

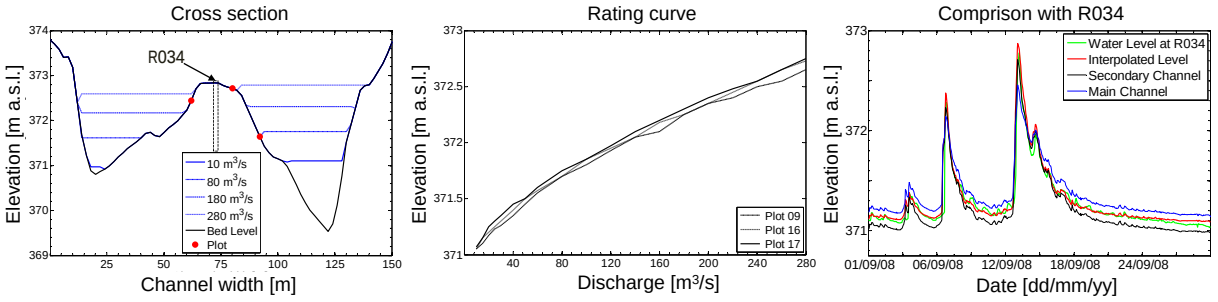

Figure 5.3: *Cross section for the plots 9, 17 and 16 with some of the stream flows used (a). On the same transect piezometer R034 is installed. The rating curve for the same plots is shown in (b). Frame (c) shows the comparison between the level read on the piezometer R034 and level computed using the rating curve method. The root mean square error (RMSE) over the the whole year is 6 cm (Schneider et al., 2011).*

This technique is further described in Schneider et al. (2011), together with its application in relation to groundwater issues and it was validated by observations from a number of piezometers spread around the island (e.g., see Figure 5.3.c), which also confirmed the almost negligible role of capillary rise in this type of soil. On this basis, we built the histogram of the frequencies of the saturated water table vertical location within the sediment at each plot location.

5.3 Root frequency distribution

From both 2009 and 2010 field campaigns, data relating to below-ground biomass development shows that cuttings from different plots developed distinct histograms (hereafter shown as frequency polygons) toward the end of the season depending on their location. Figure 5.4 shows images of both the root structure and the related histogram averaged from three samples taken from each of four plots during the last uprooting of the season (September 2009). The histogram of the vertical position frequencies of the saturated water table is also shown. Cuttings growing at low elevation, that is close to the stream at the modal flow (e.g., Plot 10) show a negatively skewed root density histogram (Figure 5.4). In contrast, as cuttings grew at higher elevations (e.g., Plot 5), and the distance between the modes of the histograms increased, then the root density histogram appears to be positively skewed and the highest root density is found in the lowermost part of the cutting or possibly below it (Figure 5.4). At intermediate elevations a more uniform root density distribution was generally observed (Plots 8 and 25 in Figure 5.4). In some cases, we also found signatures of thigmotropism bending the root locally (Figure 5.4, inset panel), likely related to the presence of big stones which is typical of the heterogeneity of alluvial sedimentary beds.

At the end of the growing season, according to whether plot locations were either close to the stream or at higher elevations, roots are respectively found in the uppermost part of the cutting (close to the soil surface) as if the dominant form of tropism would be aeration driven, or in the lowermost part of it as a possible result of hydrotropism. For plots close to the stream, we also observed the tendency of some roots to grow toward upper and better areated soil layers, as suggested by Bloom and Voesenek (1996). Eventually, the switch of the skewness from negative to positive value in relation to the distance from the modal saturated water table would suggest a clear dependence of the root distribution on river discharge characteristics.

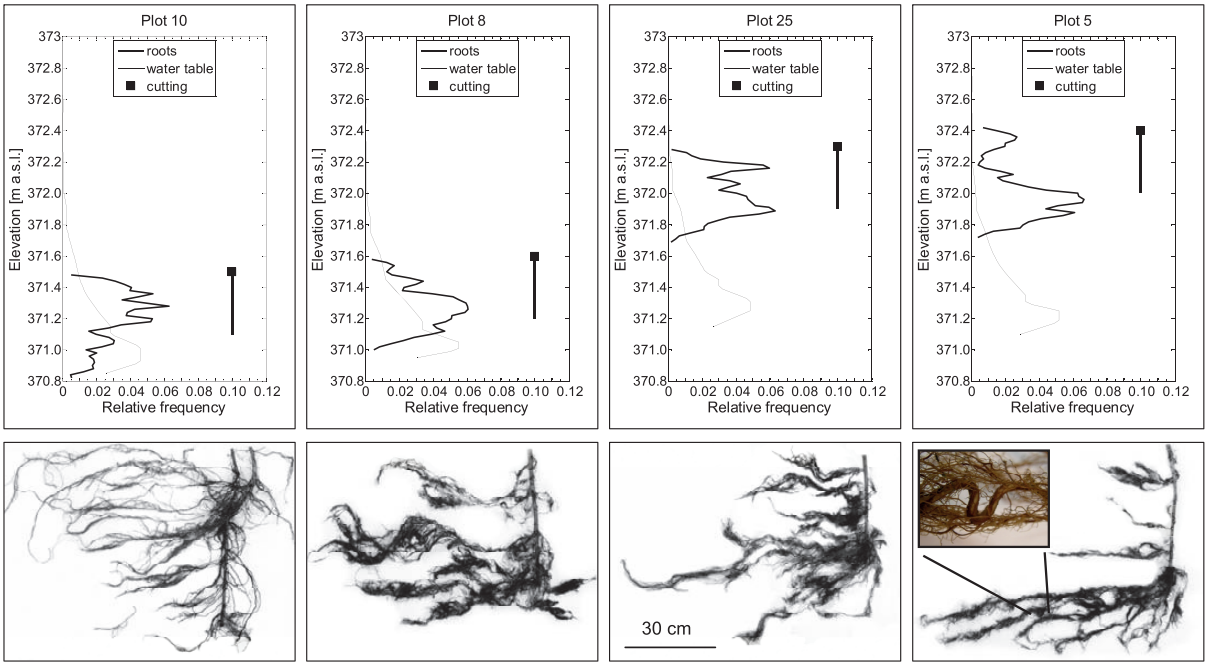

Figure 5.4: *Experimental relationship between the vertical root density distribution and the histogram of water table oscillations at each plot location for a number of exemplary plots located at different elevation. The vertical black line in the upper panels is the cutting length (when installed). The square on the top represents the original ground surface elevation of the plot. Lower panels show the root structure of one of the three uprooted exemplars per each plot location that were used to obtain the histograms. The inset panel in the root structure image for plot 5 shows the effect of mechanical impedance (thigmotropism) for which the root locally bends around a flat vertically oriented stone (Pasquale et al., 2012a).*

5.4 Root scaling relationship

While growing through the season, cutting roots showed clear time dependent root distribution as shown in the compilation of images of Figure 5.5, which refer to cuttings uprooted from Plot 10 in the 2009 campaign (corresponding location shown in Figure 5.2). Quite interestingly, roots seem to reorganize their distribution in time as in response to an external forcing, the effects of which require longer time periods (e.g, a season) to be perceived. This observation allows some supposition regarding the role played by water table fluctuation, and whether a possible scaling relationship exists as a signature of hydrotropism-driven growth for pioneering plants in such environments. The following relationship is defined (Pasquale et al., 2012a):

$$\eta = \frac{Z_r - Z_w}{Z_s - Z_r}, \tag{5.1}$$

where Z_r and Z_w are the absolute elevations (e.g., above sea level) of the mode of the distributions of the root density and of the saturated water table, respectively. The quantity Z_s is the

temporal mean over the season duration T of the soil surface elevation at each plot location. Changes in soil surface elevation due to erosion or deposition caused by floods can influence roots growth, and the history of local soil aggradation or degradation should therefore be taken into account when computing Z_s. If this information is available for a number of significant events, then it is recommend to compute Z_s as the weighted mean:

$$Z_s = \frac{1}{N} \sum_{i=1}^{N} \alpha_i z_s^i \tag{5.2}$$

with α_i being the fraction of time the variable z_s spent at a certain value z_s^i over N days.

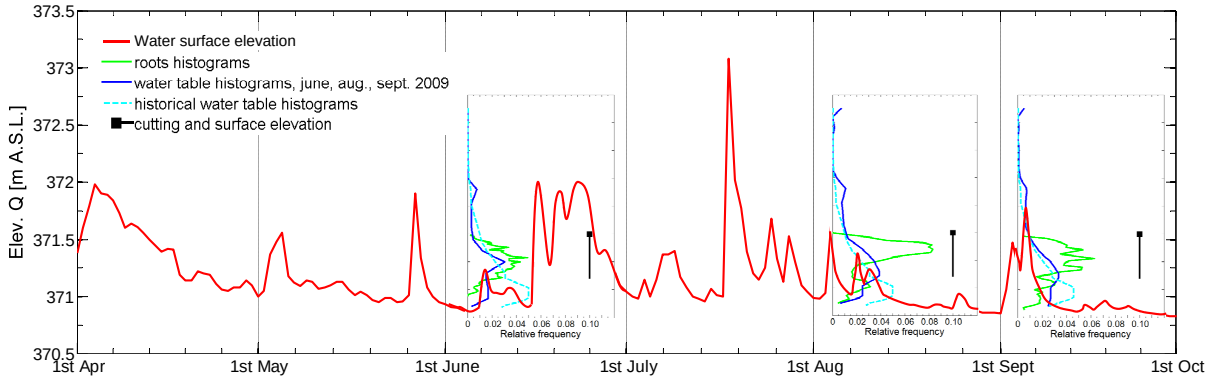

Figure 5.5: *Temporal evolution through the season of the root structure of Plot 10 (2009 field campaign) showing how the root density histogram adjusts in time to the experienced water table fluctuations. The blue line shows the experienced water table empirical histograms computed from april 2009 up to the uprooting day recorded discharge (Pasquale et al., 2012a).*

For the sake of generality and given the limited available data regarding soil topography, the scaling parameter η is computed by using the data from the 2009 campaign, and it has been later validated with the data of the 2010 campaign. As quantity for Z_s, the island topography at the time when the cuttings were planted was used, since the time and the amount of change in soil elevation caused by seasonal floods could not precisely be quantified (see Figure 5.2). A plot with the root data of the 2009 campaign rescaled with Eq.5.1 is shown in Figure 5.6. Notice, that only toward the end of the season the data (black crosses) seem to converge toward a common average value of η, equal to 1.2.

Viceversa, this ratio is quite different across the season even for cuttings belonging to the same plot, the highest value occurring at different times of the season depending on plot location. This apparently illogical root growth at the beginning of the season may be interpreted as the delayed tendency of roots to gradually adapt to changes in the saturated water table (i.e., the discharge regime) within the sediment. That is, cuttings are unable to determine if the

particular location where they were planted is going to suffer lack of water or of oxygen, as obtaining experience of this requires at least a season.

Although this conclusion may sound rather "naive", it can after all be justified by considering that precipitation is practically uniform at the spatial scale of the island. Hence, time is needed for plants to respond consistently to the surrounding environment and the scaling relationship would support the idea that the time scale required to establish such consistent responces is at least the duration of the growing season.

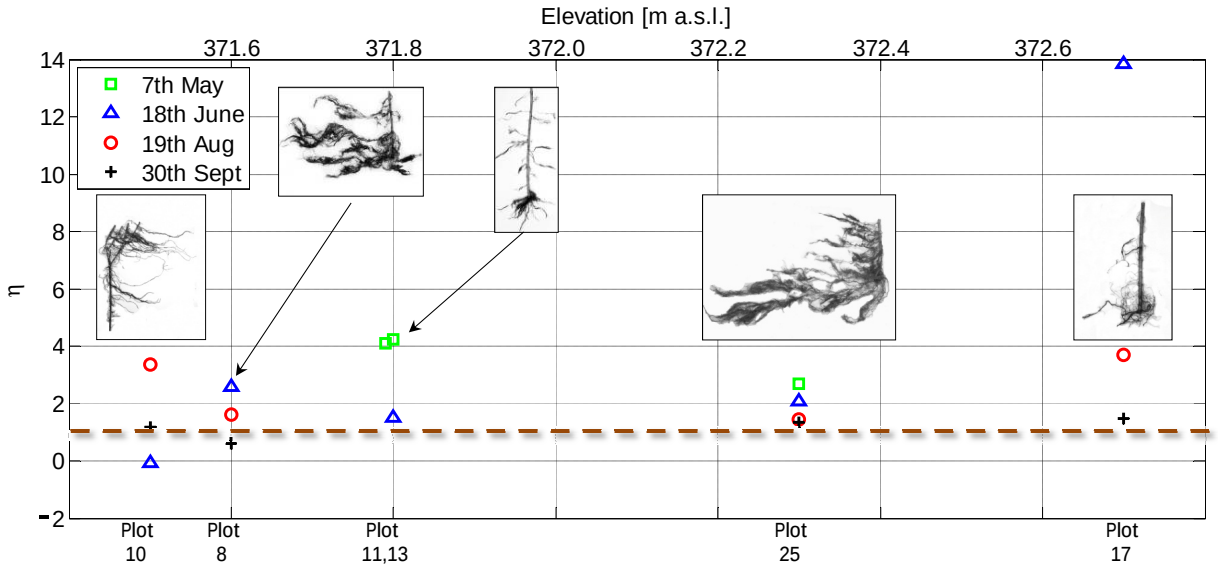

Figure 5.6: *Scaling relationship relating the depth of the highest root density (histogram mode) to that of the most frequent water table position, and the soil surface elevation. No scaling is evident until the end of the season when data eventually re-align to the scaling relationship (orange dashed line) as the root architecture assumes the form shown in the inset panels (Pasquale et al., 2012a).*

The rather unique root images and the data-based scaling relationship proposed in this work seem to support the idea that hydrotropism and oxitropism are mainly responsible for determining the vertical root density distribution on bedforms of alluvial environments.

From an engineering viewpoint, this understanding is key to developing sound mathematical frameworks for mechanisms of uprooting by flow in river bedforms (Edmaier et al., 2011) and banks (Hubble et al., 2010). For instance, such frameworks can be used to either improve or develop numerical morphodynamic models of river-vegetation interaction (e.g., see Perona et al., 2009) by including the effect of sediment texturing and added cohesion due to vegetation roots (Fan and Su, 2008).

5.5 Root scaling map and root mode depth

The scaling relationship can be rewritten in the following form (Pasquale et al., 2012a):

$$Z_r = \frac{\eta Z_s + Z_w}{1 + \eta}, \tag{5.3}$$

and it can be used to assess the expected depth Z_r of highest root density. Using the topography Z_s of the island at the beginning of the 2010 growing season, and the value of Z_w computed for this topography by using the historical river discharge data allowed to produce the spatial map shown in Figure 5.7, which is used together with the root data (average of three cuttings per plot) from the 2010 uprooting campaign in order to validate the scaling relationship proposed in Equation (5.1). The gravel bar in 2010 is an island only for river discharges above 80 m^3/s. This precluded the use of the technique described in Section 5.2 (Pasquale et al., 2011) to compute the water table in the sediment in correspondence of Plot 10 because for low flows no stream is observed on the right hand side channel, with an exception made for some pools of exfiltrating water that could still be used as boundary condition for the other plots. Hence, for Plot 10, the statistics computed from the observations of the nearby piezometer R034 was used. The results of the estimated highest root density depth are encouraging (Figure 5.8). When comparing the observed and predicted root data in 2010, the plot returns a high coefficient of determination R^2 despite the limitation of neglecting the influence of seasonal topographic changes on the quantity Z_s and the use of the water table Z_w from the nearby piezometer R034 as far as Plot 10 is concerned. All plots, wit the exception of plot 10 fit the regression curve. The reason why plot 10 does not follow the scaling relation might be reasonably two, one physiological and the other statistical. From the physiological point of view, given that this plot is located near the highest elevation, the intrinsic plant physiology may not allow to develop so deep root to reach water, as predicted by the scaling relationship. The scaling, after all, does not contain any information concerning plant characteristics. Second, the validation is done on the basis of 2009 field measurement and plot 10 of field campaign 2010 was transplanted, much higher than the plot used to determine the scaling.

The results presented so far are useful for improving our understanding of process development and vegetation uprooting by flow in alluvial sediments. *Salix* species have a dense tap root architecture (Kuzovkina and Volk, 2009), for which the anchorage is the result of the tap root itself (the cutting in our case), plus the spatial distribution and density of higher order roots (Ennos, 1993). Beside nutrient and water absorption, anchorage is the second primary function of root systems and can influence their spreading in the soil (Ennos, 1993). Roots must transfer the forces applied to the canopy into the soil in order to counter flow-induced uprooting mechanisms (e.g., see Edmaier et al., 2011).

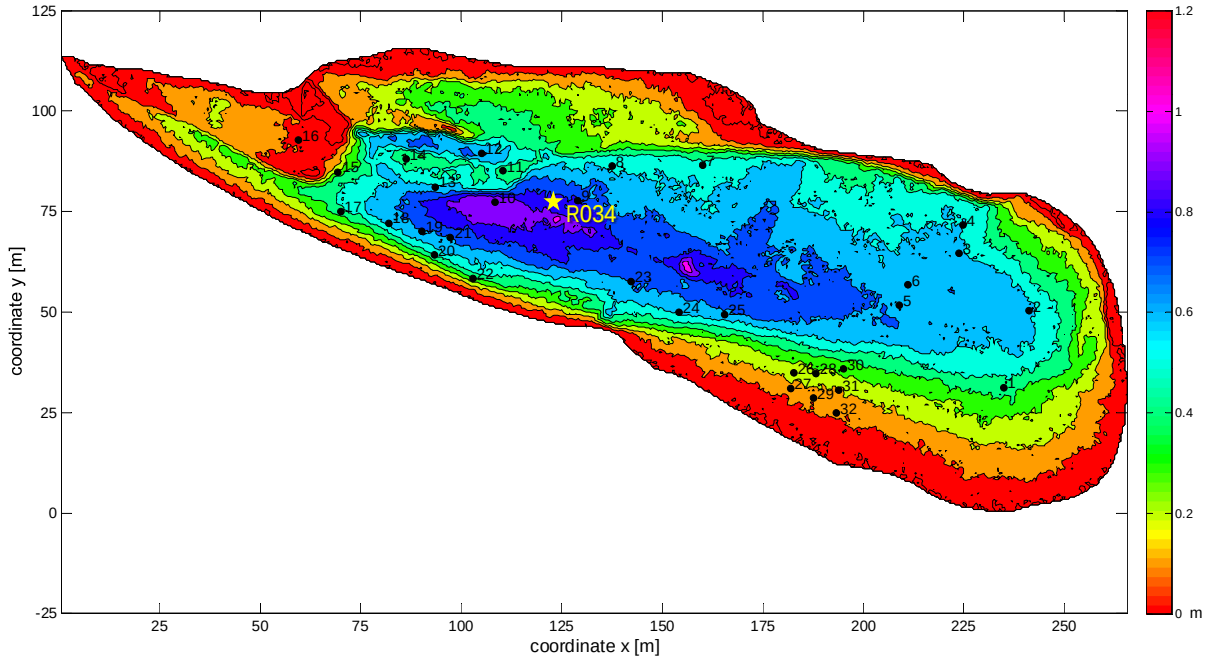

Figure 5.7: *Map of expected highest root density depth for the 2010 campaign as obtained from the scaling on 2009 data. The yellow star indicates the location of the piezometer R034 (Pasquale et al., 2012a).*

In some cases it was found that the direction of the roots might reflect the structural need of countering the direction of the external force (i.e. drag due to flow) applied to the canopy. However, given the high soil heterogeneity, root spread at certain depths was in general rather broad and only allowed for density measurements. On the one hand, this fact limits our conclusions about a possible correlation between root direction and applied forces. On the other hands, it leaves this hypothesis open to future investigations, for instance by means of controlled laboratory experiments.

By anchoring the plants to the soil, the root system reinforces the soil with an additional spurious cohesion, which helps prevent soil erosion by modifying both incipient and transport bedload conditions.

As this chapter shows, the fact that topography and hydrology may affect the location of the rooting depth density (which are common measures of below-ground biomass distribution (Schenk and Jackson, 2002b)) therefore has important implications as far as the resistance to flow erosion is concerned. A positively or negatively skewed root density distribution plays a clear nonlinear role with respect to the probability of survival to flow erosion. Not only are higher elevations reached by floods less frequently, but for the same amount of eroded sediment the roots are deeper at higher elevations, and their probability of removal is therefore smaller than simple hydrologically-based statistics would predict. In this sense, for river islands with a very pronounced topography, mortality at high elevation would essentially be the result

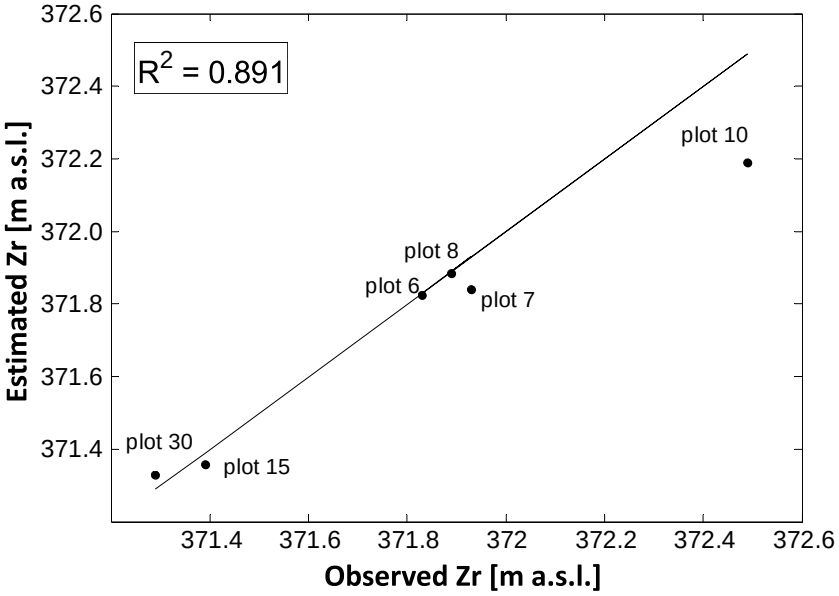

Figure 5.8: *The coefficient of determination R^2 for observed vs computed data points for the 2010 campaign at the end of the growing season (Pasquale et al., 2012a).*

of an excessive depth-to-groundwater rather than of flow damage, as directly observed by Francis (2007). The observations reported in the contest of this experimental work relate to installed cuttings for which the stem is itself a primary root from which the others have sprouted. Although this may possibly differ from naturally germinated or rejuvenated pioneering species, data hereby shown provide evidence of how water table oscillations influence the root distribution in such environments, and may particularly relate to cuttings planted as part of restoration schemes (Mallik and Rasid, 1993; Pezeshki et al., 2007).

This study refers to cuttings that had grown for one season, only. Analyzing roots from plants in successive seasons may become prohibitive because of the amount of developed biomass and the consequent difficulty in removal for data collection. Therefore, whether in successive years the vertical density distribution changes or remains the same with only an increased amount of biomass to compensate biological and mechanical (i.e. anchoring and stability) functionalities remain open questions, which may be addressed via additional experimental work and/or numerical models.

5.6 Sources of uncertainties

Both for sample uprooting and for analysis and result interpretation one should keep in mind some considerations. Some factors, which could not be under complete control in case of the

field experiments, may strongly influence the final result (in terms of root distribution). The most important ones are: i) sediment texture, ii) deposition of new layer of sediment or erosion of bed material and iii) biological characteristics.

Sediment texture may influence the direction of root growth, when the presence of large gravel particle (ϕ >10 cm) in the soil does not allow root to keep growing in the same direction. Therefore, in a coarse gravel soil, roots often diverge their growth trajectory due to thigmotropism which is the movement in which roots (and in general an organism) move or grows in response to touch or contact stimuli (in this case gravel particles).

Sediment grain size distribution may also influence soil moisture. Consequently a more sandy rich soil will trap soil moisture for a longer period than gravel soil. Floods may result in deposition or scouring of bed material. In the first case, the new deposited material, with a higher porosity (and therefore with higher breathability) and richer in nutrients is optimal for the plant to spread adventitious roots. In the second case, instead, roots previously grown in the soil may be exposed by erosion of soil layer. Those roots are likely to dry in the air and become inactive in the nutrient uptake process. It is also very easy that the exposed cutting spread juvenile shootings as it is typical for willow species.

Finally one should not forget that plants are alive organisms and the repetition of measurements may strongly be affected by large variance among the samples, due, for instance to the inherent difference among individual of the same species. The only factor that may be controlled is the accuracy of the sampling techniques. Uprooting cutting samples in a gravel soil for such analysis as the ones reported in this chapter as well as in chapter 4 must be accurately planned in advance and it must be carried out following as much as possible the recommendation of Pasquale et al. (2011).

Chapter 6

Root anchorage and soil reinforcement

The experimental evidence discussed in the previous chapters and the clear dependence of vegetation establishment on the hydraulic regime provides a good basis to formulate a pilot model of root anchorage, which depends essentially on the local hydrodynamic conditions. The model is presented in this chapter by contrasting it with a literature review of similar models and more specifically by validating against evidence of scouring at various vegetation plot locations.

6.1 Application to river banks and slopes

Many authors have considered spatial variability in root distributions at the scale of individual trees, when considering the effect of root reinforcement on stream-bank stability (Pollen, 2007). The effects of root reinforcement on soil strength is commonly quantified by two methods. The first method uses values collected from in situ shear tests of root-permeated soils to replace the value of the soil strength alone (e.g., Wu et al., 1988). However, in situ shear tests present a number of problems: while they provide a direct assessment of the amount of increased cohesion provided to the soil by the roots, they require the difficult task of isolating a block of root permeated soil to shear. Moreover the soil and the anchoring of the roots may be disturbed before shearing is undertaken. In addition to this problem, Wu et al. (1988) comment that when carrying out in situ tests of root permeated soil, the forces developed in the roots and therefore their contribution to soil shear strength, are dependent on the dimensions of the shear box.

The second method involves the development of physically based formulas to establish the relationships between the root and soil properties that cause the roots to increase the shear strength of the soil. These formulas generally form the basis for static root reinforcement

models in which the forces acting in the root-soil matrix are considered at an instant in time, usually taken as being when all of the roots reach their maximum tensile stress. One such formula is the simple perpendicular root model developed by Waldron (1977) as described by Pollen and Simon (2005) and Pollen (2007). This root reinforcement model is based on the Coulomb equation in which soil shearing resistance is calculated from cohesive and frictional forces.

The simple model of Wu et al. (1979) assumes that the roots are perpendicular to the slip plane. However, the angles of the roots in relation to the direction of the force applied to the soil are important, as this dictates the distribution of stresses within the root volume and hence the maximum tensile strength reached before failure of the root occurs (Niklas, 1992). However, Gray and Ohashi (1983) have shown from laboratory tests that perpendicular orientations of reinforcing fibers provide comparable reinforcement to randomly orientated fibers. This lends support to the use of the simple perpendicular root model, where it may be assumed that the roots are randomly orientated in the soil.

An important assumption of those models is that the full tensile strength of all the roots is mobilized when the soil shears. However, laboratory and field strength testing of stream bank materials and riparian roots show that root strength is typically mobilized at much larger displacements than soil strength (Pollen et al., 2004).

In order to solve some of the limitation of the physically based formulas, Pollen (2007) introduced a new approach based on the so called *fiber bundle* methods (FBM). The basic principle of a standard FBM is that the maximum load, which a bundle of fibers can withstood, is less than the sum of each of their individual strengths (Daniels, 1945). This is because when a load is applied to the bundle the fibers will not all break at the same time; as noted earlier, it is this very assumption that causes the Wu et al. (1979) model to overestimate the additional cohesion provided by roots in a soil. The simplest of these FBMs assume that the load from the broken fibers is distributed evenly between the remaining intact fibers, according to their diameters. This type of load redistribution is known as global load sharing (GLS) (Hidalgo et al., 2002). The alternative to GLS is a local load sharing (LLS) approach. In an LLS FBM, the load is redistributed according to the proximity of intact fibers to the broken fibers (Hidalgo et al., 2002).

This project concerns river bed form erosion of alluvial braided rivers. Therefore, a new, different approach is needed to study root reinforcement. In this context two new approaches, one more theoretical and the second more practical are introduced in the following Section.

6.2 Model of root reinforcement for river bedforms (alluvial sediments)

The theoretical approach presented in the previous sections of this chapter refers mainly to hill slope and river bank stability. River banks reach failure when soil shear resistance is exceeded along a slip plane where rupture occurs. Once a river bank reached instability it consequently collapses producing lateral erosion of the river.

Erosion of the river bed is instead a different phenomenon. Instability and erosion involve a rather more complicated process than breakage occurring along a slip plane. Erosion mechanism follows the exceeding of a threshold of particle's incipient motion condition as described in Section 2.5. In the case of river bed it is more likely a balance at the single particle scale where bed shear, produced by local hydrodynamic conditions and bed material characteristics (roughness), exceeds the stabilizing forces (i.e., particle's wetted weight eventually increased by bed armoring). Therefore, in order to describe analytically vegetation root reinforcement of river bed, a new approach is needed.

A theoretical model based on energy balance of the flow-sediment-vegetation dynamics is formulated (Section 6.2.1). The energetic method is explicit and physically based. However, due to the large number of unknowns and given the difficulties in controlling boundary condition during field experiments, the model could not be validated in the context of this project. Moreover, the intrinsic unpredictability of real field dynamics and the impossibility of monitoring all the variable of the model lead to the need of an accurate validation of the energetic method through laboratory experiments, where boundary and environmental conditions can be kept under control.

In the context of this project, due to the available data from the experimental and the monitoring field campaigns carried out, the energetic method could not be validated. Therefore, using a retrospective approach, an implicit model was formulated on the basis of the Shields' theory and of the Meyer-Peter and Müller equations (hereafter described in Sections 6.2.2 and 6.2.3). The model is still based on an energetic balance of the flood (it links the flood magnitude to the scouring depth and sediment transport) but this time it starts from the scouring depth measured from field observation.

6.2.1 Energetic Method

Vegetation canopy strongly influences local hydrodynamics. Therefore, in presence of flexible stems, such as plot of *Salix* shootings, the contribution of vegetation has to be taken into

account to compute the correct velocity profiles and bed shear stresses. Also, it has to be considered that flexible wood branches bend under flow forces, such as the ones produced by a flood event.

Figure 6.1 illustrates the conceptual bending model including stem and leaf contributions as formulated by Schnauder and Moggridge (2009). The model assumes a uniform vertical distribution of leaves, constant diameter d and flexural rigidity *EI* of the stem along its height h_{stem}. Drag contributions from stem and leaves are:

$$\mathrm{F}_{d,stem} = \frac{1}{2} c_d \rho h' d U^2 \tag{6.1a}$$

$$\mathrm{F}_{d,leaf} = \frac{1}{2} c_{d,leaf} \rho A_{\perp,leaf} U^2 \tag{6.1b}$$

where U is the mean velocity, ρ density of water and d stem diameter, h' deflected height, c_d stem drag coefficient, $A_{\perp,leaf}$ planar one-sided area of the leaf and $c_{d,leaf}$ associated leaf area drag coefficient. Several authors proposed values of the dragging coefficients expressed in Equations 6.1 (among others, Vogel, 1989; Nepf, 1999).

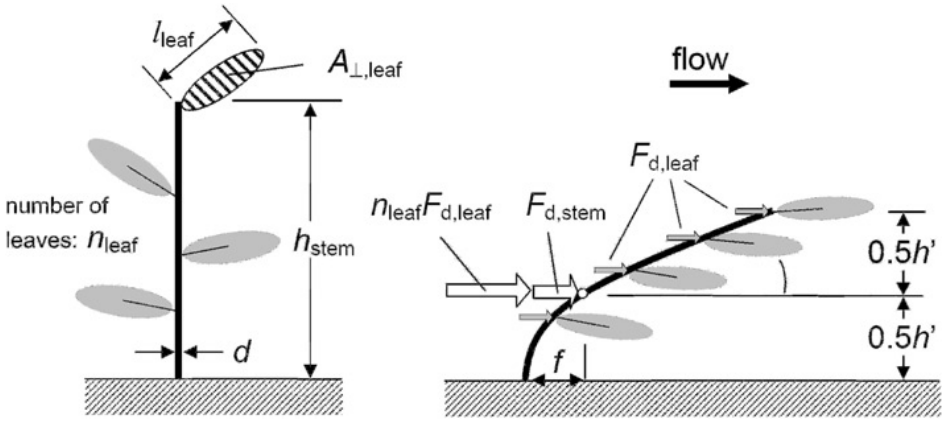

Figure 6.1: *Conceptual model for shooting deformation due to dragging on stem and leaves (Schnauder and Moggridge, 2009).*

The greatest unknown in Equations 6.1 is represented by the velocity profile U. The presence of vegetation strongly influences local hydrodynamic and the theoretical logarithmic vertical velocity profile becomes rather more complicated and several studies are currently ongoing by many authors. A method to define the velocity profile U based on the work of Katul et al. (2011) is shown in Appendix F.

Hereafter, the explicit energetic model is presented: the model is based on the energy balance of the flow and the work produced by the flow when sediments move and erosion occurs. Within the canopy, the energetic method takes also into account the presence of vegetation and the influence of stem and leaves on the local hydrodynamics.

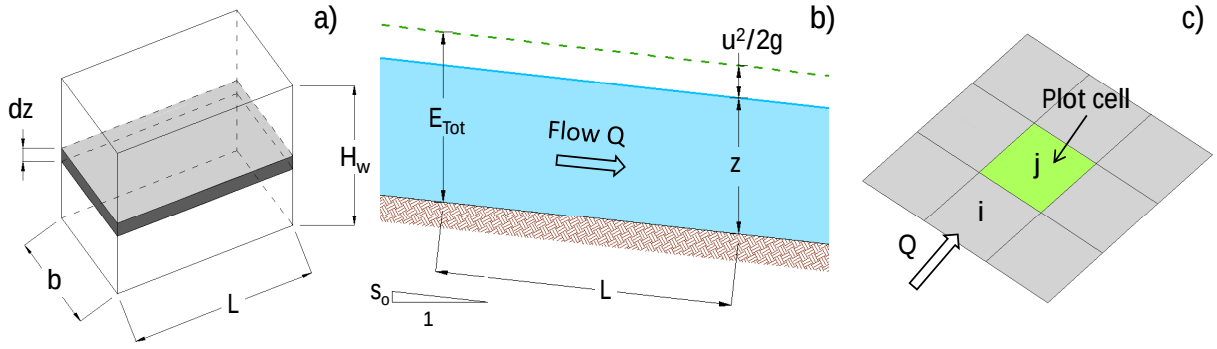

Figure 6.2: *Conceptual model of the flow energy method to assess quantification of root reinforcement in presence of a canopy layer.*

Referring to Figure 6.2 for symbols and conceptualization, the kinetic energy E_k^c of the flow, within the vegetation plot canopy is given by:

$$\mathrm{E}_k^c = \frac{1}{2}\rho b L \int_0^{H_c} u^2(z)\, dz + \int_{H_c}^{H_w} u^2(z)\, dz \;, \tag{6.2}$$

in which ρ is the density of the water, b the plot width and L is the plot length. In the case of model discretization in regular cells, b x L is the cell size (Figure 6.2.c). The first integral term describes the kinetic energy of the flow in the canopy layer, given by the exponential term of the equation by Katul et al. (2011). The second integral term, instead, is the kinetic energy above the canopy layer, i.e., where the velocity profile $u(z)$ according to Katul et al. (2011) is logarithmic. The kinetic energy of a cell outside the vegetation plot E_k may be computed considering only the mean value of vertical velocities u and the expression is given by:

$$\mathrm{E}_k = \frac{1}{2}\rho b L H_w \overline{u}^2 \tag{6.3}$$

The potential energy of the flow is function of the water level H_w only and it may be written as:

$$\mathrm{E}_p = \rho g b L H_w^2 \tag{6.4}$$

in which g is the gravity acceleration. Of course the water level H_w is dependent on the local flow velocity and friction losses. Therefore it depends on the local roughness which is strongly

modified by the presence of dense vegetation. The power of the flow is computed using the classic formula:

$$\mathrm{W} = \gamma Q \mathrm{E_{tot}} = \gamma Q \left(\mathrm{H}_w + \frac{\overline{u}^2}{2\mathrm{g}} \right) = \rho g b \mathrm{H}_w \overline{u} \left(\mathrm{H}_w + \frac{\overline{u}^2}{2\mathrm{g}} \right) \tag{6.5}$$

where $\gamma = \rho \dot{g}$, Q is the discharge and E_{tot} is the total energy given by the contribute of the kinetic and potential energy. $\mathrm{W} \cdot t$ is the energy needed to produce the power W in a given time t. Within a cell of length L, the time t to produce W is equal to the cell length divided by the flow velocity $\frac{L}{\overline{u}}$. The energy $\mathrm{W} \cdot t$ must be equal to the sum of the kinetic energy and the potential energy of the flow. Equation 6.6 shows the identity $\mathrm{W}t = \mathrm{E}_k^c + \mathrm{E}_k$:

$$\frac{1}{2} \rho b L H_w \overline{u}^2 + \rho g b L H_w^2 = \rho g b \mathrm{H}_w \overline{u} \left(\mathrm{H}_w + \frac{\overline{u}^2}{2\mathrm{g}} \right) \frac{L}{\overline{u}}. \tag{6.6}$$

The identity equation hereby defined is formulated considering a water volume flowing on a fixed channel bed. In real condition (both in laboratory and in a natural reach), channel bottom is made of moving particles. Depending on the hydrodynamic conditions, the movement of particles creates aggradation and erosion patterns, the so called river bed forms. Locally, if the total erosion (in terms of volume) produced by a certain flow can be measured, it is also possible to compute the energy due to the flow over a defined scoured area (i.e., the plot cell). The scouring energy $\mathrm{E_S}$ is the work $\mathrm{J_{tot}}$ produced by the flow to move the volume V toward the flow direction of a quantity L and lifting up the same volume of a quantity δ.

$$\mathrm{E_S} = \mathrm{J_{tot}} = \left[\overrightarrow{\mathrm{F}}_{\mathrm{D}} L + \left(\overrightarrow{\mathrm{P}} - \overrightarrow{\mathrm{A}} \right) \delta \right] \tag{6.7}$$

where δ is the depth of the scoured layer, $\overrightarrow{\mathrm{P}} - \overrightarrow{\mathrm{A}}$ is the submerged weight of the bed material, L is the length of the scoured volume and $\overrightarrow{\mathrm{F}}_D$ is the dragging force acting on the eroded volume. The submerged weight may be expressed as

$$\overrightarrow{\mathrm{P}} - \overrightarrow{\mathrm{A}} = \gamma' V (1 - \mu) = (\rho_s - \rho_w)\, \mathrm{g} \frac{4}{3} \pi \left(\frac{d}{2} \right)^3 = \frac{1}{6} \pi g \left(\rho_s - \rho_w \right) \mathrm{d}^3 \tag{6.8}$$

where γ' is the effective specific weight, V the total volume scoured in the considered cell (see Figure 6.2.c) and μ is the porosity of the bed soil layer. The dragging force on a single particle is given by:

$$\overrightarrow{\mathrm{F}}_D = \tau_0 A = \rho u_*^2 \pi \frac{d^2}{4} \tag{6.9}$$

in which $\tau_0 = \rho u_*^2$ is the shear stress on the bed layer and A the particle area equal to $\pi \mathrm{d}^2/4$. u_*^2 is the shear velocity defined in Section 2.5.1. The new identity of the energy balance, in the case of moving channel bed can be written as

$$\mathrm{E_P} + \mathrm{E_K} + \mathrm{E_S} = \mathrm{W}t. \tag{6.10}$$

Therefore, considering two cells i and j, the condition

$$\mathrm{E_P^i} + \mathrm{E_K^i} + \mathrm{E_S^i} = \mathrm{E_P^j} + \mathrm{E_K^j} + \mathrm{E_S^j} \tag{6.11}$$

can be written. Equation 6.11 states that the transformation of energy in two adjacent cell must be equal. However, if the cell j is the plot cell, the boundary conditions are different, because soil property are modified by the presence of the root system which increase soil resistance and particle cohesion. In this case the scouring energetic term of the vegetated cell will be higher, since higher is the energy needed by the flow to produce the same scouring as the one produced on the non-vegetated cell i (Figure 6.2). Equation 6.11 has to be re-written in the following way:

$$\mathrm{E_P^i} + \mathrm{E_K^i} + \mathrm{E_S^i} = \mathrm{E_P^j} + \mathrm{E_K^j} + \mathrm{E_{S,corr}^j} \tag{6.12}$$

in which $\mathrm{E_{S,corr}^j} = \mathrm{E_S^j} + \Delta\mathrm{E}^*$ and $\Delta\mathrm{E}^*$ represent the surplus energy needed to produce in the *j* cell the same scouring of *i* cell. Considering that, due to Bernoulli's theorem the sum of the kinetic and potential energy in the *i* cell, $\mathrm{E_P^i} + \mathrm{E_K^i}$, must be equal to the correspondent term of the *j* cell, $\mathrm{E_P^j} + \mathrm{E_K^j}$, in Equation 6.12 the two can be deleted and Equation 6.12 becomes:

$$\mathrm{E_S^i} = \mathrm{E_S^j} + \Delta\mathrm{E}^* \tag{6.13}$$

Once computed the scouring energy in the vegetated cell and in the non-vegetated ones in the surrounding area, once can thus compute the increment of cohesion given by the root system in terms of flow energy. Substituting the $\Delta\mathrm{E}^*$ term in Equation 6.7 and manipulating it one obtain the value of the corrected shear stress $\tau_{0,corr}$. This is the value of the shear stress to be incremented to τ_0 in order to obtain a shear stress, inside the vegetated cell, that produces the same scouring recorded in a non-vegetated cell (i.e., where there is no reinforcement effect of the root system).

Carrying out field experiments to produce reliable data to validate the model is quite a difficult task and in the contest of this project it was not feasible, at the end, due to both time and cost issues. Validation and further investigations should be carried out in a laboratory flume, where

boundary conditions are known and where measurement of the flow parameters is possible. Also, flume experiments could eventually be repeated to try a broader range of flow conditions, vegetation and sediment size.

6.2.2 Simplified root reinforcement method: theory

An alternative to the explicit energetic model is to reversely proceed from the field data to develop an implicit model. The implicit model of root reinforcement is based on the amount of scoured volume due to the sediment transport balance produced by a flood event. Because canopy strongly influences local hydrodynamic by modifying velocity profile and shear stress, the quantification of root reinforcement considering canopy contributes is a complicated task. Many authors have approached and studied those effects; however, due to the uncertainty given by field experiment, data acquisitions and definition of boundary conditions, the use of an accurate theory of velocity profile modification would be made difficult by the impossibility of any validation with the available data in this work. For this reason, during field campaigns some of the plot planted the year before have been pruned periodically, with the purpose of maintaining the root system below ground and, at the same time, to make negligible the canopy effect on the local hydrodynamic.

Two main hypotheses have to be thus considered: first, the young stems and shooting respread after each pruning are negligible in terms of influence on the hydrodynamic. Second, the portion of the cutting eventually exposed by the removal of sediment during a flood (due to erosion) does not influence the local shear stress. The first hypothesis is acceptable by the fact that young shootings are very soft and during a flood they are easily broken and quickly flushed away. The second hypothesis assumes that the effect of exposed cutting is negligible in comparison with the flooding water depth. This second hypothesis seems reasonable in consideration of the size of the cuttings relative to the water depth and is also supported by the sparse density of the cuttings in comparison to the plot area.

If the specific width $b = 1/2B$, where B is the plot width (2 meters in this case), d is the cutting diameter (0.012 m) and k the number of cuttings (6 in this case), $a = kd$ is the frontal area per unit volume of the canopy. According to Rominger and Nepf (2011), if $C_d ab \ll 1$ (where C_d is the drag coefficient) the hydrodynamic condition within the canopy are called Low Flow Blockage Canopy (LFBC). Setting $C_d = 1$ (Rominger and Nepf, 2011) in the case of the transplanted plot at the Thur site it is: $C_d ab = 1 \cdot (0.012 \cdot 6) \cdot 1 \ll 1$. In the case of LFBC, the interior adjustment region, L_0 where water profile is modified by the cuttings is function of the canopy drag length scale (Rominger and Nepf, 2011), $(C_d a)^{-1}$, that, in this case means 13 meters, a scale length much larger than the plot size (2 meters). Consequentially the effect

of the eventually exposed cutting may be neglected. In computing the scouring, this approach is consistent with the accuracy (in terms of vertical resolution) of the DEM that is being used for the analysis.

Figure 6.3 shows the scheme used for the model formulation. The green cell in the middle is the cell where vegetation plot has been transplanted. The grey cells are the surrounding bare soil cells. In correspondence of each cell the value of scouring, the d_{50} as well as the hourly hydrograph on a given time have to be known.

The integral over a given scouring period (in this case one growing season) of the scoured volume computed for cells located at the side of the vegetation plot cell (Figure 6.3.c) and perpendicular to the flow direction (Figure 6.3.b) is given by

$$\Delta V_L = \Delta z_L \cdot A_{cell} \tag{6.14a}$$

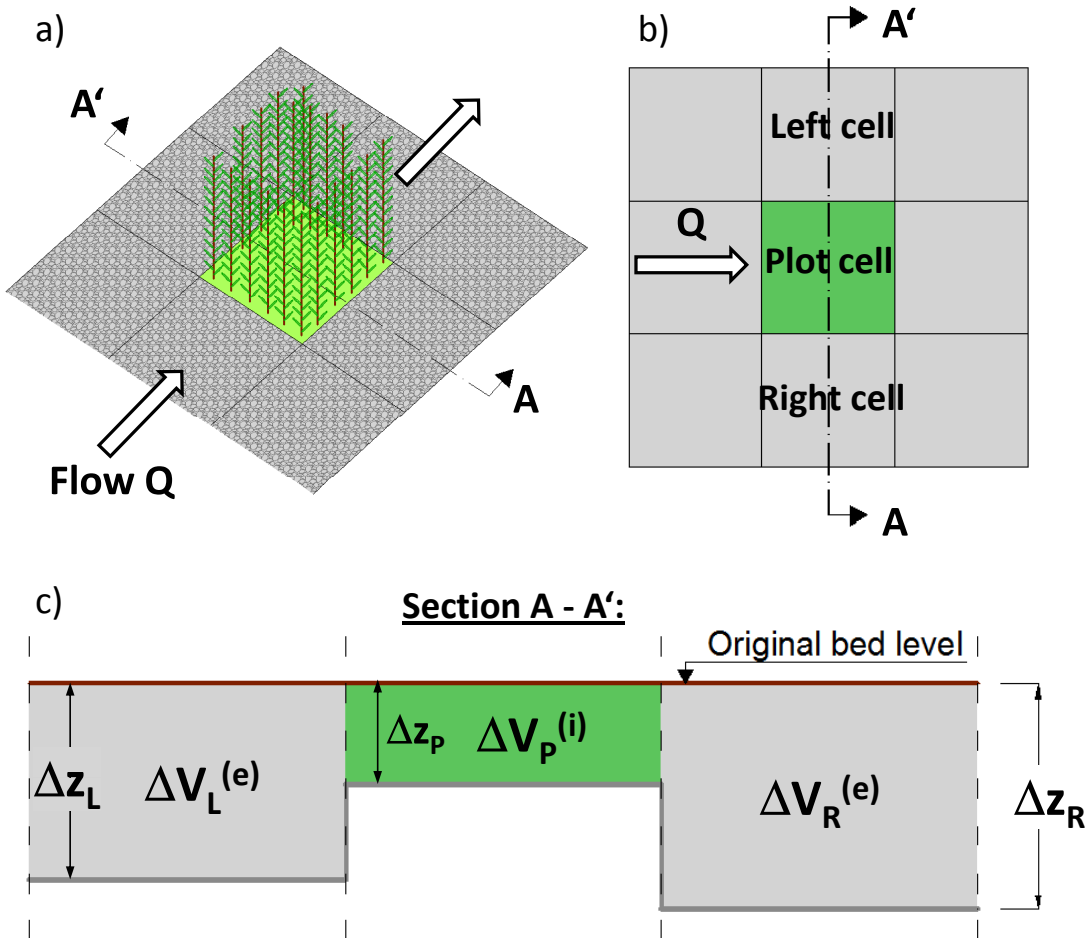

Figure 6.3: *Scheme of the cells within and surrounding the vegetation plot. The geometry here represented is used to compute vegetation root reinforcement.*

$$\Delta \mathrm{V}_R = \Delta \mathrm{z}_R \cdot \mathrm{A}_{cell} \tag{6.14b}$$

where $\Delta \mathrm{z}_L$ and $\Delta \mathrm{z}_R$ are the difference in elevation computed from the DTMs and A_{cell} is the cell size. In order to compare the volume scoured beside the plot with the volume scoured within the plot it is more practical to refer to an average of the two cell volumes computed with Equations 6.14:

$$\Delta \mathrm{V}_m^{(e)} = \frac{\Delta \mathrm{V}_1 + \Delta \mathrm{V}_2}{2}. \tag{6.15}$$

Similarly the scoured volume in correspondence of the vegetation plot is given by

$$\Delta \mathrm{V}_p^{(i)} = \Delta \mathrm{z}_{plot} \cdot \mathrm{A}_{cell}. \tag{6.16}$$

The duration $\Delta \mathrm{t}^*$ of the discharge $\mathrm{Q} > \mathrm{Q}^*$ over the year is the duration, expressed in seconds, of the flood producing scouring or deposition on the island. Dividing the scoured volume computed with Equations 6.15 by $\Delta \mathrm{t}^*$ gives the balance of sediment transport (in m^3/s) through the considered cell:

$$\Delta \mathrm{Q}_s^{(e)} = \frac{\Delta \mathrm{V}_m^{(e)}}{\Delta \mathrm{t}^*} \tag{6.17a}$$

$$\Delta \mathrm{Q}_s^{(i)} = \frac{\Delta \mathrm{V}_{plot}^{(i)}}{\Delta \mathrm{t}^*}, \tag{6.17b}$$

where now $\mathrm{Q}_s^{(e)}$ is the average sediment transport balance of the cells external to the plot and $\mathrm{Q}_s^{(i)}$ in the sediment transport balance of the plot cell. The specific sediment transport (expressed as $\mathrm{m}^3/\mathrm{s}/\mathrm{m}$) may be computed dividing the total sediment transport balance through the cell by the cell with L_{cell}:

$$\mathrm{q}_s^{(e)} = \frac{\Delta \mathrm{Q}_s^{(e)}}{\mathrm{L}_{cell}} \tag{6.18a}$$

$$\mathrm{q}_s^{(i)} = \frac{\Delta \mathrm{Q}_s^{(i)}}{\mathrm{L}_{cell}}. \tag{6.18b}$$

A formula to compute the specific bedload transport, on bare soil cells, $\mathrm{q}_s^{(e)}$, can be obtained by expressing it through Equations 2.6:

$$q_s^{(e)} = 8\sqrt{(G-1)\, g d_{50}^3}\,(\tau^* - \tau_c^*)^{3/2}. \tag{6.19}$$

For the model here formulated, once the data represented in Figure 6.3 (i.e., scouring Δz) and the duration of the flood events above a certain critical value are known, $q_s^{(e)}$ can be obtained from Equation 6.18.a. One can reformulate Equation 6.19 to explicit the value of τ_{eq}^*:

$$\tau_{eq}^* = \left[\frac{1-n}{8\sqrt{(G-1)\, g d_{50}^3}} q_s^{(e)}\right]^{2/3} + \tau_c^*, \tag{6.20}$$

where τ_{eq}^* is the equivalent shear stress for the cell external to the plot, τ_c^* is the Shields critical shear stress *n* the porosity of the soil matrix and the other terms are described in Section 2.5.2.

Considering now the vegetated cell, inside the plot, and introducing a new value $\tau_{c,mod}^*$ of the critical shear stress inside the plot where soil resistance is modified by the presence of roots, Meyer-Peter and Müller equation (Equation 2.6.a) can be written for the plot cell,

$$q_s^{(i)} = 8\left(\tau_{eq}^* - \tau_{c,mod}^*\right)^{3/2}, \tag{6.21}$$

where the balance of solid transport $q_s^{(i)}$ is known from Equation 6.18.b and the equivalent shear stress for the flow producing scouring,τ_{eq}^*, can be computed according to Equation 6.20. The only unknown of Equation 6.21 is the modified critical shear stress $\tau_{c,mod}^*$, which is a function of the root length or, even better, of the root volume $\tau_{c,mod}^* = \tau^*(RLD, RVR)$. A simple reformulation of Equation 6.21 leads to

$$\tau_{c,mod}^* = \tau_{eq}^* - \left(\frac{q_s^{(i)}}{8}\right)^{2/3}. \tag{6.22}$$

$\tau_{c,mod}^*$ can thus be written as the sum of the critical shear stress in normal condition (i.e., soil without roots) plus a linear combination of the root volume ratio RVR times a scaling factor *m*: $\tau_{c,mod}^* = \tau_c + m \cdot RVR$. The value of $\tau_{c,mod}^*$ is the new threshold of incipient movement in the Shields diagram.

In other words, the critical shear stress of the soil-root matrix, which has to be exceeded by the flow in order to produce particle movement, can considered as a virtual increase of the particle size or for the same particle size an increase of particle's specific weight (Figure 6.4).

One important thing has to be noticed: the difference in elevation for one cell is the integral of the erosion or deposition due to floods occurred between two surveys that produced the

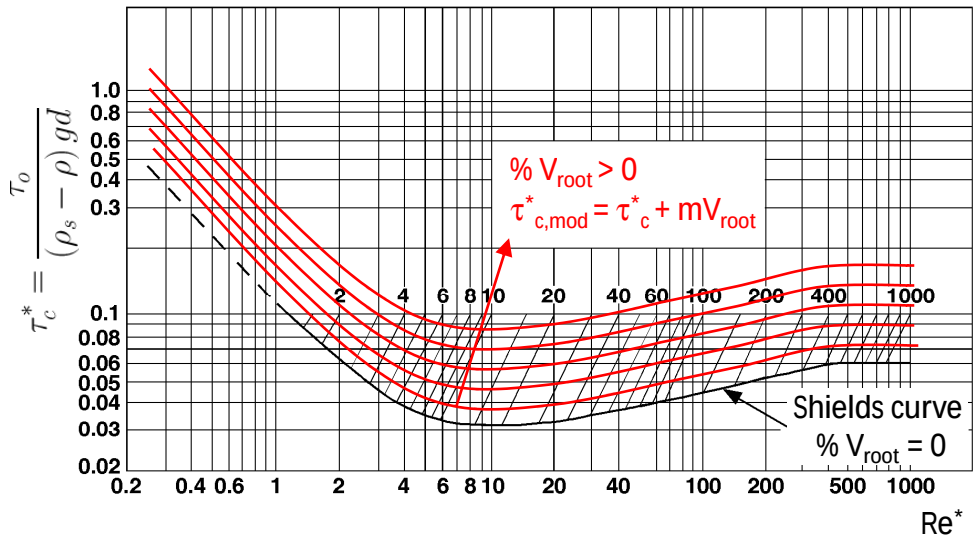

Figure 6.4: *Example of how the Shields curve of incipient motion may be modified according to percentage of root volume in the soil. For root volume $V_{root} = 0$ the curve it the same than the original computed by Shields. Increasing the percentage of V_{root}, for similar values of Re*, the curve moves towards upper values of τ_c^*.*

DTMs. Therefore the shorter is the interval between two DTM surveys the more accurate will be the results given by the model.

6.2.3 Quantification of root reinforcement and model validation from data

Considering Figure 3.7, only few plots from 2009 and 2010 may be considered for validation. All plots, where there was a positive balance of deposition, are not suitable to test the model. Among the remaining plots, all the plots where more than 40 cm of scouring was recorded, cannot be used for validation as well. Indeed, being the original cutting length nearly 40 cm, it is likely that, where erosion was deeper than this value, the entire plot died and cuttings have been flushed away.

Matrices with data used to realize Figure 3.7, are thus used here for computing the scoured volume as shown in Tables 6.1 and 6.2. After having computed the average of the external beside cell scoured volume $\Delta V_m^{(e)}$ and the plot cell scoured volume $\Delta V_p^{(i)}$ the following condition is imposed: $\Delta V_m^{(e)} > \Delta V_p^{(i)}$. In order to estimate the root reinforcement the volume scoured in correspondence of the plot must be lower than the volume scoured in the surrounding cells. Considering the strong turbulence of the flow during a flood event it may reasonably be assumed that Re*>1000 on the Shields' diagram (see Figure 2.13). In this case the Shields' critical shear stress reaches its asymptotic value $\tau_c^* = 0.047$. Given $d_{50} = 2.5$ cm, as computed from grain

size curve analysis (Section 2.2.2), a value of $\tau_c^* = 0.047$ corresponds to a discharge $Q^* = 400$ m^3/s (see Table 3.1). From both 2009 and 2010 hydrograph of the hourly discharge it is possible to compute the total duration Δt^*, over each season, of the peak flow exceeding $Q^* = 400$ m^3/s. In 2009 there was only one peak exceeding the threshold Q^* for a total of 15 hours (see Figure 5.1). In 2010 the hydrograph was more dynamic and there were several peaks along the season exceeding Q^*. Therefore the total duration Δt^* was much higher than in 2010 for a total of 50 hours (see Figure 5.1). Time in Equation 6.17 is expressed in seconds. The cell size to compute the scoured volume is, in this case: A_{cell}= 2 m x 2 m = 4 m^2.

Only three plots in 2009 and six in 2010 were suitable for validation. Table 6.1 and 6.2 show results of the validation in 2009 and 2010 respectively. Despite a low value of the average Root Volume Ratio $RVR_{2009} = 0.15$ % in September 2009 (see Figure 4.5), the average increment of $\tau^*_{c,mod,2009}$ is equal to 2.45 %.

Based on the equations described in Section 6.2.2, an explanatory example of the application of the root reinforcement model, based on the above mentioned assumptions, is given for Plot 20 in 2009 (see Table 6.1). The volume computed for the left and right cells beside the vegetation plot are (Equation 6.14):

$$\Delta V_L = \Delta z_L \cdot A_{cell} = 0.154 \cdot 4 = 0.62 \ \text{m}^3$$

$$\Delta V_R = \Delta z_R \cdot A_{cell} = 0.09 \cdot 4 = 0.36 \ \text{m}^3.$$

The reference scoured volume beside the plot cell is computed as average of the left and right cell as from Equation 6.15:

$$\Delta V_m^{(e)} = \frac{\Delta V_1 + \Delta V_2}{2} = \frac{0.62+0.36}{2} = 0.49 \ \text{m}^3.$$

Similarly the scoured volume in correspondence of the vegetation plot cell is given by Equation 6.16:

$$\Delta V_p^{(i)} = \Delta z_{plot} \cdot A_{cell} = 0.082 \cdot 4 = 0.33 \ \text{m}^3.$$

The specific sediment transport, computed for a time Δt^* (which is the duration of the considered number of flood events), is given by combining Equations 6.17 and 6.18 for the external (e) and internal (i) cells respectively:

$$\mathrm{q}_s^{(e)} = \frac{\frac{\Delta \mathrm{V}_m^{(e)}}{\Delta \mathrm{t}^*}}{\mathrm{L}_{cell}} = \frac{\frac{0.49}{4.5E-06}}{2} = 4.5\mathrm{E}-06 \ \ \mathrm{m}^3/\mathrm{s}/\mathrm{m}$$

$$\mathrm{q}_s^{(i)} = \frac{\frac{\Delta \mathrm{V}_{plot}^{(i)}}{\Delta \mathrm{t}^*}}{\mathrm{L}_{cell}} = \frac{\frac{0.33}{4.5\mathrm{E}-06}}{2} = 3.1\mathrm{E}-06 \ \ \mathrm{m}^3/\mathrm{s}/\mathrm{m}.$$

The equivalent shear stress for the cells external to the plot is given by Equation 6.20:

$$\tau_{eq}^* = \left[\frac{1-n}{8\sqrt{(G-1)gd_{50}^3}} q_s^{(e)}\right]^{2/3} + \tau_c^* = \left[\frac{1-0.3}{8\sqrt{1.65\ 9.81\ 0.025^3}\ 4.5E-06}\right]^{2/3} + 0.047 = 0.0479 \ \ \mathrm{Pa}.$$

Finally, the modified critical shear stress which takes into account the for the presence of the root within the plot cell is computed according to Equation 6.22:

$$\tau_{c,mod}^* = \tau_{eq}^* - \left(\frac{q_s^{(i)}}{8}\right)^{2/3} = 0.0479 - \left(\frac{3.1E-06}{8}\right)^{2/3} = 0.0478 \ \ \mathrm{Pa}.$$

The difference between $\tau_{c,mod}^*$ and τ_{eq}^*, and therefore between the shear stress in correspondence of the root system and the non-vegetated soil is about 1.70 %. Similar operations have been done to compute all the values reported in Table 6.1 and 6.2.

In 2010 the RVR measured from field experiment (see Section 4.2.2) was even lower, nearly a half than in 2009, and precisely $\mathrm{RVR}_{2010} = 0.09\ \%$. As a consequence the increased soil resistance estimated by the root reinforcement model described in the former section is proportionally about a half of the one in 2009: $\tau_{c,mod,2010}^*$ is equal to 1.12 %.

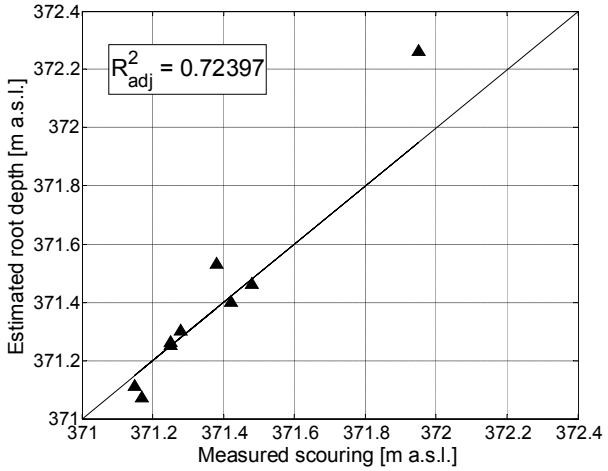

Figure 6.5: *Coefficient of determination R^2 of the observed erosion value within the plot Δz and the expected depth of the root mode, as computed with Equation 5.3 (See scaling map in Figure 5.7).*

Combining this approach with the scaling relationship expressed in Equation 5.3 (see Section 5.5), one can assess the expected depth Z_r of highest root density of the plot and determine, accordingly, the expected reinforcement, using it for model verification. Comparing the scouring data of the plot (obtained as the difference between two consecutive DTMs, as described in Section 3.3) with the expected depth of root density mode, one may investigate whether a relation exist between the two. Looking at the areas where plot 26-31 where located in Figure 5.7, would suggest a depth (from the initial surface level) of the highest root density in the range 10÷30 cm, comparable with the scouring computed in correspondence of the plot reported in Table 6.2. Therefore Equation 5.3 is used to compute precisely, the expected depth Z_r of highest root density. The so obtained Z_r are considered as estimated values whereas the scouring depths are considered as observed values to compute the coefficient of determination R^2_{adj} between the two. Results are shown in Figure 6.5, which show a positive correspondence ($R^2_{adj} = 0.7239$) between the expected root highest density depth and the observed erosion depth. This result would suggest that somehow where the root density reaches its peak, somehow the scouring potential of the flood have been reduced, resulting in a local end of the erosion process by the action of the root reinforcement.

Plot 20		
Scouring: Dz		
-0.15	-0.15	-0.20
-0.13	-0.08	-0.10
-0.08	-0.09	-0.07
τ_*^c =	0.047	
ΔV_1 =	-0.618	m^3
ΔV_2 =	-0.360	m^3
$\Delta V_m^{(e)}$ =	-0.489	m^3
$\Delta V_p^{(i)}$ =	-0.330	m^3
	YES	
$\Delta Q_s^{(e)}$ =	4.5E-06	m^2/s
$\Delta Q_s^{(i)}$ =	3.1E-06	m^2/s
$\tau_*^{(eq)}$ =	0.048	
$\tau_{c,mod}$ =	0.048	
	1.70%	

Plot 22		
Scouring: Dz		
-0.13	-0.17	-0.19
-0.11	-0.13	-0.09
-0.11	-0.11	-0.07
τ_*^c =	0.047	
ΔV_1 =	-0.692	m^3
ΔV_2 =	-0.433	m^3
$\Delta V_m^{(e)}$ =	-0.563	m^3
$\Delta V_p^{(i)}$ =	-0.518	m^3
	YES	
$\Delta Q_s^{(e)}$ =	5.2E-06	m^2/s
$\Delta Q_s^{(i)}$ =	4.8E-06	m^2/s
$\tau_*^{(eq)}$ =	0.048	
$\tau_{c,mod}$ =	0.04787	
	1.84%	

Plot 23		
Scouring: Dz		
0.00	-0.40	0.01
-0.14	-0.20	-0.01
-0.25	-0.40	-0.18
τ_*^c =	0.047	
ΔV_1 =	-1.6	m^3
ΔV_2 =	-1.6	m^3
$\Delta V_m^{(e)}$ =	-1.600	m^3
$\Delta V_p^{(i)}$ =	-0.800	m^3
	YES	
$\Delta Q_s^{(e)}$ =	1.5E-05	m^2/s
$\Delta Q_s^{(i)}$ =	7.4E-06	m^2/s
$\tau_*^{(eq)}$ =	0.049	
$\tau_{c,mod}$ =	0.04878	
	3.80%	

Table 6.1: *Results of validation of the root reinforcement model for plots in 2009. The average root reinforcement is found to be +2.45%.*

Plot 26		
Scouring: Dz		
-0.22	-0.19	-0.15
-0.21	-0.21	-0.19
-0.24	-0.25	-0.23
τ_*^c =	0.047	
ΔV_1 =	-0.762	m^3
ΔV_2 =	-0.980	m^3
$\Delta V_m^{(e)}$ =	-0.871	m^3
$\Delta V_p^{(i)}$ =	-0.832	m^3
	YES	
$\Delta Q_s^{(e)}$ =	2.4E-06	m^2/s
$\Delta Q_s^{(i)}$ =	2.3E-06	m^2/s
$\tau_*^{(eq)}$ =	0.048	
$\tau_{c,mod}$ =	0.048	
	1.10%	

Plot 27		
Scouring: Dz		
-0.23	-0.26	-0.22
-0.24	-0.23	-0.23
-0.26	-0.26	-0.27
τ_*^c =	0.047	
ΔV_1 =	-1.027	m^3
ΔV_2 =	-1.030	m^3
$\Delta V_m^{(e)}$ =	-1.029	m^3
$\Delta V_p^{(i)}$ =	-0.928	m^3
	YES	
$\Delta Q_s^{(e)}$ =	2.9E-06	m^2/s
$\Delta Q_s^{(i)}$ =	2.6E-06	m^2/s
$\tau_*^{(eq)}$ =	0.048	
$\tau_{c,mod}$ =	0.048	
	1.24%	

Plot 28		
Scouring: Dz		
-0.25	-0.23	-0.22
-0.27	-0.20	-0.20
-0.29	-0.25	-0.27
τ_*^c =	0.047	
ΔV_1 =	-0.93	m^3
ΔV_2 =	-1.015	m^3
$\Delta V_m^{(e)}$ =	-0.972	m^3
$\Delta V_p^{(i)}$ =	-0.817	m^3
	YES	
$\Delta Q_s^{(e)}$ =	2.7E-06	m^2/s
$\Delta Q_s^{(i)}$ =	2.3E-06	m^2/s
$\tau_*^{(eq)}$ =	0.048	
$\tau_{c,mod}$ =	0.048	
	1.19%	

Plot 29		
Scouring: Dz		
-0.14	-0.17	-0.14
-0.17	-0.15	-0.15
-0.28	-0.20	-0.16
τ_*^c =	0.047	
ΔV_1 =	-0.662	m^3
ΔV_2 =	-0.803	m^3
$\Delta V_m^{(e)}$ =	-0.733	m^3
$\Delta V_p^{(i)}$ =	-0.597	m^3
	YES	
$\Delta Q_s^{(e)}$ =	2.0E-06	m^2/s
$\Delta Q_s^{(i)}$ =	1.7E-06	m^2/s
$\tau_*^{(eq)}$ =	0.048	
$\tau_{c,mod}$ =	0.047	
	0.99%	

Plot 30		
Scouring: Dz		
-0.20	-0.22	-0.20
-0.17	-0.14	-0.21
-0.18	-0.21	-0.21
τ_*^c =	0.047	
ΔV_1 =	-0.892	m^3
ΔV_2 =	-0.823	m^3
$\Delta V_m^{(e)}$ =	-0.857	m^3
$\Delta V_p^{(i)}$ =	-0.573	m^3
	YES	
$\Delta Q_s^{(e)}$ =	2.4E-06	m^2/s
$\Delta Q_s^{(i)}$ =	1.6E-06	m^2/s
$\tau_*^{(eq)}$ =	0.048	
$\tau_{c,mod}$ =	0.048	
	1.11%	

Plot 31		
Scouring: Dz		
-0.19	-0.19	-0.16
-0.20	-0.15	-0.20
-0.21	-0.22	-0.24
τ_*^c =	0.047	
ΔV_1 =	-0.747	m^3
ΔV_2 =	-0.870	m^3
$\Delta V_m^{(e)}$ =	-0.809	m^3
$\Delta V_p^{(i)}$ =	-0.608	m^3
	YES	
$\Delta Q_s^{(e)}$ =	2.2E-06	m^2/s
$\Delta Q_s^{(i)}$ =	1.7E-06	m^2/s
$\tau_*^{(eq)}$ =	0.048	
$\tau_{c,mod}$ =	0.047	
	1.06%	

Table 6.2: *Results of validation of the root reinforcement model for plots in 2010. The average root reinforcement is found to be +1.12%.*

Chapter 7

Conclusions

As introduced in chapter 1, the goal of the RE.COR.D. project was to quantify the results of restoration and to scientifically approach the study of the river and riparian zone dynamics after restoration, in order to give a mechanistic tool for future restoration process. This work gives important answer to research question concerning the active role of vegetation in relation to several other ecological and hydrological aspects, such as morphodynamics.

In the contest of this PhD work, many installations have been set up and many experiment and analysis carried out with the aim of monitoring the evolution of a river corridor after restoration and to assess the quantification of root induced reinforcement. A large variety of instruments have been installed to monitor meteorological and soil moisture dynamics. In parallel transplantation of Salix cuttings have been carried out for three consecutive years of field campaign, including monitoring of the above- and below-ground biomass growth and surviving. Together with river bathymetry and sediment sorting data, DEMs (produced by aerial LIDAR survey on a yearly base) have been used to study the local hydrodynamic at restored reach scale. Aerial and terrestrial photography have been used to monitor both vegetation dynamics and morphodynamic evolution of the river corridor after restoration. Terrestrial pictures have been used to develop a new technique to calibrate hydrodynamic models via remote sensing. Some preliminary morphological analysis at the reach scale and at the river bed form scale have been produced, in order to investigate the effect of restoration on river dynamics and possibly, to link river morphodynamic to vegetation establishment, surviving and growing. Particular attention was dedicated to the erosion/deposition patters as primary factors influencing vegetation mortality.

Those analyses, together with vegetation statistics of above-ground growth and survival and with statistics on root morphology and architecture were used to formulate a model of root development as controlled by the hydrodynamic regime and the water table fluctuation, and, subsequentially, to formulate a model of root reinforcement. Both models are quite simple and

were proven to be predictive with respect to the experimental data collected during the project. Although the two models integrate the results of the entire study, this has produced several interesting outcomes, with high knowledge innovation content.

This work has investigated all the proposed topics: i) the morphologic changes of the restored reach in response to hydrologic disturbances (Chapter 3), ii) the interaction between flow, sediment and local vegetation (Chapter 4 and 5), and iii) the mechanical anchoring due to vegetation roots and its contributions (Chapter 6) in sediment stabilization.

The new challenging idea leading the project was to assess the mechanical understanding by means of different and integrated techniques, such as field experiment, monitoring and modelling (Pasquale et al., 2011). The instrumentation set up integrated with new monitoring techniques allowed answering the second research question concerning the amount of vegetation that can colonize the bare sediments. The integrated monitoring of vegetation, hydrology and morphology allowed obtaining quite unique data and results: statistics on vegetation growth, according to river hydrology, as well as vegetation establishment and surviving rate in relation to river hydrology and erosion-deposition dynamics.

The digital camera set up allowed to estimate the damage produced by the flood via remote sensing, using NDVI techniques which combine visible and infrared pictures to compute the percentage of vegetation on the soil surface (Pasquale et al., 2011). Usually those techniques are based on satellite and aerial images. To the purpose of this work we used terrestrial images which are easier to produce both in terms of costs and in terms of shooting frequency. Indeed the camera set up on the Thur River allowed shooting pictures from remote and at any time of the day. The same cameras set up was used to produce a new innovative technique to calibrate hydrodynamic models (Pasquale et al., 2012). The technique is based on an automatic pattern recognition (Pasquale et al., 2011) and it uses the combination of remote sensing and terrestrial photography to calibrate the Manning's roughness coefficient to be use in the simulation at different flow rates.

New techniques have been developed to compute the elevation of the water table starting from superficial flow simulations. The satisfactory results are also object of a scientific publication by Schneider et al. (2011). Determining the statistic distribution of the water table in correspondence of vegetation plot has allowed finding a statistical scaling relationship between the vertical root distribution and river hydrology as a main driving force (Pasquale et al., 2012a).

The root sampling work carried out in the contest of this work has produced two scientific publication (Pasquale et al., 2011, 2012a) in which new techniques for cutting uprooting are described and recommended, in case of gravel, non-cohesive soils.

Results reported in this work show how an integrated system of experiments, monitoring and

modelling is able to give a broader comprehension on the eco-geomorphological processes on a restored river reach. All the experiments carried out made possible a link among vegetation establishment, growth, surviving and mortality in relation to soil characteristics, river hydrology and morphology (erosion-deposition processes). It has been shown that hydrotropism and oxitropism are root growth and root distribution primary driving factors (Pasquale et al., 2012a). The mutual interaction between vegetation and river morphodynamic is explained in form of root reinforcement.

The quantification of root induced reinforcement is expressed in terms of increased shear stress, as for many authors did in the contest of river banks and slopes. However the originality of this project is to directly relate the increased shear stress resistance to the soil cohesion and characteristics. The proposed model uses data of erosion-deposition balance measured on the field and does not require any information on root strength resistance which is often too difficult to be quantified. The main research question behind this work, addressing the influence of vegetation roots in controlling the movement of sediment is therefore answered.

The innovative aspect of this study on vegetation root reinforcement is that it focuses on river bed sediment dynamics rather than river banks, slopes or riparian zones. The root reinforcement relation is directly included in Meyer-Peter and Müller equations and it modifies the commonly used Shields' diagram.

The modified critical shear stress $\tau^*_{c,mod}$, computed in this work as a validation of the formulated model of root reinforcement, did not show such a strong increase in soil cohesion due to the root system. The main reasons are substantially two: first, vegetation and root data used to validate the model are based on measurement involving plants in their first six months of life, after spreading. Moreover, some of the plots involved in the erosion process also suffer cutting mortality, consequently decreasing the density of vegetation per plot. As a consequence, results of the statistics on Root Volume Ratio (the ratio between the root volume and the volume of the soil matrix it fills) show a very low percentage of RVR for both field campaigns. Precisely in 2009 the measured RVR was only 1.5 per mill and in 2010 an even lower value of RVR equal to 0.9 per mill was recorded. Of course the values of the critical shear stress due to root reinforcement in presence of higher percentages of root volume per soil unit are expected to be substantially more significant.

The number of DEMs produced per year and also the way they are temporally distributed along the season is surely the second limiting factor impacting the results of $\tau^*_{c,mod}$. The erosion-deposition analysis carried out in the contest of this work, are produced using one DEM of the restored corridor at the beginning of the transplanting season (April) and one another at the end of the growing season (September of the same year). Consequently, results represent the integral of the single events occurred during the whole season. This implies the fact that it

averages a variety of different magnitude flood events with not linearly related scouring and deposition phenomena.

A possible solution in this sense would be to produce a DEM of the interested area after each significant flood event, thus to allow coupling scouring and flood magnitude in a straight way. This is likely to be possible in the next future, since innovative technologies for autonomous DEM production are becoming more and more available, accurate, repeatable and affordable.

The availability of such frequent DEMs not only would improve goodness of the root reinforcement model formulated in chapter 6. It would also allow exploring and validating the energetic method proposed as outlook of this work.

Chapter 8

References

References

Abernethy, B. and I. D. Rutherford (1998). Where along a river's length will vegetation most effectively stabilize streambanks? *Geomorphology 23*, 55–75.

Abernethy, B. and I. D. Rutherfurd (2001). The distribution and strength of riparian tree roots in relation to riverbank reinforcement. *Hydrological Processes 15*, 63–79.

Allan, D. J. and M. M. Castillo (2007). Stream ecology: Structure and function of running waters. In *Transactions of the American Fisheries Society* (2nd ed.), Volume 125, pp. 445. Springer.

Aloni, R., E. Aloni, M. Langhans, and C. I. Ullrich (2006). Role of cytokinin and auxin in shaping root architecture: regulating vascular differentiation, lateral root initiation, root apical dominance and root gravitropism. *Annals of botany 97*(5), 883–93.

Andrews, E. D. (1984). Bed-material entrainment and hydraulic geometry of gravel-bed rivers in colorado. *Geological Society of America Bulletin 95*, 371–378.

Aoki, Y., M. Hoshino, and T. Matsubara (2007). Silica and testate amoebae in a soil under pine-oak forest. *Geoderma 142*, 29–35.

Argyris, J. H. and G. Faust (1994). *An exploration of chaos: an introduction for natural scientists and engineers* (1st ed.). North-Holland, Amsterdam, Netherlands.

Aronica, G. (1998). Uncertainty and equifinality in calibrating distributed roughness coefficients in a flood propagation model with limited data. *Advances in Water Resources 22*(4), 349–365.

Aronica, G., P. D. Bates, and M. S. Horritt (2002). Assessing the uncertainty in distributed model predictions using observed binary pattern information within GLUE. *Hydrological Processes 16*(10), 2001–2016.

Ashworth, P. J., R. I. Ferguson, and M. D. Powell (1992). Bedload transport and sorting in braided channels. In P. Billi, R. Hey, C. Thorne, and P. Tacconi (Eds.), *Dynamics of gravel-bed rivers*, pp. 497–515. John Wiley & Sons LTD.

Bathurst, J. C. (2002). At-a-site variation and minimum flow resistance for mountain rivers. *Journal of Hydrology 269*, 11–26.

Battle-Aguilar, J., A. Brovelli, J. Luster, J. Shrestha, and D. A. Barry (2011). Carbon and nitrogen dynamics in a variably saturated soil profile. model application to a restored swiss riparian area. *Submitted to Science of the Total Environment*.

Beker, L. and W. W. G. Yeh (1972). Identification of parameters in unsteady open channel flows. *Water Resources Research 8*(4), 956–965.

Bendix, J. and C. R. Hupp (2000). Hydrological and geomorphological impacts on riparian plant communities. *Hydrological Processes 14*(16-17), 2977–2990.

Bengough, A. G., A. Castrignano, L. Pages, and M. G. van Noordwijk (2000). Sampling strategies, scaling, and statistics. In A. Smith (Ed.), *Root Methods: a handbook* (1st ed.)., pp. 145–173. Springer-Verlag, Berlin.

Bernardara, P., E. de Rocquigny, N. Goutal, A. Arnaud, and G. Passoni (2010). Uncertainty analysis in flood hazard assessment: hydrological and hydraulic calibration. *Canadian Journal of Civil Engineering 37*, 968–979.

Bertrand, F., E. Malysheva, Y. Mazei, M. Moretti, and E. A. D. Mitchell (2012). Toward the use of testate amoebae functional traits as indicator of flood plain restoration success. *European Journal of Soil Biology, article in press*.

Bloom, C. W. P. M. and L. A. C. J. Voesenek (1996). Flooding: the survival strategies of plants. *Tree 11*(7), 290–295.

Bouma, T. J., K. L. Nielsen, J. Van Hal, and B. Koutstaal (2001). Root system topology and diameter distribution of species from habitats differing in inundation frequency. *Functional Ecology 15*(3), 360–369.

Boussinesq, J. (1877). Essai sur la theorie des eaux courantes. In *Memoires presentes par divers savants a l'Academie des Sciences XXIII*, pp. 1–680.

Bovee, K. D. (1982). *A guide to stream habitat analysis using the in.-stream flow incremental methodology*. U.S. Fish And Wildlife Services, Fort Collins, CO.

Brasington, J., B. T. Rumsby, and R. A. McVey (2000). Monitoring and modelling morphological change in a braided gravel-bed river using high resolution GPS-based survey. *Earth Surface Processes and Landforms 25*(9), 973–990.

Bridge, J. S. (1993). The interaction between channel geometry, water flow, sediment transport and deposition in braided rivers. *Geological Society, London, Special Publications 75*, 13–71.

Brookes, A. (1988). *Channelized rivers: Prospectives for Environmental Management*. John Wiley & Sons LTD, Hoboken, NJ, USA.

Burgess, D., O. Q. Hendrickson, and L. Roy (1990). The importance of initial cutting size for improving the growth performance of Salix Alba L. *Scandinavian Journal of Forest Research 5*(1-4), 215–224.

BWG (2001). *Bundesamt für Wasser und Geologie*. Hochwasserschutz an Fliessgewüssern, Wegleitung, Biel, Switzerland.

Cairns, J. (1991). The status of the theoretical and applied science of restoration ecology. *The environmental professional 13*, 186–194.

Camporeale, C., P. Perona, A. Porporato, and L. Ridolfi (2005). On the long-term behavior of meandering rivers. *Water Resources 41*, 1–13.

Camporeale, C., P. Perona, and L. Ridolfi (2006). Hydrological and geomorphological significance of riparian vegetation in drylands. In *Drylands Ecohydrology*. Eds. Springer, The Netherlands.

Casagli, N., M. Rinaldi, A. Gargini, and A. Curinin (1999). Pore-water pressure and stream-bank stability: results from a monitoring site on the Sieve River, Italy. *Earth Surface Processes and Landforms 21*, 1095–1114.

Castellarin, A., G. Di Baldassarre, P. D. Bates, and A. Brath (2009). Optimal cross-sectional spacing in preissmann scheme 1-D hydrodynamic models. *Journal of Hydraulic Engineering 135*(2), 96–105.

Chien, N. (1954). Meyer-Peter formula for bed-load transport and Einstein bed-load function. In U. of California-Berkeley and T. M. R. Division (Eds.), *M.R.D. Sediment Series No. 7*, pp. 367–381. U.S. Army Corps of Engineers, Berkeley, CA.

Chow, V. T. (1973). *Open-channel hydraulics* (2nd ed.). McGraw-Hill Book, New York, USA.

Clifford, N. J., P. J. Soar, O. P. Harmar, A. M. Gurnell, G. E. Petts, and J. C. Emery (2005). Assessment of hydrodynamic simulation results for eco-hydraulic and eco-hydrological applications: a spatial semivariance approach. *Hydrological Processes 19*(18), 3631–3648.

Cobby, D. (2001). Image processing of airborne scanning laser altimetry data for improved river flood modelling. *ISPRS Journal of Photogrammetry and Remote Sensing 56*(2), 121–138.

Colombini, M., G. Seminara, and M. Tubino (1987). Finite-amplitude alternate bars. *Journal of Fluid Mechanics 181*, 213–232.

Corenblit, D., E. Tabacchi, J. Steiger, and A. M. Gurnell (2007). Reciprocal interactions and adjustments between fluvial landforms and vegetation dynamics in river corridors : A review of complementary approaches. *Earth-Science Reviews 84*, 56 – 86.

Coutts, M. P. (1983). Root architecture and tree stability. *Plant and Soil 188*, 171–188.

Crouzy, B. and P. Perona (2012). Biomass selection by floods and related timescales. Part 2: Stochastic modeling. *Advances in Water Resources 39*, 97–105.

Daniels, H. E. (1945). The statistical theory of the strength of bundles of threads. In *Proceedings of the Royal Society, London, Ser. A*, Volume 183, pp. 405–435.

Defries, R. S. and J. R. G. Townshend (1994). NDVI derived land-cover classifications at global-scale. *Policy 15*(17), 3567–3586.

Densmore, R. V. and K. F. Karle (2009). Flood effects on an Alaskan stream restoration project: the value of long-term Monitoring. *JAWRA Journal of the American Water Resources Association 45*(6), 1424–1433.

Diplas, P. and G. Parker (1992). Deposition and removal of fines in gravel-bed streams. In Billi, P and Hey, RD and Thorne, CR and Tacconi, P (Ed.), *Dynamic of gravel-bed rivers*, pp. 313–329. John Wiley & Sons LTD.

Dung, N. V., B. Merz, A. Bardossy, T. D. Thang, and H. Apel (2011). Multi-objective automatic calibration of hydrodynamic models utilizing inundation maps and gauge data. *Hydrology and Earth System Sciences 15*, 1339–1354.

Edmaier, K., P. Burlando, and P. Perona (2011). Mechanisms of vegetation uprooting by flow in alluvial non-cohesive sediment. *Hydrology and Earth System Sciences 15*(5), 1615–1627.

Emery, J. C., A. M. Gurnell, N. J. Clifford, G. E. Petts, I. P. Morrissey, and P. J. Soar (2003). Classifying the hydraulic performance of riffle-pool bedforms for habitat assessment and river rehabilitation design. *River Research and Applications 19*(5-6), 533–549.

Ennos, A. R. (1993). The scaling of root anchorage. *Journal of theoretical Biology 161*, 61–75.

Fabio, P., G. T. Aronica, and H. Apel (2010). Towards automatic calibration of 2D flood propagation models. *Hydrology and Earth System Sciences 14*, 911–924.

Fan, C. and C. Su (2008). Role of roots in the shear strength of root-reinforced soils with high moisture content. *Ecological Engineering 33*(2), 157–166.

Farmer, R. E. and F. T. Bonner (1967). Germination and initial growth of eastern cottonwood as influenced by moisture stress, temperature and storage. *Botanical Gazette 128*, 211–215.

Federici, B. and G. Seminara (2003). On the convective nature of bar instability. *Journal of fluid mechanics 487*, 125–145.

Fitter, H. (1987). An architectural approach to the comparative ecology of plant root systems. *New Phytologist 106*, 61–77.

Formann, E., H. Habersack, and S. Schober (2007). Morphodynamic river processes and techniques for assessment of channel evolution in Alpine gravel bed rivers. *Geomorphology 90*(3-4), 340–355.

Francis, R. A. (2007). Size and position matter: riparian plant establishment from fluvially deposited trees. *Earth Surface Processes and Landforms 32*, 1239–1243.

Francis, R. A. and A. M. Gurnell (2006). Initial establishment of vegetative fragments within the active zone of a braided gravel-bed river (River Tagliamento, NE Italy). *Wetlands 26*(3), 641–648.

Francis, R. A., A. M. Gurnell, G. E. Petts, and P. J. Edwards (2005). Survival and growth responses of Populus nigra, Salix Elaeagnos and Alnus Icana cuttings to varying levels of hydric stress. *Forest Ecology and Management 210*(1-3), 291–301.

Fread, D. L. and G. F. Smith (1978). Calibration techniques for 1-D unsteady flow models. *C. J. Hydr. Div. 104*(7), 1027–1043.

Fredlund, D. G., N. R. Morgenstern, and R. A. Widger (1978). The shear strength of unsaturated soils. *Canadian Geotechnical Journal 15*, 313–321.

Gee, G. W. and J. W. Bauder (1986). *Methods of Soil Analysis. Part I* (2nd ed.), Volume 9. ASA and SSSA, Madison, WI, USA.

Gilvear, D., R. A. Francis, N. Willby, and A. M. Gurnell (2008). Gravel bars: a key habitat of gravel-bed rivers for vegetation. In *Gravel-Bed Rivers VI: From Process Understanding to River Restoration*, Volume 2025, pp. 677–700. Elsevier.

Girard, P., I. Fantin-Cruz, S. M. Loverde de Oliveira, and K. Hamilton, S. (2010). Small-scale spatial variation of inundation dynamics in a foodplain of the Pantanal (Brazil). *Hydrobiologia 638*, 123–233.

Glenz, C. (2005). *Riparian forest dynamics in central Europe - Tool for decision-making in river restoration*. Ph. D. thesis, EPFL, Lausanne, Switzerland.

Glenz, C., R. Schlaepfer, I. Iorgulescu, and F. Kienast (2006). Flooding tolerance of Central European tree and shrub species. *Forest Ecology and Management 235*, 1–13.

Graf, W. L. (1978). Fluvial adjustments to the spread of tamarisk in the Colorado Plateau region. *Geological Society of America Bulletin 89*, 1491–1501.

Gran, K. and C. Paola (2001). Riparian vegetation controls on braided stream dynamics. *Water Resources Research 37*, 3275–3283.

Gray, D. H. and H. Ohashi (1983). Mechanics of fiber reinforcement in sand. *Journal of Geotechnical Engineering 109*, 335–353.

Greenway, D. R. (1987). Vegetation and slope stability. In M. G. Anderson and K. S. Richards (Eds.), *Slope Stability, Chap. 6*, pp. 187–230. John Wiley and Sons, Hoboken, N. J.

Gregory, K. J. and A. M. Gurnell (1988). Vegetation and river channel form and process. In *Viles, H. (Ed.), Biogeomorphology*, pp. 11–42. Blackwell, Oxford, UK.

Gregory, P. (2006). *Plant roots: Growth, activities and interaction with soils* (1st ed.). Wiley-Blackwell Publishing Ltd, Oxford.

Gurnell, A. M. and G. Petts (2006). Trees as riparian engineers : The Tagliamento River , Italy. *Earth surface processes and landforms 31*, 1558–1574.

Gurnell, A. M. and G. E. Petts (2002). Island-dominated landscapes of large floodplain rivers, a european perspective. *Freshwater Biology 47*, 581–600.

Gurnell, A. M., G. E. Petts, D. M. Hannah, B. P. G. Smith, P. J. Edwards, J. Kollmann, J. V. Ward, and K. Tockner (2001). Riparian vegetation and island formation along the gravel-bed Fiume Tagliamento, Italy. *Earth Surface Processes and Landforms 26*(1), 31–62.

Gurnell, A. M., K. Tockner, P. Edwards, and G. Petts (2005). Effects of deposited wood on biocomplexitz of river corridors. *Frontiers in Ecology and the Environment 3*, 377–382.

Guswa, A. J. (2008). The influence of climate on root depth: A carbon cost-benefit analysis. *Water Resources Research 44*(2), 1–11.

Gyssel, G., J. Poesen, E. Bochet, and Y. Li (2005). Impact of plant root on the resistance of soil to erosion by water: a review. *Progress in Physical Geography 29*, 189–217.

Hall, J. W., S. Tarantola, P. D. Bates, and M. S. Horritt (2005). Distributed Sensitivity Analysis of Flood Inundation Model Calibration. *Journal of Hydraulic Engineering 131*(2), 117–126.

Harman, I. N. and J. J. Finnigan (2007). A unified theory for flow in the canopy and roughness sub layer. *Boundary Layer Meteorology 129*, 323–351.

Hartman, H. T. and D. E. Kester (1975). *Plant propagation: Principles and practices* (1st ed.). Prentice-Hall, New Jersey.

Hey, R. D. and C. R. Thorne (1986). Stable channels with mobile gravel beds. *Journal of Hydraulic Engineering 112*, 671–689.

Hickin, E. J. (1984). Vegetation and river channel dynamics. *Canadian Geographic 28*, 111–126.

Hidalgo, R. C., F. Kun, and H. J. Herrmann (2002). Bursts in a fiber bundle model with continuous damage. *Physical Review E 066122 64*, 1–9.

Horritt, M. A. (2010). Development and testing of a simple 2D finite volume model of a sub-critical shallow water flow. *Journal for Numerical Methods in Fluids 44*, 1231–1255.

Horritt, M. S., G. D. Baldassarre, P. D. Bates, and A. Brath (2007). Comparing the performance of a 2-D finite element and a 2-D finite volume model of floodplain inundation using airborne SAR imagery. *Hydrological Processes 21*, 2745–2759.

Hubble, T. C. T., B. B. Docker, and I. D. Rutherfurd (2010). The role of riparian trees in maintaining riverbank stability: A review of Australian experience and practice. *Ecological Engineering 36*(3), 292–304.

Ikeda, S., G. Parker, and K. Sawai (1981). Bend theory of river meanders. Part 1. Linear development. *Journal of fluid mechanincs 112*, 363–377.

Inglis, C, C. (1949). The behaviour and control of rivers and canals (with the aid of models). In *Central Water Power, Irrigation and Navigation Research Station, Research pubblication 13 part 1*, pp. 298. Poona, India.

Iwahashi, M. and S. Udomsiri (2007). Water level detection from video with fir filtering. In *ICCCN*, pp. 826–831. IEEE.

Jang, C. L. and Y. Shimizu (2007). Vegetation effects on the morphological behavior of alluvial channels. *Journal of Hydraulic Research 45*(6), 763–772.

Jowett, I. G. (2003). Hydraulic constraints on habitat suitability for benthic invertebrates in gravel-bed rivers. *River Research and Applications 19*(5-6), 495–507.

Julien, P., Y. (1995). *Erosion and Sedimentation* (1st ed.). Cambridge University Press, New York, USA.

Junk, W. J., P. B. Bayley, and R. E. Sparks (1989). The flood pulse concept in river-floodplain systems. *Canadian Special Publication in Fish and Aquatic Sciences 106*, 110–127.

Karrenberg, S., P. J. Edwards, and J. Kollmann (2002). The life history of salicaceae living in the active zone of floodplains. *Freshwater Biology* (47), 733–748.

Karrenberg, S., J. Kollmann, and P. J. Edwards (2003). Root anchorage of saplings and cuttings of woody pioneer species in a riparian environment. *Functional Ecology 17*, 170 – 177.

Katul, G. G. and J. D. Albertson (1998). An investigation of higher-order closure models for a forested canopy. *Boundary Layer Meteorology 89*, 47–74.

Katul, G. G., D. Poggi, and L. Ridolfi (2011). A flow resitance model for assesssing the impact of vegetation on flood routing mechanics. *Water Resources Research 47*, 1–15.

Keim, R. (1999). Digital terrain modeling of small stream channels with a total-station theodolite. *Advances in Water Resources 23*(1), 41–48.

Kuo, S. (1996). Phosphorus. In D. L. Sparks (Ed.), *Methods of soil analysis: Part 3- chemical methods*. SSSA, Madison, WI, USA.

Kuzovkina, Y. A. and T. A. Volk (2009). The characterization of willow (Salix L.) varieties for use in ecological engineering applications: Co-ordination of structure, function and autecology. *Ecological Engineering 35*(8), 1178–1189.

Lacey, G. (1930). Stable channel in alluvium. *Proceedings of the institution of civil engineers 229*, 259–292.

Laio, F. (2006). A vertically extended stochastic model of soil moisture in the root zone. *Water Resources Research 42*(2), 1–10.

Laio, F., P. D'Odorico, and L. Ridolfi (2006). An analytical model to relate the vertical root distribution to climate and soil properties. *Geophysical Research Letters 33*(18), 1–5.

Lamouroux, N. (1995). Predicting velocity frequency distributions in stream reaches. *Water Resources Research 31*(9), 2367–2375.

Lamouroux, N. (1998). Depth Probability Distributions in Stream Reaches. *Journal of Hydraulic Engineering 124*(2), 224.

Lamouroux, N., B. Statzner, U. Fuchs, F. Kohmann, and U. Schmedtje (1992). An unconventional approach to modeling the spatial and temporal variability of local shear stress in stream segments. *Water Resources Research 28*(12), 3251–3258.

Lane, S. N., K. S. Richards, and J. H. Chandler (1994). Developments in monitoring and modelling small-scale river bed topography. *Earth Surface Processes and Landforms 19*(4), 349–368.

Lanzoni, S. (2000). Experiments on bar formation in a straight flume 2. Graded sediment. *Water Resources Research 36*(11), 3351–3363.

Lejot, J., C. Delacourt, H. Piégay, T. Fournier, M.-l. Trémélo, and P. Allemand (2007). Very high spatial resolution imagery for channel bathymetry and topography from an unmanned mapping controlled platform. *Earth Surface processes and Landforms 32*, 1705–1725.

Leopold, B. L. and M. G. Wolman (1957). River chanel patterns: Braided, meandering and straight. In U. G. Survey (Ed.), *Cross Sections*. United States Government Printing Office, WA.

Lisle, T, E., H. Ikeda, and F. Iseya (1991). Formation of stationary alternate bars in a steep channel with mixed-size sediment - A flume experiment. *Earth Surface Processes Landforms 16*(5), 463–469.

Lisle, T, E. and A. Madej, M (1992). Spatial variation in armoring in a channel with high sediment supply. In Billi, P and Hey, R, D and Thorne, C, R and Tacconi, P (Ed.), *Dynamics of gravel-bed rivers*, pp. 277–293. John Wiley & Sons LTD.

Mallik, A. U. and H. Rasid (1993). Root-shoot characteristics of riparian plants in a flood control channel: implications for bank stabilization. *Ecological Engineering 2*(2), 149–158.

Malmqvist, B. and S. Rundle (2002). Threats to the running water ecosystems of the world. *Environmental Conservation 29*(02), 134–153.

Massman, W. J. (1997). An analytical one-dimensional model of momentum transfer by vegetation of arbitrary structure. *Boundary Layer Meteorology 83*, 407–421.

Massman, W. J. and J. C. Weil (1999). An analytical one-dimensional second-order closure model of turbolence statistics and the lagrangian time scale within and above plant canopies of arbitrary structure. *Boundary Layer Meteorology 91*, 81–107.

Meyer-Peter, E. and R. Müller (1948). Formulas for bed-load transport. In *Proceedings of the 2nd Meeting of the International Association for Hydraulic Structures Research*, pp. 39–64.

Millar, R. G. (2000). Influence of bank vegetation on alluvial channel patterns. *Water Resources Research 36*(4), 1109.

Mitsch, W. (2003). Ecological engineering: A field whose time has come. *Ecological Engineering 20*(5), 363–377.

Moggridge, H. (2007). *The dispersal, establishment and growth of vegetation in riprian zones*. Ph. D. thesis, University of London, London, UK.

Molnar, P., V. Favre, P. Perona, P. Burlando, C. Randin, and R. Wolfgang (2008). Floodplain forest dynamics in hydrologically altered mountain river. *Peckiana 5*, 17–24.

Nakamura, K., K. Tockner, and K. Amano (2006). River and wetland restoration: Lessons from Japan. *BioScience 56*, 419–429.

Nepf, H. M. (1999). Drag turbolence and diffusion in flow thorugh emergent vegetation. *Water Resources Research 35*, 479–489.

Nepf, H. M. (2007). Transport in aquatic canopies. In Y. A. Gayev and J. C. R. Hunt (Eds.), *Flow and transport with complex obstructions: applications to cities, Vegetative canopies and industry.*, pp. 221–250. Springer, Berlin.

Nepf, H. M. and E. R. Vivoni (2000). Flow structure in depth-limited, vegetated flow. *Journal of Geophysical Research 105*, 28547–28557.

Nielson, K. L., J. P. Lynch, and H. N. Weiss (1997). Fractal geometry of bean root systems: correlations between spatial and fractal dimension. *American Journal of Botany 84*, 26–33.

Niklas, K. J. (1992). *Plant Biomechanics: An Engineering Approach to Plant Form and Function* (1st ed.). University of Chicago Press, Chicago, Ill.

Olde Venterink, H., J. E. Vermaat, M. Pronk, F. Wiegman, G. E. M. van der Lee, M. V. van der Hoorn, L. Higler, and J. T. A. Verhoeven (2006). Importance of sediment deposition and denitrification for nutrient retention in floodplain wetlands. *Applied Vegetation Science* (9), 163–174.

Oyanagi, A., H. Takahashi, and H. Suge (1995). Interactions between Hydrotropism and Gravitropism in the Primary seminal Roots of Triticum Aestivum L. *Annals of Botany 75*, 229–235.

Palmer, M. A. and E. S. Bernhardt (2006). Hydroecology and river restoration: Ripe for research and synthesis. *Water Resources Research 42*, W03S07.

Palmer, M. A., H. L. Menninger, and E. Bernhardt (2010). River restoration, habitat heterogeneity and biodiversity: a failure of theory or practice? *Freshwater Biology 55*, 205–222.

Pappenberger, F., K. Beven, M. Horritt, and S. Blazkova (2005). Uncertainty in the calibration of effective roughness parameters in HEC-RAS using inundation and downstream level observations. *Journal of Hydrology 302*(1-4), 46–69.

Parker, G. M., C. M. Toro-Escobar, M. Ramey, and S. Beck (2003). Effect of floodwater extraction on mountain stream morphology. *Journal of Hydraulic Engineering 11*(129), 885–895.

Pasquale, N., P. Perona, and P. Burlando (2012). Root reinforcement of alluvial river sediment model. *In preparation*.

Pasquale, N., P. Perona, R. Francis, and P. Burlando (2012a). Effects of streamflow variability on the vertical root density distribution of willow cutting experiments. *Ecological Engineering* (40), 167–172.

Pasquale, N., P. Perona, R. Francis, and P. Burlando (2012b). River morphodynamic processes and related effects on above- and below-ground salix cuttings dynamics. *Submitted to Ecological Engineering*.

Pasquale, N., P. Perona, P. Schneider, J. Shrestha, A. Wombacher, and P. Burlando (2011). Modern comprehensive approach to monitor the morphodynamic evolution of a restored river corridor. *Hydrology and Earth System Sciences 15*(4), 1197–1212.

Pasquale, N., P. Perona, A. Wombacher, and P. Burlando (2012). Hydrodynamic model calibration from non-orthorectified terrestrial photographs. *In preparation*.

Perona, P., C. Camporeale, E. Perucca, M. Savina, P. Molnar, P. Burlando, and L. Ridolfi (2009). Modelling river and riparian vegetation interactions and related importance for sustainable ecosystem management. *Aquatic Sciences 71*(3), 266–278.

Perona, P., P. Molnar, B. Crouzy, E. Perucca, Z. Jiang, S. McLelland, D. Wüthrich, K. Edmaier, R. Francis, C. Camporeale, and a. Gurnell (2012). Biomass selection by floods and related timescales: Part 1. Experimental observations. *Advances in Water Resources 39*, 85–96.

Perona, P., P. Molnar, M. Savina, and P. Burlando (2008). Stochastic sediment and vegetation dynamics in an alpine braided river. *IAHS Publ.* (325), 266–274.

Perona, P., P. Molnar, M. Savina, and P. Burlando (2009). An observation-based stochastic model for sediment and vegetation dynamics in the floodplain of an alpine braided river. *Water Resources Research 45*(9), 1–13.

Perucca, E., C. Camporeale, and L. Ridolfi (2006). Influence of river meandering dynamics on riparian vegetation pattern formation. *Journal of Geophysical Research 111*, G01001.

Perucca, E., C. Camporeale, and L. Ridolfi (2007). Significance of the riparian vegetation dynamics on meandering river morphodynamics. *Water Resources Research 43*(3), 1–10.

Peter, A., F. Kienast, and S. Woolsey (2006). A strategy to assess river restoration success. *Archives de Science 15*(1-4), 643–656.

Pezeshki, S. R., S. Li, F. D. Shields, and L. T. Martin (2007). Factors governing survival of black willow (Salix nigra) cuttings in a streambank restoration project. *Ecological Engineering 29*(1), 56–65.

Poggi, D. and G. G. Katul (2008). The effect of canopy roughness density on the constitutive components of the dispersive stresses. *Experimental fluids 45*, 111–121.

Poggi, D., G. G. Katul, J. J. Finnigan, and S. E. Belcher (2008). Analytical model for the mean flow inside dense canopies on gentle hilly terrain. *Quarterly Journal of the Royal Meteorological Society 134*, 1095–1112.

Poggi, D., C. Krug, and G. Katul (2009). Hydraulic resistance of submerged rigid vegetation derived from first-order closure models. *Water Resources Research 45*, W10442.

Poggi, D., A. Porporato, L. Ridolfi, J. D. Albertsonand, and G. G. Katul (2004). The effect of vegetation density on canopy sublayer turbolence. *Boundary Layer Meteorology 111*, 565–587.

Pollen, N. (2007). Temporal and spatial variability in root reinforcement of streambanks : Accounting for soil shear strength and moisture. *Catena 69*, 197 – 205.

Pollen, N. and A. Simon (2005). Estimating the mechanical effects of riparian vegetation on stream bank stability using a fiber bundle model. *Water Resources Research 41*, 1–11.

Pollen, N., N. Simon, and A. J. C. Collison (2004). Advances in assessing the mechanical and hydrologic effects of riparian vegetation on streambank stability. In S. Bennett and A. Simon

(Eds.), *Riparian Vegetation and Fluvial Geomorphology, Water Sciences and Applications*, Volume 8, pp. 125–139. AGU, Washington, DC.

Preti, F., A. Dani, and F. Laio (2010). Root profile assessment by means of hydrological, pedological and above-ground vegetation information for bio-engineering purposes. *Ecological Engineering 36*(3), 305–316.

Qi, J., A. Chehbouni, A. R. Huete, Y. H. Kerr, and S. Sorooshian (1994). A modified soil adjusted vegetation index. *Remote sensing Environment 126*, 119–126.

Quinn, J. M. and C. W. Hickey (1994). Hydraulic parameters and benthic invertebrate distributions in two gravel-bed New Zealand rivers. *Freshwater Biology 32*(3), 489–500.

Rankin, A. L., L. H. Matthies, and A. Huertas (2004). Daytime water detection by fusing multiple cues for autonomous off-road navigation.

Richner, W., M. Liedgens, H. Burgi, A. Soldati, and P. Stamp (2000). Root image analysis and interpretation. In A. Smith (Ed.), *Root Methods: a handbook* (1st ed.)., pp. 305–341. Springer-Verlag, Berlin.

Rodhe, S. (2004). *River restoration: potentials and limitations to re-establish riparian landscapes. Assestment and planning.* Ph. D. thesis, ETH Zurich, Switzerland.

Romanowicz, R. and K. Beven (1998). Dynamic real-time prediction of flood inundation probabilities. *Hydrological Sciences Journal 43*(2), 181–196.

Romanowicz, R. and K. Beven (2003). Estimation of flood inundation probabilities as conditioned on event inundation maps. *Water Resources Research 39*(3), 1–12.

Rominger, J. T., A. F. Lightbody, and H. M. Nepf (2010). Effect of added vegetation on sand bar stability and stream hydrodynamics. *Journal of Hydraulic Engineering 136*, 994–1002.

Rominger, J. T. and H. M. Nepf (2011). Flow adjustment and interior flow associated with a rectangular porous obstruction. *Journal of Fluid Mechanics 680*, 636–659.

Ruf, W., L. Foglia, P. Perona, P. Molnar, R. Faeh, and P. Burlando (2008). Modelling the interaction between groundwater and river flow in an active alpine floodplain ecosystem. *Peckiana 5*, 5–16.

Samaritani, E., J. Shrestha, B. Fournier, E. Frossard, F. Gillet, C. Guenat, P. a. Niklaus, N. Pasquale, K. Tockner, E. a. D. Mitchell, and J. Luster (2011). Heterogeneity of soil carbon pools and fluxes in a channelized and a restored floodplain section (Thur River, Switzerland). *Hydrology and Earth System Sciences 15*(6), 1757–1769.

Schäppi, B., P. Perona, P. Schneider, and P. Burlando (2010). Integrating river cross section measurements with digital terrain models for improved flow modelling applications. *Computers & Geosciences 36*(6), 707–716.

Schenk, H. J. and R. B. Jackson (2002a). The global biography of roots. *Ecological monographs 72*(3), 311–328.

Schenk, H. J. and R. B. Jackson (2002b). Rooting depths, lateral root spreads and belowground/above-ground allometries of plants in water-limited ecosystems. *Journal of Ecology 90*(3), 480–494.

Schirmer, M., J. Luster, N. Linde, P. Perona, E. Mitchell, D. A. Barry, A. Cirpka O, P. Schneider, T. Vogt, K. Tockner, P. Burlando, E. G. Pannatier, A. Green, E. Hoehn, J. Hollender, R. Kipfer, and E. Durisch-Kaiser (2012). River restoration: Morphological, hydrological, and ecological changes and challenges.

Schmitt, F. G. (2006). About Boussinesq's turbulent viscosity hypothesis: historical remarks and a direct evaluation of its validity. *Comptes Rendus Mecanique 335*(9–10), 617–62.

Schnauder, I. and H. L. Moggridge (2009). Vegetation and hydraulic-morphological interactions at the individual plant , patch and channel scale. *Aquatic Sciences 71*, 318 – 330.

Schneider, P., T. Vogt, M. Schirmer, J. Doetsch, N. Linde, N. Pasquale, P. Perona, and O. A. Cirpka (2011, August). Towards improved instrumentation for assessing river-groundwater interactions in a restored river corridor. *Hydrology and Earth System Sciences 15*(8), 2531–2549.

Schweizer, S. P. (2007). *Predicting the consequences fo river rehabilitation measures on morphology, hydraulics, pheriphyton and on invertebrates*. Ph. D. thesis, ETH Zürich, Switzerland.

Selby, M. J. (1993). *Hillslope Materials and Processes* (1st ed.). Oxford University Press, Oxford, UK.

Simon, A. and A. J. C. Collison (2002). Quantifying the mechanical and hydrologic effects of riparian vegetation on streambank stability. *Earth Surface Processes and Landforms 27*, 527– 546.

Soar, P. J. and C. R. Thorne (2001). *Channel restoration design for mendering rivers* (1st ed.). US Army Engineer Research and Development Center, Vicksburg, Miss., USA.

Sprott, J. C. (2003). *Chaos and time series analysis* (1st ed.). Oxford University Press, Oxford, UK.

Steiger, J. and A. M. Gurnell (2003). Spatial hydrogeomorphological influences on sediment and nutrient deposition in riparian zones: observations from the Garonne River, France. *Geomorphology 49*(1-2), 1–23.

Stewardson, M. J. and T. A. MacMahon (2002). A stochastic model of hydraulic variations within stream channels. *Water Resources Research 38*(1), 1007–1021.

Tealdi, S., C. Camporeale, E. Perucca, and L. Ridolfi (2010). Longitudinal dispersion in vegetated rivers with stochastic flows. *Advances in Water Resources 33*(5), 562–571.

Thorne, C. R. (1990). Effects of vegetation on riverbank erosion and stability. In J. B. Thornes (Ed.), *Vegetation and Erosion*, pp. 125–144. John Wiley and Sons, Hoboken, NJ.

Tockner, K. and J. a. Stanford (2002). Riverine flood plains: present state and future trends. *Environmental Conservation 29*(03), 308–330.

Trush, W. J., S. M. McBain, and L. B. Leopold (2000). Attributes of an alluvial river and their relation to water policy and management. *Proceedings of the National Academy of Sciences of the United States of America 97*(22), 11858–118663.

Tubino, M. and G. Seminara (1990). Free-forced interactions in developing meanders and suppression of free bars. *Journal of fluid mechanincs 214*, 131–159.

van der Nat, D., A. P. Schmidt, K. Tockner, P. J. Edwards, and J. V. Ward (2002). Inundation Dynamics in Braided Floodplains : Tagliamento River , Northeast Italy. *Ecosystems 5*, 636 – 647.

van Noordwijk, M. G., F. Brouwer, M. Meijboom, O. do Rosario, and A. G. Bengough (2000). Trench profile techniques and core break methods. In A. Smith (Ed.), *Root Methods: a handbook* (1st ed.)., pp. 211–233. Springer-Verlag, Berlin.

Vandersande, M. W., E. P. Glenn, and J. L. Walworth (2001). Tolerance of five riparian plants from the lower colorado river to salinity, drought and inundation. *Journal of Arid Environment 49*, 147–159.

Verones, F. (2009). *Experiments on Salix shoot and root growth on river alluvial sediment with programming for image analysis*. Ph. D. thesis, ETH Zürich, Switzerland.

Vogel, S. (1989). Drag and reconfiguration of broad leaves in high winds. *Journal of Experimental Botany 40*, 941–948.

Vreugdenhil, S. J., K. Kramer, and T. Pelsma (2006). Effects of flooding duration, -frequency and -depth on the presence of saplings of six woody species in north-west europe. *Forest Ecology and Management 236*, 47–55.

Waisel, Y., A. Eshel, and U. Kafkafy (2002). *Plant roots: The hidden half* (3rd ed.). Marcel Dekker, NY.

Waldron, L. J. (1977). The shear resistance of root-permeated homogeneous and stratified soil. *Soil Science Society of America Journal 41*, 843–849.

Walthert, L., U. Graf, A. Kammer, J. Luster, D. Pezzotta, S. Zimmermann, and F. Hagedorn (2010). Determination of organic and inorganic carbon, δ 13 C, and nitrogen in soils containing carbonates after acid fumigation with HCl. *Journal of Plant Nutrition and Soil Science 173*(2), 207–216.

Wasantha Lal, A. M. (1995). Calibration of riverbed roughness. *Journal of Hydraulic Engineering 121*(9), 664–671.

Wilson, J. S., D. S. Baldwin, G. N. Rees, and B. P. Wilson (2011). The effects of short-term inundation on carbon dynamics microbial community structure and microbial activity in floodplain soil. *River Research Applications 27*, 213–225.

Wohl, E., P. L. Angermeier, B. Bledsoe, G. M. Kondolf, L. Macdonnell, D. M. Merritt, M. A. Palmer, N. L. Poff, and D. Tarboton (2005). River restoration. *Water Resources Research 41*, 1–12.

Wohl, E, E. (1998). Uncertainty on flood estimates associated with roughness coefficient. *Journal of hydraulic Engineering 124*(2), 219–223.

Woolsey, S., F. Capelli, T. O. M. Gonser, E. Hoehn, M. Hostmann, B. Junker, A. Paetzold, C. Roulier, S. Schweizer, S. D. Tiegs, K. Tockner, C. Weber, and A. Peter (2007). A strategy to assess river restoration success. *Freshwater Biology* (52), 752–769.

Wu, J. and A. D. Tang (2010). The influence of water conveyances on restoration of vegetation to the lower reaches of Tarim River. *Environmental Earth Science 59*, 967–975.

Wu, T. H., P. E. Beal, and C. Lan (1988). In-situ shear test of soil-root systems. *Journal of Geotechnical Engineering 114*, 1376–1394.

Wu, T. H., W. P. McKinnell III, and D. N. Swanston (1979). Strength of tree roots and landslides on Prince of Wales Island, Alaska. *Canadian Geotechnical Journal 16*, 19–33.

Wu, T. H., R. M. McOmber, R. T. Erb, and P. E. Beal (1988). Study of soil-root interaction. *Journal of Geotechnical Engineering 114*, 1351–1357.

Wynn, T., S. Mostaghimi, J. A. Burger, A. A. Harpold, M. B. Henderson, and L. Henry (2004). Variation in root density along stream banks. *Journal of Environmental Quality 33*, 2030–2039.

Xie, Y., S. An, B. Wu, and W. Wang (2006). Density-dependent root morphology and root distribution in the submerged plant Vallisneria natans. *Environmental and Experimental Botany 57*, 195–200.

Zong, L. and H. M. Nepf (2010). Flow and deposition in and aroung a finite patch of vegetation. *Geomorphology 116*, 363–372.

Appendix A

Normalized Difference Vegetation Index

Live green plants absorb solar radiation in the photosynthetically active radiation (PAR) spectral region of the leaves, which they use as a source of energy in the process of photosynthesis. Leaf cells have also evolved to reflect and transmit solar radiation in the near-infrared spectral region (which carries approximately half of the total incoming solar energy), because the energy level per photon in that domain (wavelengths longer than about 700 nanometers) is not sufficient to be useful to synthesize organic molecules.

A strong absorption at these wavelengths would only result in overheating the plant and possibly damaging the tissues. Hence, live green plants appear relatively dark in the PAR and relatively bright in the near-infrared. The chlorophyll in plant leaves absorbs a large portion of visible light (from 0.4 to 0.7 μm) to use it use in photosynthesis processes. The cell structure of the leaves, on the other hand, strongly reflects near-infrared light (from 0.7 to 1.1 μm). Therefore it comes that the more a plant has leaves, the more wavelengths of light are affected. The NDVI (Normalized Difference Vegetation Index) is calculated from these visible and near infrared pictures as it follows:

$$\mathrm{NDVI} = \frac{\mathrm{RED_{IR}} - \mathrm{RED_{VIS}}}{\mathrm{RED_{IR}} + \mathrm{RED_{VIS}}} = \begin{cases} < 0 \text{ Water} \\ \cong 0 \quad \text{Soil} \\ > 0.4 \div 0.8 \text{ Vegetation} \end{cases} \tag{A.1}$$

where VIS and NIR stand for the spectral reflectance measurements acquired in the visible and near-infrared regions and RED is the red channel in the RGB sprectrum. These spectral reflectance are themselves ratios of the reflected over the incoming radiation in each spectral band individually, hence they take on values between 0.0 and 1.0. By design, the NDVI itself thus varies between -1.0 and +1.0.

In 2009, in order to monitor vegetation growth (pattern and quantity) at the field site of the

Thur river, we have collected a series of picture, visible and infrared, to compute the NDVI (Defries and Townshend, 1994; Wu and Tang, 2010). Pictures have been shooting by the cameras installed on the two towers of the southern levee, beside the restored corridor (see sections 2.1 and 2.2.3). As a first step we computed the NDVI at each month, from January to the end of July (Figure A.1). Despite pictures are taken at the same time of the day (12.00 GTM+1) there is a large difference in sun exposition and reflection. The reasons are mainly the different sun position over the horizon along the seasons and the non uniform weather conditions (clouds, air humidity etc...).

Another problem in quantifying the amount of vegetation growing on the main island is due to the fact that in Figure A.1 the NDVI is computer for a large portion of field, including the forest on the northern side and the grassy area of the levee. The NDVI also has to be calibrated since it was noticed that with the usual equation the values were too low. This is visible if one compares the histograms and the NDVI picture with the visible picture. In the histograms the percentage of values below 0 which would represent water is too high. From the picture one can see that the amount of values representing soil should be much higher than those corresponding to vegetation or water.

The intervals of the NDVI have been calibrated as it follows: amount of water (NDVI$<$ -0.3), soil (NDVI $=$ -0.3 $\div$ 0.1) and vegetation (NDVI $>$ 0.1). Once the island has been cropped from the rest of the picture (Figure A.2) histogram of the NDVI values are computed in terms of absolute frequencies of the values in specific intervals as well as percentage. The values of the pixels surrounding the cropped island are set as NaN in order to ensure exclusion in computing the histogram. The NDVI values are in Figure A.3 for the time January-May 2009.

An exemplary result, showing the variability of this index on a specific day illustrated in Figure A.4, supports the rationale for comparing different NDVI histograms throughout the season, in order to obtain an additional piece of quantitative information complementing that from field monitoring. The two set of pictures (visible and NIR) used in Figure A.4 show the island before the flood occured in 2009 (see Figure 2.15, red hydrograph) and just after. The amount of vegetation damaged, removed or covered by sediments, during the flood event, is quantified as the number of pixels (percentage) that shifted from NDVI$>$0.1 (vegetation) to NDVI $=$ -0.1$\div$0.1 (bare soil).

Figure A.4 supports the rationale for comparing different NDVI histogram throughout the season, in order to obtain an additional piece of quantitative information complementing that from field monitoring. Unfortunately, thunder storms occurred in 2009 and in 2010 systematically damaged the cameras. The high cost of repairing, substituting and maintenance the cameras set up on the field became too expensive and was therefore given up. Consequently the NDVI analysis ended at the end of summer 2009.

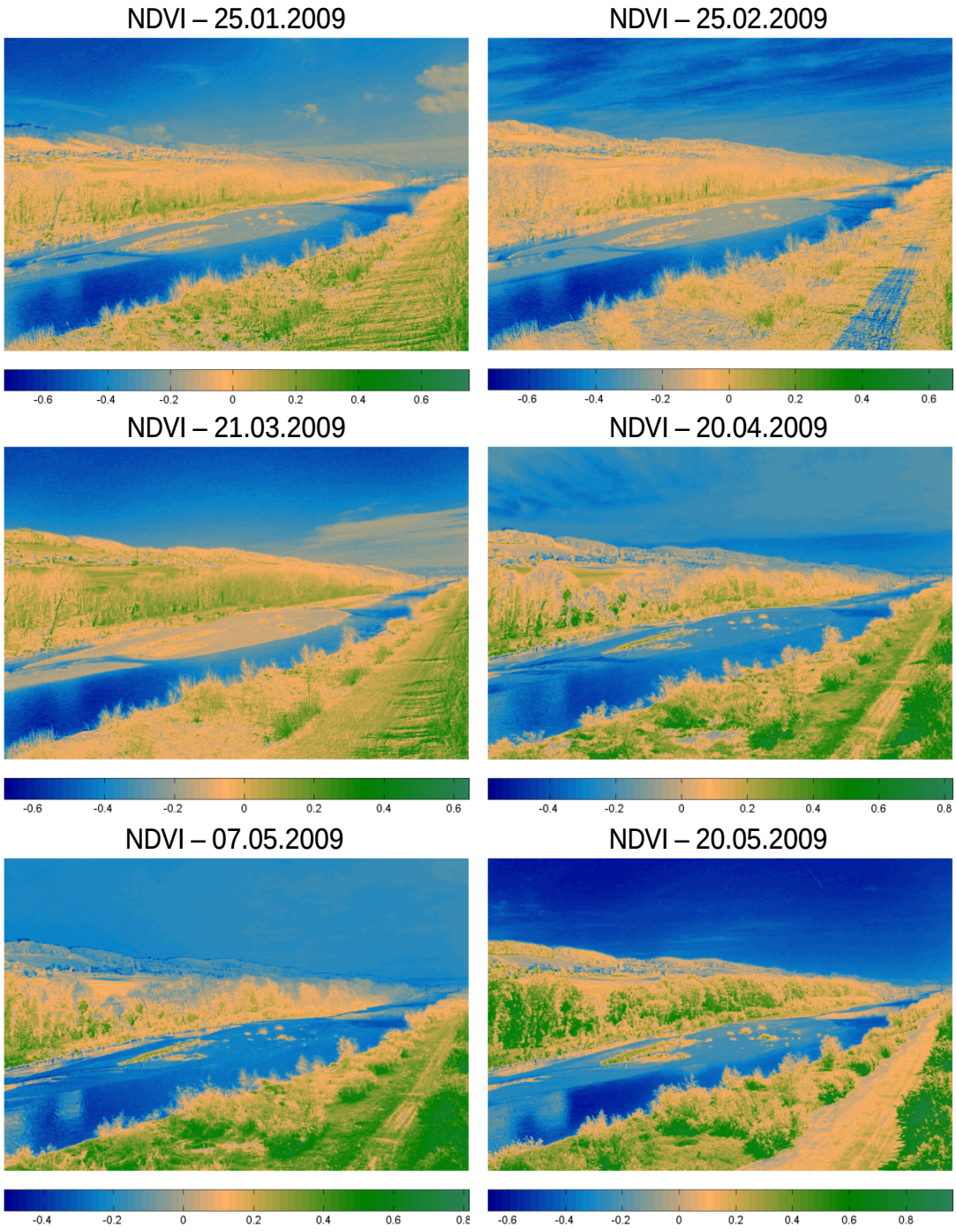

Figure A.1: *NDVI computed for representative pictures selected within single month set in 2009.*

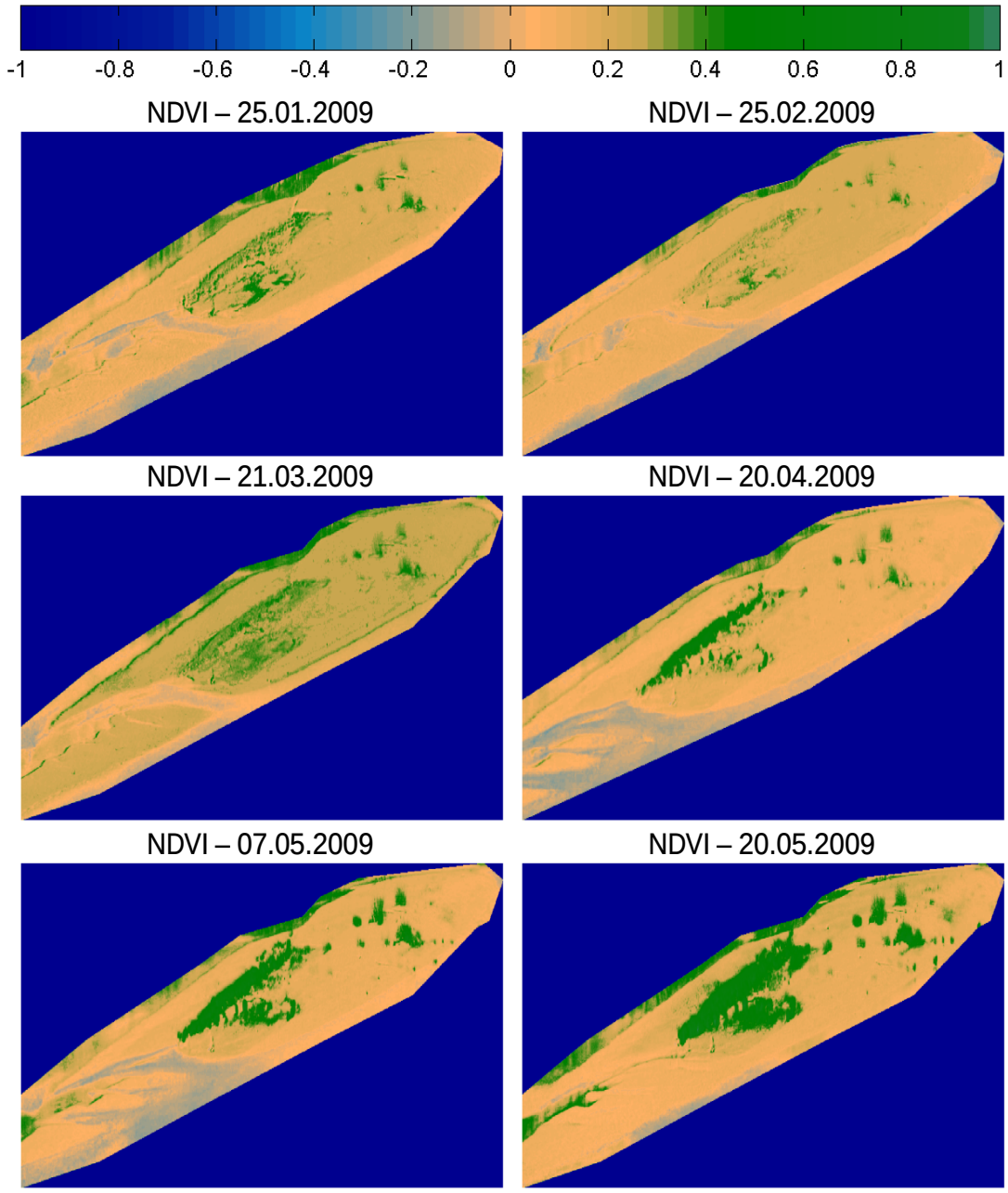

Figure A.2: *NDVI computed for the island only. First, the island has been cropped from the original picture and then separately analyzed.*

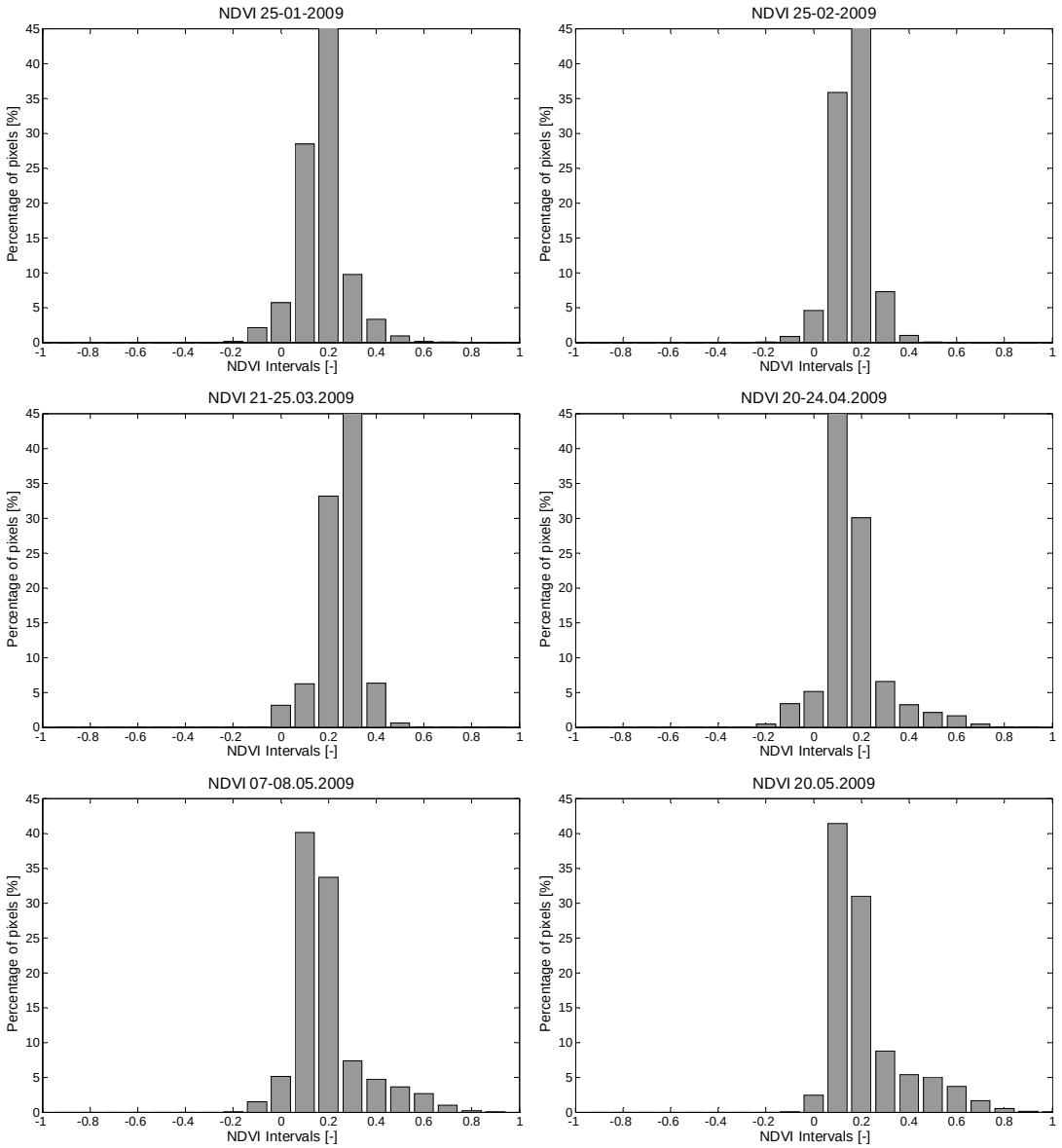

Figure A.3: *Histograms of the percentage of pixels for each class (waterm bare soil and vegetation) computed with the NDVI.*

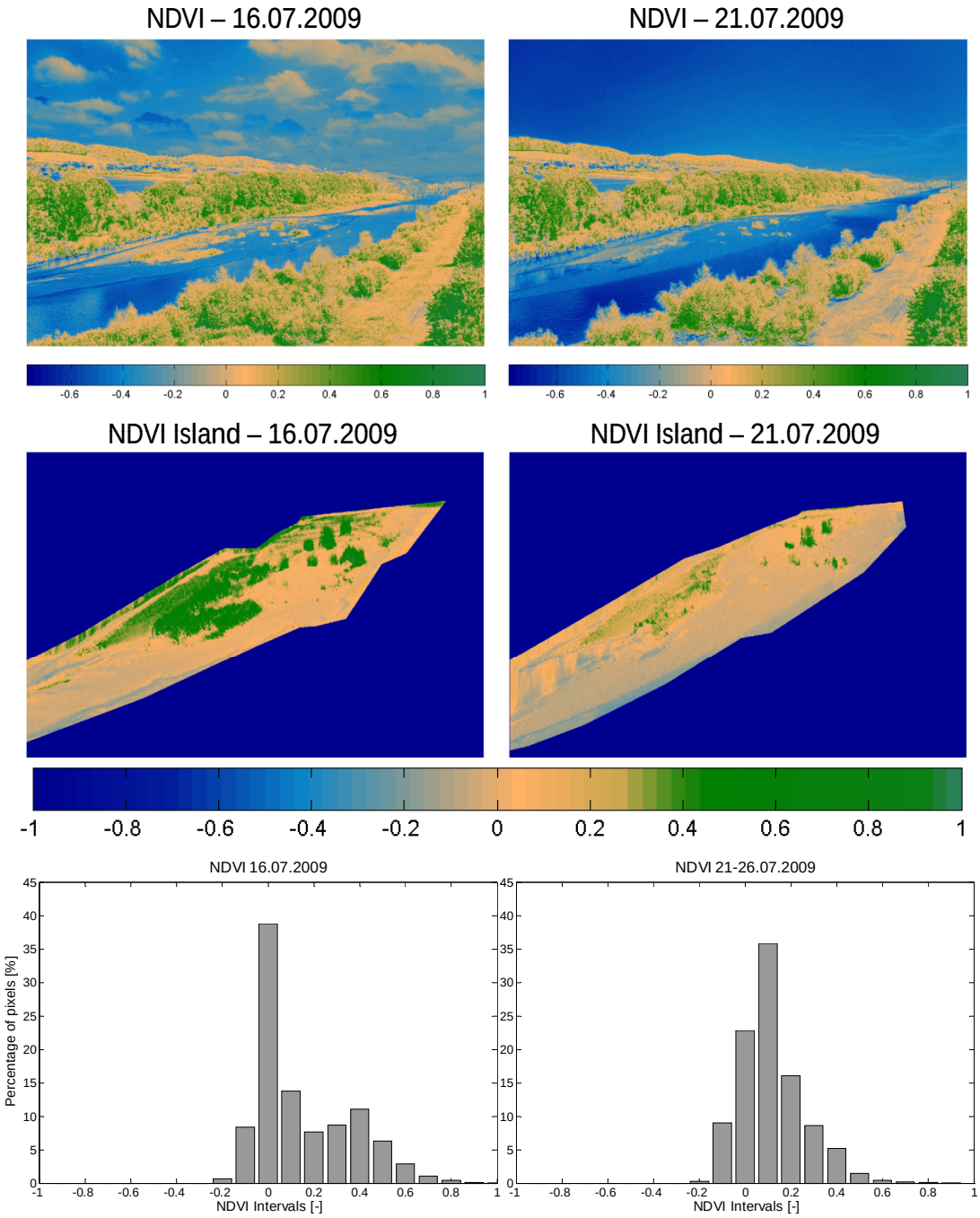

Figure A.4: *In July 2009, pictures recorded before and after a major flood allowed to quantify the amount of vegetation damaged or removed during the event.*

Appendix B

Shallow water equation and finite volume method of integration

B.1 Derivation of the shallow water equations

The approaches for the derivation of the SWEs are two:

- Integrating the three-dimensional system of Navier-Strokes equations over the depth,
- Direct approach by concerning a three dimensional control volume element of fluid.

The following boundary conditions are imposed:

1. At the top of the water surface:
   Kinetic boundary condition (no flow across the water surface can take place):

$$w_s = \frac{\partial z_s}{\partial t} + u_s \frac{\partial z_s}{\partial x} + v_s \frac{\partial z_s}{\partial y} = \frac{dz_s}{dt} \tag{B.1}$$

   Dynamic bounday condition:

$$\tau = (\tau_{Sx}, \tau_{Sy}) \text{ and } \mathrm{P} = \mathrm{P}_{atm} \tag{B.2}$$

2. At the bottom of the water body:
   Kinetic bounday condition (no flow through the bed surface can take place):

$$w_B = +u_B \frac{\partial z_B}{\partial x} + v_s \frac{\partial z_B}{\partial y} \tag{B.3}$$

Using the derivation of the depth integrated mass and momentum conservation equations from the Reynolds averaged 3-D Navier-Strokes equations, one obtains the complete set of SWE:

$$\frac{\partial h}{\partial t} + \frac{\partial(\bar{u}h)}{\partial x} + \frac{\partial(\bar{v}h)}{\partial y} = 0 \tag{B.4a}$$

$$\frac{\partial \bar{u}}{\partial t} + \bar{u}\frac{\partial(\bar{u})}{\partial x} + \bar{v}\frac{\partial(\bar{u})}{\partial y} + g\frac{\partial \bar{h}}{\partial x} = -g\frac{\partial Z_b}{\partial x} - \frac{1}{\rho h}\tau_{bx} + \frac{1}{\rho h}\frac{\partial\left[h\left(\bar{\tau}_{xx} + D_{xx}\right)\right]}{\partial x} + \frac{1}{\rho h}\frac{\partial\left[h\left(\bar{\tau}_{xy} + D_{xy}\right)\right]}{\partial y} \tag{B.4b}$$

$$\frac{\partial \bar{v}}{\partial t} + \bar{u}\frac{\partial(\bar{v})}{\partial x} + \bar{v}\frac{\partial(\bar{v})}{\partial y} + g\frac{\partial \bar{h}}{\partial y} = -g\frac{\partial Z_b}{\partial y} - \frac{1}{\rho h}\tau_{by} + \frac{1}{\rho h}\frac{\partial\left[h\left(\bar{\tau}_{yx} + D_{yx}\right)\right]}{\partial x} + \frac{1}{\rho h}\frac{\partial\left[h\left(\bar{\tau}_{yy} + D_{yy}\right)\right]}{\partial y} \tag{B.4c}$$

where *h* is the water depth (m), *g* the gravity acceleration (m/s^2), ρ the water density (kg/m^3), $\bar{x}$ and $\bar{y}$ the depth averaged velocities in x- and y directions (m/s), Z_b the bottom elevation (m), τ_{bx} and τ_{by} the bed shear stresses in x- and y direction (N/m^2), $\bar{\tau}$ the depth averaged turbulent and viscous stresses (N/m^2), *D* the momentum dispersion terms. In order to take in account energy losses between two adjacent cells of the domain closure condition are needed. The first one quantifies turbulent and viscous shear stresses according to the Boussinesq eddy viscosity hypothesis (Boussinesq, 1877; Schmitt, 2006) whereas the second one use the quadratic friction law to relate bed shear stresses and depth averaged velocities, that is:

$$\tau_{Bx} = \rho\frac{|\mathbf{u}|\,u}{c_f^2} \tag{B.5a}$$

$$\tau_{By} = \rho\frac{|\mathbf{u}|\,v}{c_f^2} \tag{B.5b}$$

in which $|\mathbf{u}| = \sqrt{u^2 + v^2}$ is the magnitude of the velocity vector and c_f the friction coefficient, related to the Manning's roughness coefficient *n* by ${c_f}^2$=R$^{1/3}$/g*n*^{2}. The two source terms in equation B.4 are the bed shear stress (τ_B/ρ = g*h*S$_f$) and the bed slope term (g*h*S$_B$. The bed shear stress is the most important physical parameter besides water depth and velocity field of a hydro- and morphodynamic model. It causes the turbulence, is responsible for sediment transport and has a non-linear effect of retarding the flow. When the effect of turbulence grows, the effect of molecular viscosity becomes relatively smaller, while viscous boundary becomes thinner and may even disappear. In that case the bed shear stress (friction) is equal to the bed turbulent stress. However, bed shear stress is usually estimated by using an empirical or semi-empirical formula sincethe vertical distribution of velocity cannot be readily obtained. In a two-dimensional system the energy slopes in x- and y- directions have the following forms:

$$S_{fx} = \frac{u\sqrt{u^2+v^2}}{gc_f^2 R}\,; \quad S_{fy} = \frac{v\sqrt{u^2+v^2}}{gc_f^2 R} \tag{B.6}$$

Bed slope terms represent the gravity forces in the form

$$S_{B,x} = -\frac{\partial z_B}{\partial x}\,; \quad S_{B,y} = -\frac{\partial z_B}{\partial y} \tag{B.7}$$

B.2 Discretisation with the finite volume method

To allow for the numerical solution of the PDEs, in a first step the computational domain in space and time has to be divided into smaller subdomains. This procedure is called discretization. It is necessary to reduce the infinite number of degrees of freedom of continuous equations to a finite number, which can be handled by the computer. The finer the discretization into smaller domains, the smaller is the approximation error. There are different ways to discretize the computational domain. Not necessarily, but often the choice of the discretization method depends on the computational method. The aim of the following paragraphs is not so much to explain the discretization methods in detail, but rather to present the different approaches and outline their advantages and disadvantages. We start with the spatial discretization. We distinguish between structured and unstructured grids.

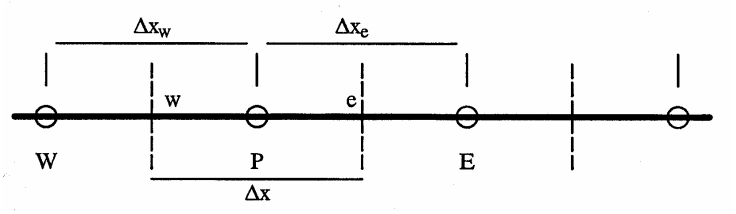

Figure B.1: *Finite volume discretization of the model problem*

Numerical methods for the calculation of flows can be compared to experimental investigations. In both cases only a limited number of flow quantities can be measured or calculated, respectively. However, their number can be chosen arbitrarily high, so that this constraint does not imply any limitation as far as practical questions are concerned. Different from experimental investigations, where primary unknowns are measured via probes in a limited number of points, numerical techniques prescribe a discrete number of grid points for the unknowns and solve the algebraic equations using a numerical algorithm. Since the focus is on variables to

be determined at a finite number of nodes, a discontinuous distribution of variables replaces the continuous one. This approach is known as discretization. The algebraic expressions are derived assuming a distribution between the unknown node-variables. The type of distribution depends on the discretization method. Since the assumed distributions are typically simple expressions, their validity is obviously restricted to a small subdomain. Such a subdomain is termed element and the subdivision that leads to such elements is called space discretization, as explained above. Up to now we have treated the discretization method in a rather general way. As mentioned, the type of equations used for the approximation of the distribution of the variables within the elements depends on the discretization method. Without outlining this for now in detail, it can be mentioned that for the finite differences method the differential form of the PDGs is used, whereas the finite volumes method uses the integral form and the finite elements method uses the weak integral form. What this means more precisely will be explained in the following on the basis of a concrete example.

For the finite volume method, we consider, for example the Poisson Equation:

$$-\frac{\partial}{\partial x}\left(\frac{\partial \Phi}{\partial x}\right) = f \tag{B.8}$$

where Φ represents velocitz potentials. We also assume homogeneous boundarz conditions on both sides, i.e., $\Phi_{(x=0)} = \Phi_{(x=1)} = 0$. Equation B.8 is integrated over the control volume, which is Δx long and extends from the western point w to the eastern point e (Figure B.1). The integration yields:

$$-\left(\frac{\partial}{\partial x}\right)_e + \left(\frac{\partial \Phi}{\partial x}\right)_w = \int_w^e f dx = 0 \tag{B.9}$$

Similar to the finite differences method, in the finite volumes method the derivatives are approximated by difference quotients. Note that the derivatives at the nodes w (west) and e (east) lie between the discretization nodes. Using the values at the nodes, Eq. B.9 is discretized as:

$$-\left(\frac{\Phi_E - \Phi_P}{\Delta x_e}\right) + \left(\frac{\Phi_P - \Phi_W}{\Delta x_w}\right) = \bar{f}\Delta x \tag{B.10}$$

where $\bar{f}$ is the average of f over the control volume. Two important advantages of the finite volumes method have not been mentioned so far: With the use of the integral form Equation B.9 the conservation of mass, momentum or energy is guaranteed in the respective transport equations, because an explicit balance between inflow, outflow and storage is required for all elements. The balance of these fluxes is in principle independent of the form of the elements, i.e. the finite volume method is much more flexible compared to the finite differences method.

For the F.V.M. we distinguish between two approaches: the cell centered method and the node centered method. The two differ by the location where the unknowns are formulated. In the cell-centered method the unknowns are placed at the center of the cell, whereas in the the node-centered method, they are located at the grid nodes (see Figure B.2). Consistency: Consistency means that the discrete equations approach (converge to) the differential equations for Δx $\rightarrow$ 0 and Δt $\rightarrow$ 0. Stability: A stable difference scheme prevents the unlimited growth of numerical error during calculation. Convergence: The discrete solution U_i^n approaches the exact solution U(x,t) of the differential equation at every point x_i = i Δx and every time t_n = n $\cdot$ Δt, if Δx $\rightarrow$ 0 and Δt $\rightarrow$ 0.

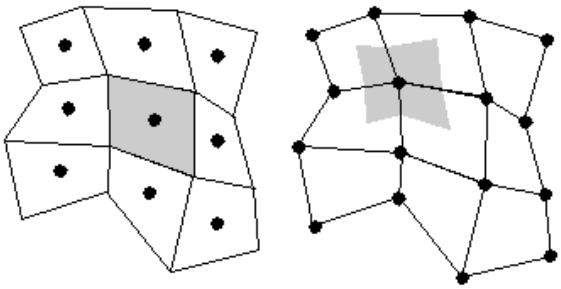

Figure B.2: *FV cell-centered method (left) and node centered method (right) and associated volume definitions.*

The discretizations in time and space are typically well separated from each other. The discretization in time can be formulated in two different ways: (1) Explicit methods compute the variables of the next time step exclusively from already known values of the variable at the previous time step. The category of explicit methods also contains the so called multiple step methods (e.g. predictor-corrector method). Explicit methods are in general easily programmed but have the restriction that they must fulfill a stability criterion. (2) Implicit methods use in addition the values of hitherto unknown values of the variables at the new time. The solution in point i therefore also depends from the still unknown solution at the neighboring points of point i. This requires solving of an equations system (as opposed to a single equation in the explicit method) and - due to non-linear terms - eventually an iterative procedure. Implicit methods involve much more effort in programming. At the same time they allow to choose larger time steps. Explicit methods gain in importance due to the progress in computer performance. They have to fulfill the Courant-Friedrich-Levy (CFL) condition. This CFL-number is a measure for the progress of a disturbance over a time step Δt related to the grid distance Δx.

$$CFL = |\lambda| \frac{\Delta t}{\Delta x} = (|u| + c) \frac{\Delta t}{\Delta x} \tag{B.11}$$

with u = flow velocity and c = wave velocity. An explicit method is only stable for small CFL-numbers (usually CFL$<$1.0). Equation B.11 thus leads to an equation for the maximum permissible time step length at fixed grid size Δx (provided the largest λ is chosen). In 2D the condition is analogous. In the explicit time discretization, variables at the new time instance depend only on values at the old time step. This means that the values of each variable at the nodes at the new time depend only on known values at the previous time step. In this way no equation solver is necessary and the solution is straightforward and easy to program. However, for too large time intervals the solution becomes instable. In contrast, the fully implicit method is strictly stable. In this method, the values at the new time depend on its neighbouring values at the new time, i.e. a system of coupled equations must be set up and solved. The variable at the new time depends both on the old and new time step. One can improve the accuracy of the time discretization using semi-implicit methods, however, the big advantage of explicit methods, which is that equation solvers are not required, is lost completely.

Appendix C

"Quasi-Automatic" Pattern Recognition

The algoritm and software for the auomatic pattern recognition described in Section 2.4.2 (Pasquale et al., 2012) have been developed in collaboration with Andreas Wombacher[1] and his group at the University of Twende, NE. The main script calls a function and two subfunctions developed by F. van der Heijden at the University of Twende.

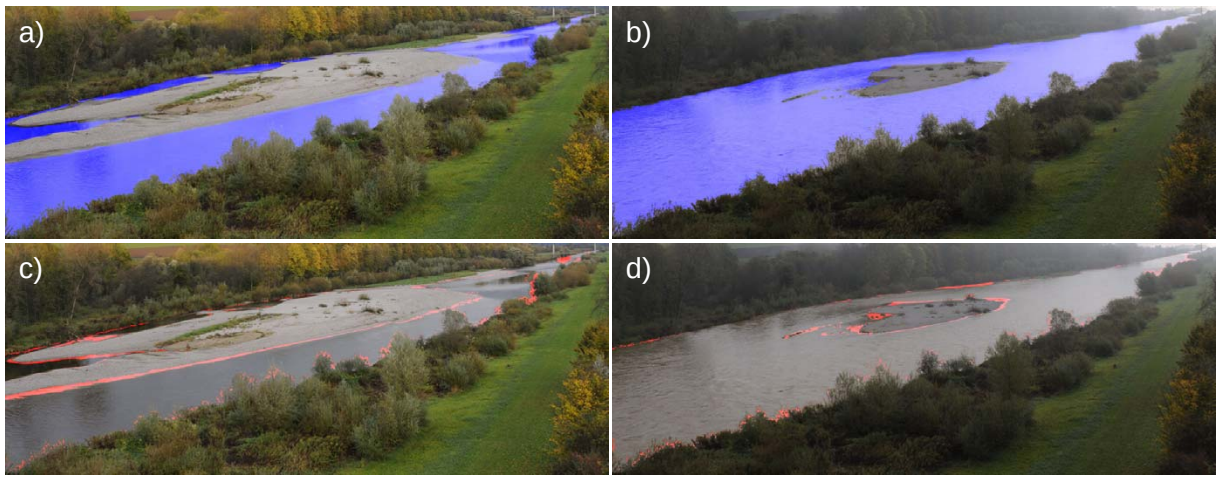

Figure C.1: *Example of water and non-water classes recognition from digital photographs under changing light and surface albedo. Such conditions are typically due to either diurnal variability or bad weather conditions (e.g., like fog or snow). Pictures (a) and (c) show a low discharge case, whereas (b) and (d) show a high discharge. Blue is the detected water (a, b). Red are the classification errors (c, d).*

[1]Prof. A. Wombacher, Database Group, Faculty of Computer Science, University of Twente, The Netherlands. Email: a.wombacher AT utwente.nl

C.1 Matlab code

```
% clear the workspace and screens
clc;
clear all;
close all;

filenames={'edge.jpg';'img/DSC_7074_s.jpg';'img/DSC_7381_s.jpg';'img/DSC_7409_s.jpg'};

fn = 1;

% open the file
img = imread(char(filenames(fn)));
img_hsv = rgb2hsv(img);
img_gray = rgb2gray( img );
[rows cols depth] = size(img);

% upper bound of rows to be considered
ub_rows = rows*0.49;

% correct edges
edgemap1 = ut_edge(img_gray, 's', 2, 'h', [0.10 0.03]);
radius = 10;
radius2 = 5;
edge_s = zeros(rows,cols);
edge_t = zeros(rows,cols);
ind = find(edgemap1==true);
edge_t(ind)=1;

for m = 1:rows
    for n = 1:cols
        if m>radius && m<rows-radius && n>radius && n<cols-radius
            edge_s(m,n) = sum(sum(edge_t(m-radius:m+radius,n-radius:n+radius)));
        end
    end
end

% red-green
res = img(:,:,2)- img(:,:,3);
redgreen = im2bw(res,0.17);

%
green_s = im2bw(img_hsv(:,:,1)-2*img_hsv(:,:,3),0.0);
green_w = im2bw(img_hsv(:,:,1)-2*img_hsv(:,:,2),0.0);

% create the result image
result = img;
mask = zeros(rows,cols);

% do the segmentation
for m = 1:rows
    for n = 1:cols
        % sand
        if img_hsv(m,n,2) <= 0.25 && img_hsv(m,n,3) > 0.70 ...
                && m >= ub_rows && (img_hsv(m,n,1)*360) <= 50
            mask(m,n) = 1;
```

```
55              result(m,n,1)=255;
            % water
            elseif ((img_hsv(m,n,2) <= 0.05 && img_hsv(m,n,3) >= 0.40) ...
                    || green_w(m,n) ) && m >= ub_rows
            end

60
            if edge_s(m,n) > radius^ 2*0.6 && m >= ub_rows
                mask(m,n) = 1;
                result(m,n,1)=255;
            end

65
            if (green_s(m,n) && m >= ub_rows )
                mask(m,n) = 1;
                result(m,n,1)=255;
            end
            %if edgemap1(m,n)
70          if redgreen(m,n) && m >=ub_rows
                mask(m,n) = 1;
                result(m,n,1)=255;
                %if result(m,n,3)==255
75              %    result(m,n,3)=img(m,n,3);
                %end
            end

        end
80  end

    % show original
    figure; imshow(img);

85  %ind = find(edgemap1);
    figure; imshow(edgemap1);

    %result(ind,2)=255;
    figure; imshow(result);
90  figure; imshow(mat2gray(mask));

    % save result
    imwrite(result,sprintf('resultsegmentation_max_\%i.jpg',fn),'JPEG','Quality',100);
```

```
function [Iout]=ut_edge(varargin)
%ut_edge        Marr-Hilderth and Canny edge detectors
%
% Iout = UT_EDGE(Iin) finds the possible edges in image Iin using an
% implementation of the Canny edge detector. The derivatives are
% calculated from a 2-D Gaussian function implemented with UT_GAUSS.
% The localization is done by finding the zero-crossings of the second
% directional derivatives (instead of directional maximum suppression
% such as implemented by EDGE from the image processing toolbox). The
% sigma (standard deviation) of the Gaussian  filtering is set to 2.
% Iout is a 2-dimensional array with the same size as Iin. The no-edge
% pixels are indicated in Iout as zeroes. Edge pixels carries the edge
% strength as grey level. The edge strength is scaled between 0 and 1.
%
% Iout = UT_EDGE(Iin,...,OPTION,OPTIONVAL,...) finds the possible edges
% with some options switched on, and with parameter(s) set to OPTIONVAL.
% The  following options are available:
%
% 'marrhildreth' or 'm': Perform Marr-Hildreth operation, i.e. Laplacian
%                        of Gaussian, rather than Canny operation.
% 'canny' or 'c':        Perform Canny operation (default).
% 'sigma' or 's':        The width (standard deviation) of the Gaussian
%                        filtering is set to OPTIONVAL (default: 2)
% 'threshold' or 't':    Return a binary (logical) edge map instead of edge
%                        strengths. The edges are detected by
%                        thresholding it at OPTIONVAL. If OPTIONVAL is
%                        omitted, the default of the threshold is 0.1.
% 'hysteresis' or 'h':   Return a binary (logical) edge map instead of edge
%                        strengths. The edge are detected by hysteresis
%                        thresholding. Two thresholds are applied. The
%                        edges detected with the higher thresholds form
%                        the seed that is propagated in the edge
%                        segments obtained by thresholding with the
%                        lower threshold. OPTIONVAL is a two-element
%                        vector. The first element specifies the
%                        fraction of pixels that will be assigned to
%                        candidate edges (detected with the lower
%                        threshold). The second element is the fraction
%                        of pixels that will be assigned to seed edges
%                        (detected with the higher threshold). If
%                        OPTIONVAL is omitted, the default of [0.1 0.03]
%                        is assumed. If OPTIONVAL is a scalar, then the
%                        default assignment to the second element is
%                        0.3*OPTIONVAL.
%
% Copyright: F. van der Heijden, F.vanderHeijden@utwente.nl
% Laboratory for Measurements and Instrumentation
% University of Twente, the Netherlands
% Version 1.2, date: 15-11-2004
%
% See also UT_GAUSS, EDGE.

[Iin,sigma,operator,threshold_method,thres_parm]=ParseInputs(varargin{:});

grad=(ut_gauss(Iin,sigma,1,0).^2+ut_gauss(Iin,sigma,0,1).^2).^0.5;
grad=grad/max(grad(:));
```

```
if strcmp(operator,'marrhildreth')
    lap=ut_gauss(Iin,sigma,2,0)+ut_gauss(Iin,sigma,0,2);
    zerocross=ut_levelx(lap,0.0);
    Iout=grad.*zerocross;
end

if strcmp(operator,'canny')
    SDGD=ut_gauss(Iin,sigma,1,0).^2.*ut_gauss(Iin,sigma,2,0)+ ...
        2*ut_gauss(Iin,sigma,1,0).*ut_gauss(Iin,sigma,0,1).*ut_gauss(Iin,sigma,1,1)+...
        ut_gauss(Iin,sigma,0,1).^2.*ut_gauss(Iin,sigma,0,2);
    zerocross=ut_levelx(SDGD,0.0);
    Iout=grad.*zerocross;
end

if strcmp(threshold_method,'threshold')
    Iout = logical(Iout>thres_parm(1));
end

if strcmp(threshold_method,'hysteresis')
    his=imhist(Iout, 100000);
    thres_parm(1) = min(find(cumsum(his) > (1-thres_parm(1))*prod(size(Iout)))) / 100000;
    thres_parm(2) = min(find(cumsum(his) > (1-thres_parm(2))*prod(size(Iout)))) / 100000;
    Iout_low = Iout>thres_parm(1);
    Iout_high = Iout>thres_parm(2);
    Iout=imreconstruct(Iout_high,Iout_low);
end


%-------------------------------------------------------------------------
% Subfunction ParseInputs
%-------------------------------------------------------------------------
function [Iin,Sigma,operator,threshold_method,thres_parm] =  ParseInputs(varargin);

error(nargchk(1,30,nargin));


Iin = double(varargin{1});
if ndims(Iin)~=2
    error('Iin must be a 2-dimensional array');
end

%defaults
Sigma=2;
operator = 'canny';
threshold_method = 'none';
thres_parm = [0.1, 0.03];

options = {'canny','c','marrhildreth','m','threshold','t','hysteresis','h','sigma','s'};

if nargin>1
    for k=2:length(varargin)
        if ischar(varargin{k})
            string = lower(varargin{k});
            j = strmatch(string,options,'exact');
            if isempty(j)
```

```
                error(['Invalid input string: ''' varargin{k} '''.']);
            end
            switch string
                case {'canny','c','marrhildreth','m'}
                    if strcmp(string,'m'), string = 'marrhildreth'; end;
                    if strcmp(string,'c'), string = 'canny'; end;
                    operator = string;
                case {'sigma','s'}
                    if nargin>k & isnumeric(varargin{k+1})
                        Sigma = varargin{k+1};
                        k=k+1;
                    end
                case {'threshold','t'}
                    threshold_method = 'threshold';
                    thres_parm = [0.1 0.03];
                    if nargin>k & isnumeric(varargin{k+1})
                        thres_parm(1) = varargin{k+1};
                        k=k+1;
                    end
                case {'hysteresis','h'}
                    threshold_method = 'hysteresis';
                    thres_parm = [0.1 0.03];
                    if nargin>k & isnumeric(varargin{k+1})
                        thres_parm = varargin{k+1};
                        if length(thres_parm)==1
                            thres_parm(2) = 0.3*thres_parm(1);
                        end
                        k=k+1;
                    end
            end
        end
    end
end

if Sigma<0
    error('Sigma must be positive');
end

if strcmp(threshold_method , 'hysteresis')
    if thres_parm(1)<0 | thres_parm(1)>1 | thres_parm(2)<0 | thres_parm(2)>1
        error('hysteresis: threshold parameters out of range');
    end
    if thres_parm(2)>thres_parm(1)
        error('hysteresis: the second threshold must be less than the first');
    end
end
```

```
function [Iout]=ut_gauss(varargin)
%ut_gauss       - 2-D filtering using Gaussian masks
%
%   H = UT_GAUSS(I,SIGMA,DX,DY) filters the data in image I with a 2-D FIR
%   filter whose PSF closely approximates a Gaussian function or one of its
%   derivatives. The width (scale; standard deviation) of the Gaussian is
%   SIGMA (default SIGMA=2).
%
%   Different types of masks can be specified by parameters DX,DY:
%
%       DX   - number of diferentiations in x direction
%       DY   - number of diferentiations in y direction
%
%   Default: DX=0,DY=0.
%
%   - DX+DY must be less or equal to 2.
%   - The size of the mask is 2*ceil(4*SIGMA)+1.
%   - The elements of the PSF are obtained by area sampling of the
%     continuous function, rather than impulse sampling. (Area sampling is
%     equivalent to impulse sampling preceded by a prefilter. The prefilter
%     prevents large aliasing errors that would otherwise occur if SIGMA is
%     too small (say, smaller than 1.5). However, the prefilter also
%     introduces a resolution error that becomes noticeable if SIGMA is
%     smaller than, say, 0.7. The response of the prefilter is a
%     rectangular function with unit width).
%   - UT_GAUSS uses IMFILTER with the replication option on.
%
% Copyright: F. van der Heijden, F.vanderHeijden@utwente.nl
% Laboratory for Measurements and Instrumentation
% University of Twente, the Netherlands
% Version 1.0, date: 25-10-2004
%
% See also IMFILTER

[Iin,sigma,typein]=ParseInputs(varargin{:});

winsiz = ceil(4*sigma);
n=2*winsiz+1;


%gaussian
if strcmp(typein,'normal')
    kernel=create_gauss_kernel(sigma,n,winsiz);
    Iout=imfilter(double(Iin),double(kernel),'replicate','conv');
    Iout=imfilter(double(Iout),double(kernel'),'replicate','conv');
end

%gauss-dx
if strcmp(typein,'dx')
    kernel=create_gauss_kernel(sigma,n,winsiz);
    Iout=imfilter(double(Iin),double(kernel'),'replicate','conv');
    kernel=create_gauss_kernel_x(sigma,n,winsiz);
    Iout=imfilter(double(Iout),double(kernel),'replicate','conv');
end

%gauss-dxdx
if strcmp(typein,'dxdx')
```

```
    kernel=create_gauss_kernel(sigma,n,winsiz);
    Iout=imfilter(double(Iin),double(kernel'),'replicate','conv');
    kernel=create_gauss_kernel_xx(sigma,n,winsiz);
    Iout=imfilter(double(Iout),double(kernel),'replicate','conv');
end

%gauss-dy
if strcmp(typein,'dy')
    kernel=create_gauss_kernel(sigma,n,winsiz);
    Iout=imfilter(double(Iin),double(kernel),'replicate','conv');
    kernel=create_gauss_kernel_x(sigma,n,winsiz);
    Iout=imfilter(double(Iout),double(kernel'),'replicate','conv');
end

%gauss-dydy
if strcmp(typein,'dydy')
    kernel=create_gauss_kernel(sigma,n,winsiz);
    Iout=imfilter(double(Iin),double(kernel),'replicate','conv');
    kernel=create_gauss_kernel_xx(sigma,n,winsiz);
    Iout=imfilter(double(Iout),double(kernel'),'replicate','conv');
end

%gauss-dxdy
if strcmp(typein,'dxdy')
    kernel=create_gauss_kernel_x(sigma,n,winsiz);
    Iout=imfilter(double(Iin),double(kernel),'replicate','conv');
    Iout=imfilter(double(Iout),double(kernel'),'replicate','conv');
end


%--------------------------------------------------------------------
% Subfunction ParseInputs
%--------------------------------------------------------------------

function [Iin,Sigma,typein] =  ParseInputs(varargin);

error(nargchk(1,4,nargin));
%MSG = NARGCHK(LOW,HIGH,N) returns an appropriate error message if
%    N is not between low and high. If it is, return empty matrix.

Iin = varargin{1};

%defaults
typein = 'normal';
Sigma=2;

methods = {'normal','dx','dxdx';'dy','dxdy','err';'dydy','err','err'};

if nargin>1
    Sigma=varargin{2};%!!!! special braces to make it numerical
end
if nargin>2
    if nargin==4
        i = varargin{3};
        j = varargin{4};
        if ((j>2)|(i>2)|(j<0)|(i<0)|(round(i)~=i)|(round(j)~=j))
            typein='err';
```

```
        else
            typein = methods{j+1,i+1};
        end
        if strcmp(typein,'err')
            disp('DX+DY must be less or equal to 2.');
            error(['Invalid input string: ',num2str(varargin{3}),',',num2str(varargin{4})
                ,'.']);
        end
    else
        error(['If DX is specified DY must be specified!!!']);
    end
end


if Sigma<0
    error('Sigma must be positive');
end
return

%------------------------------------------------------------------------
%   Subfunction create_gauss_kernel
%------------------------------------------------------------------------
function kernel=create_gauss_kernel(sigma,n,winsiz)
kernel=zeros(1,n);
c = 1.0/(sigma*sqrt(2));
for i=1:winsiz+1
    hulp(i) = erf((i-1+0.5)*c)-erf((i-1-0.5)*c);
end
accu = hulp(1);
for i=2:winsiz+1
    accu = accu+(2.0*hulp(i));
end

for i=1:winsiz
    kernel(winsiz+1-i) = (hulp(i+1)/accu);
    kernel(winsiz+1+i) = (hulp(i+1)/accu);
end
kernel(winsiz+1) = (hulp(1)/accu);
return


%------------------------------------------------------------------------
%   Subfunction create_gauss_kernel_x
%------------------------------------------------------------------------
function kernel=create_gauss_kernel_x(sigma,n,winsiz)
c =  1.0/(sigma*sqrt(2.0*pi));
sigma2=sigma^2;
kernel=zeros(1,n);

for i=1:n
    x=i-winsiz-1;
    x1 = x - 0.5;
    x2 = x + 0.5;
    kernel(i)= c*(exp(-0.5*x2*x2/sigma2)-exp(-0.5*x1*x1/sigma2));
end
return

```

```
%-------------------------------------------------------------------------
%   Subfunction create_gauss_kernel_xx
%-------------------------------------------------------------------------
function kernel=create_gauss_kernel_xx(sigma,n,winsiz)
c =  1.0/(sigma^3*sqrt(2.0*pi));
sigma2=sigma^2;
kernel=zeros(1,n);
for i=1:n
    x=i-winsiz-1;
    x1 = x - 0.5;
    x2 = x + 0.5;
    if (i==1)
        kernel(i)= c*(-x2*exp(-0.5*x2*x2/sigma2));
    else
        if (i==n)
            kernel(i)= c*(x1*exp(-0.5*x1*x1/sigma2));
        else
            kernel(i)= c*(x1*exp(-0.5*x1*x1/sigma2)-x2*exp(-0.5*x2*x2/sigma2));
        end
    end
end
return
```

```
function [Iout]=ut_levelx(varargin)
%ut_levelx  finding level crossings
%
%   IOUT=UT_LEVELX(IN,LEVEL) outputs a map of the input image IN that
%   indicates the positions where the gray levels cross the level LEVEL.
%   The contour, thus obtained, is 8 connected. The input image must be an
%   intensity image. The function is used in UT_EDGE for zero crossing
%   detection.
%
%   Default: LEVEL=0.
%
%   Copyright: F. van der Heijden, F.vanderHeijden@utwente.nl
%   Laboratory for Measurements and Instrumentation
%   University of Twente, the Netherlands
%   Version 1.0, date: 27-10-2004
%
%   See also UT_EDGE, IMCONTOUR.

[Iin,level] =  ParseInputs(varargin{:});

[m,n,o]=size(Iin);

% pad image with border and replicate pixels:
b = zeros(m+2,n+2);
b(1+(1:m),1+(1:n)) = Iin;
b(1+(1:m),1) = b(1+(1:m),2);
b(1+(1:m),end) = b(1+(1:m),end-1);
b(1,1+(1:n)) = b(2,1+(1:n));
b(end,1+(1:n)) = b(end-1,1+(1:n));
b(1,1) = b(2,2);
b(1,end) = b(2,end-1);
b(end,1) = b(end-1,2);
b(end,end) = b(end-1,end-1);
n = n+2;
m = m+2;
Iout = zeros(size(b));

% level crossings in row direction
b = b-level;
a = circshift(b,[-1 0]);
c = circshift(b,[+1 0]);
ind = find(a.*b<0);
ac = a(ind);
bc = b(ind);
ind = ind + double(abs(bc)>=abs(ac));
ind = mod(ind-1,n*m)+1;
Iout(ind) = 1;
ind = find((a.*b>=0) & (b==0) & (a.*c<0));
Iout(ind) = 1;

% level crossings in column direction
a = circshift(b,[0 -1]);
c = circshift(b,[0 +1]);
ind = find(a.*b<0);
ac = a(ind);
bc = b(ind);
ind = ind + double(abs(bc)>=abs(ac))*m;
```

```
ind = mod(ind-1,n*m)+1;
lout(ind) = 1;
ind = find((a.*b>=0) & (b==0) & (a.*c<0));
lout(ind) = 1;

% crop border:
lout = lout(2:end-1,2:end-1);



%---------------------------------------------------------------------
% Subfunction ParseInputs
%---------------------------------------------------------------------

function [lin,level] =  ParseInputs(varargin);

error(nargchk(1,2,nargin));
%MSG = NARGCHK(LOW,HIGH,N) returns an appropriate error message if
%    N is not between low and high. If it is, return empty matrix.

lin = double(varargin{1});

%defaults
level=0;

if nargin==2
      level=varargin{2};
end
```

C.2 Conversion pixel-to-area

Tarp [n° of pixels]	X_G [n° of pixels]	Y_G [n° of pixels]	AREA [m^2/pixel]
1	2559	1750	0.0226
2	2256	1788	0.0172
3	2131	1861	0.0114
4	1755	1920	0.0073
5	1484	2020	0.0055
6	563	2196	0.0048
7	598	2308	0.0021
8	177	2153	0.0054
9	1651	1848	0.0154
10	2082	1790	0.0204
11	2053	1728	0.0295
12	2216	1673	0.0586
13	2508	1686	0.0460
14	2710	1687	0.0463
15	2767	1645	0.0602
16	2935	1694	0.0406
17	2496	1777	0.0219
18	2447	1826	0.0158

Table C.1: *Conversion pixel-to-Area at each tarp location. The conversion factor is computed in correspondence of the center of mass of the tarp (X_G,Y_G).*

Appendix D

Willow cuttings transplantation and monitoring

Each year the field campaign started with transplantation of *Salix* cuttings on the bare soil of the main island. As a first step, short sticks of about 40 cm length and 1.2 cm diameter have been cut. Salix cuttings are collected from plants and bushes of willows which naturally spread on the island itself and on the riparian zone (Figure D.1.a, b). In order to have a regular distribution of plants within a plot, a matrix frame has been constructed. A thin tape bended from border to border in horizontal and vertical directions marks matrix nodes. Hammering a metal punch into the bare soil, in correspondence of each node, a hole is created, which is then filled with a single cutting D.1.c, d). The matrix, filled in every node and a particular of one cutting are shown in Figure D.1.e, f). During the growing season, from April to September, transplanted cuttings have been monitored regularly. Figure D.2 shows the phases of monitoring. Major stem length, numeber of braches and survival have been recorded in average once every two weeks. Particular effords are put in monitoring the effect of floods on single plants (damage or removal of the shootings) and on the whole plot (Figure D.3).

Figure D.1: *Phases of the cutting transplantation. Collection of cuttings (a,b) and installation of the cuttings into the soil (c,d). A regular matrix made ouf of a wood frame and a rope have been used to locate where to plant the cutting (e,f).*

Figure D.2: *Monitoring of the transplanted Salix cuttings thoughout the growing season.*

Figure D.3: *Effect of floods on the plot of transplanted Salix. During prolonged floods, the dragging force of the water damages the canopy. Erosion of the river bed produces scouring and consequent removal of material around cuttings. Roots developed by the cutting help anchoring plants, even in presence of high scour.*

Appendix E

Root empirical histograms

Figure E.1 shows 3 samples taken from plot 5 during the uprooting monitoring campaign in 2009. Pictures are analyzed using a Matlab code. Analysis parameters are set by means of the Graphical User's Interface (GUI) shown in Figure E.2. The output results are then collectend in excel sheet (Tables E.1, E.2, E.3)in order to start the data analysis process.

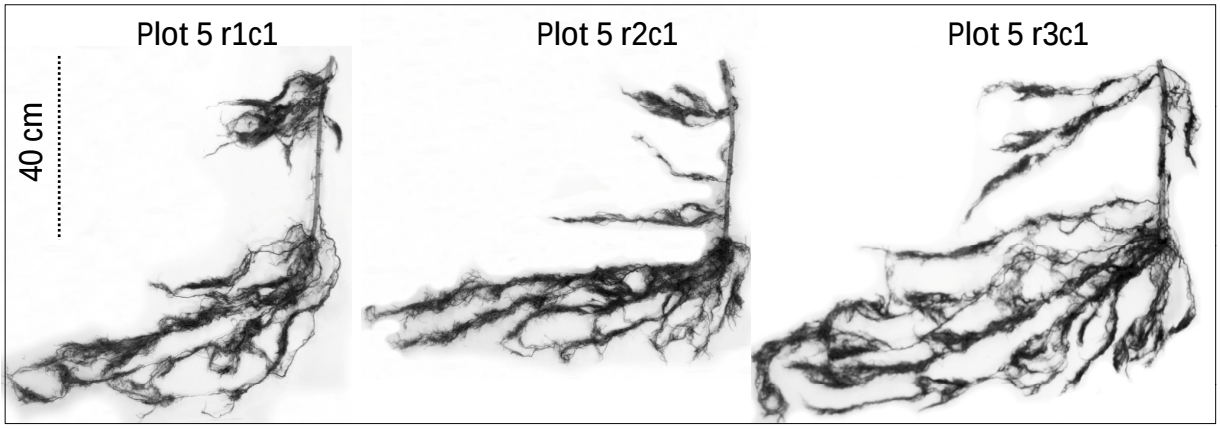

Figure E.1: *Black and White pictures of the three samples taken from plot 5 in Semptember 2009. The three pictures are then separately analyzed using the Matlab software. Input parameter for anaysis are specified by means of the user's interface of shown in figure E.2.*

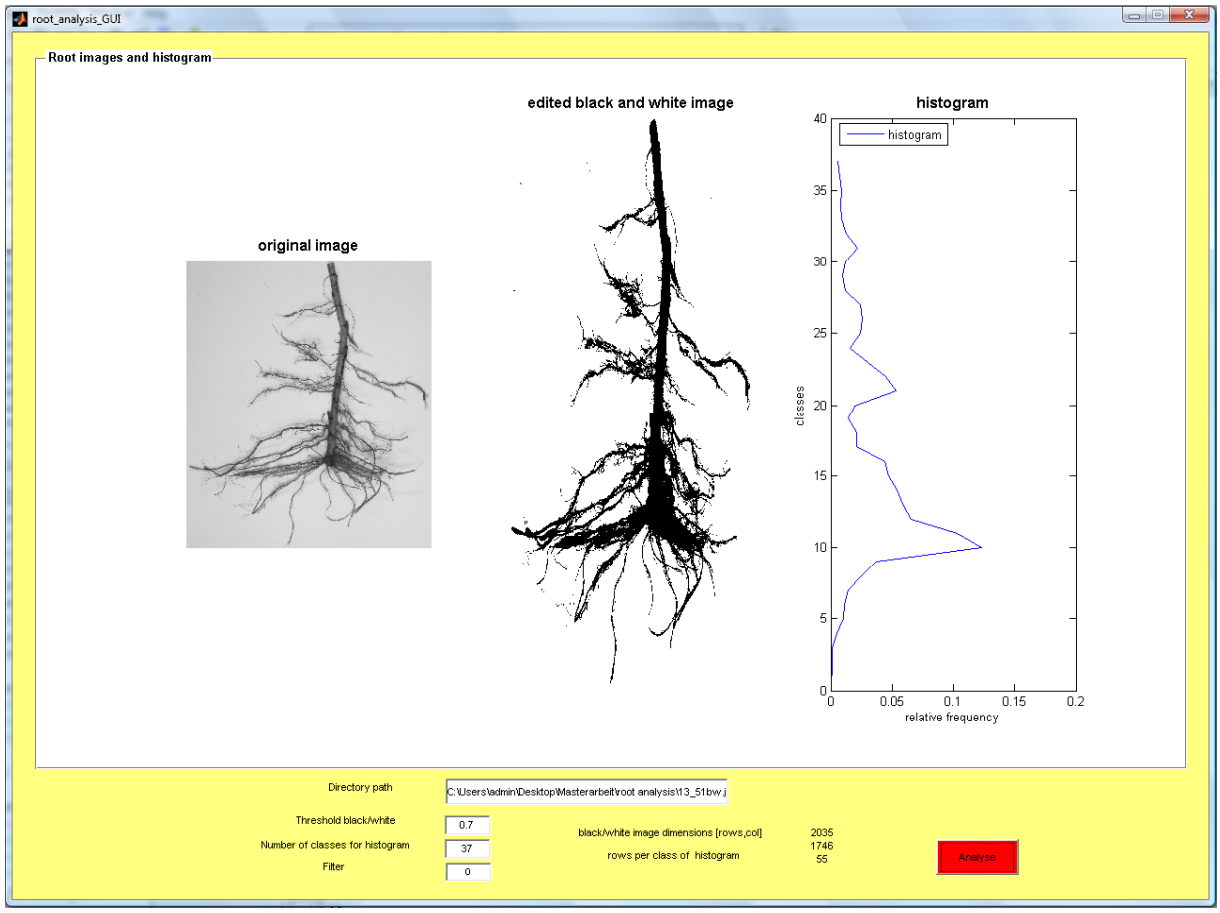

Figure E.2: *Graphical User Interface (GUI) of the MATLAB code for calculating the empirical histogram for each cutting. The picture on the left is the original, scanned picture with the original width-to-height ratio, the one in the middle shows the picture which is translated to ones (white) and zeros (black) with a chosen threshold. This picture is scaled so that height corresponds to the height of the empirical histogram, to facilitate comparison. The saved picture in MATLAB has however still the original width-to height ratio. The greyscale threshold can be chosen in the second box below the pictures. The empirical histogram of the root distribution of a cutting is shown in the right part of the picture. The first box below the pictures shows the directory path of the current original picture. For analysing a new picture this path can be changed. In the third box the number of classes can be defined. The last box allows choosing whether and how much the picture should be filtered. The size of the loaded picture (pixel height and pixel width) is shown on the right of the threshold. With the given length of the picture and the chosen number of classes the number of rows per class is displayed below the image dimensions. Pushing the red button starts the analysis of the picture indicated in the directory path.*

Plot 5, r1 c1		
class	depth	pdf roots
[n°]	[cm]	[%]
1	0	0.00007
2	0	0.00298
3	2.0	0.01060
4	4.0	0.01902
5	6.1	0.01656
6	8.1	0.03272
7	10.1	0.03334
8	12.1	0.04016
9	14.2	0.03941
10	16.2	0.02034
11	18.2	0.00693
12	20.2	0.00380
13	22.3	0.00345
14	24.3	0.00255
15	26.3	0.00289
16	28.3	0.00257
17	30.4	0.00303
18	32.4	0.00751
19	34.4	0.01530
20	36.4	0.02160
21	38.4	0.02467
22	40.5	0.02250
23	42.5	0.02781
24	44.5	0.05625
25	46.5	0.05113
26	48.6	0.04758
27	50.6	0.04452
28	52.6	0.04156
29	54.6	0.03461
30	56.7	0.06576
31	58.7	0.07170
32	60.7	0.06471
33	62.7	0.05122
34	64.8	0.04485
35	66.8	0.04689
36	68.8	0.01664
37		0.00264
38		
39		
40		

Pixel conversion	37	cm	(length picture in real)
	1280	pixel	
	0.029	cm/pixel	
pixel rows/class	70		
	2.02	cm/class	
max roots:	0.0717		
class:	31		
depth from top:	58.7	cm	
root pixel:	1158286		
	967.8	cm2	

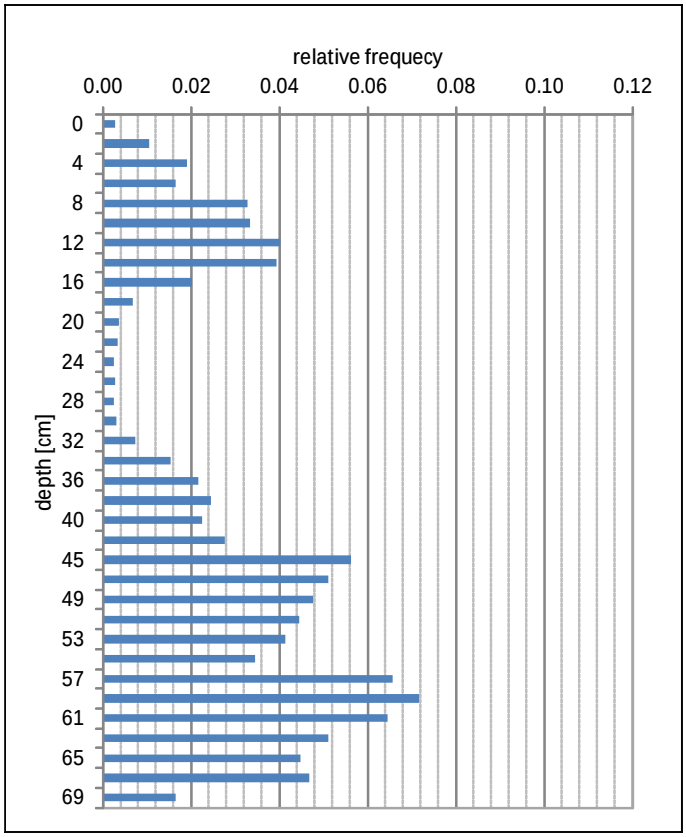

Table E.1: *Excel sheet with the output of the root analysis. Empirical histogram and classes are shown for sample "Plot5 r1c1" shown in Figure E.1.*

Plot 5, r2 c1		
class	depth	pdf roots
[n°]	[cm]	[%]
1	0	0.00000
2	0	0.00000
3	0	0.00000
4	0	0.00000
5	0	0.00000
6	0	0.00020
7	0	0.00359
8	2.0	0.00439
9	4.1	0.00735
10	6.1	0.02186
11	8.2	0.03142
12	10.2	0.03097
13	12.3	0.00790
14	14.3	0.00315
15	16.3	0.00414
16	18.4	0.00645
17	20.4	0.00522
18	22.5	0.01037
19	24.5	0.00553
20	26.6	0.00337
21	28.6	0.01184
22	30.6	0.03267
23	32.7	0.04352
24	34.7	0.00807
25	36.8	0.01344
26	38.8	0.01875
27	40.9	0.02956
28	42.9	0.07172
29	44.9	0.10063
30	47.0	0.10722
31	49.0	0.10054
32	51.1	0.10158
33	53.1	0.06100
34	55.2	0.05399
35	57.2	0.06126
36	59.2	0.03154
37		0.00674
38		0.00002
39		
40		

Pixel conversion	38	cm	(length picture in real)
	1265	pixel	
	0.030	cm/pixel	
pixel rows/class	68		
	2.04	cm/class	
max roots:	0.1072		
class:	26		
depth from top:	40.9	cm	
root pixel:	1148750		
	1036.6	cm2	

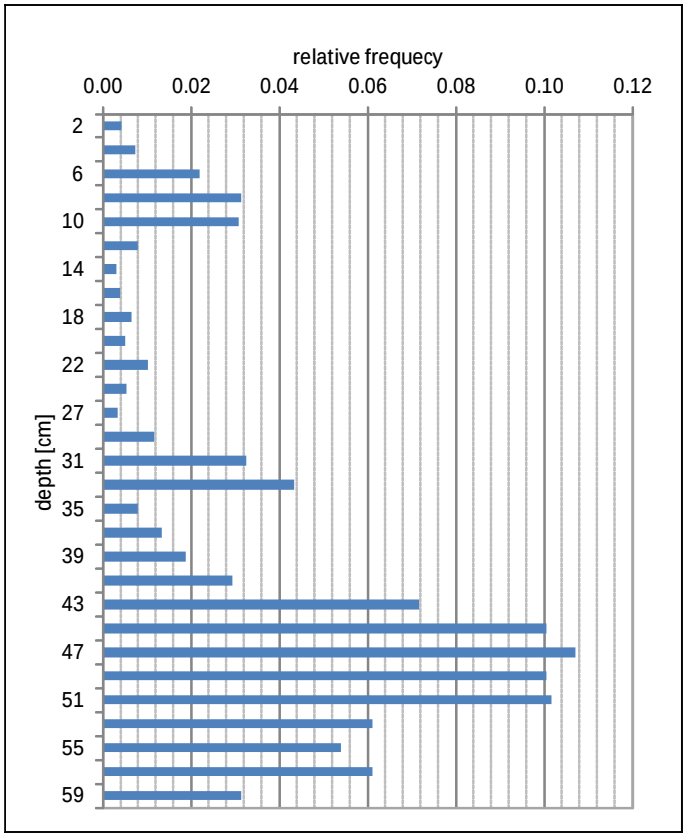

Table E.2: *Excel sheet with the output of the root analysis. Empirical histogram and classes are shown for sample "Plot5 r2c1" shown in Figure E.1.*

Plot 5, r3 c1		
class	depth	pdf roots
[n°]	[cm]	[%]
1	0	0.00000
2	0	0.00111
3	2.0	0.00598
4	4.0	0.01894
5	6.0	0.02974
6	8.0	0.01608
7	10.0	0.01279
8	12.0	0.01191
9	14.0	0.01722
10	16.0	0.01554
11	18.0	0.01185
12	20.0	0.00852
13	22.0	0.00779
14	24.0	0.00726
15	26.0	0.00578
16	28.0	0.01012
17	30.0	0.01625
18	32.0	0.02296
19	34.0	0.02304
20	36.0	0.02046
21	38.0	0.03528
22	40.0	0.04940
23	42.0	0.03389
24	44.0	0.03118
25	46.0	0.03163
26	48.0	0.05088
27	50.0	0.05043
28	52.0	0.05037
29	54.0	0.04335
30	56.0	0.05559
31	58.0	0.05890
32	60.0	0.05233
33	62.0	0.05091
34	64.0	0.04718
35	66.0	0.03892
36	68.0	0.02246
37	70.0	0.02043
38	72.0	0.01110
39		
40		

Pixel conversion	37	cm	(length picture in real)
	1240	pixel	
	0.030	cm/pixel	

pixel rows/class	68	
	2.00	cm/class

max roots:	0.0589	
class:	26	
depth from top:	48.0	cm

root pixel:	2582129	
	2299.0	cm2

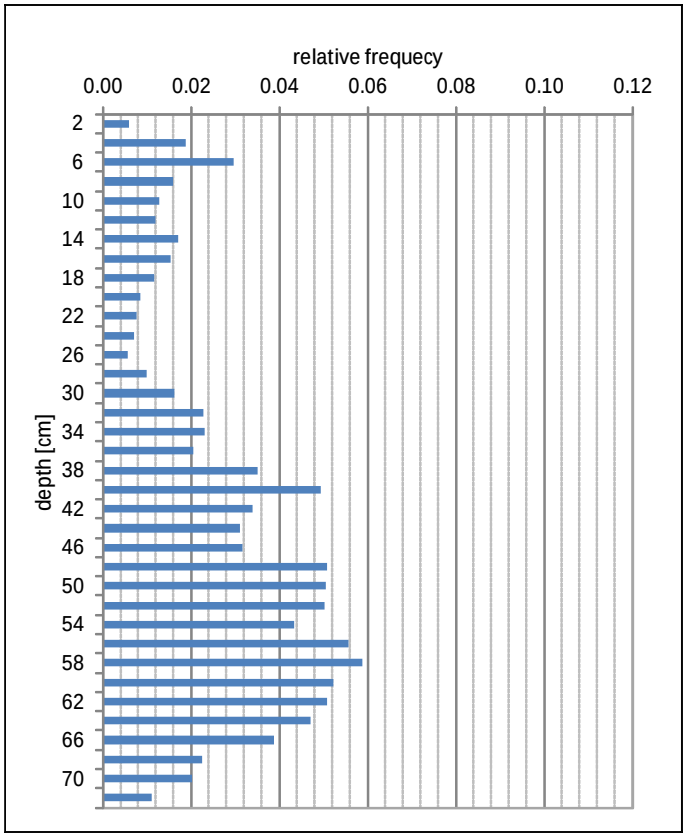

Table E.3: *Excel sheet with the output of the root analysis. Empirical histogram and classes are shown for sample "Plot5 r3c1" shown in Figure E.1.*

Appendix F

Formulation of the velocity profile in presence of a canopy layer

The greatest unknown in Equations 6.1 is represented by the velocity profile U. The presence of vegetation strongly influences local hydrodynamic and the theoretical logarithmic vertical velocity profile becomes rather more complicated and several studies are currently ongoing by many authors. To the purpose of formulation a theoretical model of root reinforcement that may include also the modification of velocity profile within the canopy and therefore local bed shear stress) here, a study by Katul et al. (2011) is summarized.

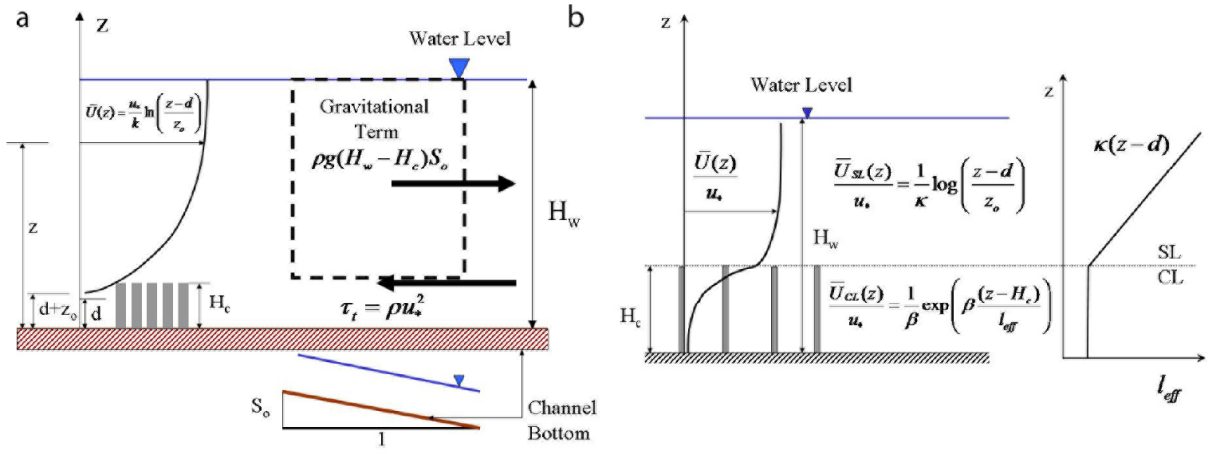

Figure F.1: *(a) Conceptual model developed by Katul et al. (2011) for the force balance above the canopy and the assumed mean velocity profile $\overline{U}(z)$ in streams where $H_w/H_c \gg 1$ (deep layer formulation). The H_w is the water depth, H_c is the canopy height, and S_0 is the bed-slope. (b) Same as (a) but using the Shallow layer formulation: $1 < H_w/H_c < 1$, (Katul et al., 2011).*

Figure F.1 schematically represents the conceptual model developed by Katul et al. (2011) for the balance above the canopy and the definition of the velocity profile. CL is the flow inside

the canopy (canopy layer) whereas the flow above the canopy (surface layer) is named SL. The difference in the mean flow between the two layers is due to the presence of a drag force which is assumed to be much larger than the bed shear stress and a constant mixing length l_{eff}. The determination of *d* and z_o in SL are based on the continuity and smoothness conditions applied to $\overline{U}(H_c)$ (Katul et al., 2011). The parameter $\beta = u_*/\overline{U}(H_c)$, where u_* is the friction velocity at the canopy top. The mixing length l_{eff} is continuous but not smooth in this formulation. The equation of the velocity profile expressed as a sum of an exponential term (within the canopy) and a logarithmic term (above the canopy) is (Katul et al., 2011):

$$\frac{U_b}{u_*} = \sqrt{\frac{8}{f}} = \frac{{H_w}^{1/6}}{n\sqrt{g}} = \overbrace{2\beta\frac{L_c}{H_w}\left[1-\exp\left(-\frac{1}{2\beta^2}\frac{H_c}{L_c}\right)\right]}^{\text{Direct Canopy Layer Effects}} + \frac{1}{2} \underbrace{\frac{1}{\kappa}\left(1-\frac{H_c}{H_w}\right)\left\{-1+\ln\left[\left(\frac{H_w-d}{z_o}\right)^{(H_w-d)/(H_w-H_c)}\left(\frac{H_c-d}{z_o}\right)^{-(H_c-d)/(H_w-H_c)}\right]\right\}}_{\text{Perturbed Log. Profile Due to Canopy Layer Effects}} \tag{F.1}$$

Equation F.1 refers to the shallow-layer formulation (i.e., the case $1 < H_w/H_c < 10$). It asymptotically converges to the deep layer formulation when $H_w \gg H_c$ and $H_w \gg \beta L_c$. Equation F.1 makes explicit the direct effects of the canopy on U_b in the CL and their modulating effect on the log-profile in SL. The momentum absorption coefficient β in Equation F.1 is known to vary with the canopy density for small *a* but saturates at about 0.33 for dense canopies as discussed by Katul and Albertson (1998), Poggi et al. (2004) and Poggi and Katul (2008).

Since $\overline{U}(z)$ is not uniform, a number of approaches can be used to model $\overline{U}(z)$ within and immediately above canopies, including first-order and higher-order closure models. In the work of Poggi et al. (2009), it was shown that a first-order closure model with an imposed mixing length (l_{eff}) that remains constant inside the canopy, hereafter referred to as to as the canopy layer or CL but varies linearly as $\kappa(z-d)$ above the canopy, hereafter referred to as surface layer or SL, reproduced measured $\overline{U}(z)$ and $\overline{u'w'}$ profiles from a wide range of experiments reasonably well. Figure F.1.b shows the assumed shape of l_{eff} in CL and SL. When variations in Lc with z are small, semianalytical models can also be used to estimate $\overline{U}(z)$. One such model can be expressed as follows (Harman and Finnigan, 2007; Massman, 1997; Massman and Weil, 1999; Poggi et al., 2008):

$$\overline{U}(z) = \begin{cases} U_{SL}(z) = \frac{u_*}{\kappa}\ln\left(\frac{z-d}{z_0}\right); & z/H_c > 1; \\ U_{CL}(z) = \frac{u_*}{\beta}\exp\left[\beta\frac{(z-H_c)}{l_{eff}}\right]; & z/H_c < 1; \end{cases} \tag{F.2}$$

where $l_{eff} = 2\beta^3 L_c$ is the constant mixing length inside the canopy and $\beta = u_*/\overline{U}(H_c)$ is a momentum absorption coefficient. The continuity (i.e., $U_{SL}(H_c) = U_{CL}(H_c)$) and smoothness $\left.\frac{d\overline{U}_{SL}}{dz}\right|_{z/H_c=1} = \left.\frac{d\overline{U}_{CL}}{dz}\right|_{z/H_c=1}$ (i.e., ensuring a continuous $\overline{u'w'}$) of the mean velocity profile at $z/H_c = 1$ necessitates unique relationships between z_0 and d as a function of β and L_c/H_c given by Katul et al. (2011):

$$\frac{d}{H_c} = 1 - \frac{2\beta^3 L_c}{\kappa H_c} \tag{F.3a}$$

$$\frac{z_0}{H_c} = 1 - \left(1 - \frac{d}{H_c}\right)\exp\left(-\kappa/\beta\right) = \frac{2\beta^3 L_c}{\kappa H_c}\exp\left(-\kappa/\beta\right) \tag{F.3b}$$

A two-layer (i.e., $z/H_c > 1$ and $z \leq H_c$) representation for the mean flow field has been used by a number of authors to arrive at approximate flow resistance formulations. It should be noticed that the mixing length is continuous but not smooth thereby resulting in a continuous and non smooth turbulent viscosity at $z/H_c = 1$. Katul et al. (2011) also shows that $\overline{U}(H_c)/u_*$ is about 3 for the atmospheric boundary layer (i.e., tall plants, such as pine forest, spruce forest, hardwood canopy etc...) experiments, which implies that $\beta = u_*/\overline{U}(H_c) \approx 1/3$, a constant for these dense-canopy experiments. For sparser canopies, β may be derived from flume experiments on rods with various densities (Poggi et al., 2004). These experiments suggest that for a fixed canopy height, $\beta = \min\left(0.135\sqrt{a}, 0.33\right)$ which is the relationship used here for the aquatic vegetation.

The specification of β is fundamentally connected to the penetration depth (δ_w), or the depth referenced from the canopy top at which 90 percent the momentum flux ($= \overline{u'w'}$) is extracted by the canopy (Nepf and Vivoni, 2000). The penetration depth is often used to categorize aquatic vegetation into sparse ($\delta_w/H_c = 1$, where the eddy penetration occurs throughout H_c) or dense ($\delta_w/H_c < 1$, Nepf (2007)). Using the mean velocity profile in Equation F.2 and a first-order closure approximation for $\overline{u'w'} = -l_{eff}^2\left(dU_{CL}/dz\right)$, the momentum flux inside the canopy is given by Katul et al. (2011):

$$\frac{\overline{u'w'}}{u_*^2} = -\exp\left(\frac{z - H_c}{\beta^2 L_c}\right). \tag{F.4}$$

Defined the vertical velocity profile modification due to the presence of low vegetation and shallow layer formulation ($1 < H_w/H_c < 10$), it is theoretically possible to compute the

dragging force as expressed by 6.1. Theoretically, with the aim of a 3-D hydrodynamic model, it would be also feasible to include the equation here presented in the model, in order to directly obtain velocity in correspondence of vegetation patterns, once the characteristics of the vegetation are defined.

Curriculum Vitae

Nicola Pasquale
Via Gabiani 11, 14100 Asti, Italy
Born 14 July 1981
Italian citizen

Education and Academic Experiences

Nov 2008 - Jul 2011	Ph.D. student in the Hydrology and Water Resources Management group, Institute of Environmental Engineering, ETH Zurich, Switzerland.
May 2007 - Mar 2008	Research Assistant in the Hydrology group, Institute of Environmental Engineering, ETH Zurich, Switzerland. Focus: development of flood-vegetation stochastic model for eco-hydrological applications. Maggia valley case study.
Nov 2007 - Feb 2008	Italian State Civil Engineer Examination, Turin, Italy.
Oct 2006 - Apr 2007	Scientific visit at the Institute fo Environmental Engineering (IfU), Swiss Federal Institute of Technology, ETH Zurich. Focus: implementation, calibration and testing of the model MIAGE for glacial Alpin basin dynamics for the master thesis.
Sep 2004 - May 2007	Master in Civil Engineering, Politecnico di Torino, Torino, Italy. Major in hydraulic constructions, geothecnical engineering and hydrology. Thesis: *Differential models for the hydrological dynamics of glacial basins*.
Sep 2000 - Oct 2004	Bachelor in Civil Engineering, Politecnico di Torino, Torino, Italy. Thesis: *Hydraulic modeling and channel protection of Rocchea creek*.

Working Experiences

Oct 2007 - Oct 2008	Project Manager, IPA LAKER Company, brick and tile fournaces and plant constructions, Asti, Italy.
Oct 2004 - Oct 2008	River 1-D modeling and sewage system design (Part time job), Arnaud Engineering, Asti, Italy.

Publications

Pasquale, N., P. Perona, and P. Burlando (2012). Root reinforcement of alluvial river sediment model. *In preparation*.

Pasquale, N., P. Perona, A. Wombacher, and P. Burlando (2012). Hydrodynamic model calibration from non-orthorectified terrestrial photographs. *In preparation*.

Pasquale, N., P. Perona, R. Francis, and P. Burlando (2012). Effects of streamflow variability on the vertical root density distribution of willow cutting experiments. *Ecological Engineering* (40), 167-172.

Pasquale, N., P. Perona, R. Francis, and P. Burlando (2012). River morphodynamic processes and related effects on above- and below-ground Salix cuttings dynamics. *Submitted to Ecologincal Engineering*.

Pasquale, N., P. Perona, P. Schneider, J. Shrestha, A. Wombacher, and P. Burlando (2011). Modern comprehensive approach to monitor the morphodynamic evolution of a restored river corridor. *Hydrology and Earth System Sciences* 15(4), 1197-1212.

Crouzy, B., K. Edmaier, **N. Pasquale**, P. Perona (2012). Impact of floods on the statistical distribution of riverbed vegetation, *Submitted to Geomorphology*.

Samaritani, E., J. Shrestha, B. Fournier, E. Frossard, F. Gillet, C. Guenat, P. a. Niklaus, **N. Pasquale**, K. Tockner, E. a. D. Mitchell, and J. Luster (2011). Heterogeneity of soil carbon pools and fuxes in a channelized and a restored floodplain section (Thur River, Switzerland). *Hydrology and Earth System Sciences* 15(6), 1757-1769.

Schneider, P., T. Vogt, M. Schirmer, J. Doetsch, N. Linde, **N. Pasquale**, P. Perona, and O. A. Cirpka (2011). Towards improved instrumentation for assessing river-groundwater interactions in a restored river corridor. *Hydrology and Earth System Sciences* 15(8), 2531-2549.

Linde, N., J. Doetsch, D. Jougnot, O. Genoni, Y. Durst, B. J. Minsley, T. Vogt, **N. Pasquale**, and J. Luster (2011). Self-potential investigations of a gravel bar in a restored river corridor. *Hydrology Earth System Sciences*, 15, 729-742.

Presentation for national and international conferences and workshops

Pasquale, N., P. Perona, A. Wombacher, U. Villero, P. Sekarsary, P. Burlando (2011). From terrestrial monitoring to non-invasive techniques for modelling river morphodynamics. River Corridor Restoration Conference, Monte Vertià, Ascona.

Pasquale, N., U. Villero, A. Wombacher, P. Perona, and P. Burlando (2011). Non-invasive calibration technique of a 2D hydrodynamic model based on pattern recognition and digital mapping. E.G.U., General Assembly, Wien.

Pasquale, N., P. Perona, P Burlando (2010). Restored reach of the river Thur: a preliminary morphodynamic evolution analysis. Latsis Symposium, CCES, Zurich.

Pasquale, N., P. Perona, P Burlando (2010). Morphodynamic evolution and Salix cutting dynamics in restored river corridors. Università degli Studi di Palermo, Eco-hydrology summer school, Palermo, Italy

Pasquale, N., P. Perona, R. Francis, P Burlando (2010). The role of river hydrology on Salix shoot and root survival statistics on the alluvial sediment of a restored river corridor. E.G.U., General Assembly, Wien.

Taube, N., **N. Pasquale**, A. Agazzi and P. Burlando (2010). Terrestrial photography of a restored river corridor and related information content about its evolution dynamics. E.G.U., General Assembly, Wien.

Pasquale, N., P. Perona, F. Verones, R. Francis, P Burlando (2009). Experimental Salix shoot and root growth statistics on the alluvial sediment of a restored river corridor. A.G.U. Fall meeting, San Francisco, CA, U.S.A.

Pasquale, N., P. Perona, Z. Jiang and P Burlando (2009). Restored river corridors: first results on the effects of flow variability on vegetation cuttings survival rate and related root architecture. E.G.U., General Assembly, Wien.

Perona, P., **N. Pasquale** and D. Molnar (2007). Mechanistic Modeling of Glaciated Alpine Basin: Case Study. E.G.U., General Assembly, Wien